A STUDY OF INCLUSIVE REACTIONS IN $K^{-}P$ COLLISIONS AT 10 AND 16 GEV/C

by

Aasim Abdul-Kareem Azooz

A thesis presented for the degree of Doctor of Philosophy of the University of London

Department of Physics,
Imperial College of Science and Technology,
London, S.W.7.

October 1973.

ABSTRACT

Inclusive production of particles and resonances from K^-p interactions at beam momenta of 10.1 and 16 GeV/c are studied in this thesis. In Chapter One, we give a review of some of the theoretical ideas associated with inclusive reactions which have appeared in literature during the last three years. In Chapter Two we discuss some of the features in our data, and some of the experimental biases from an inclusive point of view. Scaling and limiting fragmentation of single and two particle x distributions are discussed in Chapter Three. This Chapter includes a possible explanation (based on duality arguments) of the scaling behaviour of two pion distributions in certain kinematical regions. Distributions in p_T^2 are studied in Chapter Four where it is shown that resonance production plays an important role in the p_T^2 distribution of particles. Inclusive production of the $K^{*-}(890)$ resonance is studied in Chapter Five. Comparison of predictions of triple regge formalism with our data on Δ^{++} inclusive production is given in Chapter Six. In Chapter Seven it is shown that resonance production plays an important role in the observed correlations between inclusively produced particles. Inclusive and semi-inclusive production of $\bar{K}^0$ and Λ^0 are studied in Chapter Eight.

CONTENTS

CHAPTER ONE

INTRODUCTION AND THEORETICAL BACKGROUND

Notation, Kinematics and Terminology

In high energy collisions when a particle a, strikes a target b, different numbers and types of particles are produced in the final states. At the upper limit of present accelerator energies, a large number of charged and neutral particles is produced on average. Since non-strange neutral particles are very difficult to detect and, in general, identification of charged high momentum secondaries is not possible, complete analysis of the final states is difficult.

An alternative to this situation is to concentrate our study on the particular class of reactions in which a particle of type c is produced along with various numbers of other particles of unspecified type in so called "Inclusive reactions"as suggested by Feynman[1] of the type

$$a + b \rightarrow c + \text{anything} \quad . \tag{1.1}$$

In such a reaction we study the differential cross-section as a function of momentum, say, of particle c regardless of whatever else is produced.

We denote the four momentum vector of c as $(E, \bar{p})$. The object of interest is the Lorentz invariant inclusive differential cross-section: $Ed^3\sigma/d^3\bar{p}$. For notational convenience the symbol f is adopted to replace $Ed^3\sigma/d^3\bar{p}$.

$$f(s, \bar{p}) \equiv Ed^3\sigma/d^3\bar{p} \tag{1.2}$$

where s is the square of the total centre of mass energy. Analogously for two particle inclusive reactions,

$$a + b \rightarrow c + d + \text{anything} \tag{1.3}$$

we define a variable G

$$G(s, \bar{p}_c\ \bar{p}_d) \equiv E_c\ E_d\ d^6\sigma/d^3\bar{p}_c\ d^3\bar{p}_d \quad . \tag{1.4}$$

In the single particle case, the quantity $f(s,\bar{p})$ is a function of three independent variables, for which several sets may be contemplated. I list four general sets which are in common use:-

1. $(s, |\bar{p}_c|, \Omega)$
2. (s, p_L, p_T^2)
3. (s, y, p_T^2)
4. (s, t, M_x)

The common variable within the above sets is s. p_T^2 in sets 2 and 3 is the square of the component of $\bar{p}$ transverse to the direction of the incident particle. In set 1 Ω is the angle in momentum space between $\bar{p}$ and the incident projectile. In set 2 p_L is the longitudinal component of p which may be measured in different frames of references giving different subsets of set 2.

There are two more important variables to be introduced. The first variable x proposed by Feynman[1] is related to p_L^{cm}, as follows:

$$x = \frac{p_L^{cm}}{p_{max}^{cm}}$$

and $p_{max}^{cm} = \frac{1}{2\sqrt{s}} \left[\left(s - (m_a + m_b)^2\right)\left(s - (m_a - m_b)^2\right)\right]^{\frac{1}{2}}$

at large s $\quad p_{max} \rightarrow \frac{\sqrt{s}}{2}$

$$x = \frac{2\, p_L^{cm}}{\sqrt{s}} \tag{1.5}$$

The second variable is the "Rapidity"[2] y, which is defined as

$$y = \sinh^{-1}\left[p_L/(m_c^2 + p_T^2)^{\frac{1}{2}}\right] .$$

The advantages of using such a variable are two-fold:-

If one uses a set of variables defined in terms of s, y, p_T^2, the differential $d^3\bar{p}/E$ transforms into $\pi dp_T^2 dy$, which eliminates the necessity of weighting the distributions by E in order to calculate Lorentz invariant cross-sections.

Secondly, although y itself is not a Lorentz invariant variable, a longitudinal Lorentz transformation of y from one frame to another will produce the effect of changing y only by a constant, i.e.

$$y \rightarrow y' = y + \text{constant} \quad .$$

Fig. (1.1) shows how the y, p_L^{cm} and p_L^{lab} variables map into one another.

The set (s, t, M_X^2) is based on Lorentz invariants and it is the set most analogous to variables in general used for two body and quasi-two-body reactions with

$$t = (\bar{P}_c - \bar{P}_a)^2 \tag{1.6}$$

$$M_X^2 = (\bar{P}_a + \bar{P}_b - \bar{P}_c)^2 \quad . \tag{1.7}$$

For convenience we record here the phase space volume in a variety of variables for large s approximation.

$$
\begin{aligned}
d^3p/E &= d^2p_T\, dy \\
&\approx dp_T^2\, dx/x \\
&\approx dx\, (-dt) \\
&\approx \frac{dM_X^2}{s}\, dt
\end{aligned}
$$

Inclusive and Exclusive Reactions

The idea of studying reactions of type (1.1) is not new. However, the name "inclusive" was not used until recently. These reactions have been studied since the early days of high energy physics, for example through the measurements of total cross-sections of different high energy collisions. These measurements have always been most important in elucidating high energy collisions. In the new inclusive language, measurement of total cross-sections represents the simplest type of inclusive reaction which takes the form:-

$$a + b \rightarrow \text{anything} \qquad (1.8)$$

The only variable on which the cross-section depends is the total centre of mass energy for any fixed a and b pair (neglecting any polarization).

Although this type of analysis imposes itself as a technical necessity on both the experimentalist and the theorist because of the increasing number of particles in the final states, it does not follow that when we average over so many particles the results contain little

information. The inclusive study is an equivalent alternative to the exclusive one[3] and when complete it is, in principle, equally informative.

An exclusive reaction is one in which we study one particular final state where the number and type of particles are known.

The inclusive cross-section is defined averaging over exclusive ones, thus we can write

$$\frac{d\sigma^{incl}}{dp \ldots dp_n} = \sum_{\ell=0}^{\infty} \frac{1}{\ell!} \int \frac{d^{n+\ell}\,\sigma^{ex}}{dp_1 \ldots dp_n\, dp_{n+1} \ldots dp_{n+\ell}}\, dp_{n+1} \ldots dp_{n+\ell} \,. \tag{1.9}$$

In the same way one can write the exclusive cross-section in terms of inclusive ones as follows:-

$$\frac{d\sigma^{excl}}{dq \ldots dqm} = \sum_{\ell=0}^{\infty} \frac{(-1)^{\ell}}{\ell!} \int \frac{d^{m+\ell}\,\sigma^{in}}{dq_1 \ldots dqm\, dq_{m+1} \ldots dq_{m+\ell}}\, dq_{m+1} \ldots dq_{m+\ell} \tag{1.10}$$

Relations (1.9) and (1.10) are equally correct, although equation (1.10) is far less familiar. It can be understood as follows:- in order to isolate the contribution of two body channels to two body inclusive cross-sections say, we have to subtract from the latter the cross-sections where three, four etc. particles occur in the final state.

From the above discussion one deduces that a complete measurement of all inclusive cross-sections implies a complete knowledge of all exclusive cross-sections and vice versa. The two sets of measurements are entirely equivalent. This equivalence is not surprising. There is an exact parallel to this in the ordinary many body problem in quantum

mechanics, where there are two ways of describing a quantum mechanical system. Either one studies the probability of finding exactly n particles at the space co-ordinates X_1, ...X_n which is called the particle description or one asks what is the probability of finding a particle at Y_1, another at Y_2 and so on, without specifying the number of particles in the system; this is called the field description. The two descriptions are entirely equivalent, being related by a transformation of co-ordinates in the space over which the probability function is defined.

In hadron collisions the same situation occurs except it is more convenient to work in momentum space than in ordinary space. As is the case in quantum mechanics when dealing with a system of only a few particles such as the hydrogen atom, the particle description is preserved and it is fairly easy to calculate the wave function giving the probability of finding the proton and the electron at a certain co-ordinate or in a given momentum interval. However, when the number of particles is large, for example in a liquid, the field description becomes more convenient.

As is the case with exclusive measurements a complete measurement of all the inclusive cross-sections is impossible. What one hopes, is that the two will be complementary. This will help us to gain a better understanding of hadron collisions,any theory of which must be able to predict correctly both exclusive and inclusive spectra.

The Generalised Optical Theorem

A formalism for the phenomenology of inclusive reactions was provided by Mueller[4] through a generalisation of the optical theorem.

Before considering the different aspects of this generalisation, let us first recall the ordinary optical theorem. The theorem is a direct consequence of the conservation of probability, i.e. "unitarity", and

relates the total cross-section to the forward elastic amplitude in two body collisions. One of its forms is

$$\sigma_T \sim \frac{1}{s} \text{ Im } \left(A_{el}\right)_{t=0} \quad . \tag{1.11}$$

This relation can be represented schematically by the diagram of fig. (1.2.a) where σ_T is the total cross section and A_{el} is the elastic two-body scattering amplitude. When this amplitude is considered as an analytic function of s it is known to have a cut[5] on the positive real axis. It is also known that this amplitude satisfies the reality condition, which is a direct consequence of time reversal.

$$A_{el} \ (s + i\varepsilon) = \overset{*}{A}_{el} \ (s - i\varepsilon) \tag{1.12}$$

$$\therefore \quad \text{Im } A_{el} = \frac{1}{2i} \left[A_{el} \ (s + i\varepsilon) - A_{el} \ (s - i\varepsilon)\right] \tag{1.13}$$

where ε is a very small change in s.

The right-hand side of (1.13) represents a 'right-hand cut' on the (s) plane, so the optical theorem can be written as

$$\sigma_T \sim \frac{1}{s} \text{ Disc } \left[A_{el}\right]_{t=0} \tag{1.14}$$

where Disc stands for the discontinuity suffered in traversing a pole in the complex plane.

It is clear that the optical theorem relates the total cross-section, in the simplest inclusive reactions of type (1.8), to the two-body elastic amplitude, so whatever we know about one implies knowledge of the other.

Let us now consider the next simplest inclusive reaction (1.1). For such reactions the generalised optical theorem suggested by Mueller is

best represented by the diagrams of fig. (1.2.b) which is somewhat similar to fig. (1.2.a). As in the ordinary optical theorem, the Lorentz invariant single particle inclusive cross-section is related to an elastic amplitude in the forward direction of the three particles a b $\bar{c}$ as follows:-

$$f(s,\bar{P}_c) \sim \frac{1}{s} \text{ Disc}_M{}^2 A_{el} (a\ b\ \bar{c} \to \grave{a}\ \grave{b}\ \bar{\grave{c}})_{t=0} \qquad (1.15)$$

From (1.1) c is an outgoing particle. Consequently, we are not in the physical region of the reaction:

$$a\ b\ \bar{c} \to \grave{a}\ \grave{b}\ \bar{\grave{c}} \qquad (1.16)$$

In (1.16) $S_{b\bar{c}} = (P_b - P_{\bar{c}})^2$ is an effective mass while in (1.1) it is a momentum transfer and is mostly negative. Furthermore, the amplitude of (1.16) is a function of many variables and even when restricted to the physical region of (1.1) S_{ab}, S_{ab} and $S_{ab\bar{c}}$ can still have cuts. Thus, the discontinuity of fig. (1.2.b) has to be specified as follows:

$$\text{Disc } A = A\ (S_{ab} + i.\epsilon.,\ S_{ab\bar{c}} + i.\epsilon.,\ S_{a'b'} - i.\epsilon.)$$

$$-A\ (Sab + i.\epsilon,\ Sab\bar{c} - i.\epsilon,\ Sa\grave{b} - i.\epsilon) \qquad (1.17)$$

where one notices that one takes only the discontinuity across the cut $S_{ab\bar{c}}$ i.e. $M^2_{(x)}$. Because of these complications one sees that analytic continuation is needed for the amplitude of reaction (1.16) off its physical region.

The importance of the generalised optical theorem is that it relates the inclusive cross-section to an elastic amplitude which might have a similar behaviour to that of the ordinary two-body elastic amplitude.

Thus, it changes the nature of the problem to a form which can be solved in terms of the more traditional s-matrix elements.

From the above discussion we may generalise to more than one body inclusive reactions simply by relating the n - body inclusive cross section to the $2 + n \to 2 + n$ body forward elastic amplitude.

Finally, just as the optical theorem does not solve all the problems related to σ_T the generalised optical theorem can not be expected to answer all the questions about inclusive reactions, and merely changes the nature of the problem. The question now is to formulate these $(2 + n \to 2 + n)$ elastic amplitudes. Because the 2-2 body elastic amplitude is the simplest member of the family of these n-n amplitudes several approximations which were used before for the two body case are being extended to the other members[6]. These include the traditional Regge expansion and Veneziano B_n functions.

Feynman's Scaling Hypothesis

It was first Feynman in 1969[1] who suggested that the study of inclusive spectra could be very useful, not only for experimental ease but also from the theoretical point of view. One of his main predictions about the behaviour of inclusive spectra at high energy is the well known hypothesis of scaling. The scaling hypothesis can be stated simply as that "The inclusive cross-section should become energy independent at sufficiently high s when studied in terms of x and P_T^2".

$$\lim_{s \to \infty} \quad f(s,x,P_T^2) \to g(x,P_T^2) \tag{1.18}$$

This hypothesis can be understood using a picture of what happens in a collision similar to that of Fig. (1.3.a). Looking at the collision in the centre of mass of the two particles a and b we see that the two

particles suffer a Lorentz contraction along the z direction which is defined as the collision axis. This Lorentz contraction changes the shape of the two particles to disc-like objects. Feynman suggests that when the collision takes place there is a sudden mixing and reversal of direction of motion of some part of the hadronic stuff constituting the two original hadrons. The result of the mixing is a disc-like "hot" material or source of radiation. The radiation produced from this source will be in the form of material particles. The momentum spectrum of the emitted particles is determined by the momentum space spectrum of the source.

If the radiated secondaries are produced from the central source in a similar way to that of electro-magnetic radiation from classical currents, then the momentum spectrum of the particles is a Fourier transform of the energy density of the source.

If we assume that the role s plays in the interaction is merely to produce the Lorentz contraction, then increasing s merely gives a thinner disc source. Thus, at very high energy, the energy density of the disc source will have a delta function distribution. The Fourier transform of such a delta function is uniform in momentum dp. If we further assume that the field energy is uniformly distributed among the various kinds of particles in fixed ratios independent of s, we conclude that the mean number of particles of any kind at fixed P_T is distributed as dP_L/E where E is the energy of the particle in the centre of mass. Thus the probability of finding among all emitted particles a particle of kind c with mass m, in a transverse momentum interval $d\bar{P}_T$ and in the longitudinal momentum interval dP_L is of the form

$$f\,(P_T,\ P_L/W)\ dP_L\ d^2\bar{P}_T\ /E \qquad (1.19)$$

where W is the energy in the centre of mass. In terms of x:-

$$f_i\ (P_T^2,\ x)\ dx\ d^2\bar{P}_T/E \qquad (1.20)$$

which is independent of s and has a finite value at x = o.

It is useful to see what this means in terms of the rapidity variable y.

We can write

$$\sinh y^{cm} = \frac{p^L_{cm}}{(m^2 + P_T^2)^{\frac{1}{2}}} \quad .$$

At large s,

$$\sinh y^{cm} = \frac{x\sqrt{s}}{2(m^2 + P_T^2)^{\frac{1}{2}}}$$

$$x = \frac{2(m^2 + P_T^2)^{\frac{1}{2}}}{\sqrt{s}} \sinh y^{cm} \quad . \qquad (1.21)$$

The small region near x = o, i.e. p^L_{cm} = o, is wider when expressed in terms of the rapidity variable y. This can easily be seen with the aid of fig. (1). Thus if scaling of the x distribution is valid, the y_{cm} distribution will develop a plateau over a region Δy of width comparable to $s^{\frac{1}{2}}$ and centered round y_{cm} = o. This is called the plateau hypothesis.

The rate at which scaling is approached may depend on the type of particle and on the value of x. This can be explained if one keeps in mind that in the energy region considered in this thesis, for example, the cross-section for 4 and 6 prong events is nearly constant whereas it rises steeply for events with more than 10 prongs. For events with large numbers of particles the mean value of x is small. Furthermore, each particle of a specified type from a certain event is counted once in the inclusive spectrum, so events with high multiplicity contribute with large

weight to the overall distribution. Consequently, we should expect the Feynman scaling to be approached less rapidly for x small than x large.

The Hypothesis of Limiting Fragmentation

Another form of energy independence of the inclusive cross-section has been proposed by Benecke, Chou, Yang and Yen[7]. They believe that it is more useful to use the target and the projectile rest frames as the frames of reference in which to study the momentum spectrum of inclusively produced particles at high energies. In their view if one considers the laboratory system L, some of the produced particles tend to have increasing lab. velocities β as s increases, and others tend to have limited velocities. These are those slow particles in the lab frame which are the ones expected to approach a limiting distribution as s becomes large.

To make this suggestion more plausible, one may imagine the incoming beam (a) particles as Lorentz contracted discs in the lab frame, in which the target b is at rest. The passage of these discs through the hadron b causes b to split up into fragments.

One can see from fig. (1.3.b) that as the energy increases, the disc becomes thinner. Once the thickness is below a certain minimum, an increase in energy should not appreciably affect the fragmentation of b. Thus, all inclusive distributions of particles of type c say, with momentum $|P_c| \ll \sqrt{s}$ in the target rest frame should approach a constant limit, independent of s. The limit $|P_c| \ll \sqrt{s}$ is necessary because if we have $|P_c| \sim \sqrt{s}$ then from the uncertainty principle we get a resolution in z of $\Delta z < \frac{1}{\sqrt{s}}$ in the experiment. Such resolution is equal to the rate at which the apparent thickness of a decreases with increasing s.

The above argument can be applied equally well in the projectile rest frame. This means particles produced as fragments of a approach

a limiting momentum distribution as $s \to \infty$ provided that $|P_c| << \sqrt{s}$ in the projectile rest frame. Consequently, two kinematical regions can be defined, one the target fragmentation region where the momentum of an inclusively produced particle is measured in the target rest frame and a projectile fragmentation region where the momentum of the measured particle is in the projectile rest frame. In both regions the condition of $|P_c| << \sqrt{s}$ has to be satisfied. These two regions can be mapped in terms of x as the regions of $x < o$ and $x > o$ respectively. The region of $x = o$ is called the pionization region.

Pionization is best represented as evaporation[8] of slow moving particles, mostly pions, in the centre of mass system. If the hypothesis of limiting fragmentation is true, then one does not expect pionization to take place because if all particles are produced in either of two fragmentation regions they must have $|P_c| < \sqrt{s}/2$ measured in either frame of reference. This means that no particles should be produced with $|P_c| \approx \frac{\sqrt{s}}{2}$ in either regions which is the value of $x \approx o$ because values of $P_z^{lab} \approx \frac{\sqrt{s}}{2}$ or $P_z^{proje} = \frac{\sqrt{s}}{2}$ are values which can not be defined in the target or projectile frame of reference.

The above point forms the major difference between Feynman's scaling hypothesis and the hypothesis of limiting fragmentation. The former makes definite predictions about scaling near $x \approx o$ while the latter cannot define this region. The two hypotheses are equivalent for ranges of $|x| >> o$.

Model Independent Relations

Some very useful relations concerning inclusive reactions may be derived without using any prior assumptions or dynamical models such as Feynman scaling or limiting fragmentation. These fundamental relations are direct consequences of well-known kinematics and conservation laws and they are very important, for they provide useful tests on consistency

of both theory and data. Some of these relations will be discussed in this section; many others are present in the literature[7].

Starting with the single particle inclusive cross-section we have

$$\int f(s,\bar{p})\, d^3\bar{p}/E = 1.\sigma_{1c} + 2.\sigma_{2c} + 3.\sigma_{3c} \ldots\ n\sigma_{nc} = \sum_{n=1}^{n} n\sigma_{nc} \qquad (1.22)$$

where σ_{nc} is the contribution to the cross section from final states involving the production of precisely n particles of type c. If we define $\langle n_c \rangle$ as the average number of particles of type c produced in all channels, then:

$$\langle n_c \rangle = \frac{0.\sigma_{0c} + 1.\sigma_{1c} + 2.\sigma_{2c} + 3.\sigma_{3c} + \ldots + n\sigma_{nc}}{\sigma_{0c} + \sigma_{1c} + \sigma_{2c} + \sigma_{3c} + \sigma_{4c} + \ldots \sigma_{nc}} = \sum_{n=1}^{\infty} n\,\sigma_{nc}/\sigma_T \qquad (1.23)$$

Therefore

$$\int f(s,\bar{P})\, d^3p/E = \langle n_c \rangle\, \sigma_T \qquad (1.24)$$

where σ_T is the total cross-section for a b collision.

It is interesting to note that equation (1.24) can be used to get a crude prediction about the behaviour of f(s,p) with energy. It is not at all surprising to expect that above a certain threshold, the energy dependence of f(s,p) should not be much different from that of σ_T. Such behaviour is expected if we take into consideration the empirical fact that to a first approximation the integration of the phase space volume d^3P/E should be carried out in the longitudinal direction only because of the transverse momentum cut off at small values well below the kinematical limits. In such a case the available phase space volume is a slowly varying function of s "approximately" as ln (s). This is more or less the same behaviour of $\langle n \rangle$ so unless f(s,p) is of a pathological nature its dependence on s should be roughly the same as

that of σ_T.

Next let us consider a conserved additive quantity like electric charge. It is obvious that

$$Q_a + Q_b = \sum_c \int d^3\bar{p}_c \, Q_c \left(\frac{1}{\sigma_T} \frac{d^3\sigma}{d\bar{p}_c}\right) \tag{1.25}$$

and four momentum vector conservation gives

$$(p_a + p_b)^\mu = \sum_c \int d^3\bar{p}_c \quad \bar{p}_c \quad \frac{1}{\sigma_T} \frac{d^3\sigma}{dp_c} \tag{1.26}$$

where the summation over c means taking into account all possible choices of particles c.

The introduction of symmetries can produce further constraints on inclusive reactions. Some of these are quite obvious like

$$f(a\ b \to cx) = f(\bar{a}\ \bar{b} \to \bar{c}\ \bar{x})$$

where $\bar{a}$, $\bar{b}$, $\bar{c}$ and $\bar{x}$ are the conjugates of a, b, c and x respectively.

For higher particle distributions it is useful to introduce a new quantity called the correlation function. This quantity has been defined in several ways. The most popular one is the so called normalized correlation function. For the two particle case, this function is given by[9]

$$C(s\ \bar{p}_c\ ,\ \bar{p}_d) = G(s, \bar{p}_c, \bar{p}_d) - \frac{1}{\sigma_T} f(s, \bar{p}_c)\ f(s, \bar{p}_d) \tag{1.27}$$

with G and f as defined in (1.2) and (1.4) respectively.

For a completely independent emission of particles C should be equal to zero. In such a case the two particles are said to be uncorrelated. This situation never occurs because we always have some

correlation due to well known kinematical reasons like energy and momentum conservation even in the absence of all other dynamical factors.

The correlation function can be related to the average multiplicities of particles c and d by integrating both sides of relation (1.27) over all momenta, from which we get:-

$$c(s) = \langle n_c \times n_d \rangle - \langle n_c \rangle \langle n_d \rangle \qquad (1.28)$$

If particles c and d are identical particles with multiplicity n then

$$c(s) = \langle n\,(n-1) \rangle - \langle n^2 \rangle$$

where c(s) is called the overall correlation.

Phenomenological Models

The phenomenological models proposed by different authors to predict or parametrise inclusive spectra can be classified into two main categories which use different approaches to evaluate the inclusive spectrum. In the first category a general $2 \to n$ reaction is parametrized using standard s-matrix techniques for such a process, squaring and integrating over all allowed phase space for each n then summing over all n to find the inclusive cross section. The second approach tries to predict the inclusive spectrum without going into detailed assumptions about any particular $2 \to n$ process.

Well known examples in the first category are the multiperipheral models[10]. In the second category we can include Feynman scaling, limiting fragmentation, models based on Mueller's generalized optical theorem like the dual resonance models[11] and Mueller regge analysis and statistical type models like the thermodynamics model[12]. I shall give a very brief summary of the basic physical ideas behind these models

leaving detailed discussion until the predictions are compared with our data; further reference to these models is contained in a review article by Frazer et al[13].

Multiperipheral Models

These models were first developed for exclusive analysis by Amati, Fubini and Stanghellini[14]. The basic idea in such models is that many body reactions are very peripheral. In this case the interaction is expected to proceed via virtual particle exchanges. Using off-mass-shell particle particle scattering amplitudes one can construct amplitudes for many $2 \rightarrow n$ particle high energy processes provided that the off-mass shell behaviour of the low energy particle amplitudes are known.

Inclusive spectra can be obtained in principle by averaging over all the exclusive ones. The results depend solely on the assumptions made concerning the off-mass shell behaviour of the scattering amplitudes and which exchanges are important. Not many detailed calculations exist in the literature for inclusive spectra derived using these models.

Semiclassical Radiation Models

In these models the production of particles in the final states is considered as a process of radiation emitted by current sources. This idea was used by Feynman to predict scaling. The amplitudes for these radiation processes are derived from the Fourier transform of the current source. Again there are no detailed predictions, with which experimental data can be compared, apart from the scaling hypothesis.

Dual Resonance Models

The generalized optical theorem provided a good starting point to use Veneziano type models which are based on narrow resonance dominance in all channels. These are called dual resonance models. Scaling laws and early limiting fragmentation criteria were demonstrated. The defects

with these models are that internal quantum numbers cannot be introduced in a realistic way to correspond to realistic experimental resonances and that unitarity cannot be satisfied implicitly.

Regge Pole Models

The idea of using a regge expansion for the $n \to n$ amplitude to describe and parametrize inclusive spectra has been used extensively and fairly successfully in different kinematical regions such as the two fragmentation regions and the central regions[15]. I shall come back to these models in a later chapter where a comparison with our data has been carried out.

Hagedorn Thermodynamical Model

Hagedorn's model is a statistical model based on thermodynamic arguments coupled with the use of arbitrary distribution functions of longitudinal momentum. It predicts approximate forms of transverse momentum distributions and the dependence of these distributions on outgoing particle masses. It is the only model that predicts the latter explicitly. These predictions are obtained using Bose-Einstein or Fermi Dirac single particle distribution functions of a system in local thermodynamic equilibrium. Ranft and Ranft[16] extended this model to predict the nature of the correlation function in two particle inclusives.

REFERENCES (1)

1. R.P. Feynman, Phys. Rev. Letters 23, 1415 (1969).
2. K.G. Wilson, Acta Physica Austriaca 17, 37 (1963).
3. Chan Hong-Mo, Rutherford Laboratory Preprint RPP/T/17.
4. A.H. Mueller, Phys. Rev. D2, 2963 (1970).
5. Hong-Mo Chan, Rutherford Laboratory Preprint RPP/T/21.
6. M. Virasoro, Phys. Rev. D1, 2834 (1971).
7. J. Benecke, T.T. Chou, C.N. Yang and E. Yen, Phys. Rev. 188, 2159 (1969).
8. T.T. Chou and C.N. Yang, Phys. Rev. Letters 25, 1072 (1970).
9. E.L. Berger, ANL Preprint HEP/7134 (1971).
10. C.E. de Tar, Phys. Rev. D3, 128 (1971).
11. D. Gordon and G. Veneziano, Phys. Rev. D1, 2116 (1971).
12. R. Hagedorn, Nucl. Phys. B24, 93 (1970).
13. W.R. Frazer et al., La Jolla Preprint (June, 1971).
14. D. Amati, S. Fubini and S. Stanghellini, Nuovo Cimento 26, 896 (1962).
15. Chan Hong-Mo, C.S. Hsue, C. Quigg and Jiunn-Ming Wang, Phys. Rev. Letters 26, 672 (1971).
16. G. Ranft and J. Ranft, Phys. Lett. 32B, 209 (1970).

FIGURE CAPTIONS (1)

(1-1) Sections of phase space for a single pion from $Kp \to \pi +$ anything at 16 GeV/c. Variables are transverse momentum of the pion against its:-

(a) Centre of mass rapidity,

(b) Centre of mass longitudinal momentum,

(c) Lab. longitudinal momentum.

Solid lines represent the boundaries of phase space. Dashed lines of constant y denoted A, B, C, D and E in (a) are mapped into those with the same labels in parts (b) and (c).

(1-2) Shown schematically are the optical theorem for total cross-section and Mueller's generalized unitarity relationship which connects the invariant inclusive cross-section to a discontinuity of the 3 to 3 forward elastic amplitude.

(1-3) Schematic representation of:-

(a) Feynman's scaling picture in the centre of mass system,

(b) Limiting fragmentation picture in the target rest frame.

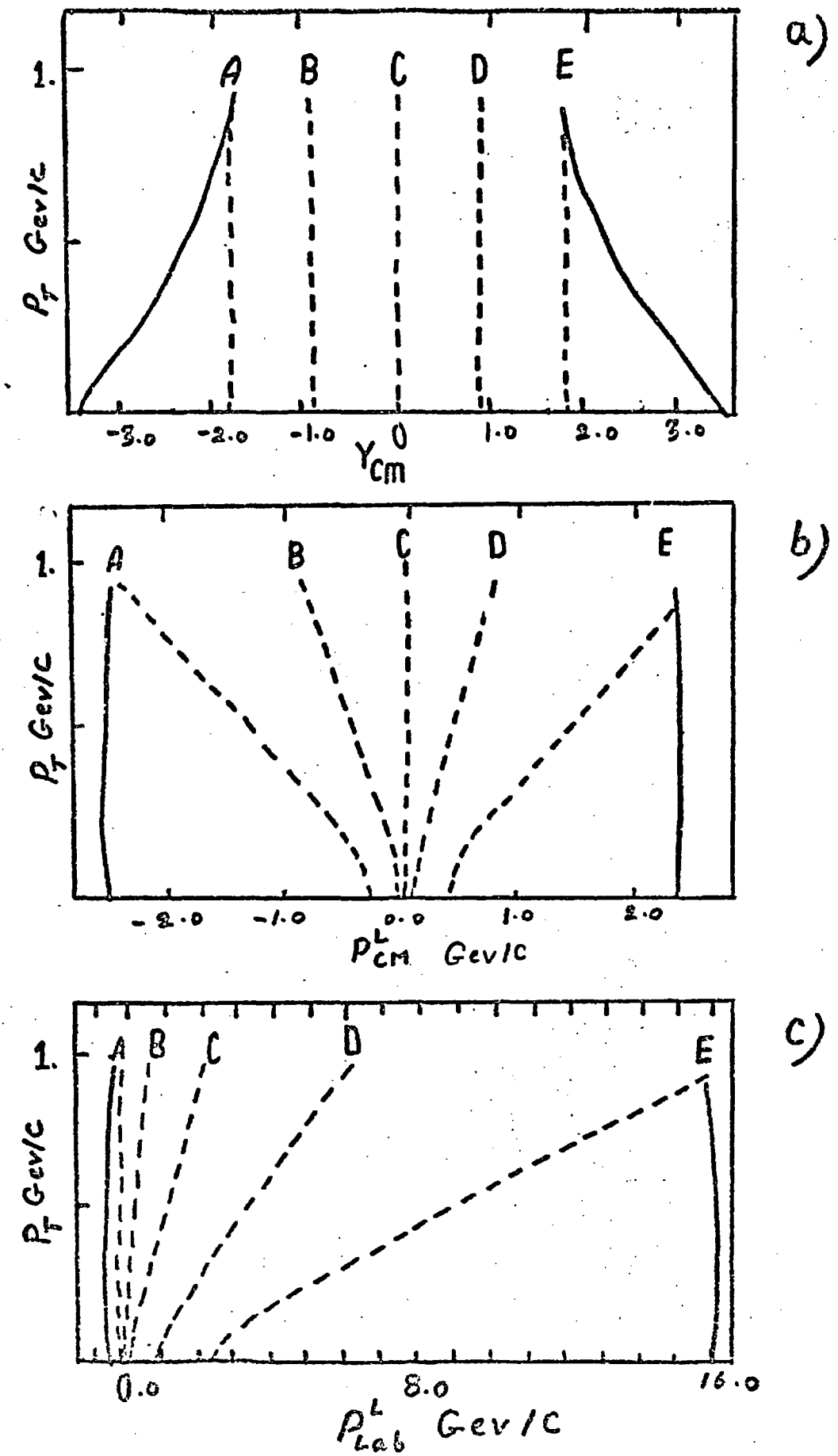
a)
1.
A
B
C
D
E
P_T Gev/c
-3.0
-2.0
-1.0
0
1.0
2.0
3.0
Y_{CM}
b)
1.
A
B
C
D
E
P_T Gev/c
-2.0
-1.0
0.0
1.0
2.0
P^L_{CM} Gev/c
c)
1.
A
B
C
D
E
P_T Gev/c
0.0
8.0
16.0
P^L_{Lab} Gev/c

Fig (1-1)

a

$$\sigma_{tot} = \sigma(ab \to X)$$

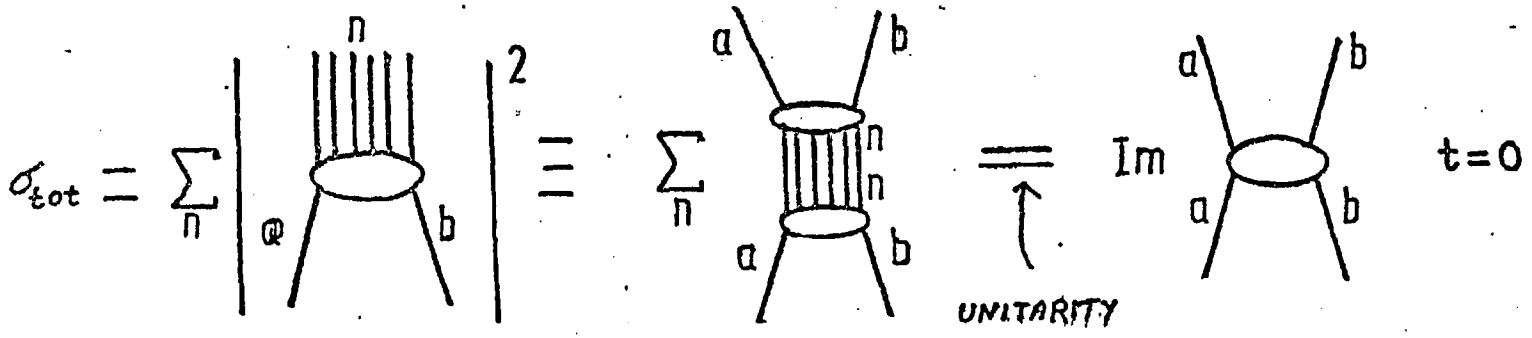

FIG 1.2

b

$$f = \sigma_{INCLUSIVE} = E\, d^3\sigma(ab \to cX)/d^3\bar{p}_c$$

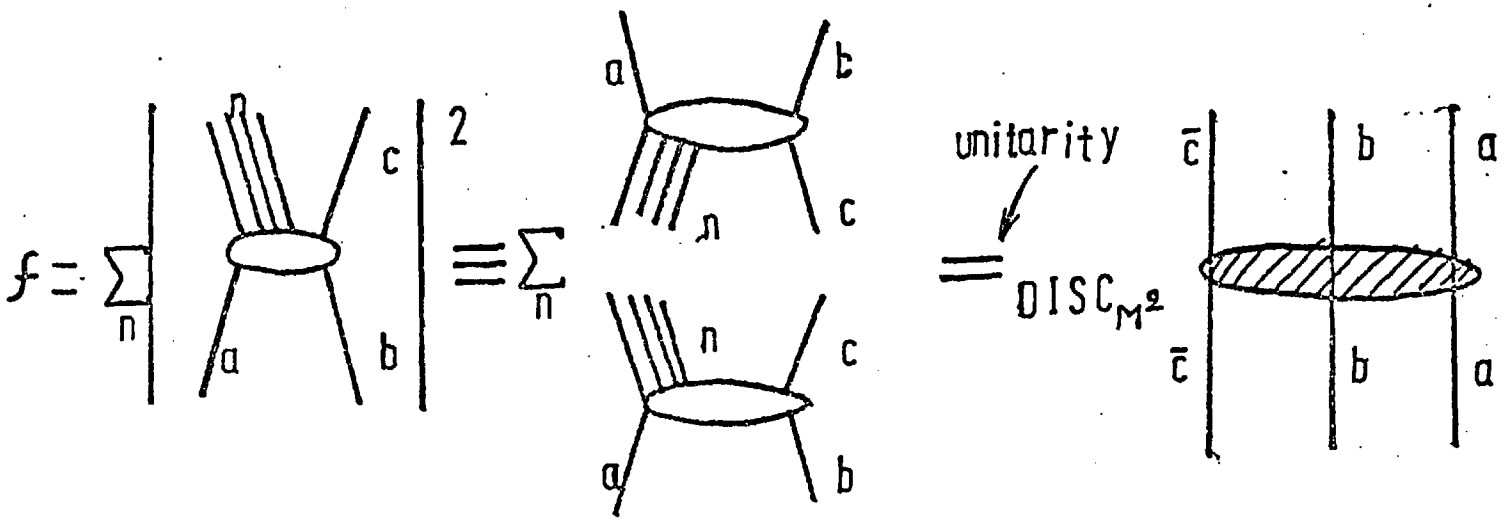

a)

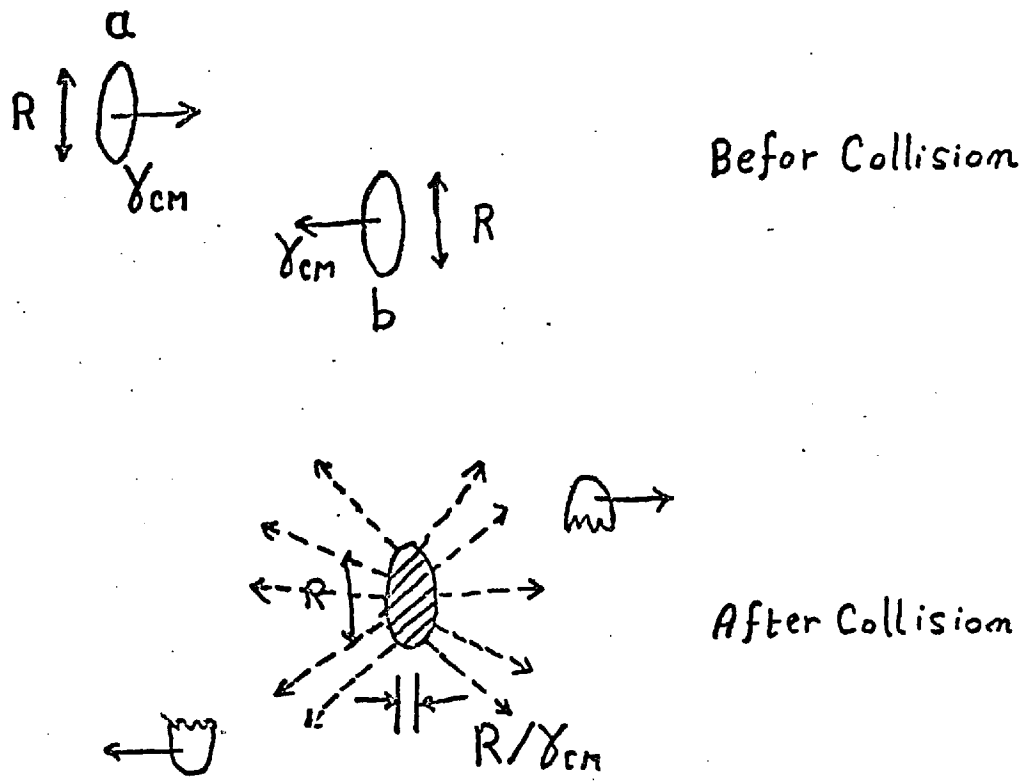
a
R
γ_{cm}
γ_{cm}
R
b
Befor Collision
R
R/γ_{cm}
After Collision

b)

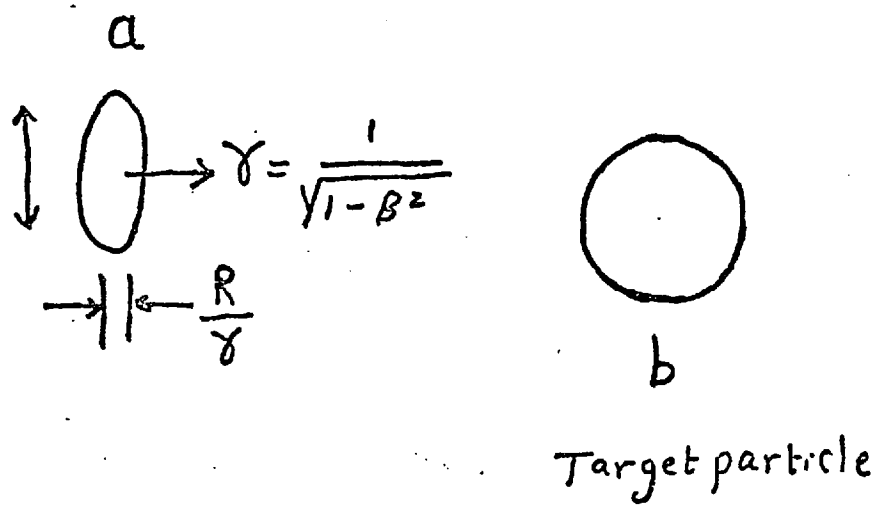
a
$\gamma = \frac{1}{\sqrt{1-\beta^2}}$
$\frac{R}{\gamma}$
b
Target particle

FIG(1.3)

CHAPTER TWO

10 AND 16 GEV/C K^-P DATA FROM INCLUSIVE POINT OF VIEW

History of the 10 and 16 GeV/c Experiments

The 10 GeV/c K^-p experiment on which this thesis is partially based was originally proposed at the beginning of 1965. The first period of beam tuning and bubble chamber exposure began in April of the same year. This was followed by three additional runs with the same beam momentum. In total some 700,000 photographs of the bubble chamber were taken.

The beam-line used to produce the K^- beam for this experiment was equipped with two radio frequency cavities. This type of separator was used because at such high energies electrostatic separation is unsuitable for a good separated K^- beam. R.F. separation is essentially a time of flight method for distinguishing between different particles moving with different velocities. Each R.F. separator consists of two radio frequency oscillating cavities. By adjusting the frequency and the distance between the two cavities one can get very efficient separation of the beam particles required for the experiment.

The first 10 GeV/c run was taken in the British 1.5 meter chamber. The rest of the pictures were taken in the CERN 2 meter bubble chamber. Five European research groups have collaborated in all stages of the experiment. These groups are listed below.

Aachen (Physikalisches Institut der Technischen Hochschule)

Berlin (Institut für Hochenergiphysik der Akademie der Wissenschaften der DDR)

CERN (European Organization for Nuclear Research)

London (Physics Department, Imperial College)

Vienna (Institut für Hochenergiephysik der Österreichischen Akademie der Wissenschaften)

The final data summary tape, (D.S.T.), of all events which were scanned, measured and fitted was completed recently. This tape contains about 250,000 ~~events~~ hypotheses.

The original purpose of this experiment was to study the mechanisms by which particles and resonances could be produced in exclusive channels. At the time when this experiment was started the techniques of inclusive analysis of high energy collisions were not developed.

Because of the increasing interest in diffractive processes during the period when the data from the 10 GeV/c experiment were being analysed, it became desirable to study such processes at higher energies. The need for such high energy K^-p data was partially fulfilled with a new K^-p experiment at 16 GeV/c beam momentum. The first run for bubble chamber photographs taken at this energy was in April 1971. The author was involved in the beam tuning and picture quality control of this run and was also partially involved in the day to day work of check scanning and grind checking of the films. This run was followed by two more and in all about 700,000 photographs at this energy have been taken so far. A proposal for another 1,000,000 photographs is being considered by the collaboration. The first data summary tape at this energy containing about 75,000 events was ready by May 1972 and very recently about double this number became available. The data from this experiment represent events from the highest K^- beam momentum available before the MIRABELLE 32 GeV/c K^-p photographs from which no fitted events are yet available.

10 and 16 GeV/c Inclusive Interactions

During the year 1971 and the years that followed after the Helsinki Conference[1] inclusive analysis of high energy collisions became fashionable. The first application of this idea by the collaboration was in a paper on production of $\bar{K}^0$ particles at 10 GeV/c[2], before the 16 GeV/c data became available. The new developments in this field and

the prediction of the scaling behaviour of inclusive cross sections gives the opportunity to test many predictions about scaling between these two energies. An encouraging feature of the data is that both experiments used the same beam line and were analysed by the same groups. This is a great advantage which helps in performing a consistent analysis with reduced biasses.

Most scaling criteria are made in the framework of constructing exotic combinations of particles, a, b and $\bar{c}$ in single particle inclusive reactions. Such combinations are severely lacking in single particle K^-p interactions. For such reasons more attention was paid to two body inclusive reactions and resonance inclusive production. Not many theoretical predictions exist in these cases and this led us to reduce our task from one which was more concerned with comparisons of theoretical predictions with our data to another which is more concerned with the production of data in the hope that theoretical interpretations will come at a later stage.

Data Processing

As was stated in the first article of this Chapter this set of experiments was originally intended to study production mechanisms in exclusive channels. Our inclusive analysis was developed some time after the experiment was first started. Because of this situation one naturally had to expect some problems in trying to look at the data inclusively. The first problem which one had to face was the inappropriate form in which the 10 GeV/c data existed at the beginning of this work. Data for different exclusive channels were scattered on many data summary tapes. The first stage in making the D.S.T.s usable for our study was to collect everything on the minimum number of tapes. This was done for the 10 GeV/c data independently and in a later stage the CERN group produced the data on mini-DST which were designed for inclusive study. For a part

of the work this CERN D.S.T. was used. When the 16 GeV/c data was produced it was produced directly in the inclusive format.

The 10 GeV/c data used comes from about 140,000 events on tapes. These include both fitted and unfitted channels. Those at 16 GeV/c consisted of about 75,000 events including "fits" and "no-fits".

In order to minimise the number of D.S.T.s, the events are stored in "packed" form on the tape. The unpacking of the information required for each SUMX run, requires a substantial amount of CDC 6600 computer time. Furthermore, because in every run one has to test every event for the particle or particles whose inclusive distribution is being studied, more c.p. time is required than for typical jobs for studying exclusive reactions when one deals with a small fraction of the data. Consequently, all jobs for inclusive analysis are of a high category which is usually given low priority when being processed. The turnround for such jobs on the University of London CDC 6600 computer varies from two days as a minimum up to two weeks in some cases, depending on the existing backlog.

The Selection of Physics Topics

The selection of physics topics was decided with two major factors in mind. The first one was the theoretical significance of what one does and the second was the experimental feasibility of doing it. The latter factor is determined mainly by the quality of the data for the particular type of analysis. For example one would be very interested in studying the scaling behaviour of inclusively produced K^-'s. Unfortunately, the K^-/π^- ambiguity which will be discussed later does not allow one to draw strong conclusions about this reaction even though this reaction may have some theoretical significance because of the $b\bar{c}$ exoticity. This is only one example of topics which one could not study. In the following sections we shall investigate the different experimental biases associated with

the topics discussed in the following chapters.

The Data

Tables (2-1) and (2-2) show the general structure of the data used in terms of the number of prongs and "seen" decay modes of neutral particles. The total number of events in those tables corresponds to about 75% of the number of hypotheses on our DST's. This is because, as one would naturally expect, not all events are uniquely identified. Some of the events are ambiguous between two or three hypotheses and in such cases each hypothesis has been given an ambiguity weight equal to 1/Number of hypotheses accepted. For example each hypothesis for an event which can be interpreted in terms of two acceptable hypotheses is given a weight of 0.5. Events which correspond to more than three hypotheses were accepted as ambiguous events with all particles which could not be identified by ionization assumed to be pions and the event given a special ambiguity flag. Ambiguities tend to occur more often with higher multiplicity events than with low multiplicity ones.

On the same tables we give the topological cross sections. These cross sections and the microbarn equivalents per event for the different topologies were calculated from the scanning and pass rate informations for each topology.

Errorsand Biases

As stated before, a substantial number of events do not have a unique assignment. This is mainly due to failure to identify the charged particle tracks or to a large number of missing neutrals. Due to these reasons one would naturally expect some of our distributions to be biased to a certain extent. The main important sources of biases are those due to failure to assign negative tracks between K^-'s and π^-'s

and positive tracks between protons and π^+. The task of estimating the actual amount of bias in each inclusive distribution in order to correct for it is not trivial. However, an attempt was made to estimate the possible size of the errors on our positive and negative pion distributions using a technique which we shall discuss below.

It is well known in the field of bias and error estimate that one can use an unbiased sample of events to estimate the biases in a biased sample if the two samples come from the same population. This technique is most useful in cases where one cannot obtain an unbiased sample which is large enough to fulfil requirements and, therefore, must use a larger but biased sample of data.

The situation that occurs in our case is not exactly of this type but to a first approximation the same idea can be used to estimate the errors due to the biases in our data. To do this we selected on that particular part of the data where our events are uniquely identified. From comparison of the distributions of "inclusively" produced particles in such events with distributions from all the data one in principle at least can obtain some idea about the size of the errors due to biases. However, the situation is not that straightforward. This is because one's estimator is not really an unbiased sample of data. Ambiguities tend to occur more often at high multiplicities, thus reducing the chances of having uniquely identified events at high multiplicities.

To overcome this problem we weighted each of the uniquely identified events by a factor such that the proportion of each topology in the overall data is maintained in our uniquely identified sample of events. Our main interest was to calculate errors on the x distributions of charged particles in different kinematical regions. For this reason we plotted the x distributions for these particles coming from the weighted estimator sample of events. After normalizing the total distributions of these particles and the overall inclusive distribution of all events

we compared the two sets of distributions. To reduce the effect of statistical fluctuations we preferred not to calculate the percentage error for each bin in x but to average such errors over a whole kinematical region.

The results of such calculations are shown in table (2-3).

These errors must be added to the statistical errors of each distribution to get the total errors.

From table (2-3) one deduces that the errors due to this type of bias are not very large for the cases of π^-'s and π^+'s and they are not expected to have a great effect on our conclusions when we compare our data from the two energies. However, those errors tend to be large enough to wash out any differences that may be observed in K^- or proton distributions. For this reason no attempt was made to carry out any comparison of these two distributions at the two energies.

The same technique could be used to predict the errors on our p_T^2 distributions for charged particles. However, this was not considered necessary because these distributions tend to be less sensitive to ambiguities than the x distributions.

In our calculations on reactions involving neutral strange particles we always used events with decays of such particles in the chamber. To correct for particles which decayed outside the visible region of the chamber and for those which decay very near to the vertex, the events were assigned a weight calculated from the formula:-

$$W = 1\Big/\Big[(\exp(-L_{min}/\nu\tau) - \exp(-L_{max}/\nu\tau)\Big] \qquad (2.1)$$

where L_{min} is the minimum detectable length between the decay vertex and the primary vertex, L_{max} is the potential length available for the V^0 particle to decay within the specified fiducial volume along its direction, ν is the velocity of the particle and τ is its mean life time.

To allow for unseen decay modes and long lived strange particles I-spin weighting was used to calculate cross sections whenever they were needed. For this reason the quality of the data on $\bar{K}^0$ inclusive production is extremely reliable because in the majority of events (where we do not have K^+K^- or $\bar{p}p$ pair production) there is no ambiguity in identifying π^-'s.

A possible source of bias in strange particle inclusive reactions is kinematic ambiguity of $\bar{K}^0$ with Λ^0. However, such a bias is expected to be very small because in the majority of cases these ambiguities are resolved by ionization measurement of the decay tracks to identify the proton from Λ^0 decay. A more important source of bias is that due to misidentification of Λ^0 with Σ^0 where the Σ^0 decays into $\Lambda^0\gamma$ and the decay secondary vertex is fitted to a Λ^0 and the Λ^0 is used to fit the primary vertex. No attempt was made to devise a method to correct for such error.

The proton-π^+ ambiguity is not expected to cause large biases on our Δ^{++} triple regge analysis, because our main study is carried out in the small t range, where the protons are slow, and such contamination is reduced. This is supported by the fact that after we selected on these events with $M(p\pi^+)$ in the Δ^{++} region we found that only about 2% of the events were counted more than once to have a Δ^{++} combination in the region. In such a case we accepted only the one with $M(p\pi^+)$ nearer to the Δ^{++} central mass value.

REFERENCES (2)

1. Proceedings of International Colloquium on Multiparticle Dynamics, Helsinki, May 1971.

2. J.V. Beaupre et al., Aachen-Berlin-CERN-London-Vienna and Bruxelles-CERN Collaborations, Nucl. Phys. B30, 381 (1971).

TABLE CAPTIONS (2)

(2-1) Topological cross sections and microbarn equivalents per event for each topology produced from K^-p at 10.1 GeV/c.

(2-2) Topological cross sections and microbarn equivalents per event for each topology produced from K^-p at 16 GeV/c.

(2-3) Estimated percentage errors on single particle inclusive x distributions for particles produced from K^-p at

(a) 16 GeV/c,

(b) 10.1 GeV/c,

in different kinematical regions.

Table (2-1)

TOPOLOGICAL CROSS SECTIONS FOR K^-P AT 10.1 GEV/C			
TOPOLOGY	σ(mb)	EVENTS ON DST	μb/EVENT
2 Prong	8.206 ∓ 0.110	57000.0	0.144
2 Prong V^0	1.768 ∓ 0.021	13591.5	0.130
4 Prong	6.140 ∓ 0.086	43504.7	0.142
4 Prong V^0	1.477 ∓ 0.018	10617.7	0.139
6 Prong	1.962 ∓ 0.038	10533.0	0.186
6 Prong V^0	0.322 ∓ 0.015	1557.5	0.207
8 Prong	0.203 ∓ 0.021	663.0	0.306
8 Prong V^0	0.021 ∓ 0.011	51.0	0.412
10 Prong	0.009 ∓ 0.003	7.0	1.286
10 Prong V^0	0.002 ∓ 0.001	3.0	1.500

Table (2-2)

TOPOLOGICAL CROSS SECTIONS FOR K^-P AT 16 GEV/C			
TOPOLOGY	σ(mb)	EVENTS ON DST	μb/EVENT
2 Prong	6.220 ∓ 0.155	23840.0	0.226
2 Prong V^0	1.406 ∓ 0.041	4220.0	0.333
4 Prong	6.170 ∓ 0.175	25115.0	0.246
4 Prong V^0	1.650 ∓ 0.049	4570.5	0.361
6 Prong	3.034 ∓ 0.088	10722.0	0.283
6 Prong V^0	0.716 ∓ 0.023	1758.0	0.407
8 Prong	0.788 ∓ 0.025	2111.5	0.373
8 Prong V^0	0.138 ∓ 0.006	253.0	0.545
10 Prong	0.038 ∓ 0.005	21.0	4.666
10 Prong V^0	0.016 ∓ 0.002		

Table (2-3-a)

K^-P AT 16 GEV/C		
PARTICLE	REGION	% ERROR
proton	TR	1
=	CR	8
=	PR	16
Λ^0	TR	2
=	CR	2
=	PR	4
$\bar{K}^0$	TR	3
=	CR	6
=	PR	6
K^-	TR	2
=	CR	20
=	PR	18
π^+	TR	1
=	CR	3
=	PR	2
π^-	TR	2
=	CR	3
=	PR	5

TR x less than -0.1

CR x between -0.1 and 0.1

PR x bigger than 0.1

Table (2-3-b)

K^-P AT 10.1 GEV/C		
PARTICLE	REGION	% ERROR
proton	TR	2
=	CR	7
=	PR	15
Λ^0	TR	1
=	CR	1
=	PR	3
$\bar{K}^0$	TR	4
=	CR	6
=	PR	6
K^-	TR	3
=	CR	18
=	PR	18
π^+	TR	1
=	CR	2
=	PR	2
π^-	TR	2
=	CR	3
=	PR	6

TR x less than -0.1

CR x between -0.1 and 0.1

PR x bigger than 0.1

CHAPTER THREE

ENERGY DEPENDENCE OF SINGLE AND TWO PARTICLE DISTRIBUTION FUNCTIONS

Introduction

The hypotheses of limiting fragmentation and Feynman scaling discussed in Chapter One are predicted to be satisfied in the asymptotic limit in which s is very large. They do not tell us anything about the behaviour of distribution functions at lower energy where data is available. Furthermore, they do not predict the threshold at which energy independence is expected to be valid. However, we can compare our data with some subsequent predictions about the dependence of particle distributions on energy and extract from this comparison a good estimate of the rate at which scaling and limiting fragmentation are approached.

The first prediction about the rate at which scaling is approached came from Chan, Hsue, Quigg and Wang (CHQW)[1] in 1971. They used the Mueller generalised optical theorem to relate the single particle distribution function to the forward elastic amplitude to predict the energy dependence in the fragmentation region and the central region. This was done by assuming that the 3-3 amplitude has a Regge behaviour and the single particle distribution function in the fragmentation region of one of the particles, the target b say, is

$$f(s,t,M_X^2) \rightarrow \sum_i \beta_i(s,t,M_X^2)\, s^{\alpha_i(0)-1} \qquad (3.1)$$

where the summation corresponds to the expansion over all possible Regge trajectories as in the figure below.

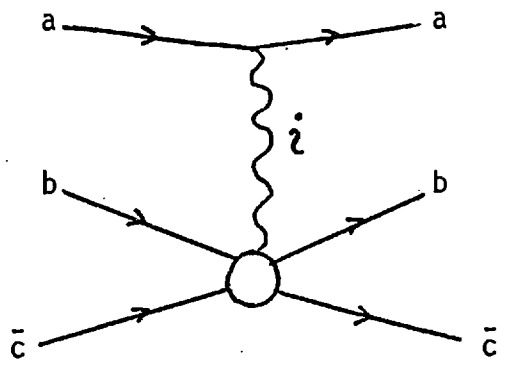

The behaviour of f as $s \to \infty$ depends on what Regge singularities are assumed to dominate. If we assume the leading trajectories to be the pomeron with $\bar{\alpha}(0) = 1$, and the nearly degenerate meson trajectories ρ-f-ω-A_2 with $\alpha_M(0) = 0.5$, one has

$$f(s,t,M_X^2) \to \beta_P(s,t,M_X^2) + \beta_M(s,t,M_X^2)\, s^{-\frac{1}{2}} \quad . \qquad (3.2)$$

The ratio of β_M/β_P governs the rate of approach to scaling and the value of it depends on the quantum numbers of particles a, b and c. CHQW used the duality argument similar to that applied to the total cross-section of two body reactions, where one expects energy independent cross-sections if the two particles are exotic in the s-channel, and they predict that pomeron exchange should be dominating in the figure above if the quantum numbers of the a b $\bar{c}$ combination are exotic. Thus energy independence is expected in both fragmentation regions for reactions like $K^+p \to \pi^- + X$, while reactions of the type $K^-p \to \pi^- + X$ should be energy dependent in general. However, they claim that while the a b $\bar{c}$ exoticity condition is sufficient, it may not be necessary.

Ellis, Finkelstein, Frampton and Jacob (EFFJ)[2] disagree with the CHQW prediction. They claim that a b $\bar{c}$ being exotic is not a sufficient condition for early scaling, for this will merely suppress energy dependent contributions from terms in the direct a b $\bar{c}$ channel only. They

suggest that non-exotic ab can give an energy dependent term to the 3-3 amplitude. They further argue that a $\bar{c}$, b $\bar{c}$ need not be exotic for early scaling to be satisfied; this is because they are below threshold. They predict that the sufficient condition for early scaling is a b $\bar{c}$ and a b both exotic.

Logan[3] requires a b c, a b and b $\bar{c}$ all to be exotic for energy independence of the cross-section in the fragmentation region of a.

Kugler, Lipkin and Rittenberg (KLR)[4] and Freeman say that if CHQW condition is sufficient for early scaling to be valid then meson contributions in (3.2) also cancel if a c is exotic and then they also prove that in this case it is not necessary for a b $\bar{c}$ to be exotic.

All the above predictions are formulated in the fragmentation region of a or b. In the central region, which we can represent by the diagram below, the asymptotic Regge expansion takes the form

$$f(U,t,K) = \sum_i \sum_j B_{ij}(K)\ (U)^{\alpha_i(o) - 1}\ (t)^{\alpha_j(o) - 1}$$

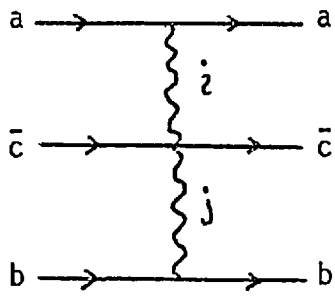

where K is called the transverse energy given by

$$K = P_c^2 + M_c^2$$

and U and t are the squared four vector momentum transfers from the incident particles to c.

If we again assume that our leading trajectories are the pomeron

and the degenerate meson trajectories we get

$$f(s,t,u) \to B_{PP}(K) + B_{PQ}(K)\, t^{\alpha_Q(o)-1} + B_{QP}(K)\, u^{\alpha_Q(o)-1}$$

where Q stands for a meson trajectory.

The term B_{PP} is the pomeron-pomeron - $\bar{c}$ Regge residue, which is energy independent and so represents the scaling part of f. The other two terms are energy dependent through the $\alpha_Q(o)$ dependence. Their dependence is upon $\alpha_Q(o)$. Considering $\alpha_Q(o)$ to be a typical meson trajectory intercept $\approx$ 0.5 one can see that the approach to scaling is given by $s^{-\frac{1}{2}(\alpha_Q(o)-1)} = s^{-\frac{1}{4}}$ which is very slow. This leads us to expect that scaling is violated more in the central region than in the fragmentation regions.

In the following sections of this chapter we will give a comparison of our data with the above theoretical predictions. Furthermore, we will give the two particle distributions for some exotic and non-exotic combinations in order to try to determine which of the above predictions is supported by experiment. In some cases we will use published data from other reactions as well.

π^+ Single Particle Distribution

The Lorentz invariant x distribution for positive pions in our experiments at 10 and 16 GeV/c are shown in fig. (3-1). In this reaction neither a b nor a b $\bar{c}$ is exotic. The only exotic combination we have is a $\bar{c}$ which is $K^-\pi^-$. In this case, if we accept the CHQW condition as being sufficient but not necessary, early scaling is not required in either fragmentation region. On the other hand the EFFJ condition requires a b to be exotic as well as a b $\bar{c}$ as the necessary condition. In such a case we should not expect early scaling. Furthermore, according to KLR if a b $\bar{c}$ exoticity is sufficient then this reaction must scale in the projectile fragmentation region because a $\bar{c}$ is exotic.

A close study of fig. (3-1) shows that there is indication of early scaling in the projectile fragmentation region. This is in good agreement with the KLR prediction of a $\bar{c}$ exotic being sufficient for early scaling in a fragmentation region. This may be taken as an indirect evidence in support of CHQW a b $\bar{c}$ exotic being sufficient condition for scaling.

In the central and target fragmentation region the cross-section seems to be increasing with energy.

π^- Single Particle Distribution

The distribution in the Feynman variable x for this channel at 10 and 16 GeV/c beam momenta is shown in fig. (3-2). In this channel none of the combinations a b $\bar{c}$, a b, b $\bar{c}$ or a $\bar{c}$ are exotic. Scaling is not to be expected in any region if we adopt any of the suggested scaling criteria except that of CHQW which does not require any necessary condition for scaling. In fig. (3-2) we notice that the cross-section is falling with energy in both the projectile fragmentation region and in the central region. In the target fragmentation region of < -0.2 we see that the distributions at the two energies are approaching each other within the experimental errors.

A possible explanation for such an effect is that suggested by Brower. He points out that the ratio of the differential cross-sections in x for the reactions $K^-p \to \pi^- + X$ and $K^+p \to \pi^- + X$ can be related to universal constants representing the ratios of the different Regge residues associated with the exchanges of the degenerate Regge trajectories. He comes to this conclusion by assuming that $F^f = F^\omega$ and $F^{A2} = F^\rho$ where F^α is the Regge residue for the α trajectory. Furthermore, he depends on the exchange degeneracy for ρ and f^o and CHQW exoticity condition for $\pi^+p \to \pi + X$ to relate F^ρ and F^f through the relation $F^\rho/F^f = \epsilon$. Then from

$$E\frac{d\sigma}{d^3\bar{p}}(K^{\mp}p \to \pi^{-} + x) = F^{P} + \frac{1}{\sqrt{s}}(F^{f} \pm F^{\omega} + F^{A2} \pm F^{\rho})$$

one gets

$$E\frac{d\sigma}{d^3\bar{p}}(K^{-}p \to \pi^{-} + x) \;/\; E\frac{d\sigma}{d^3\bar{p}}(K^{+}p \to \pi^{-} + x) = 1 + \frac{2(1+\delta)}{\varepsilon\sqrt{s}}$$

where $\delta = F/F^{f}$.

Using Feynman's form of the Regge expansion in the triple Regge limit one gets for the ratios of the two differential cross sections at fixed x the value of $(1 + c/\sqrt{1-x})$ with $c = 2(1+\delta)/\varepsilon\sqrt{s}$.

The above ratio for the two energies were compared with the data using the data on $K^{+}p \to \pi^{-} + x$ published by Ko and Lander[6] at 12 GeV/c. The centre of mass energy of the $K^{+}p$ data is not important in the calculation because experimental as well as theoretical evidences suggest that this reaction scales even for energies below 12 GeV.

The comparison was carried out in the proton fragmentation region using the unweighted x distribution. This was done simply because the K^{+} data was published in this form. The logarithms of the above-mentioned ratios were fitted with curves deduced from the expression $\log(1 + c\sqrt{1-x})$ where c was left as the free parameter. The fitting was not extended to include values of x near the boundary when $x \simeq 1$ or in the central region where $x \simeq 0$. The values of the constant $2(1+\delta)/\varepsilon$ were calculated for both energies and following values were obtained.

$$2(1+\delta)/\varepsilon = 0.37 \pm 0.05 \text{ at } 10.1 \text{ GeV/c}$$
$$2(1+\delta)/\varepsilon = 0.40 \pm 0.05 \text{ at } 16 \text{ GeV/c} \quad .$$

These values are not in disagreement with each other. Using these results and some published data on $\pi^{\mp}p \to \pi^{-} + x$[15] and assuming that

factorization is valid, it was found that this gives a value of ≈ 0.5 for the ratio between the coupling of the above degenerate trajectories to the kaon to that of the same trajectories to the pion. This suggests that the Brower formalism which is a direct result of exchange degeneracy and a b $\bar{c}$ exoticity condition of CHQW is not inconsistent with our data. This may be taken as an indirect evidence in favour of the CHQW prediction that a b $\bar{c}$ exotic can be taken as a sufficient condition for scaling.

$\bar{K}^0$ Single Particle Distribution

$\bar{K}^0$ inclusive production at 10.1 GeV/c was studied in reference (7). Fig. (3-3) shows the x distributions for both 10.1 and 16 GeV/c. No significant change in the shape of the distribution is evident between these two momenta. It should be noted that the total $\bar{K}^0$ production cross-section forms about 40% of the total K^-p inelastic cross-section. This fraction seems to have only weak dependence on energy. This characteristic does not seem to be restricted to charge exchange production of $\bar{K}^0$. It is reported elsewhere[9] that this 40% ratio applies to most leading particles produced via charge exchange.

It is worth mentioning here that Bialas, Muryn and Zalewski[8] have pointed out that such results are difficult to describe by the nova model, unless double nova production is assumed to form a substantial part of the production process. This is because in a single nova production model the number of $\bar{K}^0$ produced is expected to be very small if the nova is produced at the proton vertex because this will lead to diffractive production off K^-'s.

Returning to fig. (3-3) we find that the majority of the events populate the positive x region. However, we do not see strong leading particle effects, for the distribution is not flat for positive x but peaks at about 0.2. This is probably due to the fact that most K^0's come from decays of K^* resonances.

Λ^0 Single Particle Distribution

The reaction $K^-p \rightarrow \Lambda^0$ + anything cannot be considered as an inclusive reaction in the sense suggested by Feynman. This is because at our two energies the events contributing to this reaction involve the production of pions only. At such energies the cross-sections for other channels which involve the production of $p\bar{p}$, $\Lambda^0\bar{\Lambda}^0$, K^+K^- or $K^0\bar{K}^0$ are very small, forming only about 4% of the total Λ^0 production cross-section at 10 GeV/c and about 8% at 16 GeV/c. For such reasons this reaction is called "partially inclusive"[9]. The scaling properties of this reaction between 4.2 and 10.1 GeV/c beam momenta were studied in ref. (10). It was observed that the x distribution does not scale when the Lorentz invariant inclusive cross-section is used. However, when the cross-section is normalized by the total Λ^0 inclusive cross-section the normalized function does scale. Further detailed analysis of exclusive Λ^0 channels was done at 10 GeV/c by Kumar[11]. We present here a comparison of the above results with our 16 GeV/c data.

Fig. (3-4) shows the invariant differential cross-section for the data at 10 and 16 GeV/c. It can be seen that the two distributions have different shapes. The cross-section is falling with energy over most of the range of x. However, the cross-section seems to be decreasing more rapidly in the forward direction than in the backward direction. This is in contrast with the behaviour observed at lower energies in ref. (10).

This effect is not very surprising. The difference in the rate at which the cross-section is decreasing with energy could be due to the difference in the exchange mechanisms by which forward and backward Λ^0's are produced. For Λ^0 produced in the forward direction one would expect baryon exchange to dominate while in the backward direction strange meson exchange is expected to be dominant.

Further analysis of inclusive Λ^0 production is given in Chapter Eight.

π^-/π^+ Ratio

The ratio between different particle production cross-sections in the fragmentation regions and in the central region is of considerable importance. This is because the limiting behaviour of this ratio for large values of S can be taken as an indication of whether the pomeron is a leading trajectory or not in any particular region.

The importance of the π^-/π^+ cross-section ratio in our case is restricted to the central region, where the Mueller Regge diagram shown in section (1) of this chapter is expected to be valid. If the production of pions in this region takes place via double pomeron exchange then factorization suggests that the pomeron particle coupling is equal to the pomeron antiparticle coupling[12]. Hence one would expect the ratio of the two cross-sections to be unity.

Fig. (3-5-a) and (3-5-b) show this ratio over the whole range of x for 10 and 16 GeV/c data respectively. In both cases one can see that this ratio is generally different from unity, in the central region and both fragmentation regions. This ratio is low for backward moving pions and is high for forward moving pions.

In the central region we have a significant structure with the highest value of about 0.9. The errors on the values of this ratio in this region are very small and the existence of this structure, which cannot be produced by double pomeron exchange, is definite. This can be taken as an explanation for the strong violation of scaling by both π^+ and π^- in the central region.

Two Particle Distributions

The study of single particle distributions, although very useful, cannot yield a definite conclusion about the most efficient scaling criteria for K^-p interactions. This is because it is nearly impossible to obtain an a b $\bar{c}$ exotic combination which is the basic condition for scaling in most of the proposed criteria.

To overcome this problem the idea was extended to include two particle inclusive reactions. This extension was done only for two pion inclusive reactions for two reasons:

1. Interactions involving pions as our detected particles are the nearest approximation to the ideal inclusive reactions in this energy range when one expects many particles to be produced.
2. Choosing pions as our detected particles offers a large variety of exotic and non-exotic combinations which can be composed of K^-p and two pions and in particular the combination $a\ b\ \bar{c}\ \bar{d}$ exotic which we cannot get in single particle inclusive.

One here may speculate that if $a\ b\ \bar{c}$ is a sufficient condition for scaling in the single particle case, then $a\ b\ \bar{c}\ \bar{d}$ exotic may be a sufficient condition for scaling in the two particle case.

The disadvantage of this type of study is that one is restricted to only that part of the data where at least the two particles are produced, which reduces the statistics, but as will be shown, this problem is not very serious because the error bars on the data do not affect our conclusions severely.

The function $G = \frac{E_1 E_2}{s}\ d^2\sigma/dx_1 dx_2$ for the reaction $K^-p \to \pi^+ + \pi^+ +$ anything at 10 and 16 GeV/c is plotted in fig. (3-6) for different regions in $X(\pi_1^+)$. One can see that all these plots clearly show very strong energy dependence of the function except in fig. (3-6-d) in the region which corresponds to both pions moving in the forward direction, i.e. the K^- fragmentation region. The difference in G between the two energies in all other regions cannot be accounted for by the error bars on the data.

Fig. (3-7) shows similar plots for the $\pi^-\pi^-$ distribution function. In this case again strong energy dependence is clear in all regions except where both π^-'s are in the proton fragmentation region where the energy dependence is very weak and the error bars are larger than the difference

in G between the two energies.

In both cases a b $\bar{c}$ $\bar{d}$ is exotic corresponding to $K^-p\pi^-\pi^-$ in the first case and $K^-p\pi^+\pi^+$ in the second. The conclusion from both cases is that a b $\bar{c}$ $\bar{d}$ exotic is not a sufficient condition for scaling in all regions at our energies.

Plots of G for the $\pi^+\pi^-$ case where a b $\bar{c}$ $\bar{d}$ is not exotic are shown in fig. (3-8). The behaviour of G shows that it is energy dependent in general in all regions and no strong evidence for scaling can be observed in any of them.

Using the above experimental results to speculate about possible scaling criteria, we notice that apparent energy independence was observed in some regions when a b $\bar{c}$ $\bar{d}$ was exotic but not when a b $\bar{c}$ $\bar{d}$ is not exotic, so one may conclude that although a b $\bar{c}$ $\bar{d}$ being exotic is a necessary condition for scaling, it is not at all sufficient. A second thing one notices is that the scaling behaviour of G was observed in those regions where the particles c and d can be considered as fragments of a particle with which $\bar{d}$ $\bar{c}$ can form an exotic combination, e.g. $G(\pi^-\pi^-)$ scales in the proton fragmentation region and $G(\pi^+\pi^+)$ scales in the K^- fragmentation region.

Possible Explanation of the Observed Behaviour of Two Particle Distributions

In order to try to understand the nature of the observed scaling behaviour in two particle inclusive reactions considered in the previous section, we try here to use arguments based on two component duality. Such arguments have been used to predict the scaling behaviour in single particle inclusive reactions through applying them to constrain 3-3 amplitudes.

In our two particle case we shall try to use similar arguments to consider 4-4 amplitudes. Before doing so we shall summarise the general way 3-3 amplitudes have been treated as a sum over all possible distinguishable configurations of dual diagrams. These diagrams are

constructed from the original quark diagrams representing the exchange of quarks between particles. The Harari-Freund two component duality for two body amplitudes extends to a seven component picture for 3-3 amplitudes. To see this let us recall how the two components arise in the 2-2 amplitude in fig. (3-9). Fig. (3-9-a) contains a single resonance production in the a b s channel where a and b are attached to the same quark loop. This diagram vanishes if a b has exotic quantum numbers. The configuration shown in fig. (3-9-b) contain two resonances in the intermediate state and the two particles are connected to two separated quark loops. These two cases are considered to represent two components of the amplitude. In the second component the pomeron is expected to be the leading exchange between the two quark loops if the amplitude is to have a regge behaviour. In such a case if a b is exotic then one would expect the total a b scattering cross-section to be energy independent.

Now going to the 3-3 case we can see that there can be three independent configurations for a single resonance intermediate state, three configurations for a double resonance intermediate state and one configuration for a triple resonance intermediate state. These configurations are shown in fig. (3-10-a) and the corresponding quark dual diagrams are shown in fig. (3-10-b).

Using this type of representation of the 3-3 amplitude many authors have predicted various scaling criteria for different kinematical regions of the single particle inclusive spectrum. Some of these criteria have been discussed in previous sections.

Now we shall try to use the same procedure applied to the 4-4 amplitude to explain some of the features observed in the two particle distribution functions observed in the data of the previous section. We shall concentrate our attention on the case where our detected particles are two pions of like charge. This is because restriction to this type of reaction simplifies the procedure for dealing with a

general a b $\bar{c}$ $\bar{d}$ - a b $\bar{c}$ $\bar{d}$ amplitude and trying to establish the conditions under which the amplitude becomes energy independent.

In the case of a general a b $\bar{c}$ $\bar{d}$ → a b $\bar{c}$ $\bar{d}$ amplitude we can construct eight independent configurations representing cases where we can have a single resonance in the intermediate state, twelve independent configurations for a two resonance intermediate state, eight configurations for a three resonance intermediate state and two independent configurations for a four resonance intermediate state. This will give us an amplitude which can be represented in terms of thirty independent dual diagrams. All the thirty configurations for a general a b $\bar{c}$ $\bar{d}$ case are shown in fig. (3-11) where the wavy lines represent resonances in the intermediate states such resonances are assumed to form the discontinuities in the 4-4 amplitude. The dual quark loop diagrams can be obtained directly from squaring such resonance diagrams.

It is apparent that it is very difficult to consider contributions of all these diagrams or their corresponding quark loops diagrams for the general a b $\bar{c}$ $\bar{d}$ case. Hence we shall stick to our two particular reactions where two pions of like charge are produced. This can be done through substitution for a, b $\bar{c}$ and $\bar{d}$ by the corresponding particles in each case. We shall use two duality rules to reduce the number of diagrams which have to be considered. These two rules are:-[13]

1. Diagrams with exotic combinations of quantum numbers of particles attached to the same quark loop are expected to vanish.
2. Reggeons are expected to be exchanged between particles attached to the same quark loop while the pomeron is expected to form the leading trajectory exchanged between different quark loops.

The quark loop diagrams for the reaction $K^-p \rightarrow \pi^+\pi^+ + X^{--}$ are

shown in fig. (3-12). If we apply the first one of the above two rules we can see that we get contributions to the amplitude from the following diagrams only:-

13, 20, 23, 24, 25, 28, 29 and 30

Now diagram 13 has been constructed from diagram 13 in fig. (3-11), where one can see that particle c is far away from particle a, and hence is not expected to have a large contribution in the region of small t_{ac} but would contribute to the region of small t_{bc}. In this case its contribution to the projectile fragmentation region may be neglected. This diagram contains an energy dependent part due to reggeon exchanges. The same argument can be applied to diagrams 20, 24, 25 and 28. All these diagrams can give non-scaling terms but to a first approximation they contribute only to cases where at least one of the pions is produced in the target fragmentation region. Diagrams 23, 29 and 30 give energy independent contributions to all regions including the case where the two particles are produced in the fragmentation region. This may explain the energy independence observed for this reaction in this region.

The situation with the reaction $K^-p \to \pi^-\pi^-$ + anything is somewhat more complicated than in the previous case. In this reaction we expect to have contributions to the amplitude from quark loop diagrams 10, 12, 13, 15, 16, 17, 19 and 22 to 30 of fig. (3-13). Diagrams 10, 15 and 16 are expected to have stronger contributions when one of the pions is produced in the target fragmentation region than when both pions are produced in the same fragmentation region. Furthermore, contributions from these diagrams are expected to suppress contributions from diagrams 22 - 28 when both sets contribute to the same kinematical region. This argument is based on predictions of narrow width duality[14]. Diagrams

12, 13, 17 and 19 are expected to contribute strongly to the proton fragmentation region with the last three contributions to the K^- fragmentation region as well. All these diagrams are expected to give some energy dependence. This may lead us not to expect any energy independence in any region. But if we look at the main contribution to the proton fragmentation region we can see that we always have one of our pions produced via a pomeron exchange mechanism on a single quark loop coupled to another quark loop containing the rest of the particles. The latter quark loop is nothing but a dual diagram for the amplitude $K^-p\pi^+ \to K^-p\pi^+$ which was observed to show little energy dependence in a previous section at this energy range. Therefore, the scaling of the two π^+'s inclusive spectrum in the proton fragmentation region may be closely related to the observed weak energy dependence of single particle π^- inclusive distributions in this energy range.

It must be mentioned at this stage that all our arguments are based on simple planar duality which although successfully explaining many experimental results is still incomplete, at least, because of the fact that baryons are treated in the same way as mesons when constructing our diagrams.

Conclusions

The main aim of this chapter was to study the scaling behaviour in single and two particle inclusive reactions. Experimental distributions were compared with existing theoretical scaling criteria. In the single particle case one was limited to a certain extent by the fact that no a b $\bar{c}$ exotic combination was possible and so no definite direct conclusion can be drawn from these except that a b exotic may not be a necessary condition for early scaling. This is because scaling was observed in some cases only in certain regions. The data are not in disagreement with CHQW prediction although one cannot say whether a b $\bar{c}$ being exotic is a sufficient condition for early scaling or not.

In the two particle case evidence was shown that a b $\bar{c}$ $\bar{d}$ being exotic cannot be a sufficient condition for scaling in all regions. Furthermore, a crude extension of duality arguments was developed and the observed scaling in some regions in the two particle case was explained on that basis. The main result is that for scaling in the two particle case we need a b $\bar{c}$ $\bar{d}$ and b $\bar{c}$ $\bar{d}$ to be exotic in order to have early scaling in the target fragmentation region and a b $\bar{c}$ $\bar{d}$, a $\bar{c}$ $\bar{d}$ to be exotic in order to have scaling in the projectile fragmentation region.

REFERENCES (3)

1. Chan Hong-Mo, C.S. Hsue, C. Quigg and Jiunn-Ming Wang, Phys. Rev. Letters 26, 672 (1971).
2. J. Ellis, J. Finkelstein, P.H. Frampton and M. Jacob, Phys. Letters 35B, 227 (1971).
3. R.K. Logan, University of Toronto, Preprint (1971).
4. M. Kugler, H.J. Lipkin and R. Rittenberg, Weizmann Institute Preprint (1971).
5. R.C. Brower, CERN Preprint, TH.1390 (1971).
6. W. Ko and R. Lander, Phys. Rev. Letters 26, 1064 (1971).
7. Aachen-Berlin-CERN-London-Vienna and Brussels-CERN Collaborations, Nucl. Phys. B30, 381 (1971).
8. Private communication to D.R.O. Morrison, CERN/D.PhII/1972-19.
9. D.R.O. Morrison Review Talk given at the Fourth International Conference on High Energy Collisions (Stony Brook Series), Oxford, 1972.
10. Aachen-Berlin-CERN-London-Vienna and Amsterdam-Nijmegen Collaborations, Nucl. Phys. B39, 287 (1972).
11. R. Kumar, Ph.D. Thesis, London University (1972).
12. A.H. Mueller, Phys. Rev. D2, 2963 (1970).
13. Chan Hong Mo, Rutherford Laboratory Preprint, RPP/T/17 (1972).
14. D.P. Roy, Rutherford Laboratory Preprint RPP/T/41 (1973).
15. H.I. Miettinen, Rutherford Laboratory Preprint, RPP/C/35.

FIGURE CAPTIONS (3)

(3-1) Lorentz invariant x distributions for π^+ inclusive production from K^-p at 10 and 16 GeV/c.

(3-2) Lorentz invariant x distributions for π^- inclusive production from K^-p at 10 and 16 GeV/c.

(3-3) Lorentz invariant x distributions for $\bar{K}^o$ inclusive production from K^-p at 10 and 16 GeV/c.

(3-4) Lorentz invariant x distributions for Λ^o inclusive production from K^-p at 10 and 16 GeV/c.

(3-5) The ratio of π^-/π^+ inclusive cross-section versus x from K^-p at:-

(a) 10 GeV/c

(b) 16 GeV/c.

(3-6) Lorentz invariant two particle inclusive distributions for the reaction $K^-p \rightarrow \pi^+\pi^+ + x^{--}$ at 10 and 16 GeV/c.

(3-7) Lorentz invariant two particle inclusive distributions for the reaction $K^-p \rightarrow \pi^-\pi^- + x^{++}$ at 10 and 16 GeV/c.

(3-8) Lorentz invariant two particle inclusive distributions for the reaction $K^-p \rightarrow \pi^+\pi^- + x^o$ at 10 and 16 GeV/c.

(3-9) 2 to 2 elastic amplitude represented in terms of dual resonance diagrams which in turn can be represented in terms of dual quark loops to demonstrate two component duality picture of the amplitude.

(3-10) 3 to 3 elastic amplitude expressed as:-

(a) a sum of dual resonance diagrams, and

(b) a sum of quark loop diagrams.

(3-11) 4 to 4 elastic amplitude for the process $a\,b\,\bar{c}\,\bar{d} - a\,b\,\bar{c}\,\bar{d}$ represented in terms of dual resonance diagrams.

(3-12) Quark loop representation of the amplitude for $K^-p\pi^-\pi^- - K^-p\pi^-\pi^-$ elastic scattering.

(3-13) Quark loop representation of the amplitude for $K^-p\pi^+\pi^+ - K^-p\pi^+\pi^+$ elastic scattering.

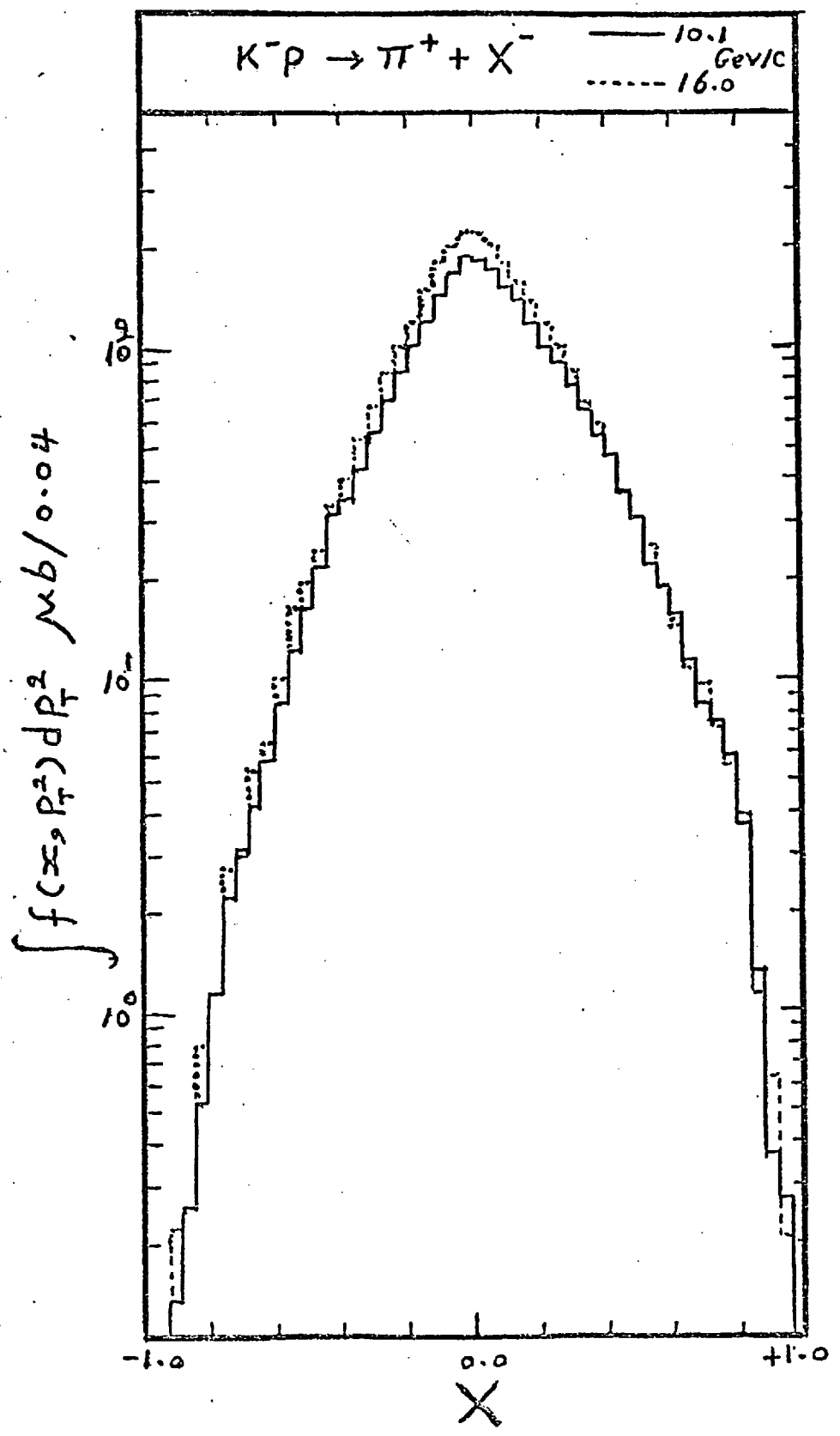
$K^- p \rightarrow \pi^+ + X^-$
10.1 Gev/c
16.0
$\int f(x, p_T^2) dp_T^2$ μb/0.04
10^0
10^{-1}
-1.0
0.0
+1.0
X

FIG(3-1)

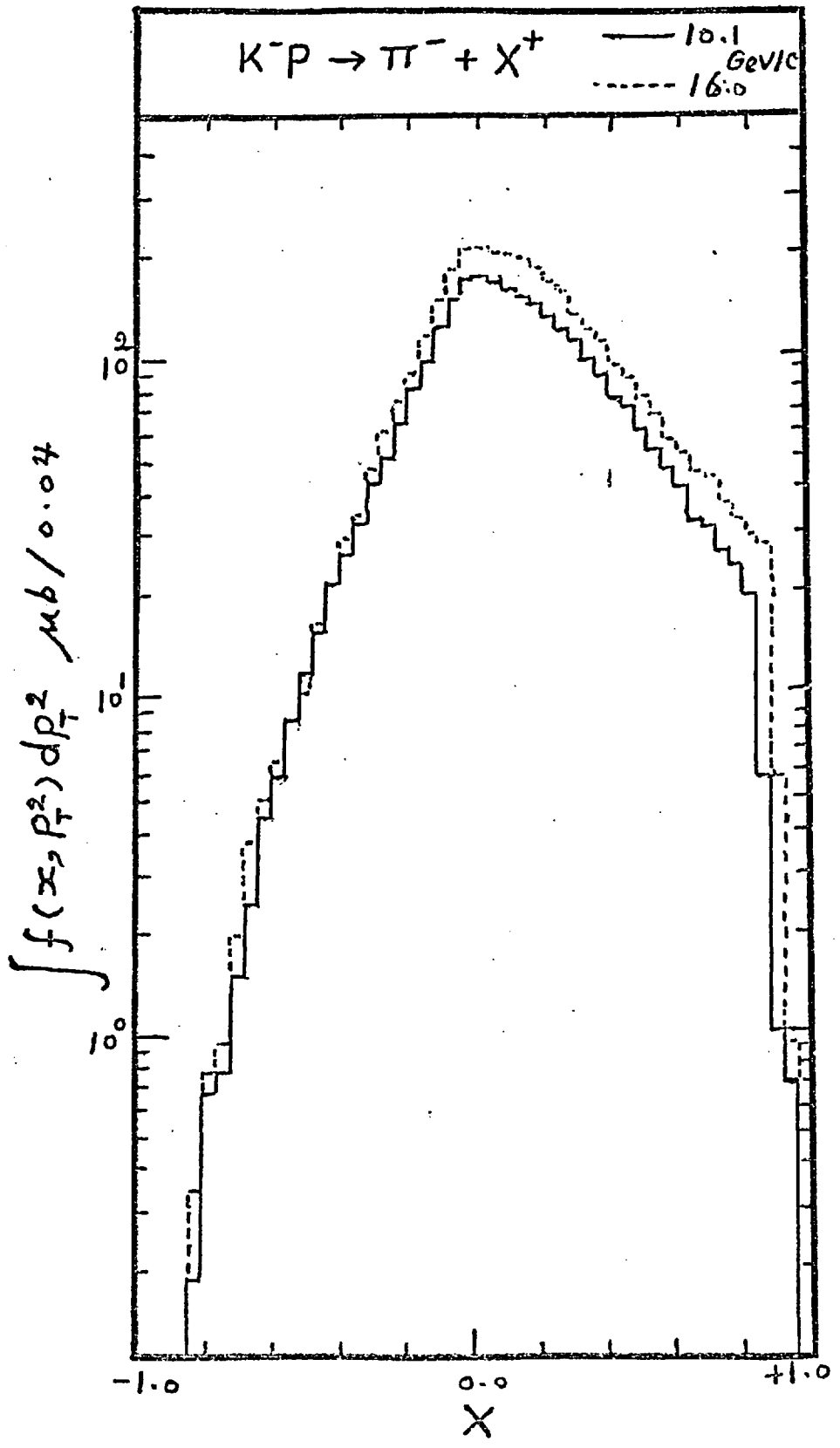
$K^-P \to \pi^- + X^+$
10.1 GeV/c
16.0
$\int f(x, p_T^2)\, dp_T^2$ μb / 0.04
10^2
10^1
10^0
-1.0
0.0
+1.0
X

FIG(3-2)

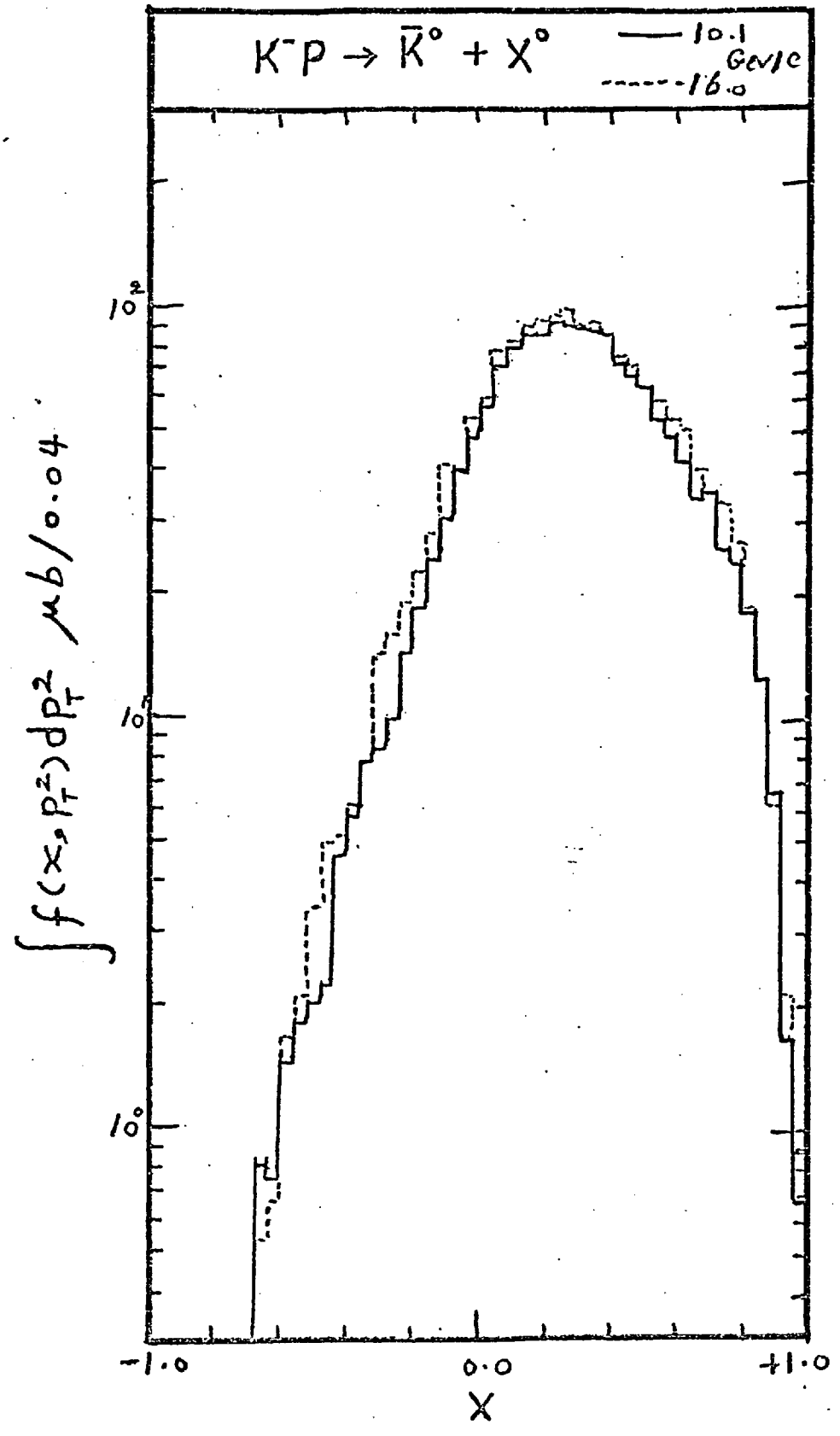
$K^-P \rightarrow \bar{K}^\circ + X^\circ$
10.1 GeV/c
16.0
$\int f(x, p_T^2) dp_T^2$ μb/0.04
10^2
10^1
10^0
-1.0
0.0
+1.0
X

FIG(3-3)

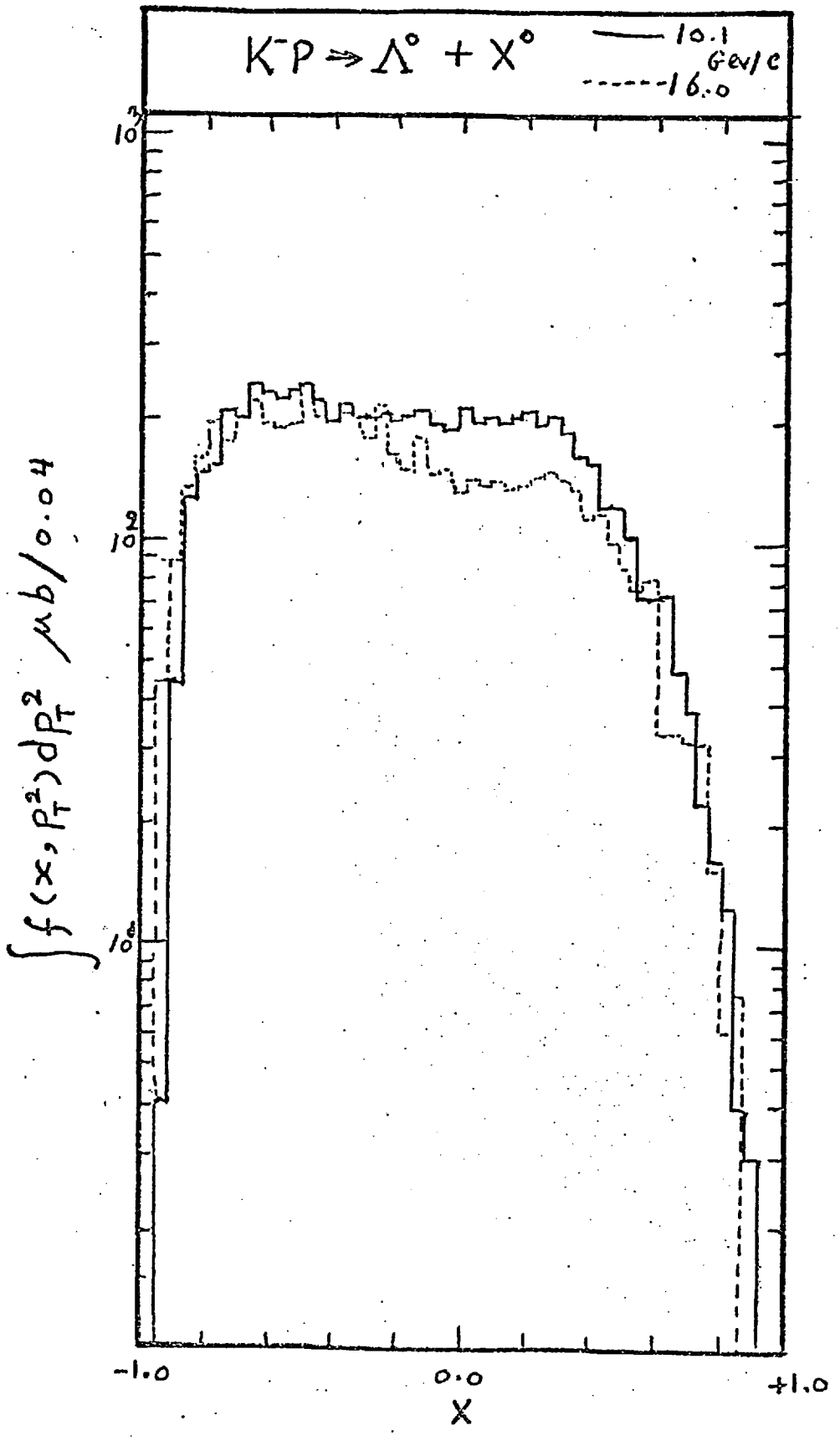
$K^-P \Rightarrow \Lambda^\circ + X^\circ$
10.1 Gev/c
16.0
$\int f(x, P_T^2) dP_T^2$ μb/0.04
10^3
10^2
10^1
-1.0
0.0
+1.0
X

FIG(3-4)

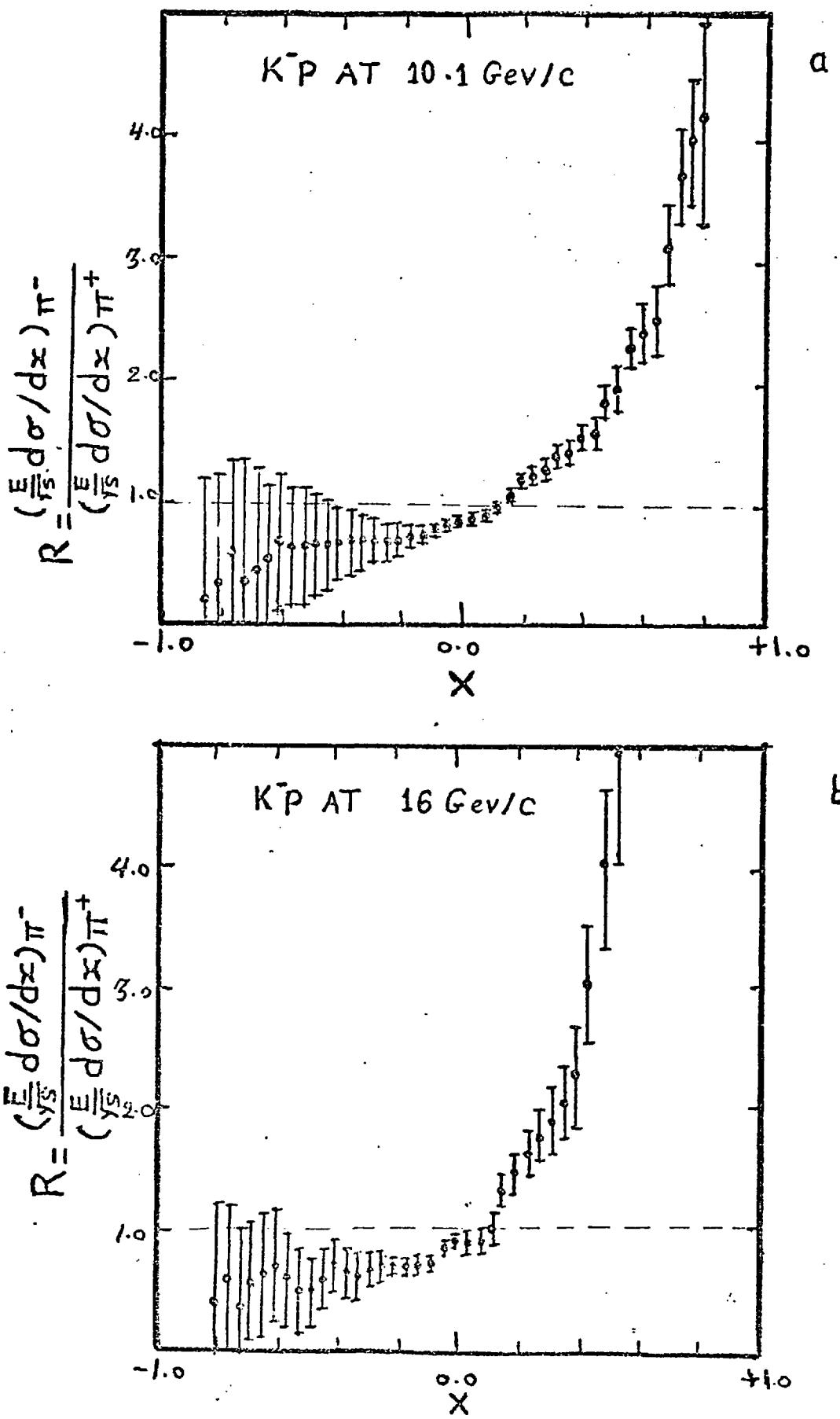
K⁻P AT 10·1 Gev/c
a
$R = \frac{(\frac{E}{p^3}\frac{d\sigma}{dx})_{\pi^-}}{(\frac{E}{p^3}\frac{d\sigma}{dx})_{\pi^+}}$
4.0
3.0
2.0
1.0
-1.0
0.0
+1.0
X
K⁻P AT 16 Gev/c
b
$R = \frac{(\frac{E}{p^3}\frac{d\sigma}{dx})_{\pi^-}}{(\frac{E}{p^3}\frac{d\sigma}{dx})_{\pi^+}}$
4.0
3.0
2.0
1.0
-1.0
0.0
+1.0
X

FIG(3-5)

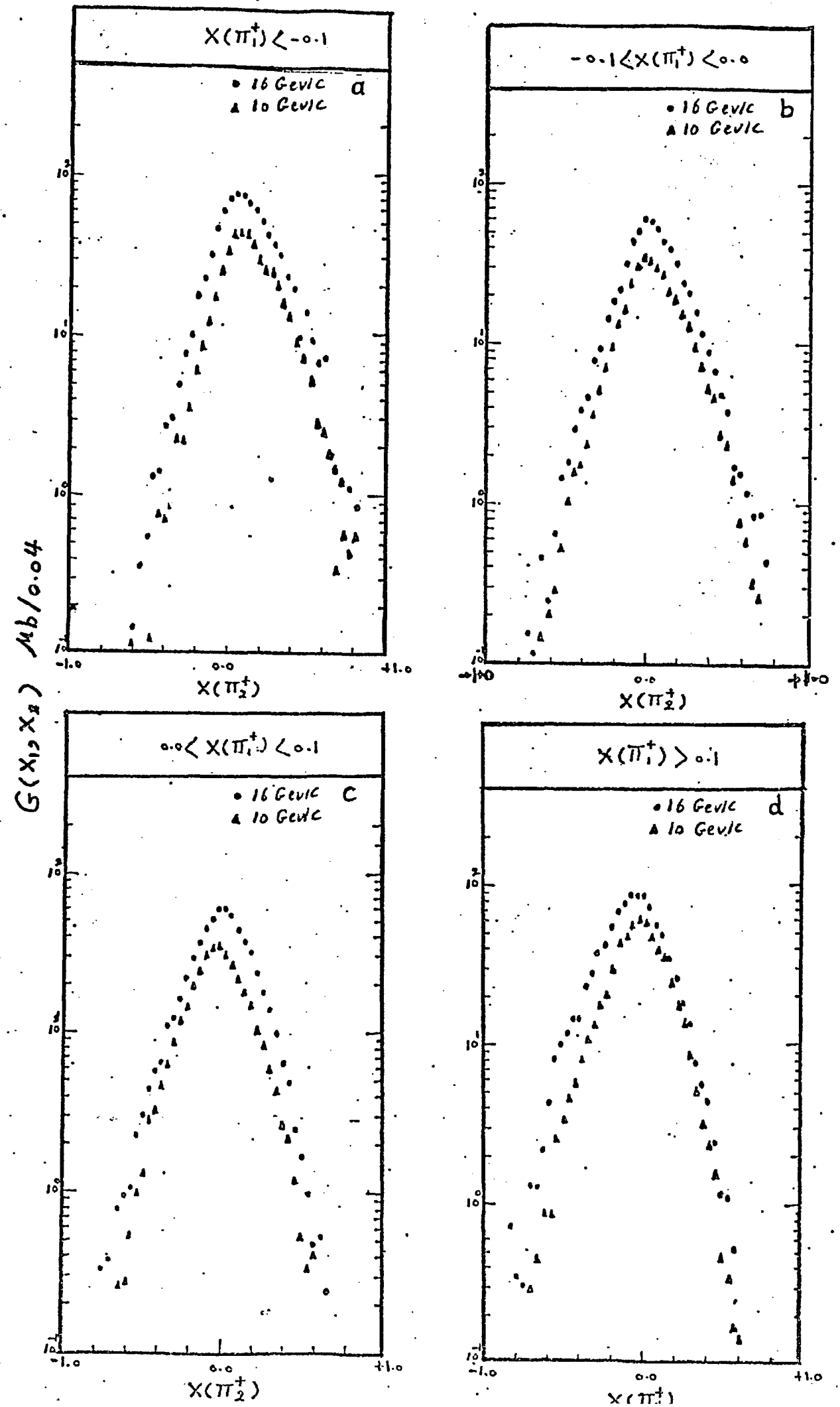
$X(\pi_1^+) < -0.1$
• 16 GeV/c
▲ 10 GeV/c
a
$-0.1 < X(\pi_1^+) < 0.0$
b
$0.0 < X(\pi_1^+) < 0.1$
c
$X(\pi_1^+) > 0.1$
d
$G(x_1, x_2)$ $\mu b/0.04$
$X(\pi_2^+)$
-1.0
0.0
+1.0

FIG(3-6)

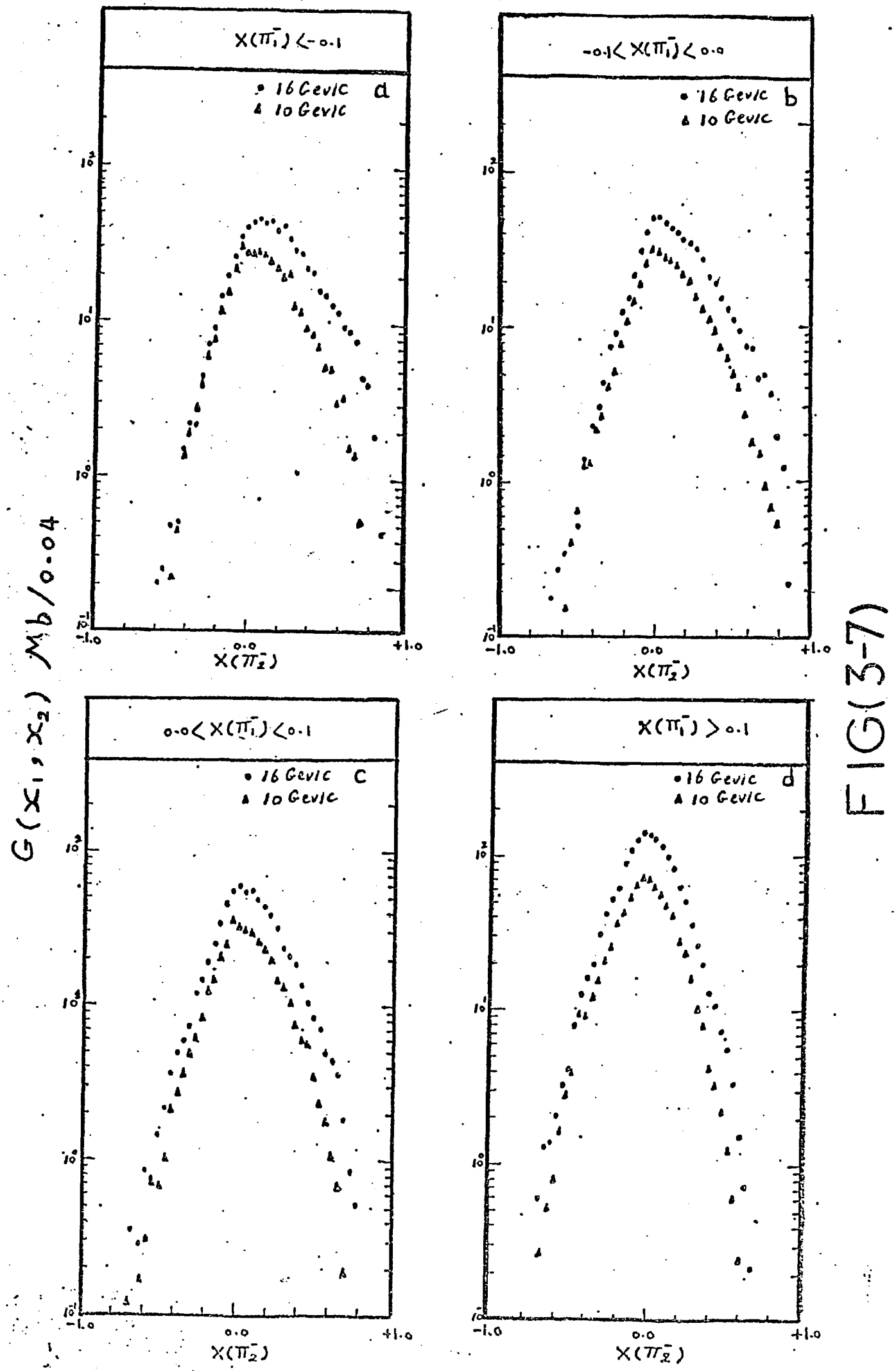
$X(\pi_1^-) < -0.1$
• 16 GeV/c a
▲ 10 GeV/c
$-0.1 < X(\pi_1^-) < 0.0$
• 16 GeV/c b
▲ 10 GeV/c
$0.0 < X(\pi_1^-) < 0.1$
• 16 GeV/c c
▲ 10 GeV/c
$X(\pi_1^-) > 0.1$
• 16 GeV/c d
▲ 10 GeV/c
$G(x_1, x_2)$ mb/0.04
$X(\pi_2^-)$
-1.0
0.0
+1.0

FIG(3-7)

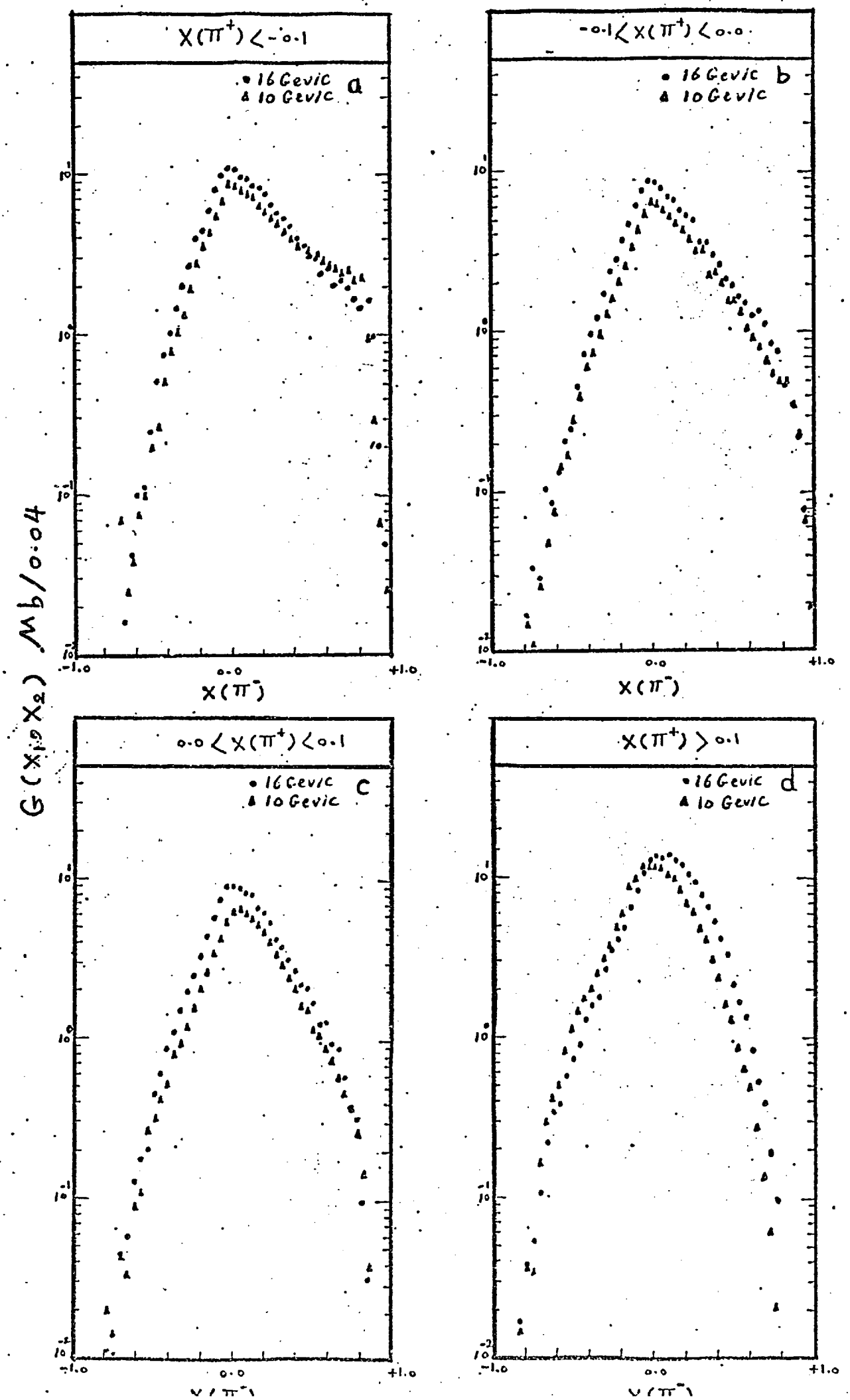
X(π⁺) < -0.1
• 16 GeV/c
▲ 10 GeV/c
a
-0.1 < X(π⁺) < 0.0
b
0.0 < X(π⁺) < 0.1
c
X(π⁺) > 0.1
d
G(X₁, X₂) Mb/0.04
X(π⁻)
-1.0
0.0
+1.0

FIG(3-8)

a

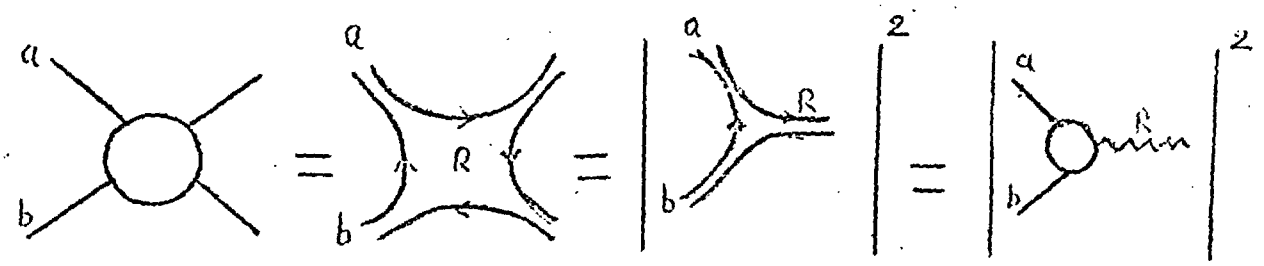

b

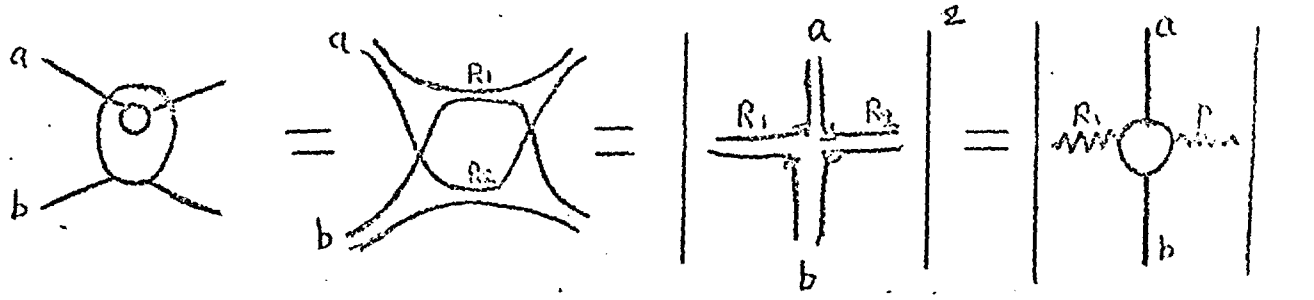

FIG(3-9)

---

a

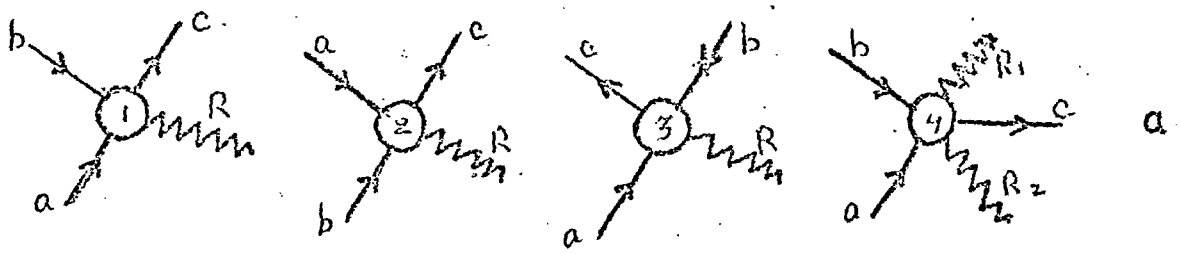

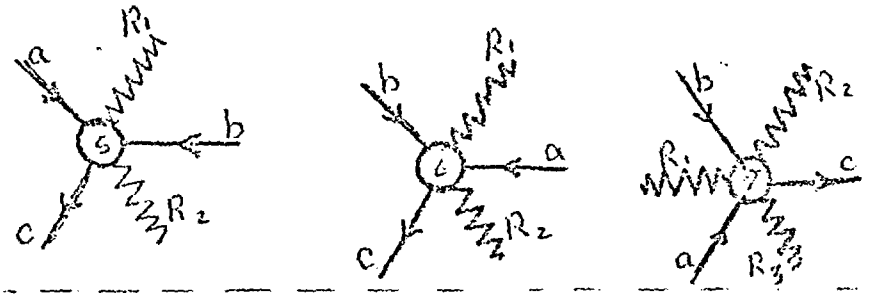

b

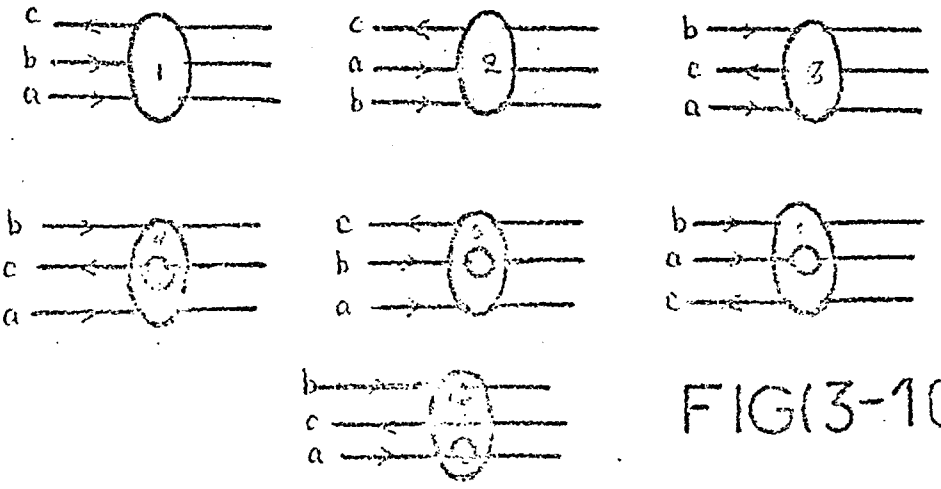

FIG(3-10)

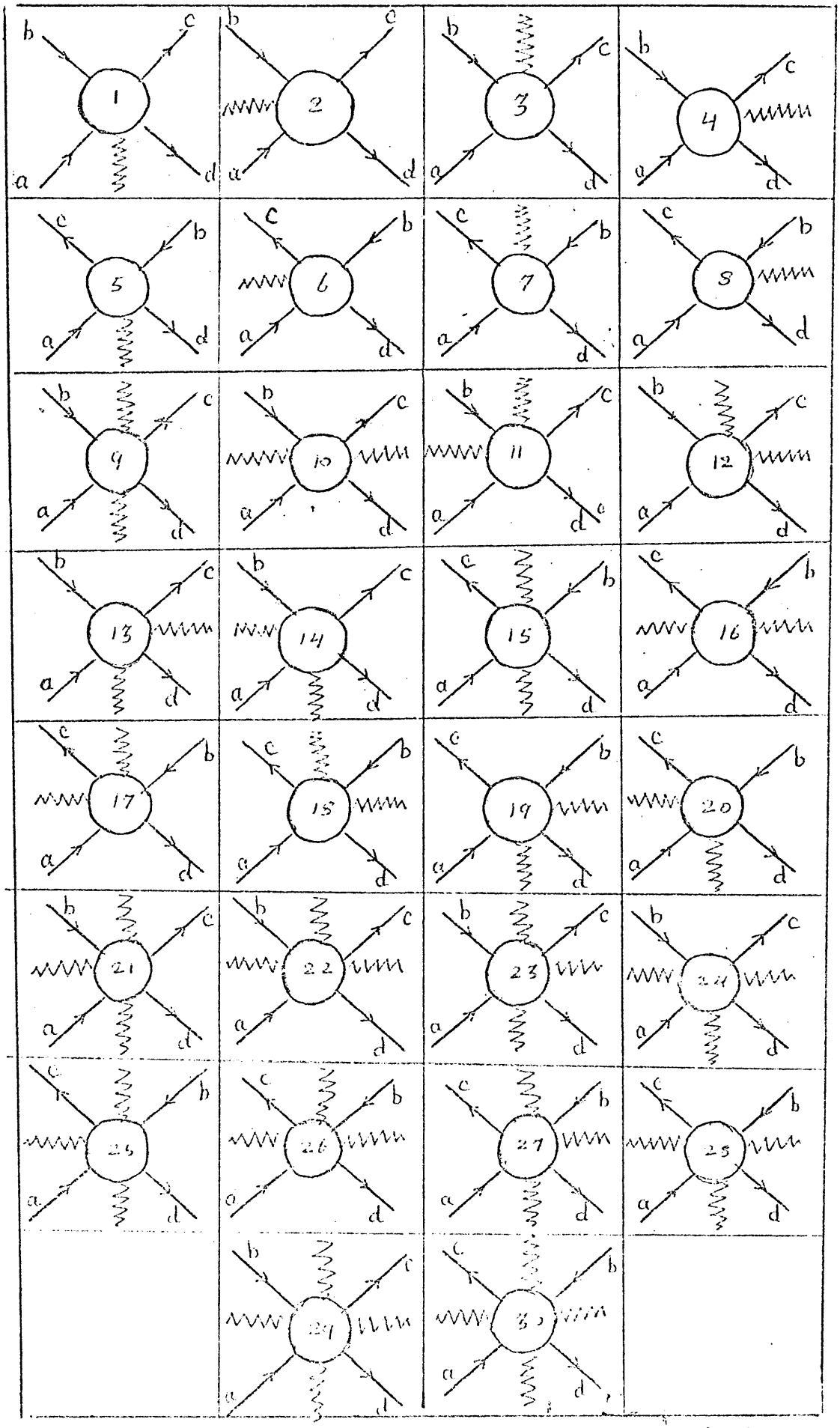
1
2
3
4
5
6
7
8
9
10
11
12
13
14
15
16
17
18
19
20
21
22
23
24
25
26
27
28
29
30
a
b
c
d

FIG(3-11)

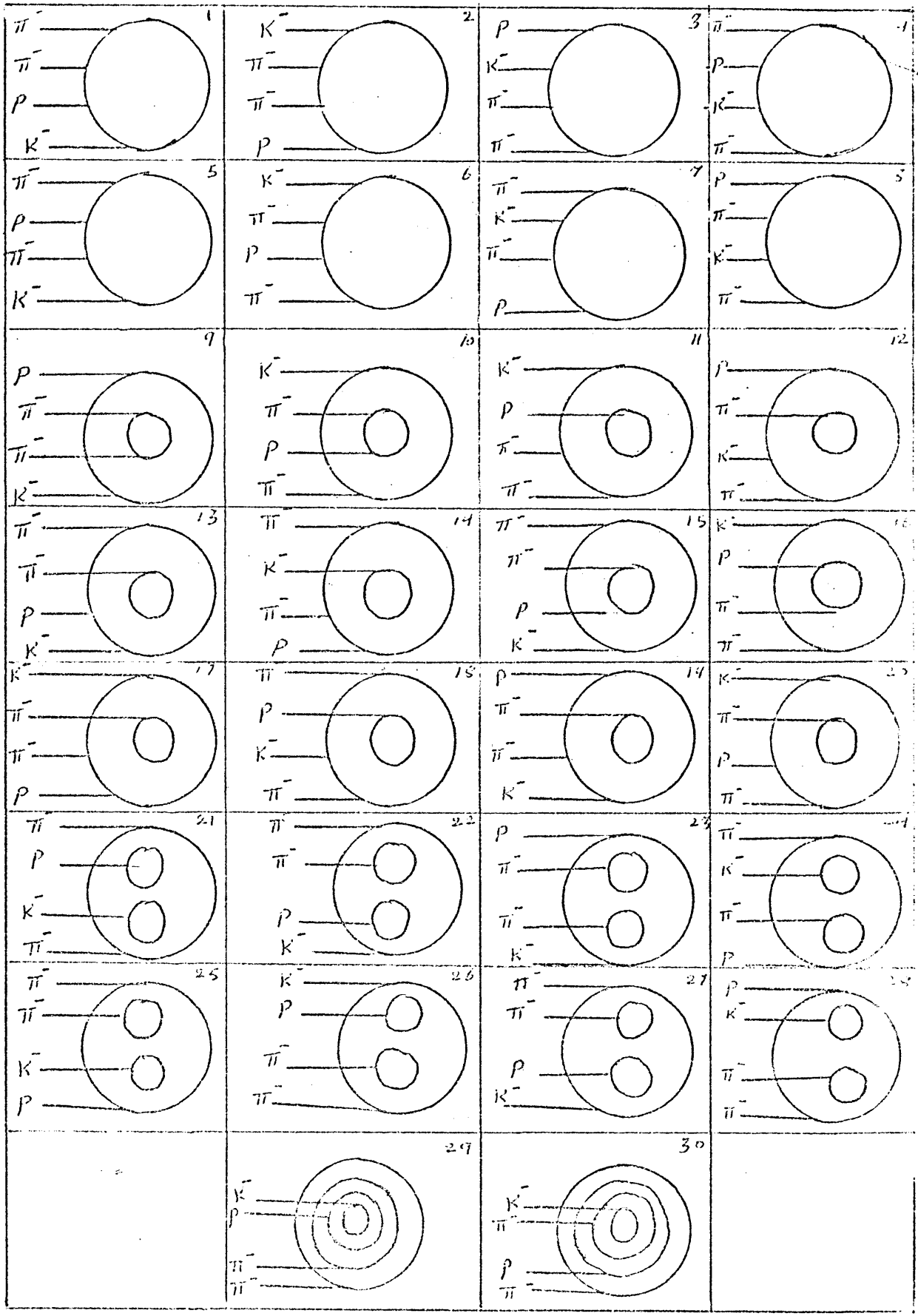
1
2
3
4
5
6
7
8
9
10
11
12
13
14
15
16
17
18
19
20
21
22
23
24
25
26
27
28
29
30

FIG (3-12)

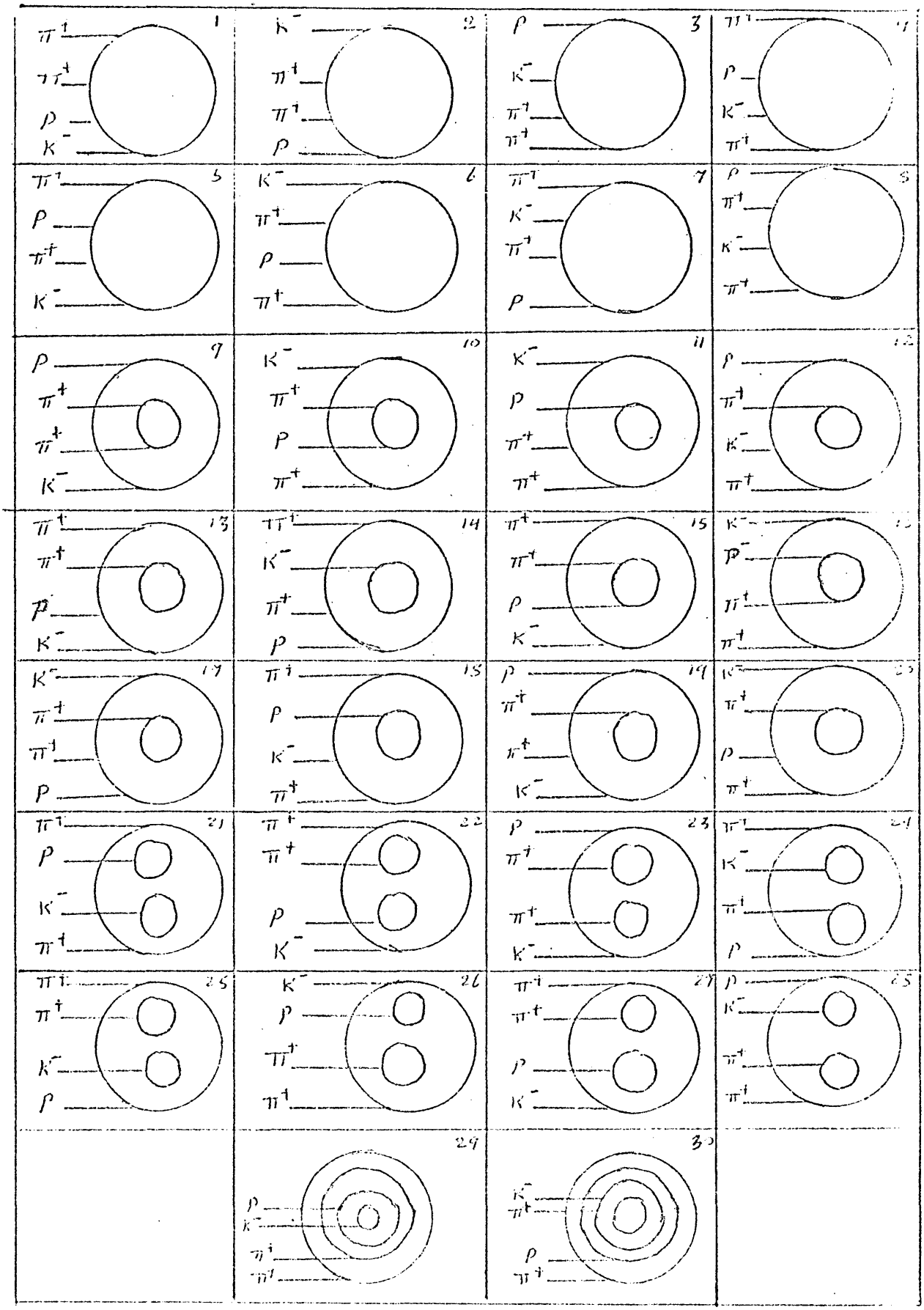
1
π^+
π^+
p
K^-
2
K^-
π^+
π^+
p
3
p
K^-
π^+
π^+
4
π^+
p
K^-
π^+
5
π^+
p
π^+
K^-
6
K^-
π^+
p
π^+
7
π^+
K^-
π^+
p
8
p
π^+
K^-
π^+
9
p
π^+
π^+
K^-
10
K^-
π^+
p
π^+
11
K^-
p
π^+
π^+
12
p
π^+
K^-
π^+
13
π^+
π^+
p
K^-
14
π^+
K^-
π^+
p
15
π^+
π^+
p
K^-
16
K^-
p
π^+
π^+
17
K^-
π^+
π^+
p
18
π^+
p
K^-
π^+
19
p
π^+
π^+
K^-
20
K^-
π^+
p
π^+
21
π^+
p
K^-
π^+
22
π^+
π^+
p
K^-
23
p
π^+
π^+
K^-
24
π^+
K^-
π^+
p
25
π^+
π^+
K^-
p
26
K^-
p
π^+
π^+
27
π^+
π^+
p
K^-
28
p
K^-
π^+
π^+
29
p
K^-
π^+
π^+
30
K^-
π^+
p
π^+

FIG(3-13)

CHAPTER FOUR

TRANSVERSE MOMENTA OF PRODUCED PARTICLES

General Features

One of the most persistent features of hadron collisions is that the transverse momenta of all particles produced in the final states are very small compared with the values allowed by phase space and with the longitudinal momenta of these particles. This behaviour is independent of energy over a wide range starting as low as two or three GeV and up to ISR energies. This effect is largely independent of the type of the incident particle or of the secondary particles. Apart from some effect at very small values of p_T^2 the distributions can be parametrized with a simple exponential formula of the form:-

$$\frac{d\sigma}{dp_T^2} = \text{Const. } \exp(-kp_T^2) \qquad (4.1)$$

Another surprising feature is the value of the parameter k. For different reactions, different particles produced and different incident energies the value of k does not seem to change much. The value of k is usually between 3 and 4. The behaviour near small values of p_T^2 is somewhat more complicated and varies with the type of reaction. This point will be studied in the following sections.

The third characteristic feature which is related to the p_T^2 distributions is that the average value of p_T^2 depends on the mass of the particle. For example, it is higher for protons than for kaons and higher for the latter than it is for pions.

To demonstrate the above features in our data we present in fig. (4-1) and fig. (4-2) the p_T^2 distributions for different particles produced at 10 and 16 GeV/c respectively. The solid lines correspond to a simple

parametrization of the data in the region of $p_T^2 > 0.5$ (GeV/c)^2 with equation (4.1). The corresponding values of the parameter k are given in table (4-1). The region of $p_T^2 < 0.5$ (GeV/c)^2 needs a steeper slope and the value of k in this region differs from one particle to another. However, it can be clearly seen that the value of the cross-section in this region is higher than that expected from extrapolating the fitted line from the other region into this region. We shall come back to this point in more detail in a subsequent section. At the moment one can only say that such effects depend on the particle produced.

Fig. (4-3) shows the value of $\langle p_T \rangle$ of particles plotted against their masses. The relation is approximately linear. The proton, however, has a $\langle p_T \rangle$ value (which was calculated excluding elastic events) appreciably smaller than this simple scheme would indicate.

It is clear from figs. (4-1) and (4-2) that none of the properties associated with transverse momenta are dependent on the incident beam momentum apart from the overall normalization of the cross-section which can be considered as a direct consequence of the non-scaling part of the cross-section discussed in the previous chapter. All other properties like the shape of the distribution and the value of k are hardly affected by the change of the beam momentum from 10 to 16 GeV/c.

Comparison with the Thermodynamic Model

The nature of the Hagedorn[1] thermodynamical model mentioned in Chapter One makes it a very useful model in attempting to describe transverse momentum distributions of particles produced in high energy collisions. The advantage that this model enjoys over other models in this respect is that one reduces the effects of leading particles, which in the thermodynamic language are assumed to be associated with the so called drift velocity λ. Hence, from the basic assumption of the thermodynamical model which assumes that in a hadronic collision

at high energy one would expect that some kind of hadronic "hot-stuff" is formed and reaches some kind of thermal equilibrium state before emitting particles, in a way which is similar to that of black body radiation, one would expect the transverse momentum distributions of produced particles to be described by the formula

$$f(p_T, s) = \text{Const} \left[\frac{1}{(\exp (K/T \mp 1)} \right] \qquad (4.2)$$

where K is called the transverse energy of the particle given by $K^2 = m^2 + \bar{p}^2$ and T is the "temperature" of the hadronic stuff produced in the collision. The model suggests that this value is universal for all particles produced from collisions where hadronic thermal equilibrium is reached.

The positive sign in relation (4.2) is taken when dealing with fermion particles which are described by Fermi Dirac statistics while the negative sign is taken for bosons.

Equation (4.2) was used to parametrize the overall transverse momentum distribution of each of the distributions shown in fig. (4.1) and fig. (4.2). The method of least squares was used to fit for both normalization constants and temperature parameters. The quality of the fits obtained was very poor in terms of the ratio of χ^2 to the number of degrees of freedom. Furthermore, the values of the temperature parameter T obtained from those fits were not in good agreement with the predicted value of Hagedorn of 140 MeV.

In order to try to improve the quality of the fits, we selected particles produced with small values of the centre of mass longitudinal momenta in the region of $|x|$ smaller than 0.1. The distributions were fitted separately with formula (4.2). The quality of the fits, however, was not much better than the previous case. The values of the temperature parameter were in good agreement with the predicted 146 MeV value for $\bar{K}^0$ and Λ^0 only. Table (4-2) shows the values of T and the values of

χ^2/N where N is the number of degrees of freedom for each of the particle distributions fitted.

From this we conclude that in spite of its success in describing the p_T^2 distributions of $\bar{K}^o$ and Λ^o, this thermodynamic model does not give good fits for the distributions of pions produced. This behaviour is difficult to explain by possible biases in the data due to misidentifications of particles because we get results which are very similar for both π^+ and π^- while the nature of the ambiguity in each case is different.

It is clear that in this energy range the thermodynamical model is not completely adequate to describe the p_T distribution even for pions, while other particles are known to be produced via certain exchange mechanisms rather than via a process like black body radiation.

Transverse Momenta in Multiperipheral Models

Multiperipheral models contain within their physical concept the facility to explain the observed experimental cut off of transverse momenta of produced particles qualitatively if not quantitatively. This can be easily understood in two ways. The first way is through the consideration of the physical assumption involved in these models that particles produced are decay products of some type of cluster of various angular momentum states produced along a multiperipheral ladder. The decay of these clusters with a low Q value is the main reason behind the observed low values of p_T^2, where the Q value represents the mass difference between the cluster and its decay products. The second way to explain this effect is very much linked to the first explanation: At any vertex of a multiperipheral diagram the p_T^2 value of any particle produced at that vertex is approximately proportional to the squared four vector momentum transfer to that point. Because of the fact that regge exchanges are expected to be the momentum transfer carriers, one would expect to have small values of t's between different parts of the multiperipheral ladder. This in turn can give small values to the transverse

momenta possessed by produced particles.

Although detailed quantitative predictions about p_T^2 distributions using these models do not exist at the moment, one can to a first approximation consider pions to be the best particles with which to test these models. This is because, as was shown in Chapter Three, pions are produced mostly in the central region which is equivalent to producing particles half way up a multiperipheral ladder. This, coupled with the fact that in most cases the nucleon and the strange meson are produced as leading particles, leaves us with pions produced half way between the two and in the multiperipheral ladder. These may be considered as decay products of slow moving resonances such as the ρ. This is only true for models which do take into account resonance production.

Steven Pinsky [2] has shown that in a simple model, in which all pions are produced as decay products of a low mass unpolarized cluster with a transverse momentum distribution that peaks near $p_T^2 = 0.0$, the transverse momentum of the produced pions exhibits a turning over near $p_T^2 = 0$. This effect is strictly kinematical and will appear in any similar model.

To compare this with our data we selected those pions produced in the central region. The p_T^2 distribution for those events is plotted in fig. (4-4). The solid curve represents the Pinsky and Stevens prediction; because of the form in which this prediction was given no detailed fits were made and we fitted our data only to the shape of their curve with the overall normalization as a free parameter. Although the agreement between the data and the predicted curve is not bad for large p_T^2 there is disagreement in the region where a turnover is expected. Our data show no such effect. This may be taken as an indication against the assumption that all particles produced in the central region come from the decay of the low mass meson resonances produced on the multiperipheral ladder.

Although the above statement does not take into account any of the details involved in this type of model, it gives a general comparison with the behaviour of the distribution expected from such models. However, the evidence here against these models is not very strong and the only disagreement is that one associated with the turnover at small p_T^2.

Comparison with Dual Resonance Model

Most dual resonance models (DRM) predict the observed dynamical cut off in the p_T^2 distributions of inclusively produced particles. The particular model which we are going to use in this context is that formulated by de Tar et al[3]. They used the relation between the inclusive distribution function and the discontinuity in the 3-3 amplitude to predict the transverse momentum distributions. The latter discontinuity was derived using seven configurations corresponding to seven different dual diagrams contributing to the inclusive single particle distribution function. To obtain quantitative results on p_T^2 distributions these dual diagrams were expressed in terms of B_6 functions. The results of these calculations were shown to predict transverse momentum distributions of the form

$$f(p_T^2) = \exp\ (-\ 4\alpha'\ p_T^2) \qquad (4.3)$$

for large values of p_T^2.

Where α' was claimed to be a universal slope related to those trajectories which were assumed to be exchanged.

It was shown in the first section of this chapter that the simple exponential form assumed for $f(p_T^2)$ distribution offers a good parametrization for large values of $p^2 > 0.5\ (GeV/c)^2$. However, the values of the slope parameter for different particles are somewhat different and may

depend among other factors on the mass of the particle. Thus one concludes that the evidence in support of the universality of the value of the slope parameter α' is not strong. Another DRM calculation[4] predicts the same kind of behaviour without requiring α' to be universal.

The Seagull Effect

In most high energy interactions if one plots the average value of the square of the transverse momentum variable versus the Feynman variable x or the longitudinal momentum of an inclusively produced particle one gets a dip in $\langle p_T^2 \rangle$ values near x = 0. This type of behaviour is called the seagull effect. The depth of the dip depends on the mass of the particle considered. It is usually smaller for particles with higher mass than it is for those with smaller mass.

Fig. (4-5) shows plots of $\langle p_T^2 \rangle$ values against x for some particles produced at 10 GeV/c. The behaviour at 16 GeV/c is similar. The values in this figure were calculated from the Lorentz non-invariant $d\sigma/dx$ distributions. The mass dependence of the dip is clear. For example, the dips in the curves of the two pions are much larger than they are for the proton or the lambda. This behaviour led many people to believe that the effect may be due to kinematical reasons coming from the fact that we are not using the Lorentz invariant distribution. The Lorentz non-invariant distribution does not contain the $\frac{1}{E}$ factor and hence can give a dip in p_T^2 for x = 0 if E = 0. To avoid this the Lorentz invariant $Ed\sigma/dx$ distributions were also used and fig. (4-6) shows the resulting plots. It is clear that although this procedure reduces the dip to some extent it is not true that the effect can be fully accounted for by the $\frac{1}{E}$ factor in the Lorentz non-invariant differential cross-section. The plots of fig. (4-6) show the effect is still there and the type of mass dependence observed in fig. (4-5) is again present.

Berger[5] relates the kind of behaviour observed to the nature of the p_T^2 distributions of the particles considered. He explains the seagull

effect as a reflection of the heavily populated region on the p_T^2 distribution near $p_T^2 = 0.0$. Furthermore, Berger argues that both the seagull effect and the peak near $p_T^2 = 0$ can be explained as a result of kinematic effects produced as consequences of resonance production. If one considers a resonance to be produced with small p_T^2 value then in the centre of mass frame of that resonance one may expect the decay products to be produced with very small p_T^2 values provided that the Q value for that decay mode of the resonance is small. In a very small Q value approximation the decay products of the resonance will share the original momentum of that resonance with ratios proportional to their masses when measured in the overall centre of mass. Now the effect of the Q value of the decay can be bounded between two extreme cases when the additional momentum is either added or subtracted to the momentum shared between the two particles. For small Q values this will only form a small perturbation to the momentum of the particles. In the longitudinal direction the effect of the decay can be neglected completely remembering that the massive particle takes the largest proportion of the longitudinal momentum with it and the particle with small mass will have the smaller proportion. This will lead to production of decay products with p_T^2 and x very small.

In order to check whether the above argument can explain the observed seagull effect in the data it was first thought that one should not expect such an effect when one studies resonances themselves rather than their decay products. The two most abundant resonances in our experiment, the K^{*-} and the Δ^{++}, were chosen and plots of p_T^2 versus x are shown in fig. (4-7) for each of them. Indeed the effect disappears and in the case of the Δ^{++} values of p_T^2 are higher near x = 0 than anywhere else and the two resonances tend to have an overall $\langle p_T^2 \rangle$ higher than that of the $\bar{K}^0$ and the protons.

An argument against this type of analysis is that by choosing the resonances we have automatically increased the masses which, as was seen

in section one, has the effect of increasing $\langle p_T^2 \rangle$. The answer to that is that the K^{*-} and the Δ^{++} have nearly the same masses as the proton and the Λ^0 and yet we do not observe the seagull effect for the former two while it is clear for the latter two particles.

A different type of analysis was carried out by classifying particles into two samples depending on whether or not they are decay products of a particular resonance and the $\langle p_T^2 \rangle$ - X correlation for the two samples are compared. The resonances chosen for this study were the Δ^{++}, K^{*-} and Y^{*-}.

In the Δ^{++} case, pions coming from inside and outside the Δ^{++} mass region are compared using the $\langle p_T^2 \rangle$ dependence on x in fig. (4-8-a). It can be seen that the two samples of pions are different in the sense that those coming from Δ^{++} decay have substantially smaller $\langle p_T^2 \rangle$ values than those which do not. Furthermore, it is clear that resonance decay products occupy a very limited region in x around zero. Although there is a small dip in the plot for pions coming from outside the Δ^{++} region the dip is much smaller than it is for the case of all pions. This dip is due to other resonances which were not separated. The same kind of behaviour can be observed with protons although to a much less significant degree.

The situation in the K^{*-} and the Y^{*-} follow the same pattern and on the whole one observes that particles coming from the decay of a resonance tend to have smaller $\langle p_T^2 \rangle$ values than those which do not, as is shown in fig. (4-9) and (4-10).

To check whether this effect is due to the cut on a low mass cluster and not due to the resonance formation we imposed cuts on different regions of the background outside the resonance regions on both sides. No effect indicating differences between those regions was observed and in all cases $\langle p_T^2 \rangle$ were larger than that of the resonances decay products. This leads us to conclude that Berger's explanation of the seagull effect does explain a substantial part of this effect at least, if not the whole structure.

Reflections on Correlations

Although the study of correlations between two inclusively produced particles is going to be treated in some detail in following chapters, we find it necessary to deal with one aspect of this subject at this stage. This can be justified if one tries to remember that the simplest and most direct method to study correlations between two particles is being done through studying structures in their effective mass distributions. In the previous section we discussed possible reflections of structures in the effective mass distributions due to resonances on the single particle transverse momentum distributions. In this section we are going to demonstrate that structures in the effective mass distribution are reflected in other kinematical variables of the two particles.

At this stage we want to introduce a new method for studying correlations between two particles. This is done through the study of the dependence of $\langle p_T^2 \rangle$ of one of the particles on the longitudinal variable x of the other. The first particle is usually chosen to be a pion while the second may be taken to be any particle. Although this method is a very simple one, we find that it has many advantages which help in extracting information concerning the observed $\langle p_T^2 \rangle$ distributions in single particle inclusive reactions. The main advantages that we have here are:-

1. If the two particles are independently produced and are completely uncorrelated, then one would simply expect the flat distribution of $\langle p_T^2 \rangle$ values of one particle against the x values of the other over the whole range of x.
2. With the first particle chosen to be a pion one has the means of exploiting the useful fact that correlations due to energy momentum conservation are the same for both π^+'s and π^-'s inclusive reactions. Therefore, one can extract at least part of the dynamics involved simply by comparing results from reactions involving a π^+ and a π^- produced with another particle.

In this section the type of dynamics we are looking at are those due to resonance production. To do this we choose the following reactions:-

$$K^- p \rightarrow \bar{K}^0 \pi^{\mp} + \text{anything}$$
$$K^- p \rightarrow \Lambda^0 \pi^{\mp} + \text{anything}$$
$$K^- p \rightarrow p \pi^{\mp} + \text{anything}$$

The above reactions form a typical sample which represent most of the known production mechanisms that may take place. Reactions involving $\bar{K}^0$ as one of the detected particles represent two extreme cases where one of them has a strong resonance production mainly through $K^{*-}(890)$ and $K^{*-}(1420)$ production while the other has the exotic combination. If the method is sensitive enough one might expect some difference between values of $\langle p_T^2 \rangle$ between the two reactions especially when the $\bar{K}^0$ is fast moving in the forward direction. Indeed, from fig. (4-11) one finds that first the average $\langle p_T^2 (\pi^+) \rangle$ are nearly independent on the x values of $\bar{K}^0$ while there exists some dependence in the π^- case. The difference between the two becomes larger for higher values of $X(\bar{K}^0)$ and we conclude that there must exist some effect other than phase space which tends to suppress the values of $p_T^2 (\pi^-)$ when the $\bar{K}^0$ is moving fast in the forward direction. The only difference we know of is the resonance production involved in one but not in the other. So one may conclude that K^{*-} production may have a significant effect in suppressing further the values of $p_T^2 (\pi^-)$ produced.

The situation with reactions when the proton and a pion are produced and detected is similar except that we have contributions from resonances in both π^+ proton and π^- proton combinations. However, this is not a very serious problem because the main resonances in both cases are the Δ^{++} and the Δ^0 respectively which have the same mass. Furthermore, many

studies of exclusive channels have shown that the cross-section for Δ^{++} production is much higher than that of Δ^{o} (6). Fig. (4-12) shows a substantial difference in values of $\langle p_T^2 \rangle$ for π^+ and π^- over a wide range of X(p) with those of π^+ lying below the corresponding values for π^-. The two cases become nearly equal when $X(p) \to -1$. This may be explained by the fact that the majority of fast backward moving protons are produced via diffractive dissociation of K^- where no resonance is being formed in the proton vertex.

The results from the study of the $\Lambda^o\pi^{\mp}$ inclusive reaction are somewhat different. IN this case both Y^{*+} and Y^{*-} are strongly produced resonances. However, the cross-section for Y^{*-} production is a little higher than that of Y^{*+} (6). Fig. (4-13) shows values of $\langle p_T^2 \rangle$ which are nearly equal although one may observe some values of $\langle p_T^2\ (\pi^-) \rangle$ which are a little bit higher than the corresponding ones for $\langle p_T^2\ (\pi^+) \rangle$.

By combining the results of the above three pairs of cases one can deduce that resonance production plays a strong role in suppressing the values of p_T^2 of the particles involved. This effect reflects itself in the observed transverse momentum distributions of particles through the production of large population density of events near small values of p_T^2 and also in the observed structure called the seagull effect observed for most particles.

Conclusions

In this chapter, single particle transverse momentum distributions were studied. These distributions were compared with predictions from the Hagedorn thermodynamical model, the multiperipheral model and the dual resonance type model. The observed higher values of the cross-section at small values of p_T^2 were investigated in the light of the assumption that the effect is due to resonance production. The data seems to be in agreement with Hagedorn model for Λ^o and $\bar{K}^o$ but not

for π^+ and π^-. No strong evidence in support of a multiperipheral model was found. The higher population density in the $\langle p_T^2 \rangle$ distribution and the observed seagull effect was proved to be due, partially at least, to those particles coming from decays of resonances. A new method of studying correlations between pions and other particles was introduced. This method depends on the suppression of the values of $\langle p_T^2 \rangle$ for particles produced as decay products of resonances.

REFERENCES (4)

1. R. Hagedorn, Nucl. Phys. B24, 93 (1970).
2. S. Pinsky, University of Utah Preprint (1972).
3. C.E. de Tar et al., Phys. Rev. D3, 128 (1971).
4. G.H. Thomas, ANL Preprint, ANL/HEP 7144 (1971).
5. E. Berger, ANL Preprint, ANL/HEP 7134 (1971).
6. A. Mutalib, Ph.D. Thesis (1972).

TABLE CAPTIONS (4)

(4-1) Values of the slope parameter k obtained from exponential fits to inclusive p_T^2 distributions for different particles produced from K^-p interactions at

(a) 10 GeV/c

(b) 16 GeV/c.

On the tables are also shown the values of χ^2/N where N is the number of degrees of freedom.

(4-2) Values of the temperature parameter T obtained from thermodynamical model fitting to inclusive p_T^2 distributions for particles produced in the region $|x| < 0.1$ from K^-p at

(a) 10 GeV/c

(b) 16 GeV/c.

TABLE (4-1-a)

K^-P AT 10 GEV/C		
Particle	$k(GeV/c)^{-2}$	χ^2/N
p	4.14	0.93
π^+	3.36	0.54
π^-	3.62	0.58
Λ^0	3.08	0.59
$\bar{K}^0$	3.56	0.26
K^-	3.34	0.85

TABLE (4-1-b)

K^-P AT 16 GEV/C		
Particle	$k(GeV/c)^{-2}$	χ^2/N
p	4.32	1.07
π^+	3.41	0.50
π^-	3.54	0.63
Λ^0	3.04	1.14
$\bar{K}^0$	3.42	1.07
K^-	4.08	0.91

TABLE (4-2-a)

K^-P AT 10 GEV/C		
Particle	Temperature Parameter	χ^2/N
p	102	0.21
π^+	221	2.23
π^-	196	2.52
Λ^o	121	0.36
$\bar{K}^o$	145	0.47
K^-	135	0.56

TABLE (4-2-b)

K^-P AT 16 GEV/C		
Particle	Temperature Parameter	χ^2/N
p	101	1.05
π^+	186	4.60
π^-	166	5.60
Λ^o	135	1.20
$\bar{K}^o$	142	0.43
K^-	131	0.40

FIGURE CAPTIONS (4)

(4-1) $f(p_T^2)$ single particle inclusive distributions for the reaction $K^- p \to c$ + anything at 10.1 GeV/c where c is a proton, π^+, π^-, $\bar{\Lambda}^0$, $\bar{K}^0$ and K^-.

(4-2) $f(p_T^2)$ single particle inclusive distributions for the reaction $K^- p \to c$ + anything at 16 GeV/c where c is a proton, π^+, π^-, Λ^0, $\bar{K}^0$ or K^-.

(4-3) Average value of p_T for different particles produced from $K^- p$ collisions at 10.1 GeV/c plotted against their masses.

(4-4) $f(x, p_T^2)$ for pions in the region of $|x| < 0.1$ from $K^- p$ collisions at 10 and 16 GeV/c. Solid lines represent predictions of multiperipheral model if those pions are decay products of a low mass cluster.

(4-5) $\langle p_T^2 \rangle$ for particles produced from $K^- p$ collisions at 10.1 GeV/c plotted against their longitudinal variable x. Values of $\langle p_T^2 \rangle$ are calculated from Lorentz non invariant x distributions.

(4-6) $\langle p_T^2 \rangle$ values versus x. Values of $\langle p_T^2 \rangle$ are calculated from Lorentz invariant x distributions.

(4-7) $\langle p_T^2 \rangle$ values versus x for

(a) the Δ^{++} resonance

(b) the $K^{*-}(890)$ resonance.

$\langle p_T^2 \rangle$ values are calculated from Lorentz non invariant x distribution for the resonance in each case.

(4-8)

(a) Comparison of $\langle p_T^2 \rangle$ versus x for pions which are decay products of the Δ^{++} with those which are not.

(b) Comparison of $\langle p_T^2 \rangle$ versus x for protons which are decay products of the Δ^{++} with those which are not.

(4-9)
(a) Comparison of $\langle p_T^2 \rangle$ versus x for pions which are decay products of the K^* with those which are not.

(b) Comparison of $\langle p_T^2 \rangle$ versus x for protons which are decay products of the K^* with those which are not.

(4-10)
(a) Comparison of $\langle p_T^2 \rangle$ versus x for pions which are decay products of the Y^* with those which are not.

(b) Comparison of $\langle p_T^2 \rangle$ versus x for protons which are decay products of the Y^* with those which are not.

(4-11) $\langle p_T^2 \rangle$ of pions plotted against x of $\bar{K}^0$ in the two reactions $K^- p \to \bar{K}^0 \pi^{\pm} + X$ at 10 GeV/c.

(4-12) $\langle p_T^2 \rangle$ of pions plotted against x of protons in the two reactions $K^- p \to p\pi^{\mp} + X$ at 10 GeV/c.

(4-13) $\langle p_T^2 \rangle$ of pions plotted against x of Λ^0 in the two reactions $K^- p \to \Lambda^0 \pi^{\mp} + X$ at 10 GeV/c.

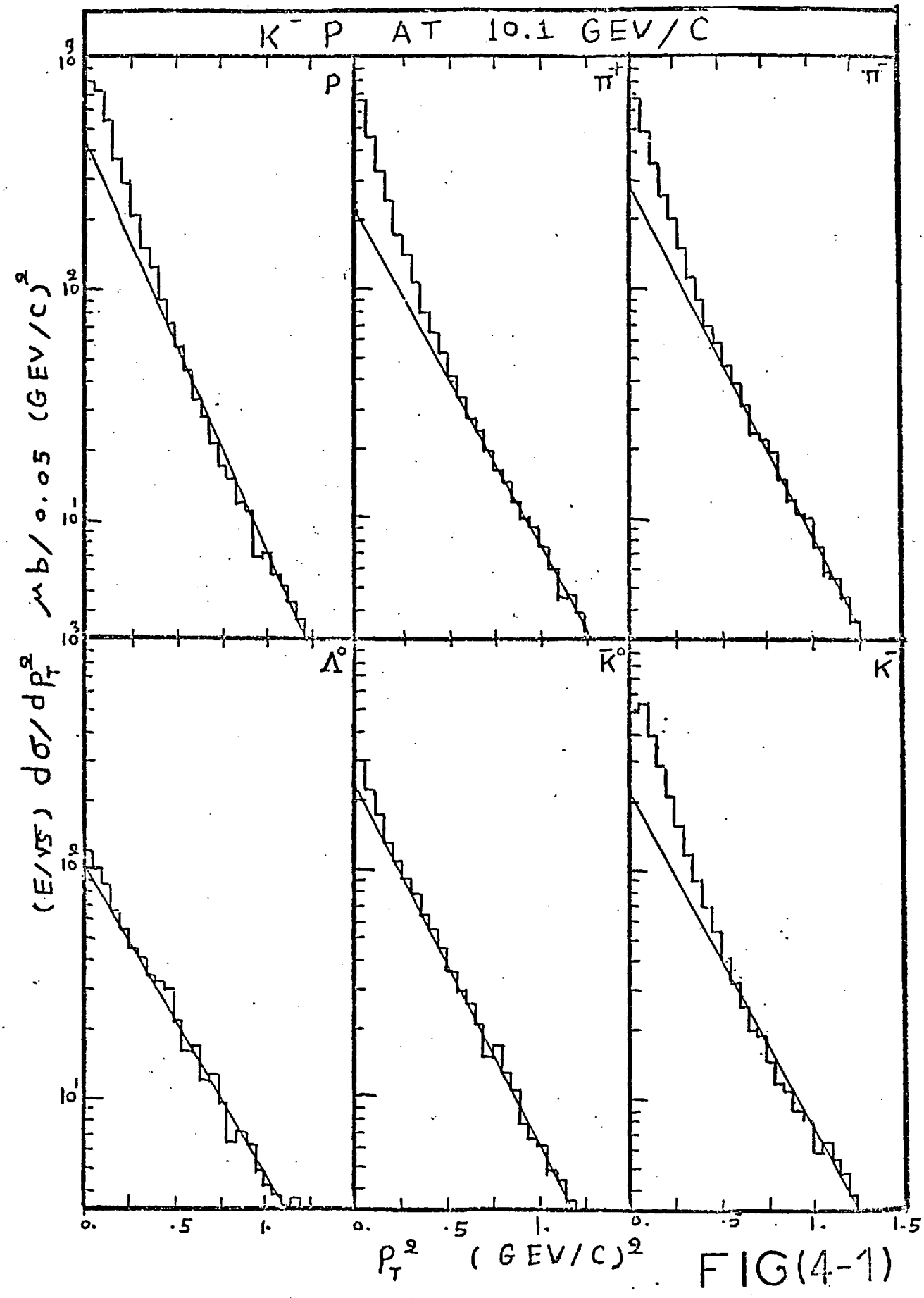

FIG(4-1)

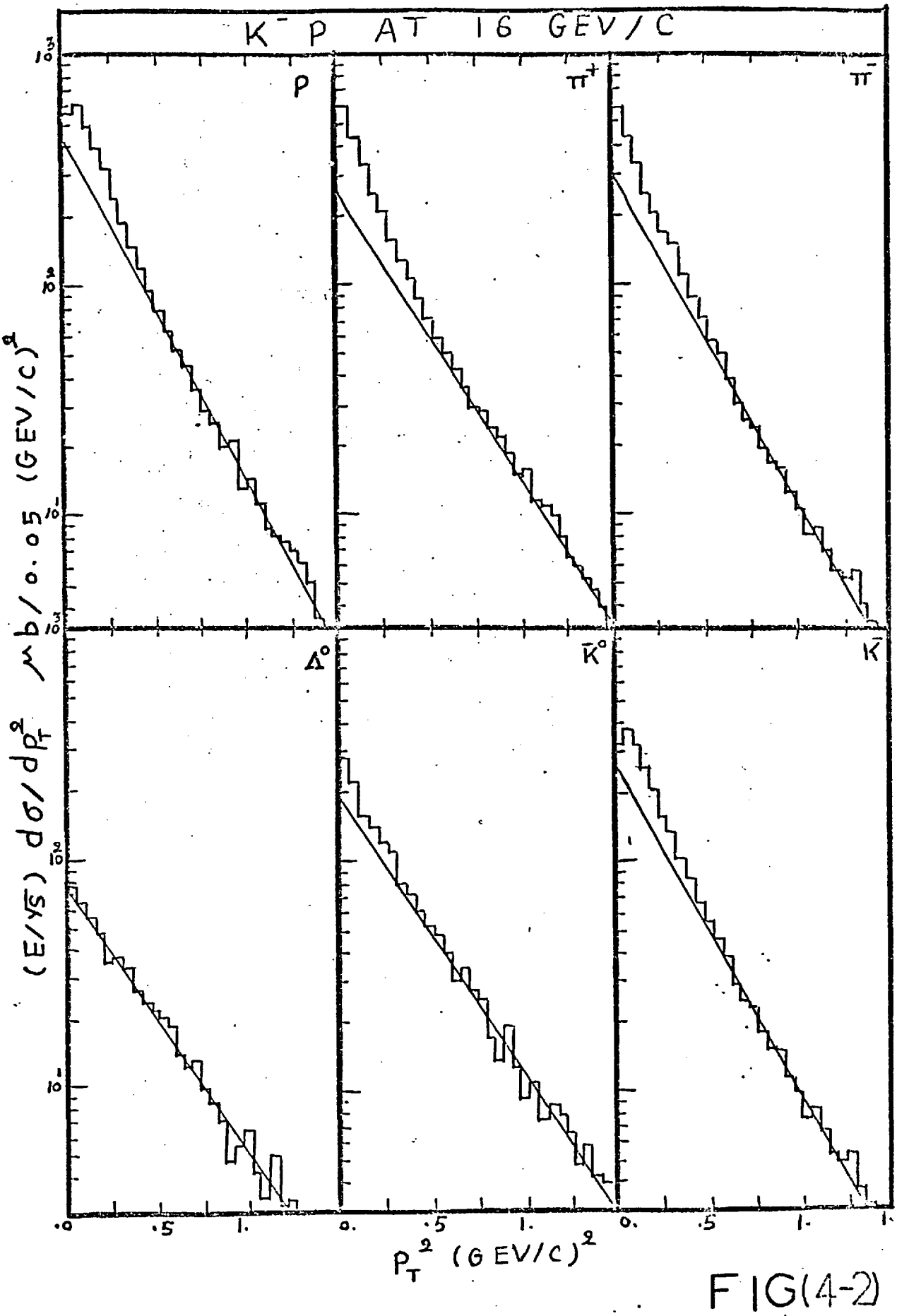

FIG(4-2)

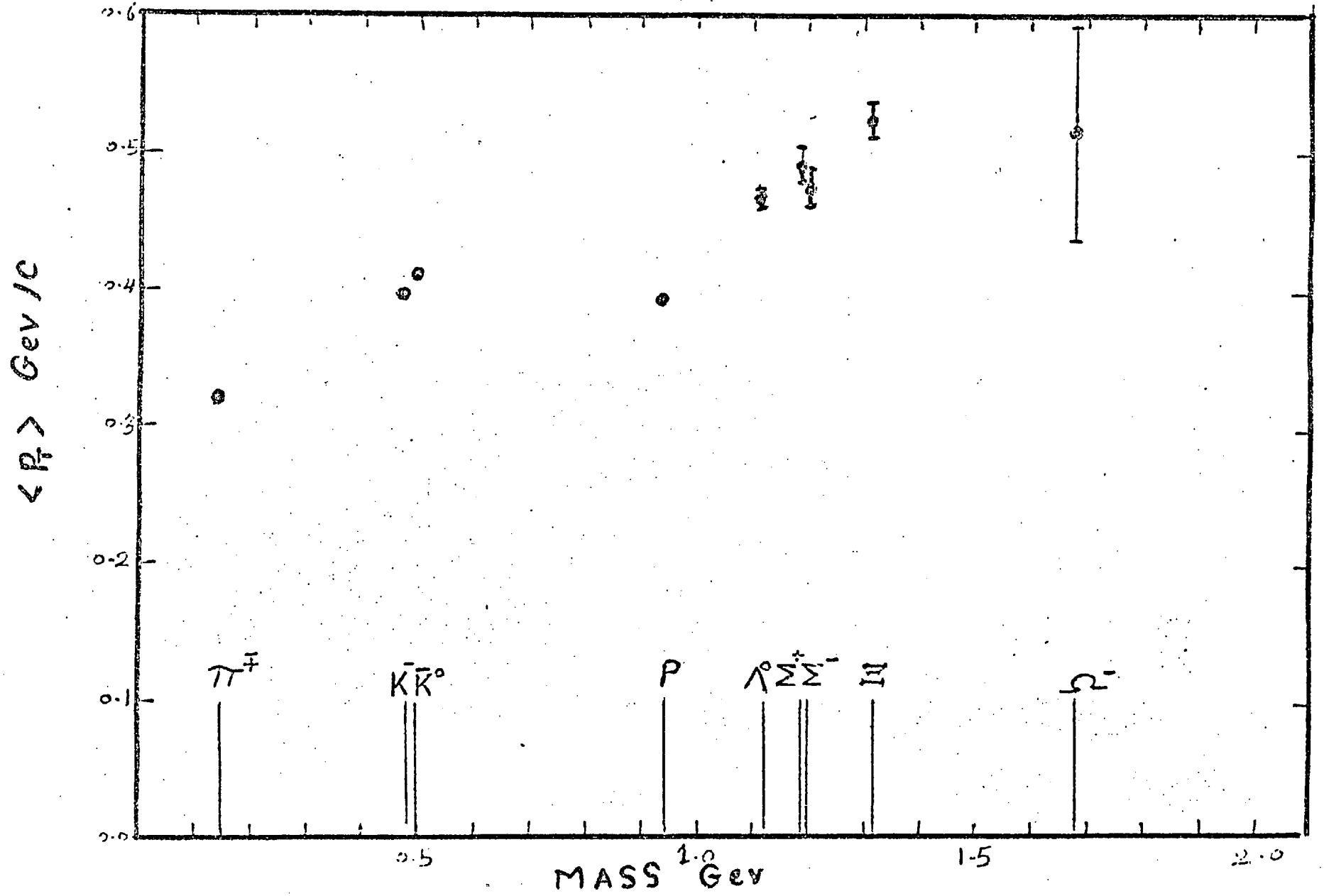
$\langle P_T \rangle$ Gev/c
0·6
0·5
0·4
0·3
0·2
0·1
0·0
$\pi^{\mp}$
$K\bar{K}^{\circ}$
P
$\Lambda^{\circ}\Sigma^{+}\bar{\Sigma}^{-}$
Ξ
Ω^{-}
0·5
1·0
1·5
2·0
MASS Gev

FIG(4-3)

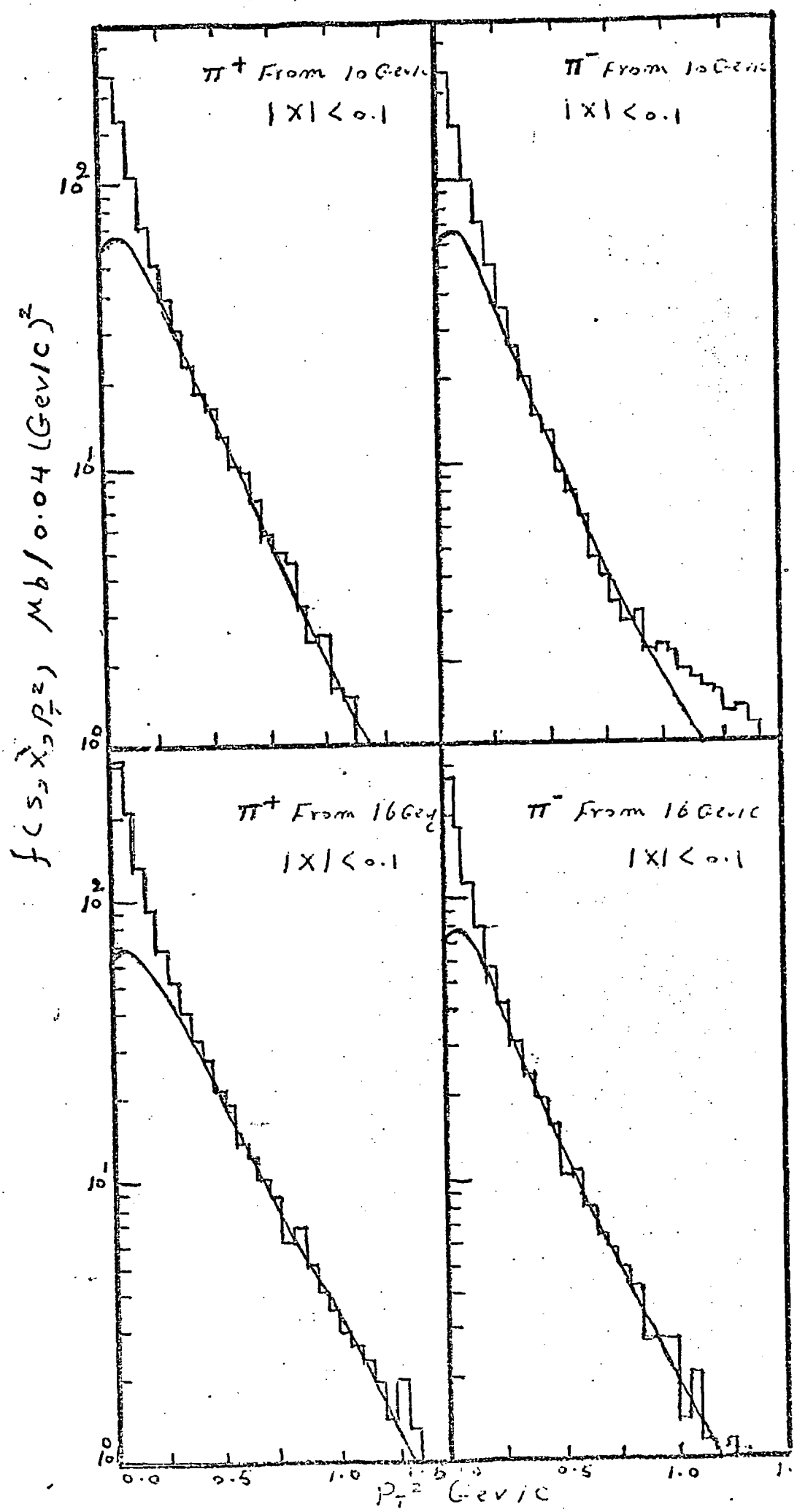
π⁺ From 10 Gev/c
|X| < 0.1
π⁻ From 10 Gev/c
|X| < 0.1
π⁺ From 16 Gev/c
|X| < 0.1
π⁻ From 16 Gev/c
|X| < 0.1
f(s, x, p_T²) Mb/0.04 (Gev/c)²
p_T² Gev/c
0.0
0.5
1.0
1.5

FIG(4-4)

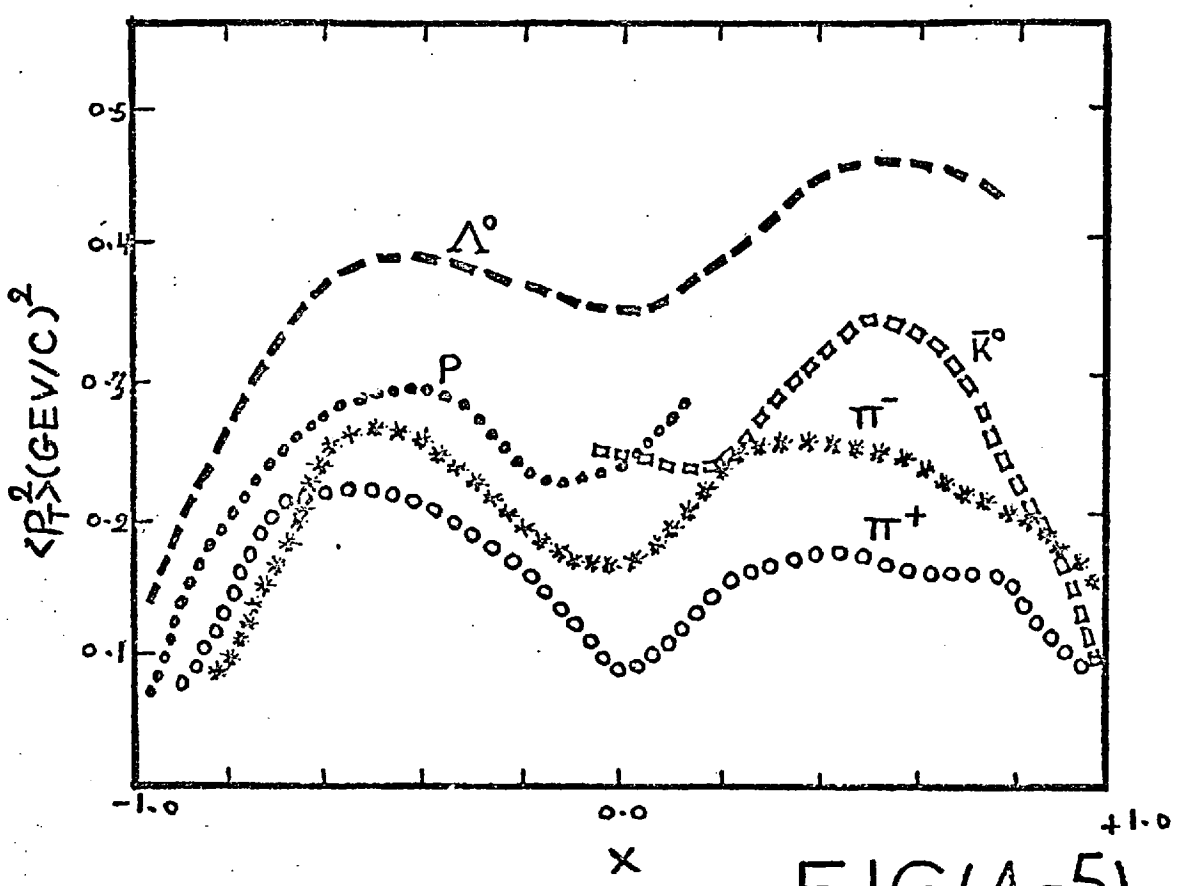
0.5
0.4
0.3
0.2
0.1
$\langle P_T^2 \rangle (GEV/C)^2$
Λ°
P
$\bar{K}^\circ$
π^-
π^+
-1.0
0.0
+1.0
X

FIG(4-5)

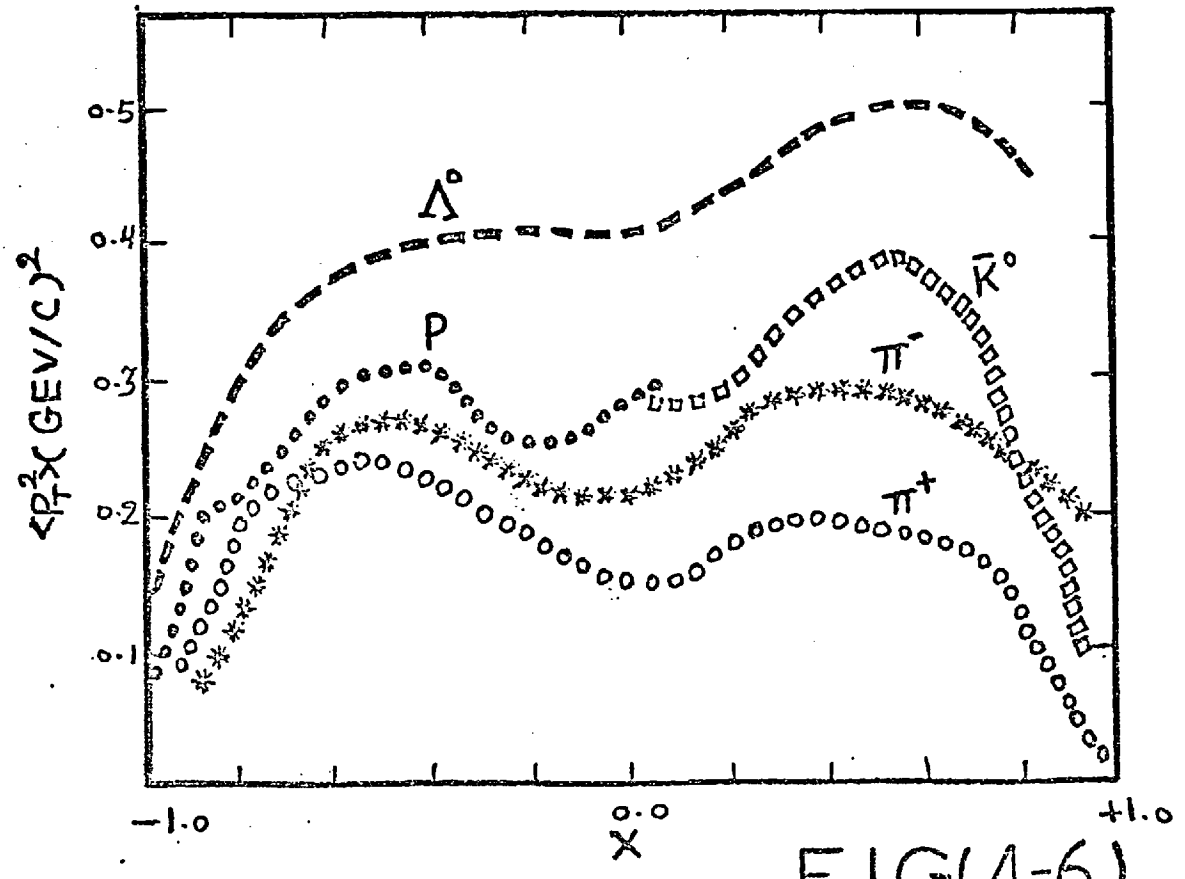
0.5
0.4
0.3
0.2
0.1
$\langle P_T^2 \rangle (GEV/C)^2$
Λ°
P
$\bar{K}^\circ$
π^-
π^+
-1.0
0.0
+1.0
X

FIG(4-6)

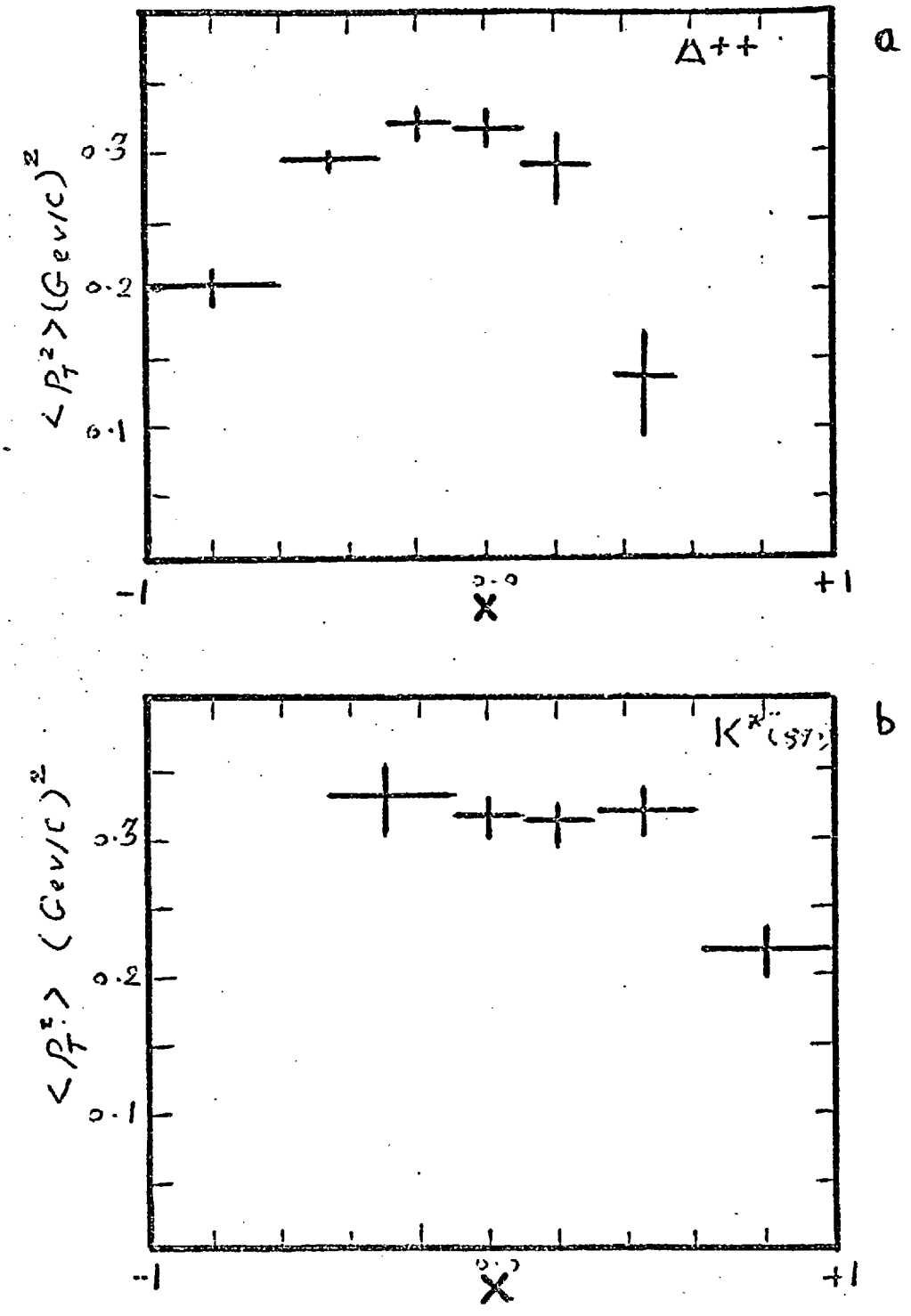
a
Δ++
$\langle P_T^2 \rangle (GeV/c)^2$
0.3
0.2
0.1
-1
0.0
+1
X
b
$K^{*0}(892)$
$\langle P_T^2 \rangle$ $(GeV/c)^2$
0.3
0.2
0.1
-1
0.0
+1
X

FIG(4-7)

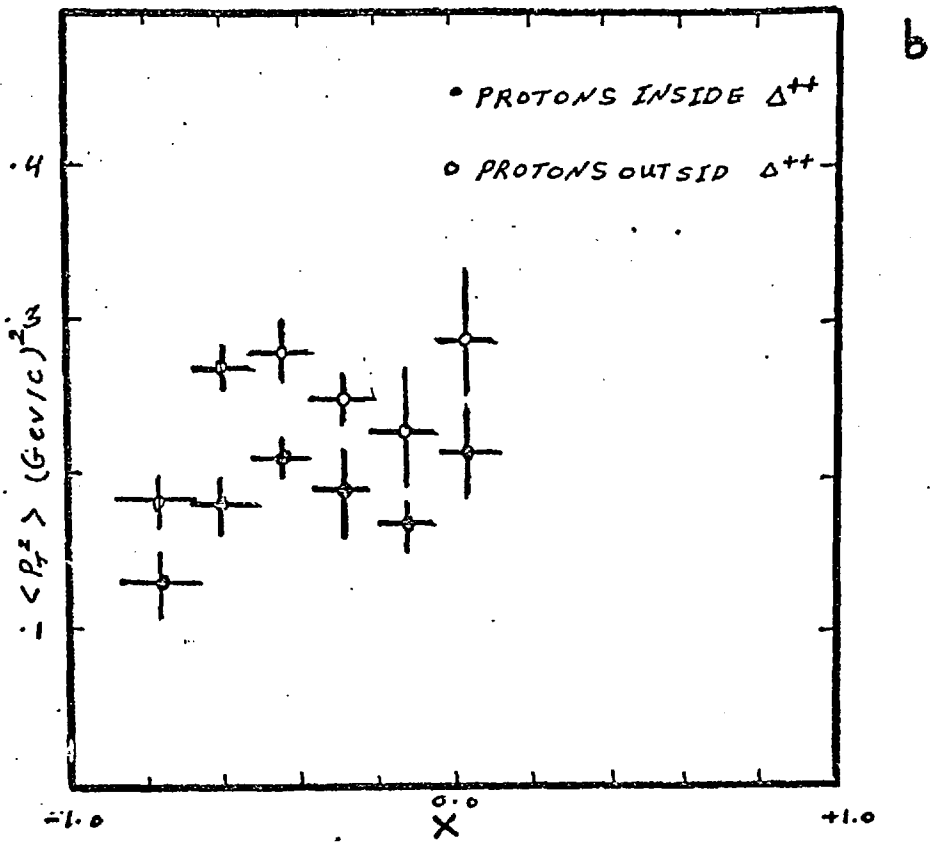
b
• PROTONS INSIDE Δ++
o PROTONS OUTSID Δ++
.4
$< P_T^2 >$ (Gev/c)^2
-1.0
0.0
+1.0
X

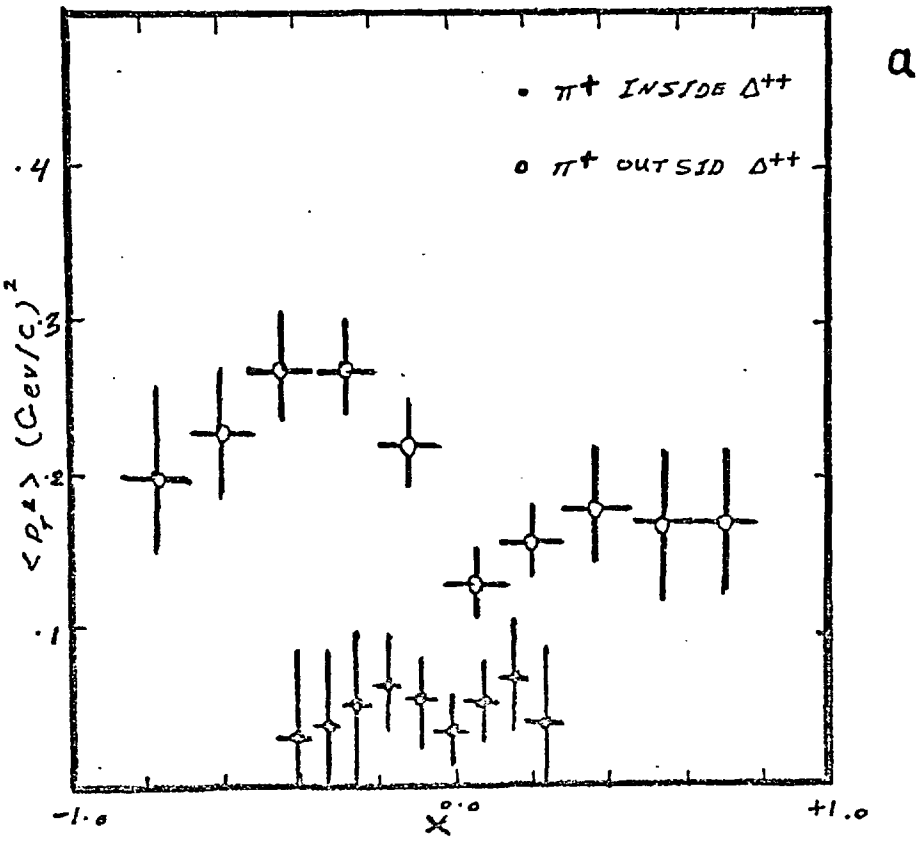
a
• π+ INSIDE Δ++
o π+ OUTSID Δ++
.4
.3
.2
.1
$< P_T^2 >$ (Gev/c)^2
-1.0
0.0
+1.0
X

FIG(4-8)

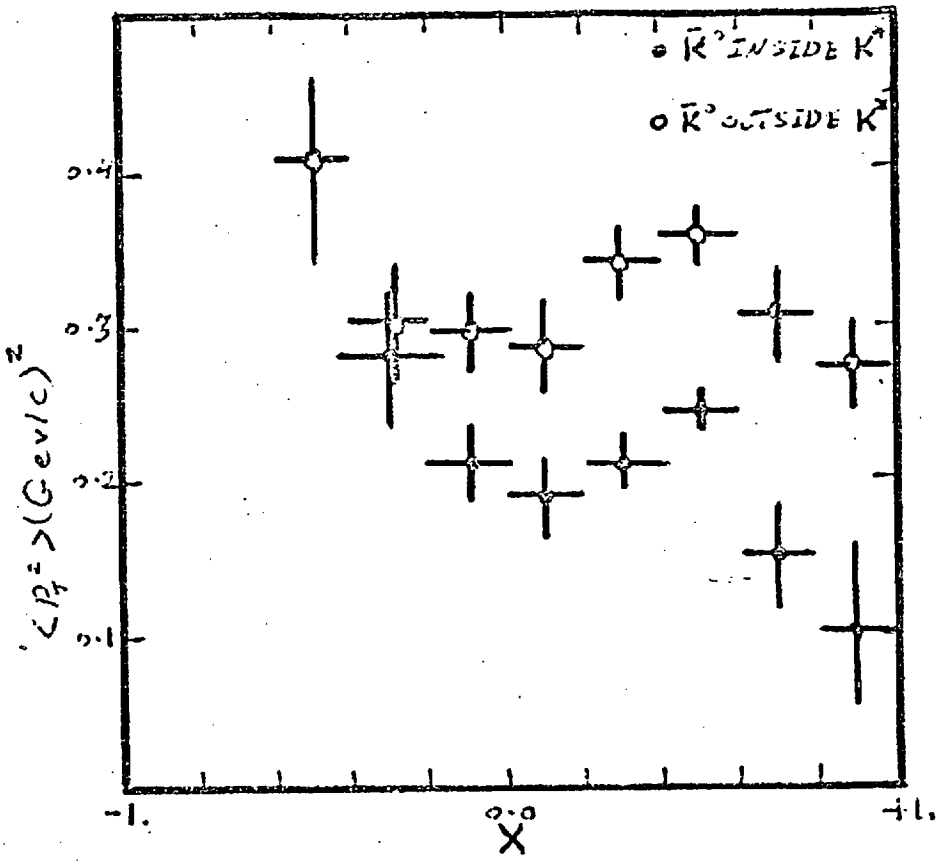
• $\bar{K}^0$ INSIDE K^*
o $\bar{K}^0$ OUTSIDE K^*
$\langle P_T^2 \rangle$ (Gev/c)^2
0.4
0.3
0.2
0.1
-1.
0.0
+1.
X

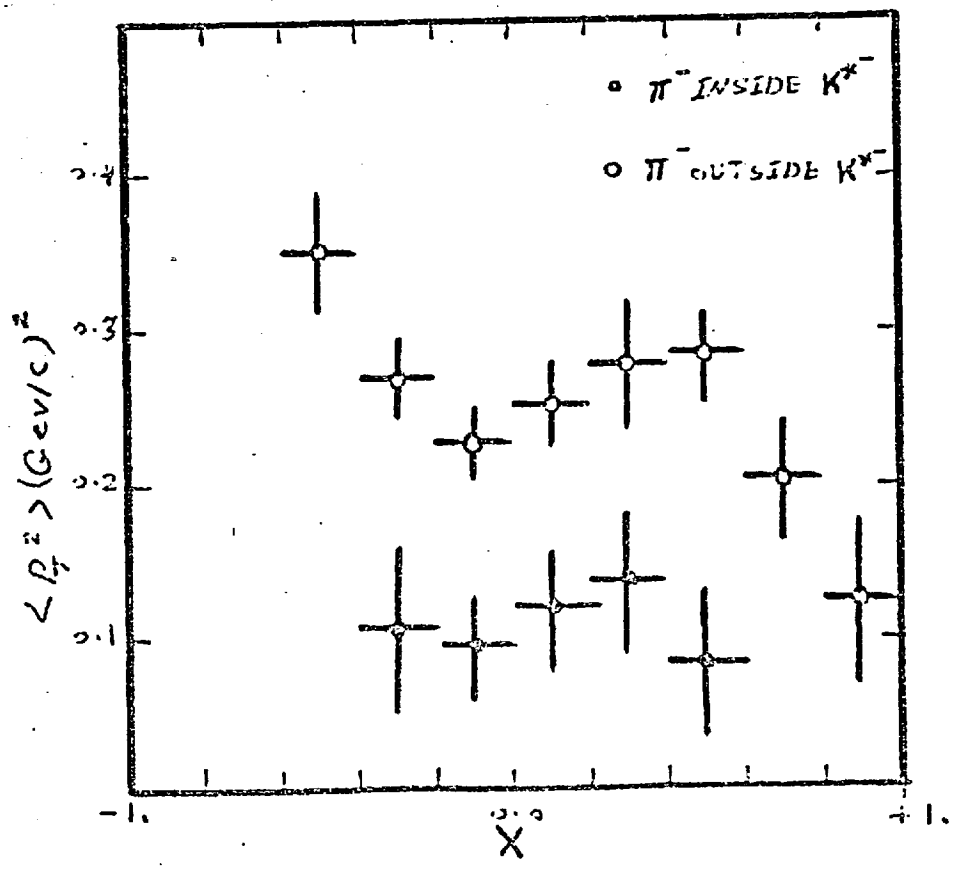
• π^- INSIDE K^{*-}
o π^- OUTSIDE K^{*-}
$\langle P_T^2 \rangle$ (Gev/c)^2
0.4
0.3
0.2
0.1
-1.
0.0
+1.
X

FIG(4-9)

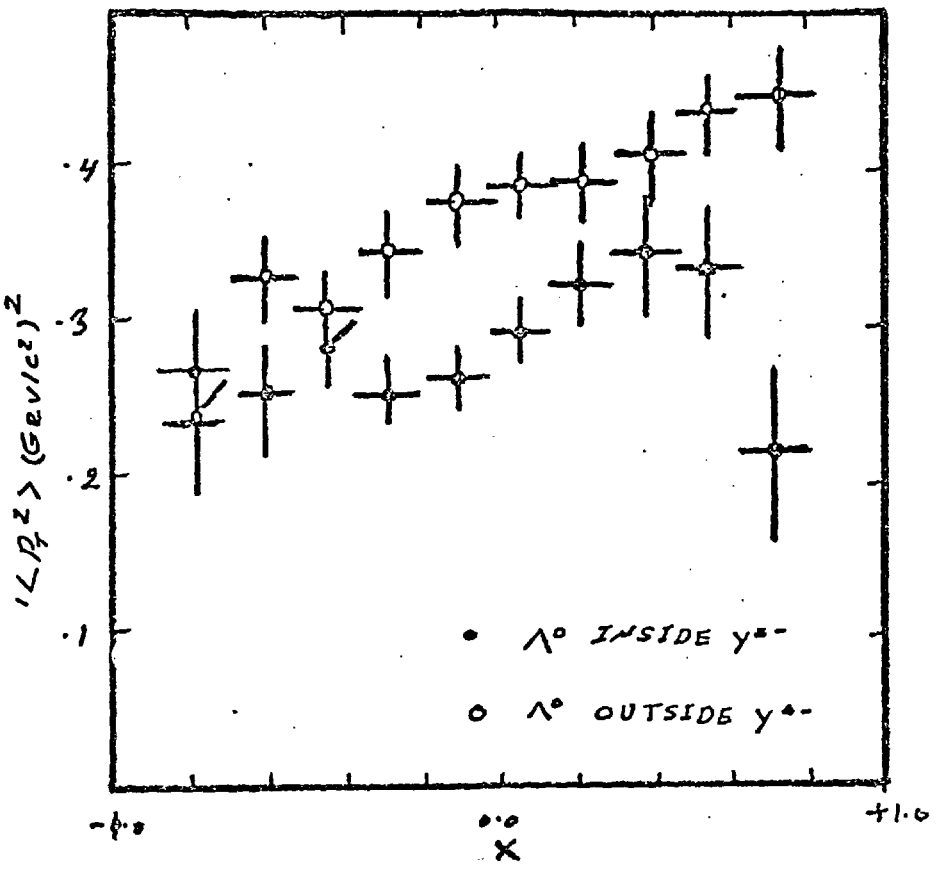
$\sqrt{\langle p_T^2 \rangle}$ (GeV/c)^2
.4
.3
.2
.1
• Λ^0 INSIDE y^{a-}
o Λ^0 OUTSIDE y^{a-}
-1.0
0.0
+1.0
X

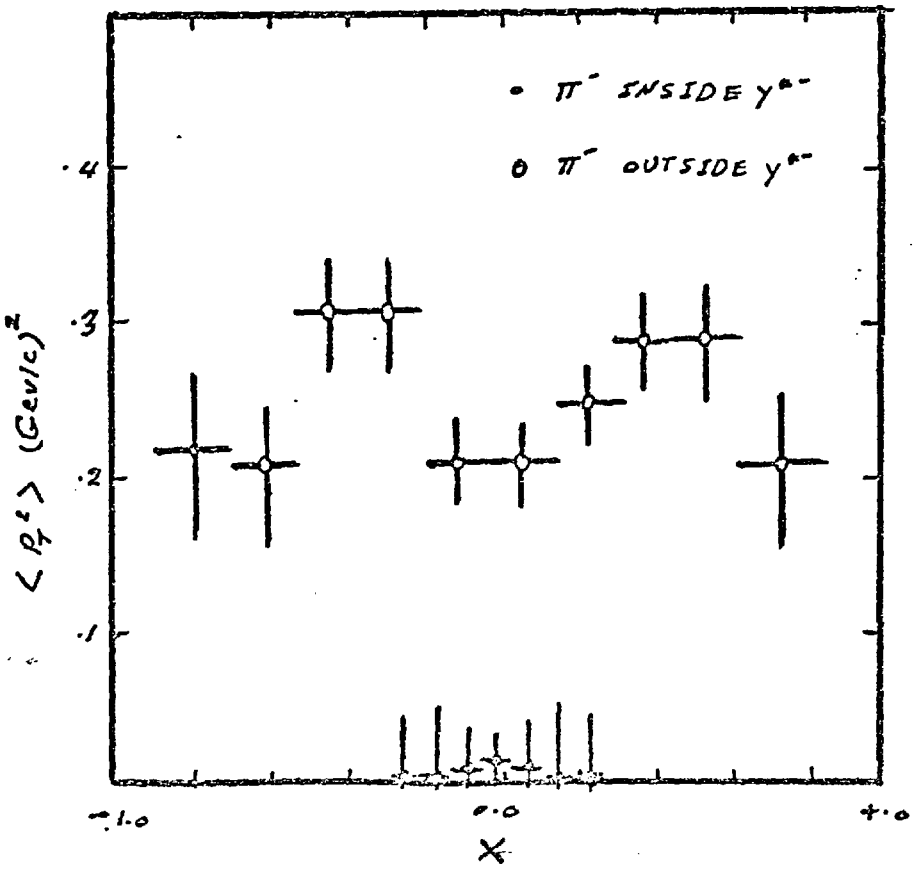
$\langle p_T^2 \rangle$ (GeV/c)^2
.4
.3
.2
.1
• π^- INSIDE y^{a-}
o π^- OUTSIDE y^{a-}
-1.0
0.0
+1.0
X

FIG (4-10)

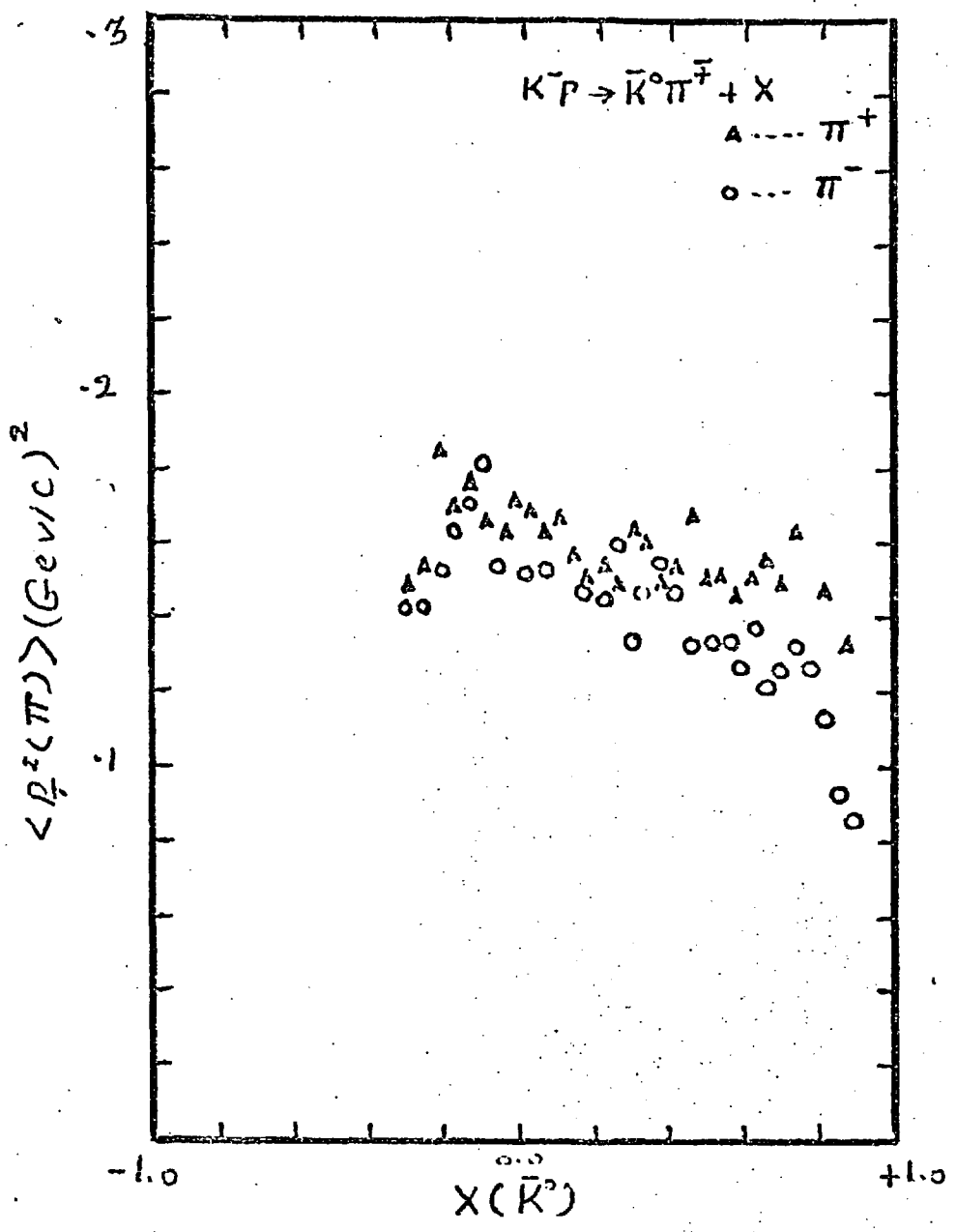
$K^- p \to \bar{K}^0 \pi^{\mp} + X$
π^+
π^-
$\langle p_T^2(\pi) \rangle (GeV/c)^2$
.3
.2
.1
-1.0
0.0
+1.0
$X(\bar{K}^0)$

FIG(4-11)

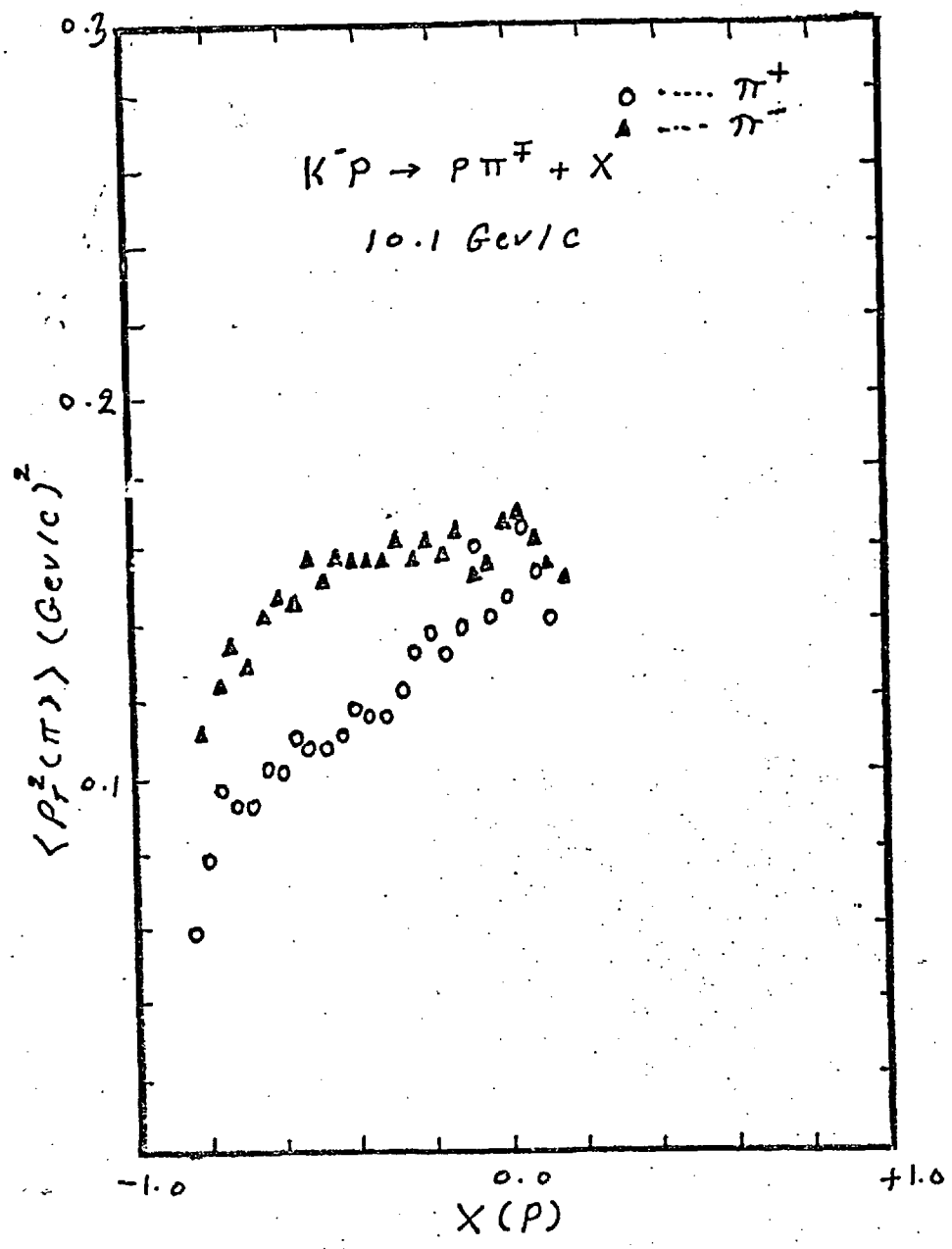
0.3
0.2
0.1
$\langle p_T^2(\pi) \rangle$ (GeV/c)^2
o ..... π^+
▲ ---- π^-
$K^- p \rightarrow p \pi^{\mp} + X$
10.1 GeV/c
-1.0
0.0
+1.0
X(P)

FIG(4-12)

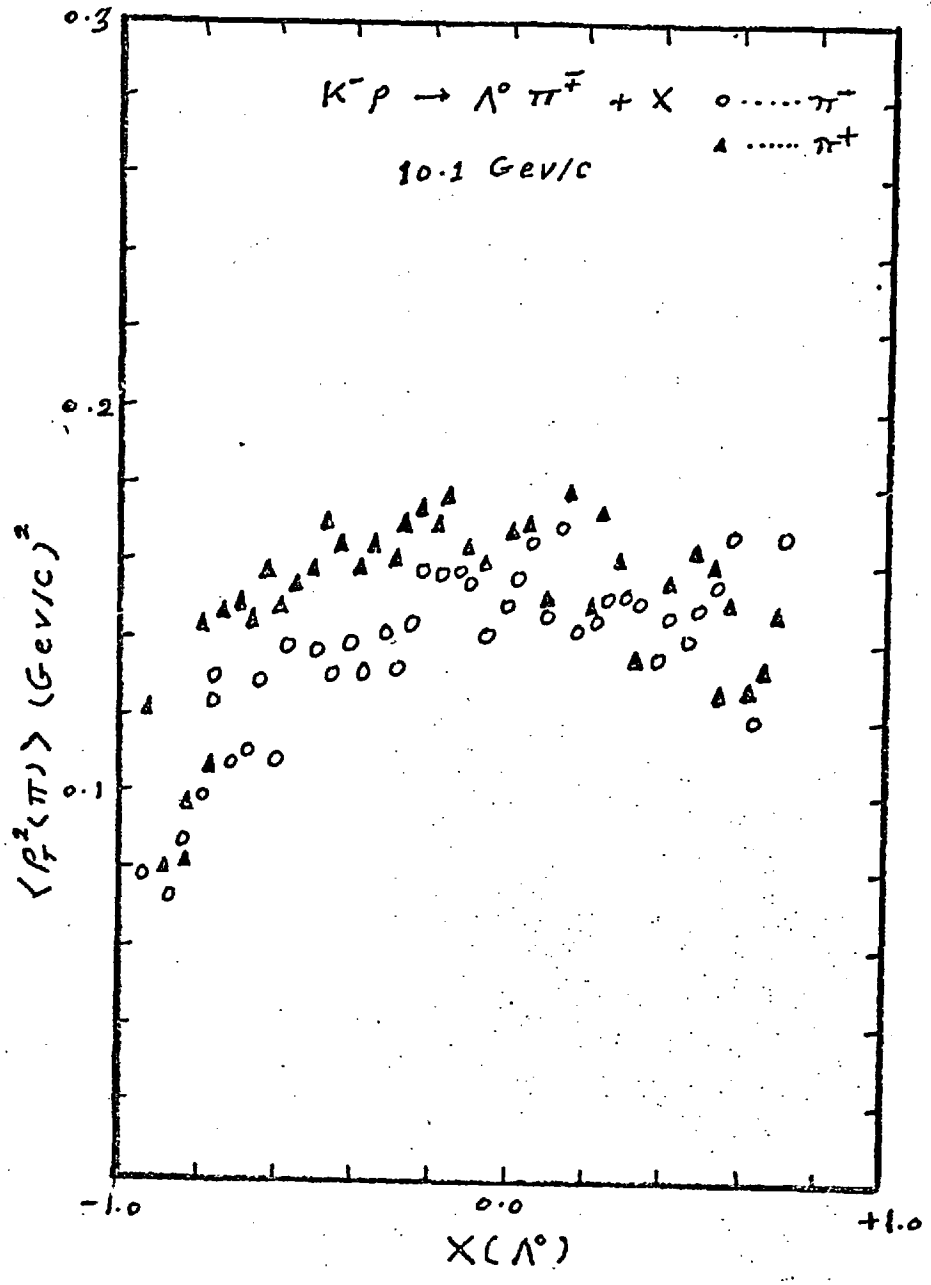
$K^- p \rightarrow \Lambda^0 \pi^{\mp} + X$
o ..... π^-
▲ ..... π^+
10.1 Gev/c
0.3
0.2
0.1
$\langle p_T^2(\pi) \rangle$ (Gev/c)^2
-1.0
0.0
+1.0
X(Λ^0)

FIG(4-13)

CHAPTER FIVE

$K^-P \rightarrow K^{*-}(890) + ANYTHING$

Inclusive Resonance Production

In the inclusive approach to the study of hadron-hadron interactions, it is tempting to study reactions of type (1.1) where particle c is a resonance rather than a stable particle. This type of study represents an intermediate step between single and two particle inclusive reactions. As noted in Chapter Four, reflections due to resonance production show themselves in single particle distributions and such reflections contribute to give two particle correlations. Therefore, the temptation to study resonance production specifically is not unjustified if one wants to understand the different aspects of high energy collisions in the framework of inclusive reactions.

It is not surprising that the amount of published work on this subject is small compared to what has been published on stable particle inclusive production. This is because the study of resonance production is more complicated than that for stable particles. In inclusive resonance analysis just as in exclusive analysis, the reliability of the data can be a decisive factor in one's chances of performing a successful study. For inclusives, the situation is worse because one has to sum over all channels which include the particular resonance under consideration, including those which are kinematically unconstrained, and this imposes severe restrictions on what one can do. The second problem is that one is technically limited to certain types of "clean" resonance where the signal to background ratio is not too small. This problem becomes very serious when one tries to study resonances, such as the ρ^0, which can be formed from many combinations of particles. In this case, for example, one may need to consider up to twenty-five combinations in some ten pronged

events. Of course not all these combinations can contribute to the ρ^0 and consequently will form a major contribution to the background. When an effective mass plot for all these combinations was produced the ρ^0 region was observed as a very broad bump over a wide range of effective mass.

The theoretical situation with this type of study is again not very clear. Although it is in principle true that all of the predictions that do exist concerning single particle production can be used to describe resonance inclusive production, they cannot be fully exploited because they are either of a very general nature or are restricted to a small region of phase space where the errors on the data are too large to perform a fruitful comparison of theory with experiment. However, there exists some demand by many theoretician authors for data not only on single particle distributions but on resonance inclusives as well[1,2].

In spite of the above problems, inclusive resonance analysis can add a new dimension to the inclusive approach because of the valuable information it provides about exchange mechanisms through the study of decay angular distributions yielding spin space density matrix elements, which, in general, single stable particle analysis does not provide.

In our experiments if one takes into account all the above factors, one is left with two resonances about which useful data can be produced. The first one is the $K^{*-}(890)$ and the second is the $\Delta^{++}(1236)$ resonance and an inclusive study of these is presented in this chapter and the next.

$K^{*-}(890)$ Total Cross Section

Here we give the values of the total cross-sections for inclusive K^{*-} production at 10 and 16 GeV/c. These values have been calculated from the effective mass plots of $\bar{K}^0\pi^-$ combinations. Before doing so, one

has to account for the background under the resonance. This was done by subtracting from the $\bar{K}^0\pi^-$ effective mass plot the $\bar{K}^0\pi^+$ effective mass spectrum. In the latter case one does not expect K^* production in the mass plot. However, because there are some events where the seen decay corresponds to a K^0 rather than a $\bar{K}^0$, there is a signal in the resonance region. This bias has been estimated to be about 10% for K^-p at 14.2 GeV/c[3]. Consequently, the $\bar{K}^0\pi^+$ effective mass plot was scaled by a factor of 0.9. The dotted lines on fig. (5-1) correspond to the background expected using this technique.

The results of such subtractions are shown on the same figure. These show a clear K^* signal.

The values of the cross-sections were estimated by counting events in the K^{*-} region in the plots whose backgrounds have been subtracted.

The values of the cross-sections are given in table (5-1) for both beam momenta. In the same table the value of the cross-section at 8.2 GeV/c is given[4]. These values show a cross section which tends to remain constant with increasing incident energy.

Production Features

The x distributions for K^*'s produced at our two energies are shown in fig. (5-2). Although most K^*'s are produced in the forward direction in both cases, no strong forward peak near x = 1.0 is observed. This can be taken as an indication of the lack of K^* production through diffractive dissociation. The distribution peaks at both energies at a value of x of about 0.3 and then falls rapidly as x increases. This leads one to expect that the leading trajectories are mainly those of the p, A_2, ω, f in addition to π exchange.

When one compares the distributions of fig. (5-2) with the corresponding ones for K^{*+} produced from K^+p [5] interactions one observes that the distribution in the latter case is flatter in the

positive x region with a pronounced peak near x = 1 in contrast with our results.

The t distributions in fig. (5-3) are very similar to those for K^{*+}. The missing mass distributions in fig. (5-4) show a one bin peak coming from the exclusive channel $K^- p \rightarrow K^{*-} p$. It is interesting to note that the height of this peak at 16 GeV is about 75 microbarns, which is well below the values obtained for the exclusive cross section of this channel at lower energies. This value is in good agreement with the prediction of the Gribov-Morrison[6] rule for the variation of the cross section of this channel with the lab momentum of the incident beam. This does not support the value obtained for this cross section from the RHEL $K^- p$ experiment at 14.2 GeV/c [7] which shows some flattening effect in the cross section.

The distributions of squared transverse momentum in fig. (5-5) can be well represented by a simple exponential parametrization. These distributions do not possess a higher population density near $p_T^2 = 0$ which has been observed in single particle distributions.

Decay Angular Distributions

It is well known that the study of decay angular distributions in a frame of reference where the resonance is considered to be at rest, such as the Jackson frame, can yield useful information about the exchange mechanism in exclusive channels in which the resonance is produced.

If one argues that there exists some kind of similarity between the quasi two body reaction of the form

$$a + b \rightarrow a' + b' \qquad (5.1)$$

where in this case a' is a decaying resonance, then one might think of using the same technique to study the inclusive exchange mechanism.

However, the technique may not be applied in such a straightforward manner. This is because in the quasi two body case the resonance under study is usually recoiled from another particle or resonance which is a definite angular momentum state, while in the inclusive case the recoiling mass "anything" is a mixture of defined and undefined angular momentum states. Thus one does not expect that such analysis can yield the same information which one can get from a quasi two body analysis.

To get some insight about the extent to which the analogy between the two cases can be carried, let us consider the basic definition of an inclusive resonance cross section

$$d\sigma(a + b \to a' + X) = \sum_i d\sigma(a + b \to a' + X_i) \tag{5.2}$$

where X_i is a given set of particles specified in number and type. It is clear that X_i is not a well defined angular momentum state, but is a mixture of many possible states. Taking into account all such states q_j of the particular state X_i then relation (5.2) may be rewritten as

$$d\sigma(a + b \to a' + X) = \sum_i \left| \sum_j F_{ij} \right|^2 \tag{5.3}$$

where F_{ij} is the amplitude for producing a state X_i with quantum numbers q_j. From this one would not expect the density matrixelements to satisfy the relation

$$\rho_{\lambda\lambda'} = (-1)^{\lambda-\lambda'} \rho_{-\lambda, -\lambda'} \tag{5.4}$$

for a particular n body final state with $n > 2$. However, Ader, Meyer and Salin (AMS) [19] pointed out that when one integrates over all i to find the inclusive cross section, one finds out the relation (5.4) is

satisfied. Furthermore, they showed that all quantities which are measurable in the quasi two body case are measurable in the inclusive case as well with the same relations for the decay probability distributions derived for the former case.

Consequently, the decay angular distributions in θ and ϕ in the Jackson [8] frame have been calculated. The Jackson frame is defined as the resonance rest frame with the z direction taken as the incident beam direction. The X-Y plane has been defined by the direction of the momentum of the recoiling mass and the normal to this direction and the beam direction. A schematic diagram of this frame and the definitions of θ and ϕ are given in fig. (5-6).

In this frame the angular distribution function for a spin one resonance is given by [9]

$$W(\cos\theta,\phi) = \frac{3}{4\pi}\left[\tfrac{1}{2}(1-\rho_{00}) + \tfrac{1}{2}(3\rho_{00}-1)\cos^2\theta - \rho_{1,-1}\sin^2\theta\cos 2\phi - \sqrt{2}\,\mathrm{Re}\,\rho_{10}\sin^2\theta\cos\phi\right]. \qquad (5.5)$$

Angular Distributions Versus the Missing Mass and t

The distributions in the Jackson angles for different regions in the missing mass variable for the $K^*(890)$ produced in the 10 GeV/c data are shown in fig. (5-7). The first thing one may notice in this figure is the change in shape of the Cos θ distribution between the first two mass intervals. This effect is not very surprising because, through the introduction of such a mass cut, one is actually selecting on those exclusive events where the K^{*-} is produced with the proton. This channel is known to be dominated by natural parity exchange. However, what is interesting is the continuation of the general trend to show more unnatural parity exchange for higher values of missing mass.

For higher values of missing mass one notices that the ϕ angular distribution is no longer symmetric. This may be explained because the

$K\pi$ combinations selected with a simple mass cut is not a pure 1^- object for such high values of missing mass. This type of asymmetry is not unexpected from AMS calculations and they expect this kind of behaviour after integrating over all quantum numbers in the missing mass.

When one studies these angular distributions as a function of t integrating over all values of missing mass in fig. (5-8) one observes that there exists a gradual change of the exchange mechanism when we go to higher values of t. Again here one observes that there is some degree of asymmetry in the ϕ distributions, due to the overall integration over the missing mass. Natural parity exchange tends to be stronger for smaller values of t, being replaced by unnatural parity exchanges at a higher value of t.

Decay Angular Distributions versus X and p_T^2

Although the momentum transfer and missing mass variables are the ones which are in common use to study angular distributions and density matrix elements in quasi two body reactions, one tends to favour the pair of x and p_T^2 when dealing with inclusives. This is mainly because by using the latter set of variables one reduces biases produced by mass cuts which might select particular exclusive channels rather than producing simple kinematical cuts on the whole inclusive cross section. Here we are going to demonstrate that there exists some dependence of decay angular distributions on x and p_T^2 only.

In figs. (5-9) we studied the angular distributions versus the variable p_T^2 for three regions in x. It can be observed that in both regions where x is positive there exists a gradual change of the exchange mechanism depending on the values of p_T^2. For the lowest bins in p_T^2 one observes that we get more unnatural parity exchange, decreasing as we go toward higher values of p_T^2. High values of $|x|$ serve as mass cuts of small missing masses with the advantage of selecting on forward and

backward moving K^*'s separately without biasing the sub sample severely with a particular type of exclusive events.

For values of x which are negative one cannot draw any conclusions about the nature of the exchange mechanism. When the $K\pi$ effective masses were plotted for these events the signal to background ratio was observed to be very small. This indicates that cuts in x can serve the purpose of reducing background.

Density Matrix Elements

Depending on the results of AMS which suggest that relation (5.4) is, indeed, a correct relation for describing the decay angular distribution of a spin one particle in its centre of mass we used this relation to calculate the spin density matrix elements for the K^* resonance. The method used here is the method of moments where the density matrix elements are given by

$$\rho_{oo} = \tfrac{1}{2}(5\,\overline{\text{Cos}\,\theta^2} - 1)$$

$$\rho_{1,-1} = -\frac{5}{4}\,\overline{\text{Sin}^2\,\theta\,\text{Cos}\,2\phi}$$

$$\text{Re}\,\rho_{10} = -\frac{5}{4\sqrt{2}}\,\overline{\text{Sin}^2\,\theta\,\text{Cos}\,\phi}$$

In fig. (5-10) we show these density matrix elements computed in different regions of t' and M_X. It is apparent that values of both $\rho_{1,-1}$ and Re ρ_{10} are consistent with zero over a wide range of values of M and t within the statistical error bars.

For the smallest t bin the values of ρ_{oo} are increasing with increasing values of M_X. Starting from zero for the lowest bin in M_X which corresponds to the $K^-p \to K^{*-}p$ channel, up to values which are slightly less than one for $M_X \approx 1.4$ GeV for values of M_X above this range the values

seem to have some structure. It is interesting that the same type of behaviour has been observed for K^{*+} produced in K^+p interactions [5]. The selection on our data was done in such a way as to allow comparison between the two cases. The same kind of behaviour is followed for higher values of ρ_{00} but to a less significant degree.

From this one may conclude that natural parity exchange dominates in the region of small M_x and t. For higher values of t and M_x where more pions are being produced unnatural parity exchange tends to be the main contribution to the exchange mechanism.

The dependence of these density matrix elements on x and p_T^2 is shown in fig. (5-11). In this case one observes from fig. (5-11-b) that the values of $\rho_{1,-1}$ are increasing with increasing x and p_T^2. K^* moving fast in the forward direction with large transverse momenta have the highest values of $\rho_{1,-1}$ of about 0.25. All events with $p_T^2 \approx 0$ have $\rho_{1,-1} \approx 0$ and the values of $\rho_{1,-1}$ are decreasing with decreasing x and p_T^2. The values of $\rho_{1,-1}$ for backward moving K^*'s are comparable with zero for all values of p_T^2.

No indication of values of Re ρ_{10} which are different from zero can be deduced from fig. (5-11-c), indicating that ρ_{10} is largely imaginary.

The same conclusion that has been drawn from the study of decay angular distribution versus p_T^2 can be deduced from the study of ρ_{00} in fig. (5-11-a). In all three regions of x the values of ρ_{00} are highest for very small values of p_T^2 which indicate a larger contribution of unnatural parity exchange for these p_T^2 values. This contribution decreases with increasing p_T^2 values where ~~pion~~ natural parity exchange tends to take over.

Comparison with a Dual Resonance Model

The model with which we are going to compare our experimental values of the $K^*(890)$ density matrix elements has been formulated by Randa[10]. Mueller's generalised optical theorem is used in this model to express

the two body inclusive cross section in terms of the discontinuity in the 4-4 amplitude. In this type of model n - n amplitudes are represented by β functions. This model uses the assumption that the reaction

$$a + b \rightarrow R + \text{anything}$$
$$\hookrightarrow c + d$$

to be a special case of two particle inclusive reactions. In the dual resonance framework these reactions are related through the optical theorem to the 4-4 amplitude which is assumed to have a β_8 behaviour. In this special case where particles c and d are decay products of the resonance R, this β_8 function can be expanded to a linear combination of β_6's because of cancellation of contributions from many dual diagrams. In this model only contributions from the diagrams of fig. (5-12) are considered. Another major assumption used in this model is that all trajectories are linear and in the actual numerical calculations all trajectories are taken to be equal to the π trajectory. This was justified in two ways. First, because the model is mainly concerned with some features of the production process at a fixed energy, such as the p_T^2 distribution and density matrix elements, rather than with the energy dependence of these features, Randa argues that one can tolerate having all trajectories to have zero intercepts even that of the pomeron. The second argument is that the model tries to impose scaling in an explicit form by normalizing the cross section to ab total cross section to allow for scaling even with the pomeron intercept being zero.

After reducing the β_8 mathematical form to a linear combination of β_6 functions, using only those dual resonance diagrams which are assumed to contribute to the fragmentation region of a, and performing detailed

mathematical and numerical calculations using the meson trajectory as the only trajectory, the model predicts a transverse momentum distribution, and also uses the explicit relation derived by Mueller[11] to relate the spin density matrix elements to the discontinuity in the three to three amplitude. This relation is given by

$$\rho_{\lambda\lambda} = \frac{1}{N} \text{Disc}_{M_X^2} \langle a\ b\ \bar{R}\ (\lambda)|T|a\ b\ \bar{R}\ (\lambda)\rangle$$

where

$$N = \sum_{\lambda} \text{Disc} \langle a\ b\ \bar{R}\ (\lambda)|T|a\ b\ \bar{R}\ (\lambda)\rangle \quad .$$

One can very easily see that the spin density matrix constructed from the density matrix elements defined above does, indeed, satisfy the trace condition.

The solid lines on fig. (5-13) and fig. (5-14) show the predicted behaviour of the two density matrix elements ρ_{00} and Re ρ_{10} with t' for two regions of M_X^2/s given by M_X^2/s = 0.1 and 0.2. The data points on those two figures are the experimental values of the density matrix elements calculated for the corresponding values of M_X^2/s which were chosen to be between 0.05 - 0.15 and 0.15 - 0.25 for the particular t bins shown in the figures. It may be noted here that in the above mass cuts the channel $K^- p \to K^* p$ has been excluded automatically. This channel is known to be dominated by natural parity exchange.

We note that in both figures the data are not in very good agreement with the predictions of the model. The values of ρ_{00} measured are substantially lower than the corresponding predicted ones for the small t region especially for the lower range of M_X^2/s values. This difference between the two tends to be reduced in the higher range of M_X^2/s values, but the values of ρ_{00} are still far below the ones expected from the

model. No evidence of a pronounced dip in ρ_{00} near $t' = 0.7$ GeV^2 can be observed.

The situation with Re ρ_{10} is no better and there is a substantial amount of disagreement between the measured and predicted values of this quantity over a wide range of t' and for both M_X^2/s ranges.

This disagreement is not too surprising. For this model not only suffers from the weakness that it does not satisfy unitarity (because it has been built on the β's Veneziano type amplitudes which all have this problem), but furthermore it involves severe constraints on the type of the exchanged trajectories. Such constraints may not produce substantial problems when tested against p_T^2 distributions but one would certainly expect their effect to be more noticeable when dealing with density matrix elements. This is because we know that our K^*'s are not produced by a process of pure pion exchange but that there is a noticeable amount of natural parity exchange as well. In such a case one needs to feed in more realistic trajectories to be able to take into account contribution from such exchanges.

The other problem with this model is that the pomeron is introduced in a rather artificial way. In order to do this in a natural way one needs to consider more dual diagrams in addition to those of fig. (5-12). These dual diagrams would each contain more than one quark loop. This will avoid the problem of having to normalize by σ_T to take care of the scaling part of the amplitude.

However, this comparison may be useful in the sense that it gives us some idea about the possible sensitivity of dual resonance models to changes in the trajectories used. Such sensitivity is difficult to obtain when the predictions of such models are compared with the data using quantities other than spin density matrix elements, such as longitudinal and transverse momentum distributions, which seem to be well described by most models of this type without much dependence on the kinds of trajectories used in the actual calculations.

Conclusions

In this chapter, data on K^{*-} inclusive production have been presented. These include the study of the dependence of the total production cross section on energy. The study of the x distributions does not give any strong evidence of a forward diffractive peak. The study of decay angular distributions and density matrix elements shows that there is a substantial amount of natural parity exchange in addition to unnatural exchange. Comparison with a dual resonance model was carried out. Although this model does provide a good exponential parametrization of the p_T^2 distribution, the predictions concerning the variation of ρ_{00} and Re ρ_{10} with M and t were not compatible with our data. This might be due to the fact that this model substitutes the π trajectory for all others in the actual numerical calculation. Furthermore, the pomeron was not introduced in the proper sense.

REFERENCES (5)

1. E.L. Berger, ANL Preprint, ANL/HEP 7134 (1971).
2. L. Masperi and C. Rebbi, CERN Preprint, TH-1526, CERN (1972).
3. K. Paler et al., RHEL-Paris-Saclay Collaboration, RPP Preprint, to be published in Physics Letters.
4. Athens-Democritus-Liverpool-Vienna Collaboration, Nucl. Phys. B58, 178 (1973).
5. P. Chliapnikov, O. Czyzewski, Y. Goldschmidt-Clermont and M. Jacob, Nucl. Phys. B37, 336 (1971).
6. D.R.O. Morrison, Phys. Rev. 165, 1699 (1968).
7. R. Barloutaud et al., Phys. Letters 38B, 257 (1972).
8. K. Gottfried and J.D. Jackson, Nuovo Cimento 33, 309 (1964).
9. N. Schmitz, Proceedings of the 1965 CERN Easter School, CERN Yellow Report, CERN 65-24.
10. J. Randa, University of Illinois Preprint, ILL-(TH)-72-11.
11. A.H. Mueller, Phys. Rev. D2, 2963 (1970).
12. J.P. Ader, C. Meyers, Ph. Salin, Universite de Bordeaux I Preprint PTB-47 (1972).

TABLE CAPTION (5)

(5-1) Inclusive total cross section for the reaction $K^- p \to K^{*-}$ + anything at three different energies.

TABLE (5-1)

$K^- p \rightarrow K^{*-} + X^+$	
P_{Lab} GeV/c	σ mb
8.25	2.4 ∓ 0.3
10.1	2.0 ∓ 0.5
16	2.5 ∓ 0.5

FIGURE CAPTIONS (5)

(5-1) Effective mass distribution for $\bar{K}^0\pi$ systems at 10 and 16 GeV/c. The solid lines represent the inclusive cross section for $\bar{K}^0\pi^-$ system. The dotted lines represent the inclusive cross section for $\bar{K}^0\pi^+$ system. The shaded area is the result of subtraction of the $\bar{K}^0\pi^+$ distribution from the $\bar{K}^0\pi^-$ distribution.

(5-2) X distributions for K^{*-} inclusive production from K^-p at

(a) 10 GeV/c

(b) 16 GeV/c.

(5-3) t distributions for K^{*-} inclusive production from K^-p at

(a) 10 GeV/c

(b) 16 GeV/c.

(5-4) Missing mass distributions for the reaction $K^-p \rightarrow K^{*-}$ + anything at

(a) 10 GeV/c

(b) 16 GeV/c.

(5-5) Squared transverse momentum distribution for K^{*-} inclusive production from K^-p at

(a) 10 GeV/c

(b) 16 GeV/c.

(5-6) Schematic diagram of the Gottfried-Jackson[8] frame defining the angles θ and ϕ.

(5-7) Cos θ and ϕ decay angular distributions for $K^{*-}(890)$ for different missing mass regions.

(5-8) Cos θ and ϕ decay angular distributions for $K^{*-}(890)$ for different values of t.

(5-9) Cos θ and ϕ decay angular distributions for $K^{*-}(890)$ versus p_T^2 in three different x regions.

(5-10) Values of ρ_{00}, $\rho_{1,-1}$ and Re ρ_{10} plotted against $t' = (t - t_{minimum})$ for different regions of the missing mass.

(5-11) ρ_{00}, $\rho_{1,-1}$ and Re ρ_{10} plotted against p_T^2 for different x regions.

(5-12) Dual resonance diagrams used in ref.(11) to construct the 3-3 amplitude for vector resonance inclusive production.

(5-13) Comparison of the values of ρ_{00} for K^{*-} decay from our 10 and 16 GeV/c data with predictions of ref.(11).

(5-14) Comparison of the values of Re ρ_{10} for K^{*-} decay from our 10 and 16 GeV/c data with predictions of ref.(11).

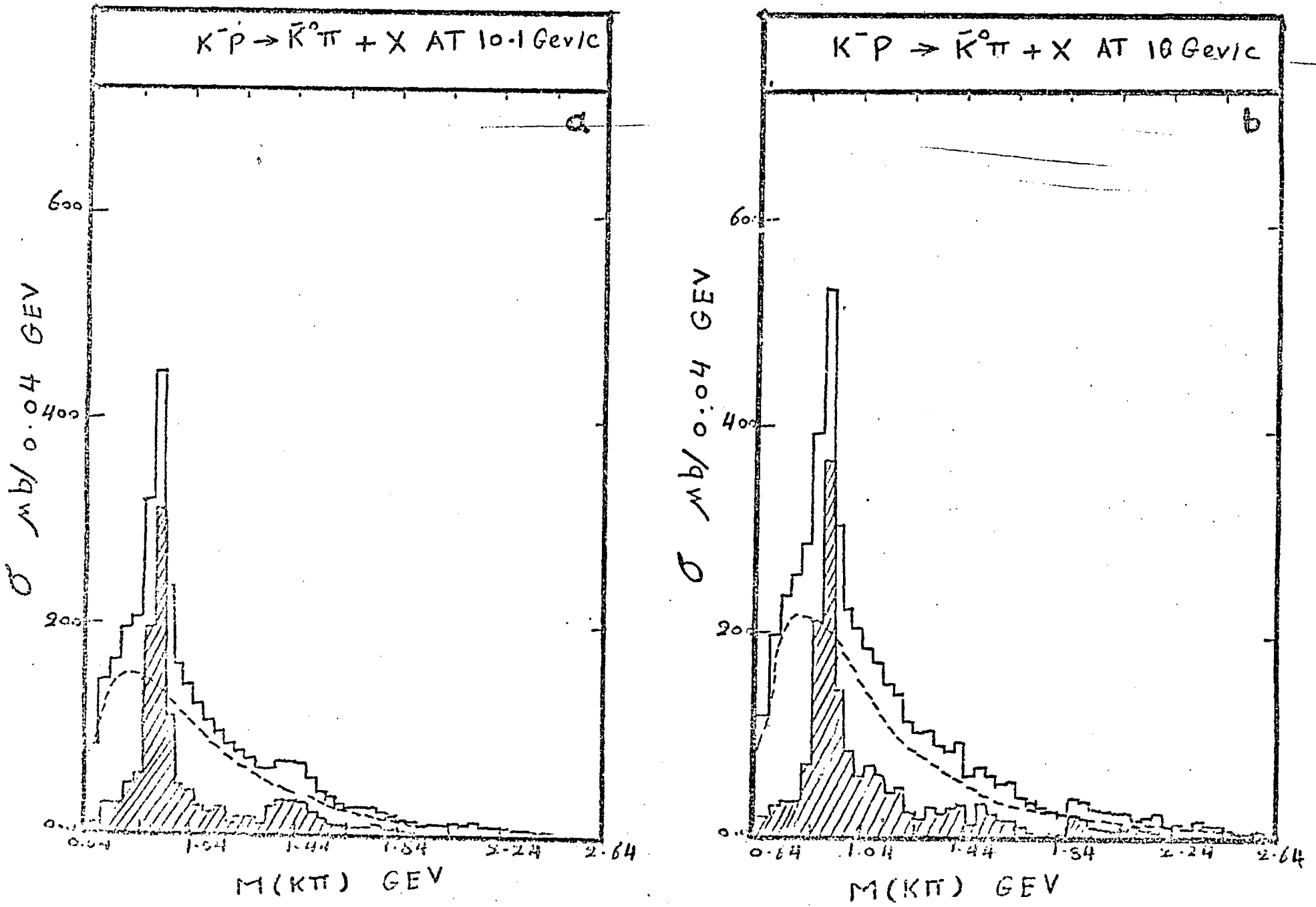
K⁻P → K̄°π + X AT 10·1 Gev/c
a
600
400
200
0
σ mb/ 0·04 GEV
0·64
1·04
1·44
1·84
2·24
2·64
M(Kπ) GEV
K⁻P → K̄°π + X AT 18 Gev/c
b
60
40
20
0
σ mb/ 0·04 GEV
0·64
1·04
1·44
1·84
2·24
2·64
M(Kπ) GEV

FIG(5-1)

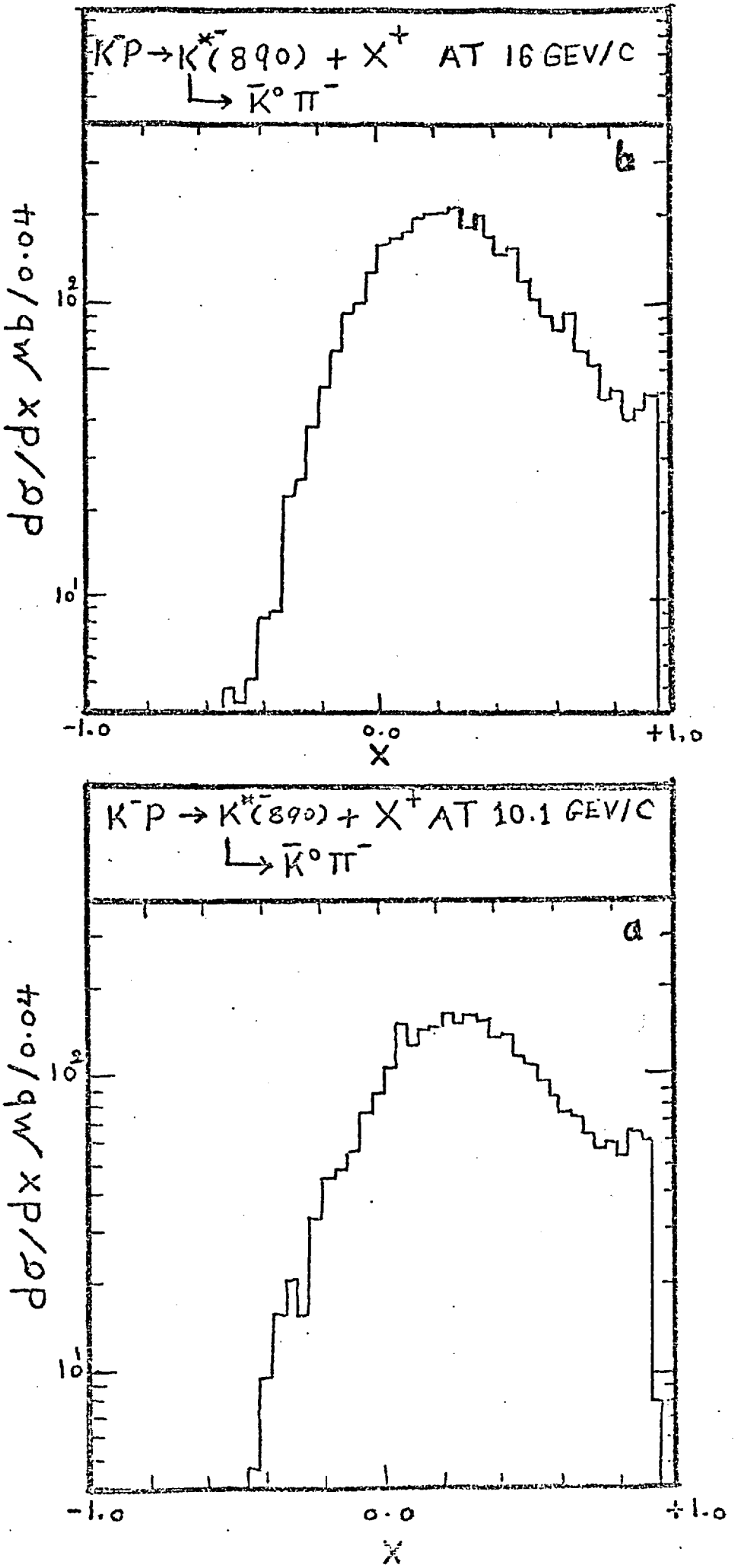
K⁻P → K*⁻(890) + X⁺ AT 16 GEV/C
→ K̄° π⁻
b
dσ/dx mb/0.04
10²
10¹
-1.0
0.0
+1.0
X
K⁻P → K*⁻(890) + X⁺ AT 10.1 GEV/C
→ K̄° π⁻
a
dσ/dx mb/0.04
10²
10¹
-1.0
0.0
+1.0
X

FIG(5-2)

FIG(5-3)

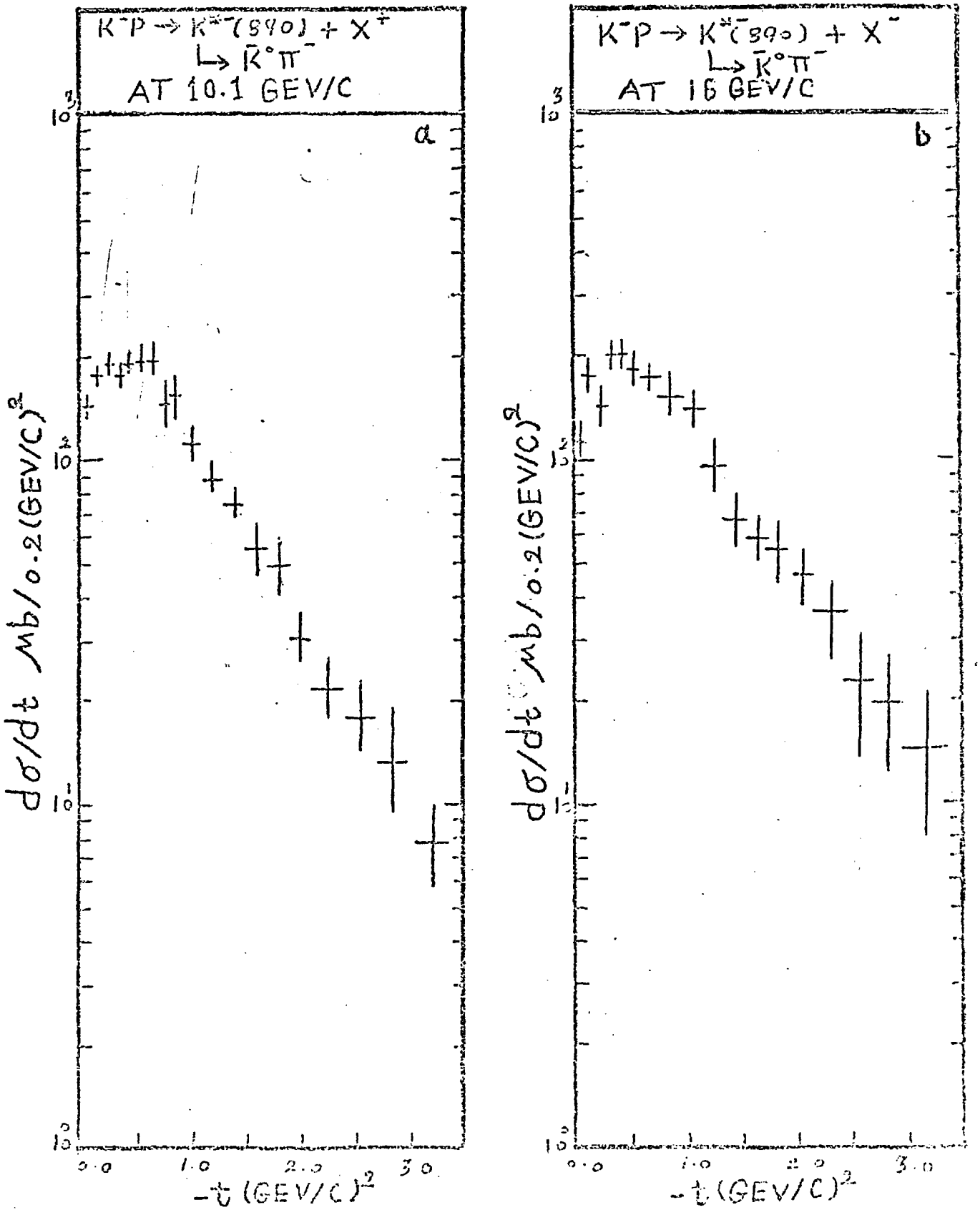
K⁻P → K*⁻(890) + X⁺
↳ K̄°π⁻
AT 10.1 GEV/C
a
dσ/dt mb/0.2(GEV/C)²
-t (GEV/C)²
K⁻P → K*⁻(890) + X⁻
↳ K̄°π⁻
AT 16 GEV/C
b
dσ/dt mb/0.2(GEV/C)²
-t (GEV/C)²

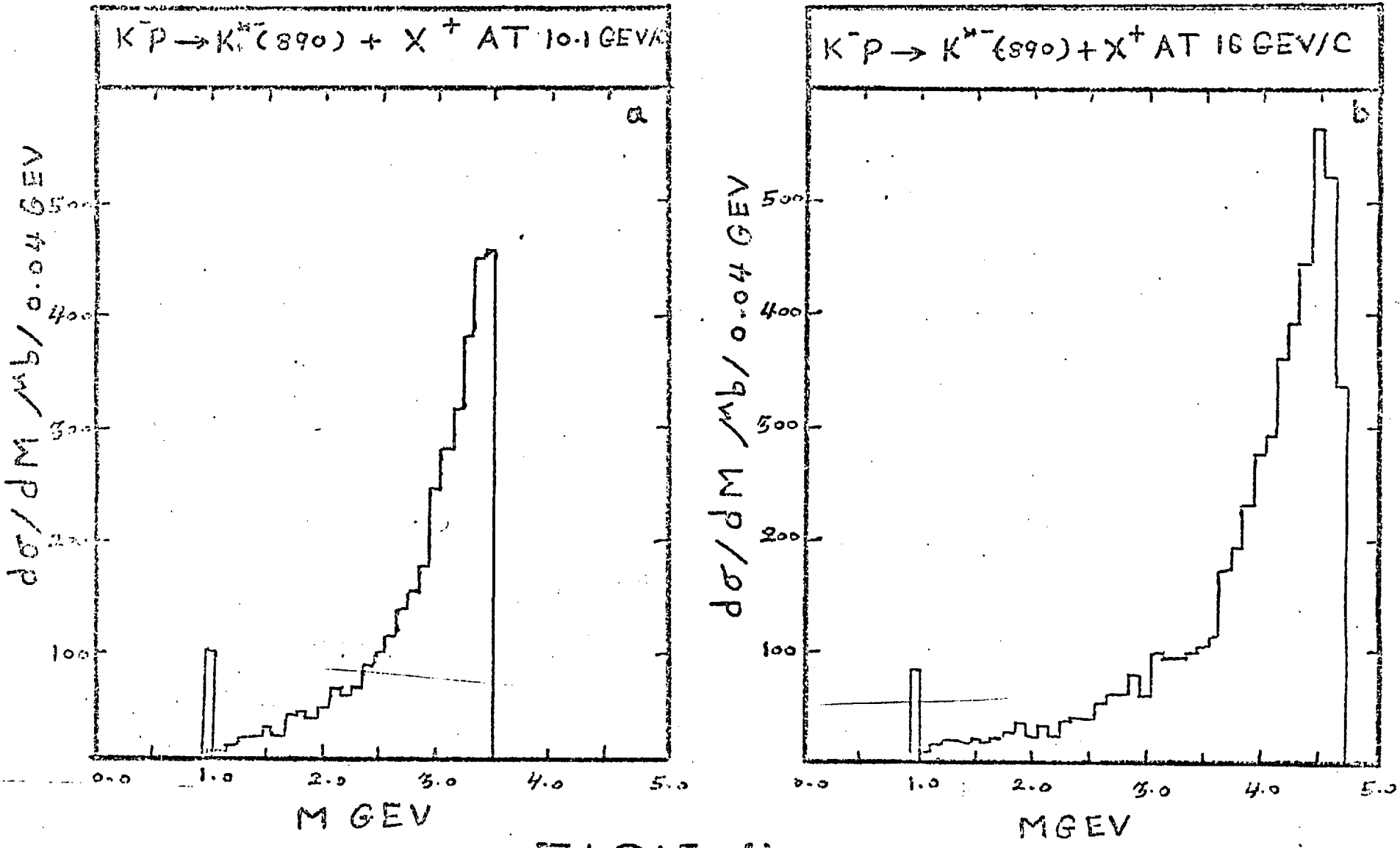
K⁻P → K*⁻(890) + X⁺ AT 10.1 GEV/C
a
dσ/dM /μb/ 0.04 GEV
100
200
300
400
500
0.0
1.0
2.0
3.0
4.0
5.0
M GEV
K⁻P → K*⁻(890) + X⁺ AT 16 GEV/C
b
dσ/dM /μb/ 0.04 GEV
100
200
300
400
500
0.0
1.0
2.0
3.0
4.0
5.0
M GEV

FIG(5-4)

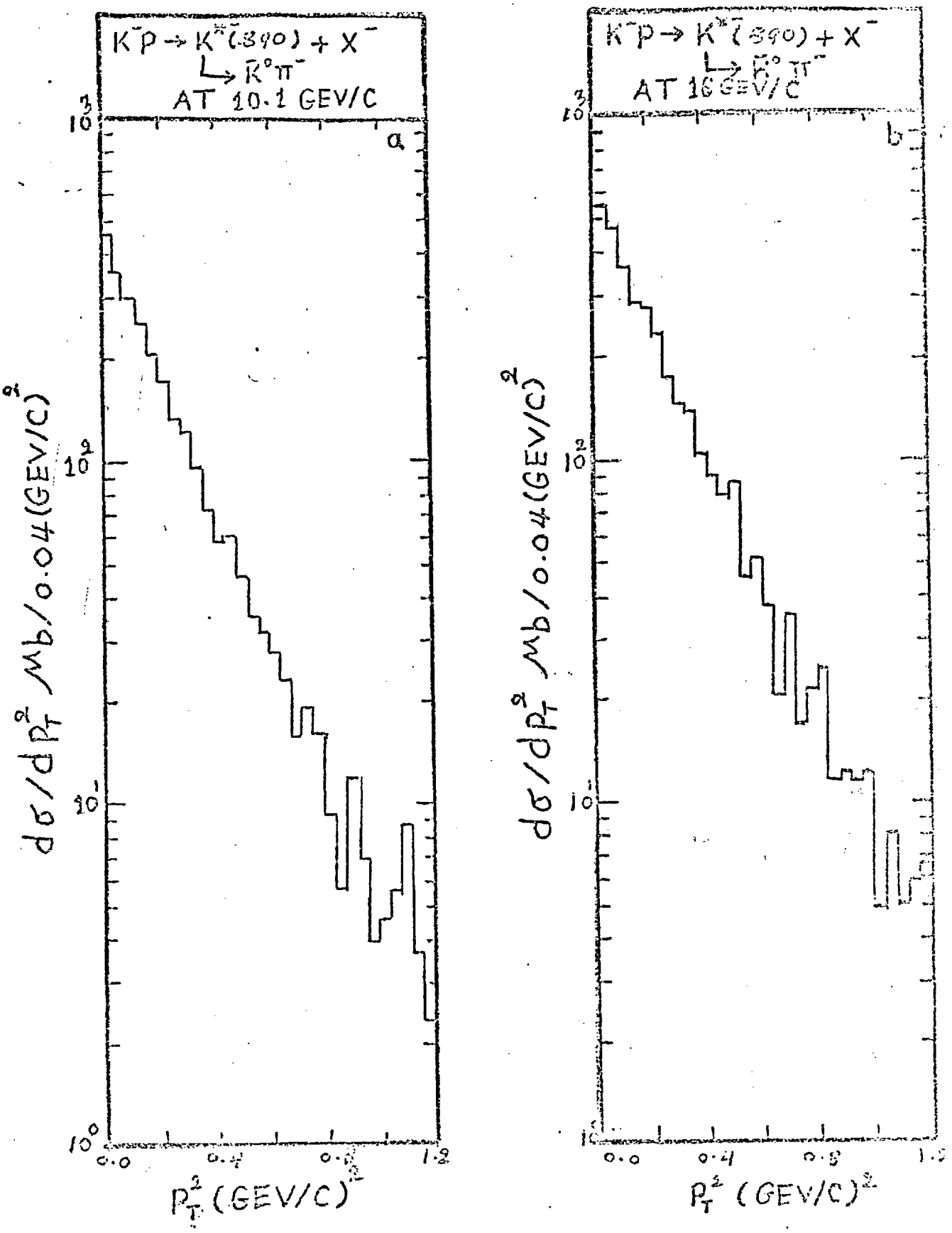
K⁻P → K*⁻(890) + X⁻
↳ K⁰π⁻
AT 10.1 GEV/C
a
dσ/dP_T² Mb/0.04(GEV/C)²
P_T² (GEV/C)²
K⁻P → K*⁻(890) + X⁻
↳ K⁰π⁻
AT 16 GEV/C
b
dσ/dP_T² Mb/0.04(GEV/C)²
P_T² (GEV/C)²

FIG(5-5)

Gottfried - Jackson Frame

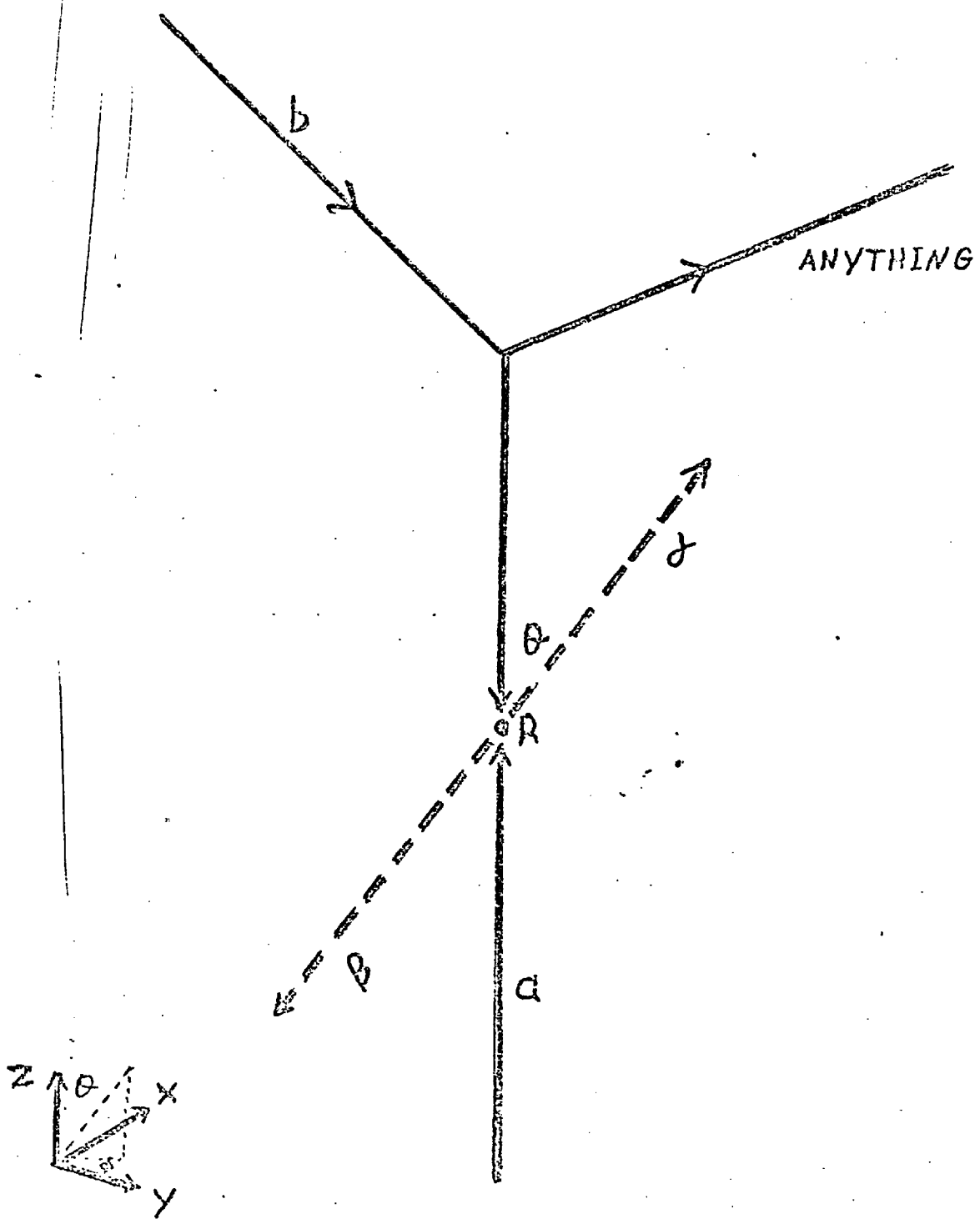

FIG(5-6)

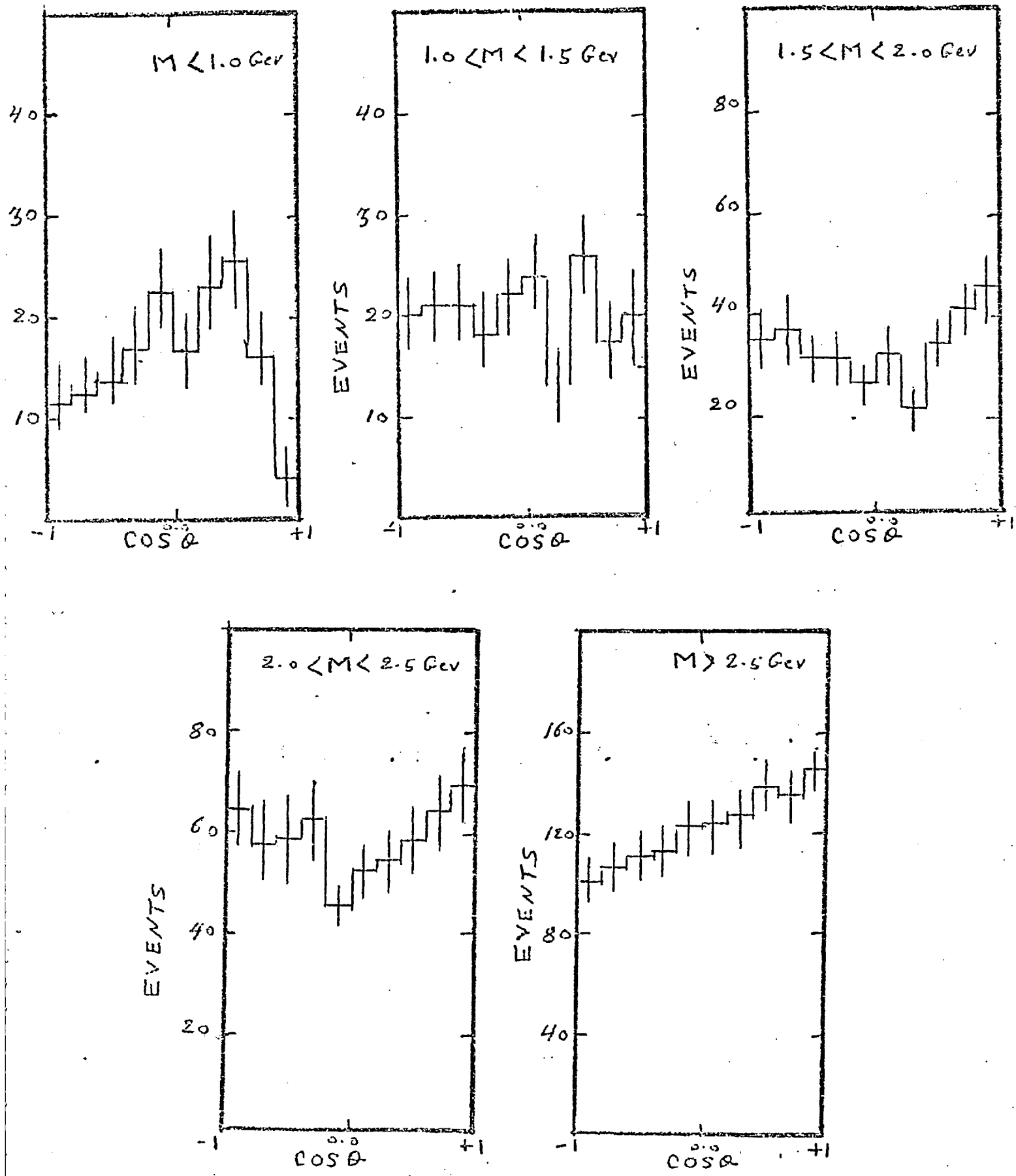
M < 1.0 Gev
1.0 < M < 1.5 Gev
1.5 < M < 2.0 Gev
2.0 < M < 2.5 Gev
M > 2.5 Gev
EVENTS
COS θ
-1
0.0
+1

FIG(5-7-9)

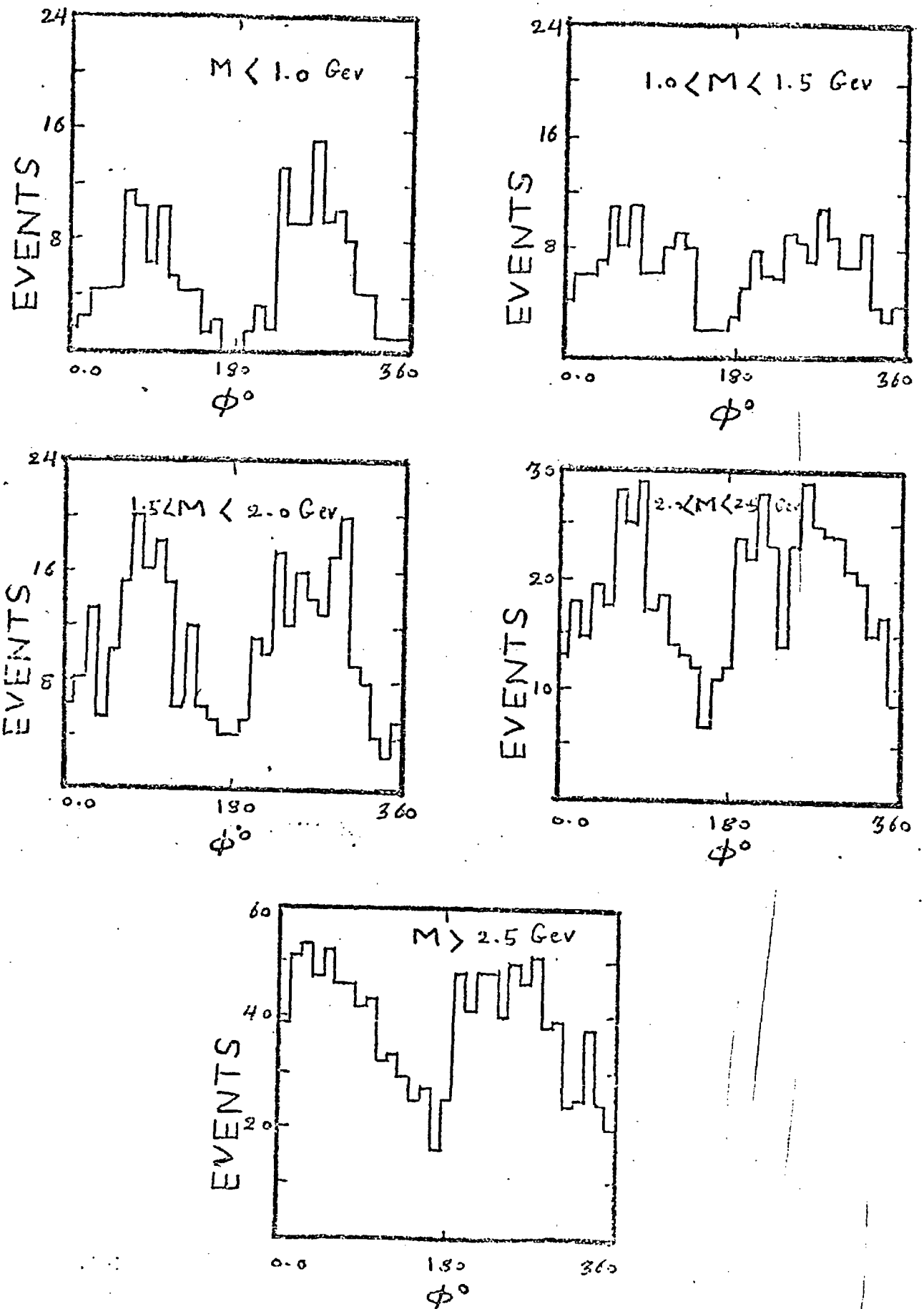
M < 1.0 Gev
1.0 < M < 1.5 Gev
1.5 < M < 2.0 Gev
2.0 < M < 2.5 Gev
M > 2.5 Gev
EVENTS
φ°
0.0
180
360

FIG(5-7-b)

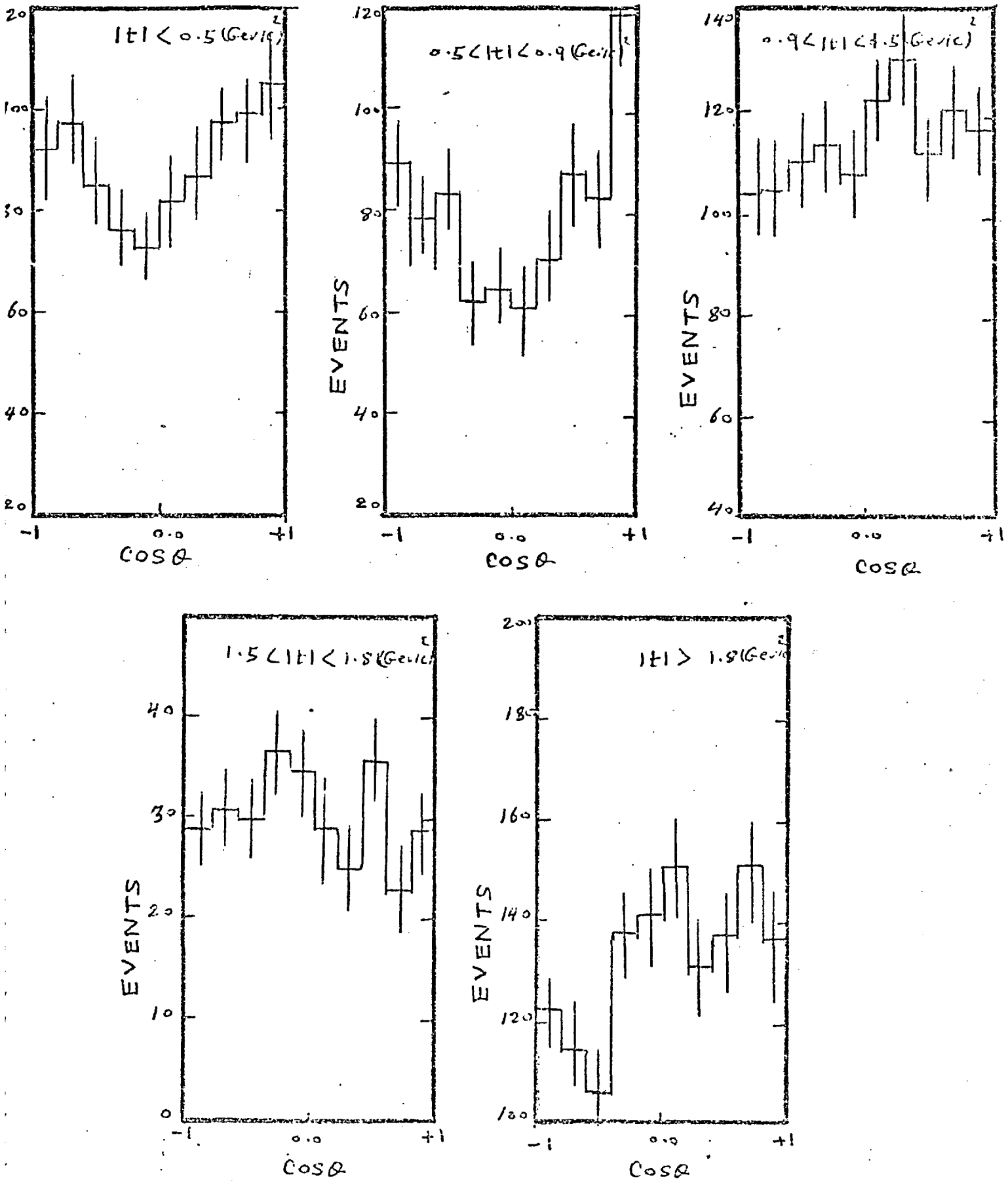
|t| < 0.5 (GeV/c)²
0.5 < |t| < 0.9 (GeV/c)²
0.9 < |t| < 1.5 (GeV/c)²
1.5 < |t| < 1.8 (GeV/c)²
|t| > 1.8 (GeV/c)²
EVENTS
Cos θ
-1
0.0
+1

FIG(5-8-a)

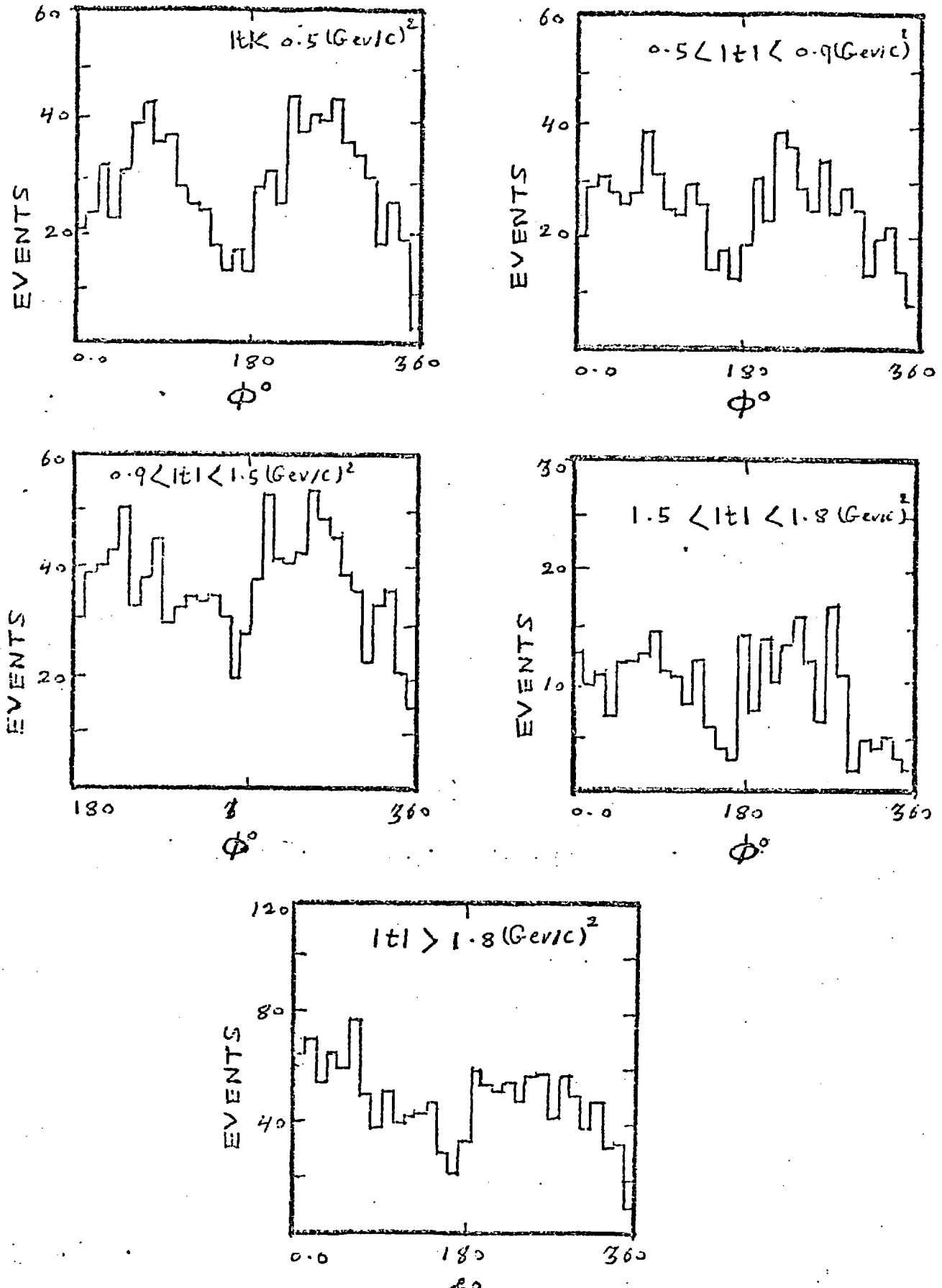
|t|< 0.5 (Gev/c)²
0.5 < |t| < 0.9 (Gev/c)²
0.9 < |t| < 1.5 (Gev/c)²
1.5 < |t| < 1.8 (Gev/c)²
|t| > 1.8 (Gev/c)²
EVENTS
Φ°
0.0
180
360

FIG(5-8-b)

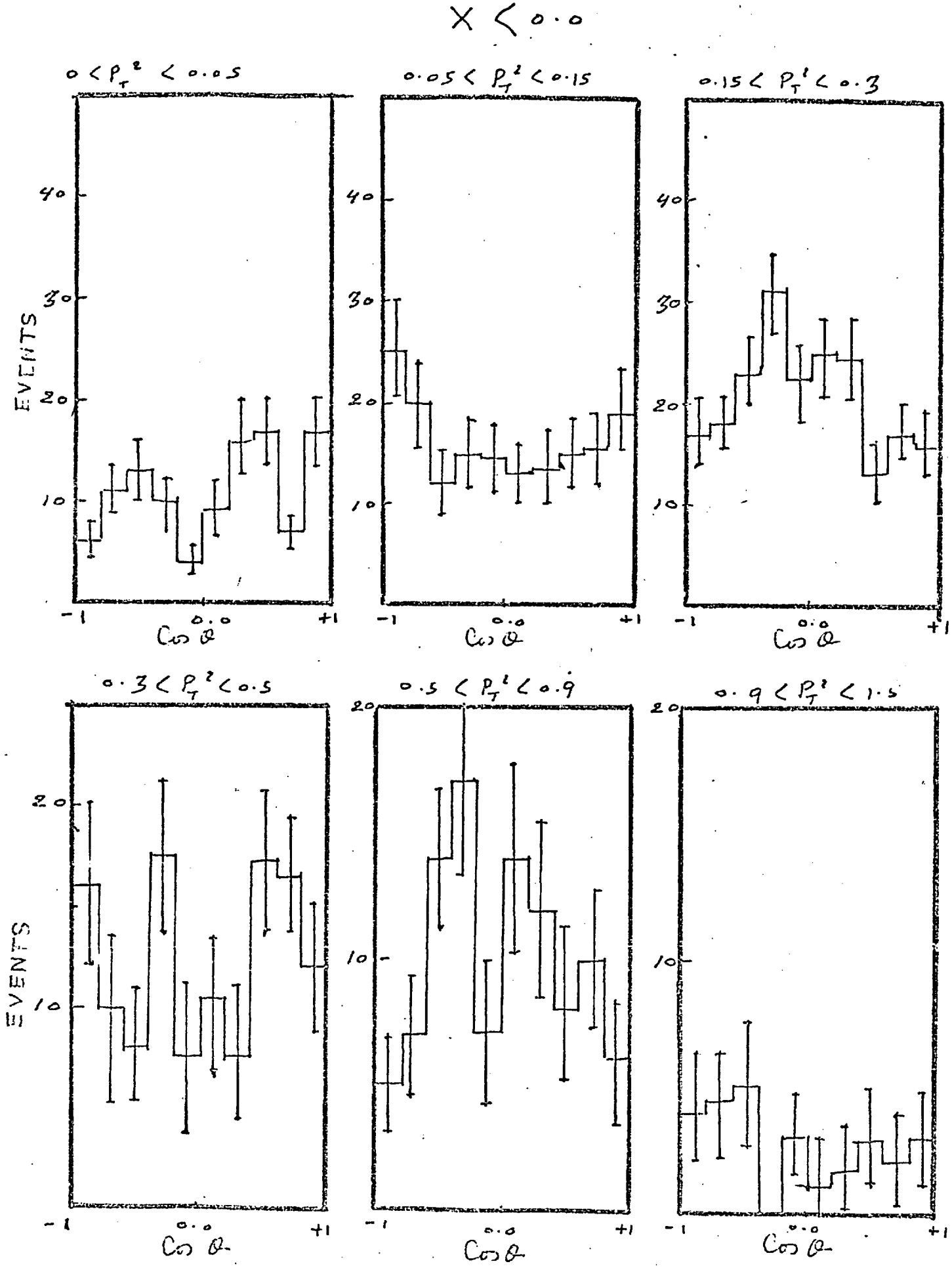
X < 0.0
0 < P_T^2 < 0.05
0.05 < P_T^2 < 0.15
0.15 < P_T^2 < 0.3
0.3 < P_T^2 < 0.5
0.5 < P_T^2 < 0.9
0.9 < P_T^2 < 1.5
EVENTS
Cos θ
-1
0.0
+1

FIG(5-9-a-1)

$K^- p \rightarrow K^{*}(890) + X^+$ AT 10 GeV/c

$-1.0 < x < 0.0$

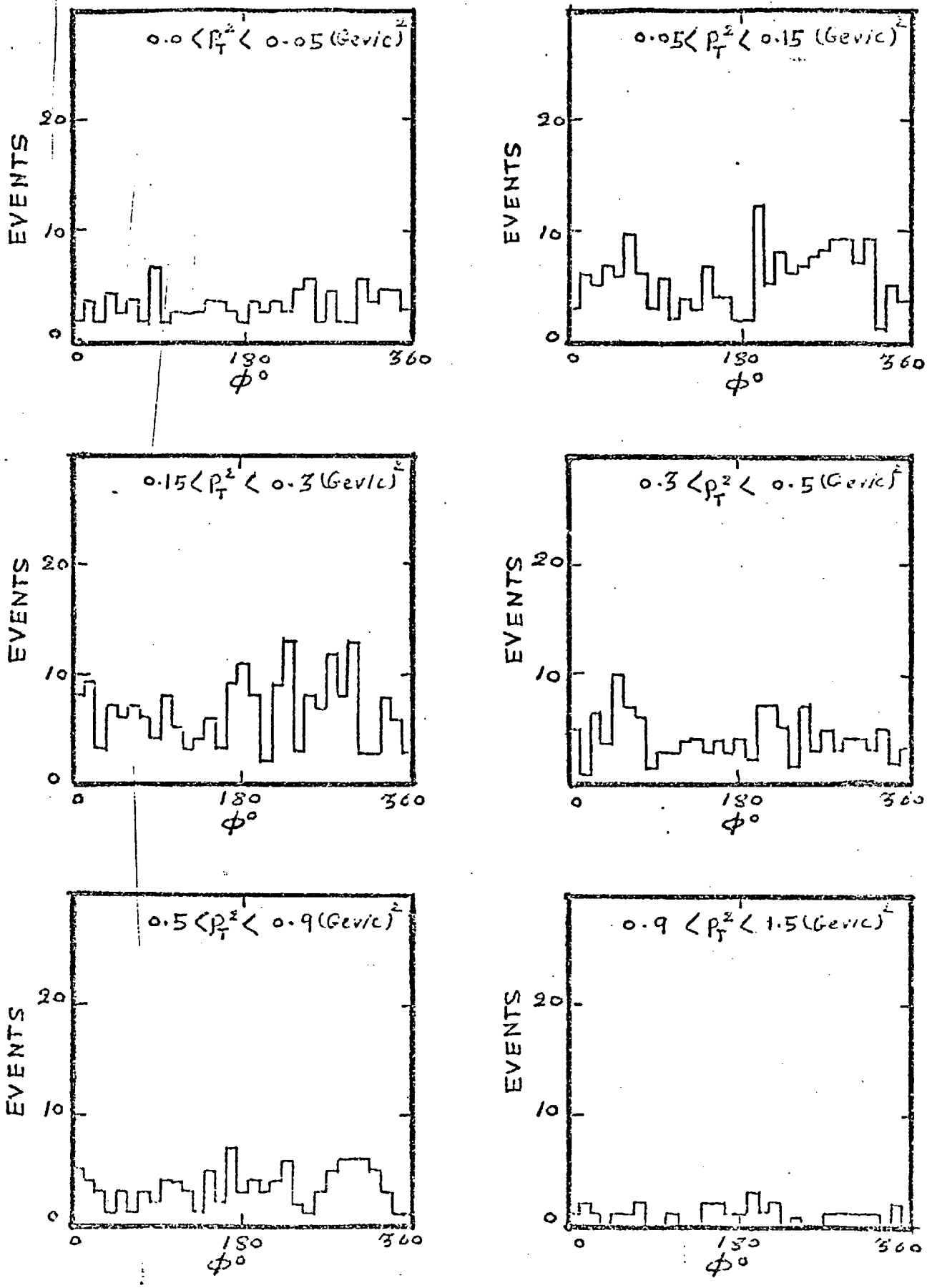

FIG(5-9-a-2)

$K^- P \rightarrow K^{*}(890) + X^+$ AT 10.1 GEV/C

$0.0 < X < 0.5$

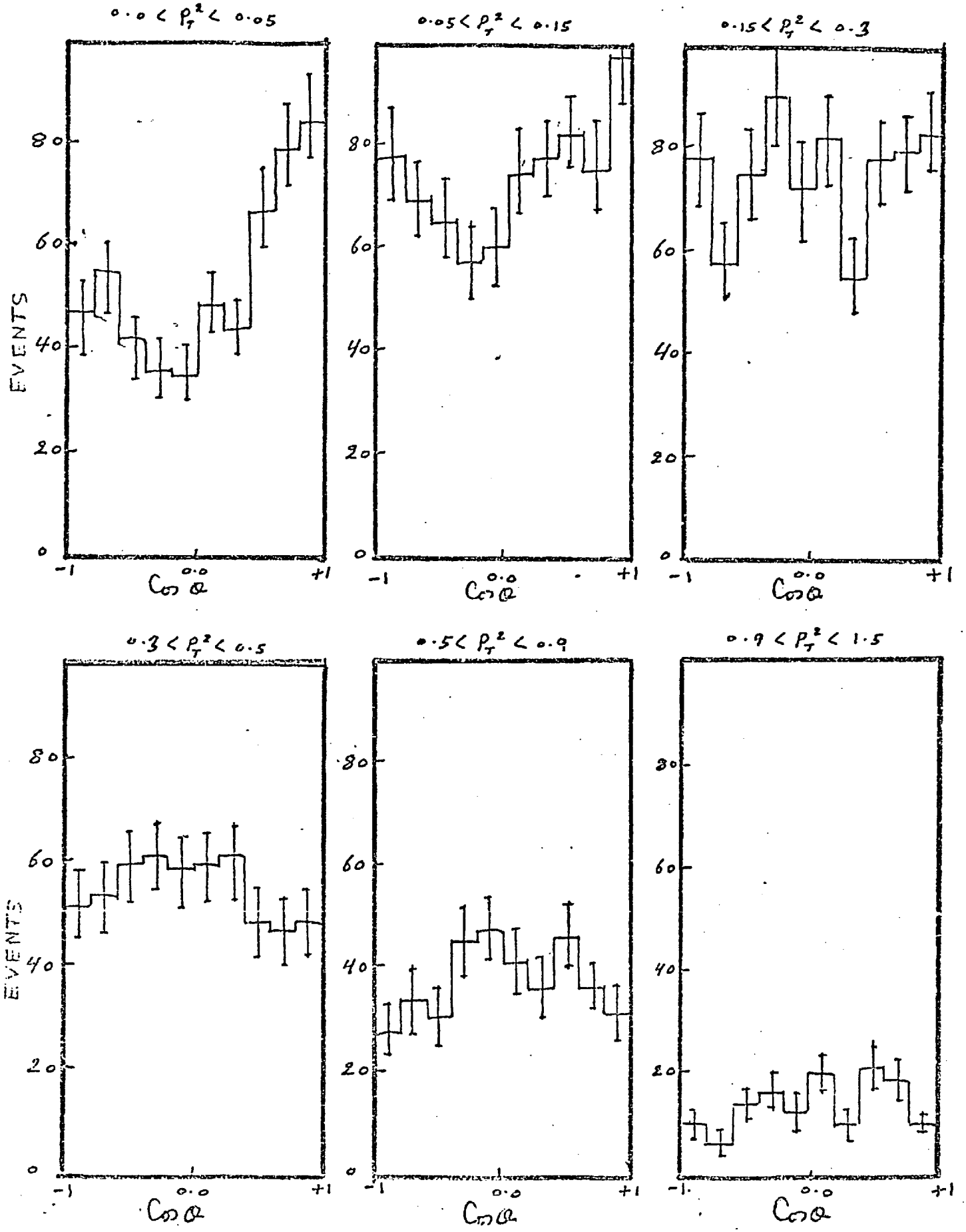

FIG(5-9-b-1)

$K^- p \rightarrow K^{*}(890) + X^+$ AT 10 GeV/c
$0.0 < x < 0.5$

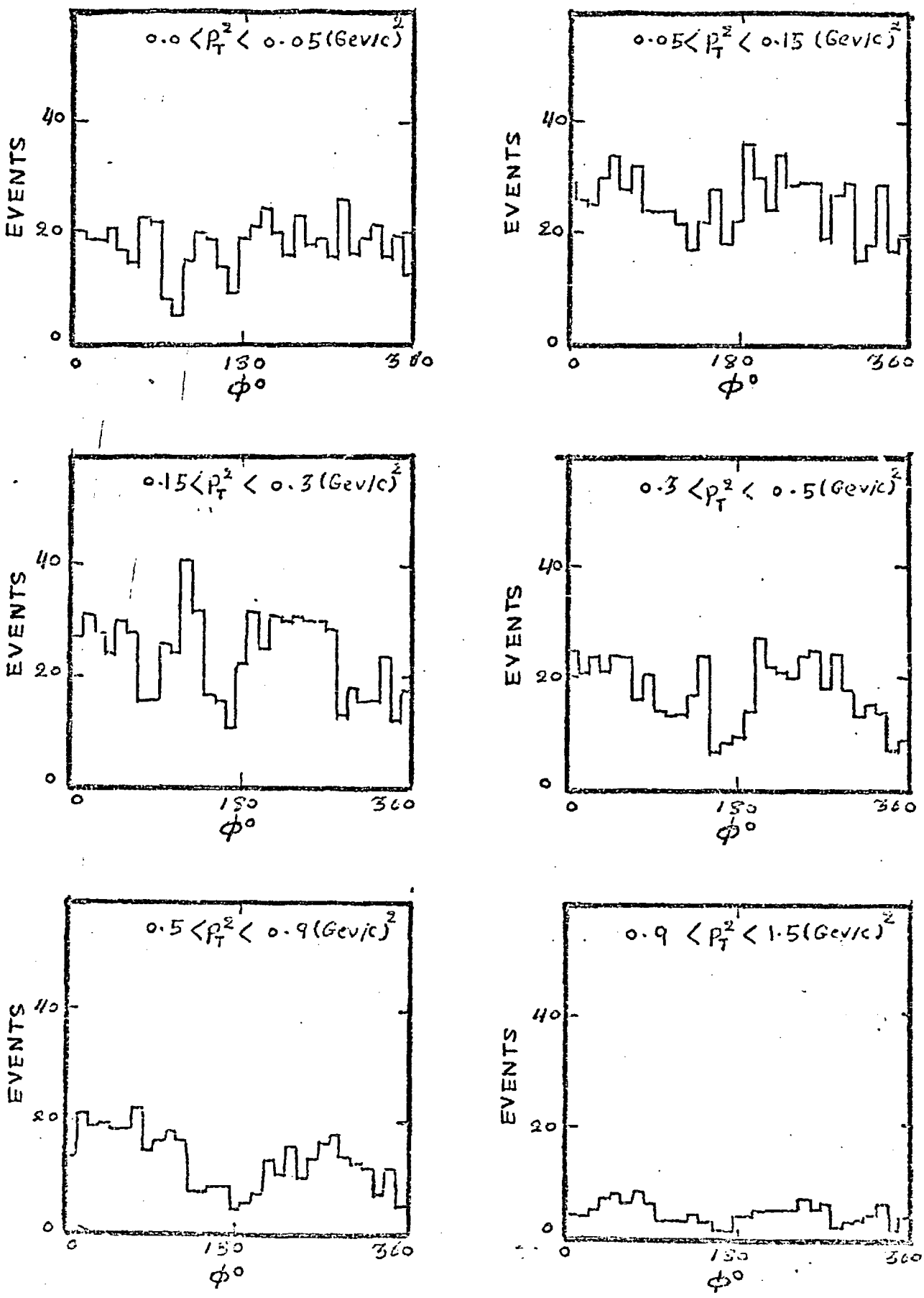

FIG(5-9-b-2)

$K^- P \rightarrow K^{*}(890) + X^+$ AT 10.1 GEV/C

$1.0 > X > 0.5$

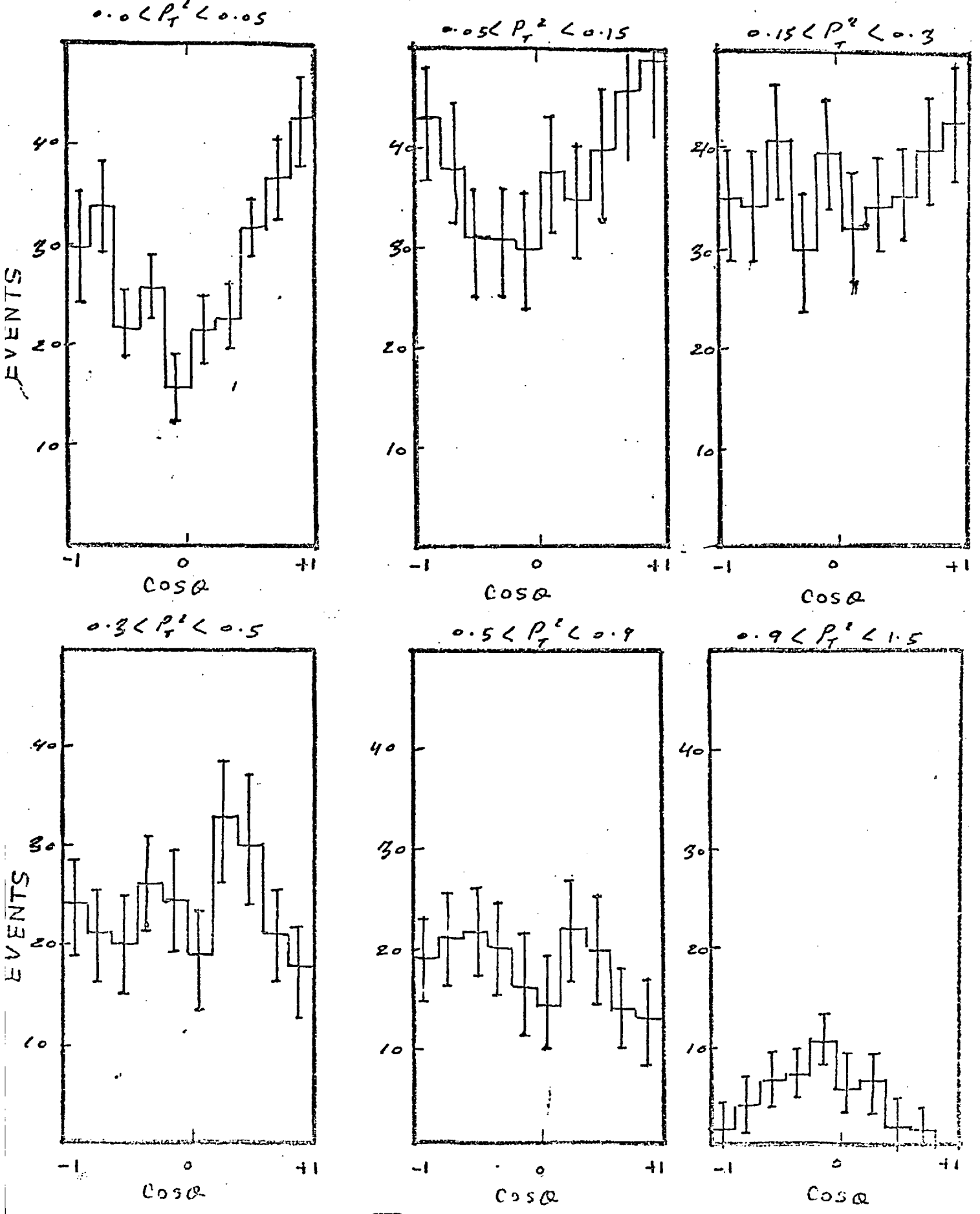

FIG(5-9-C-1)

$K^- p \rightarrow K^{*-}(890) + X^+$ AT 10 Gev/c

$1.0 > X > 0.5$

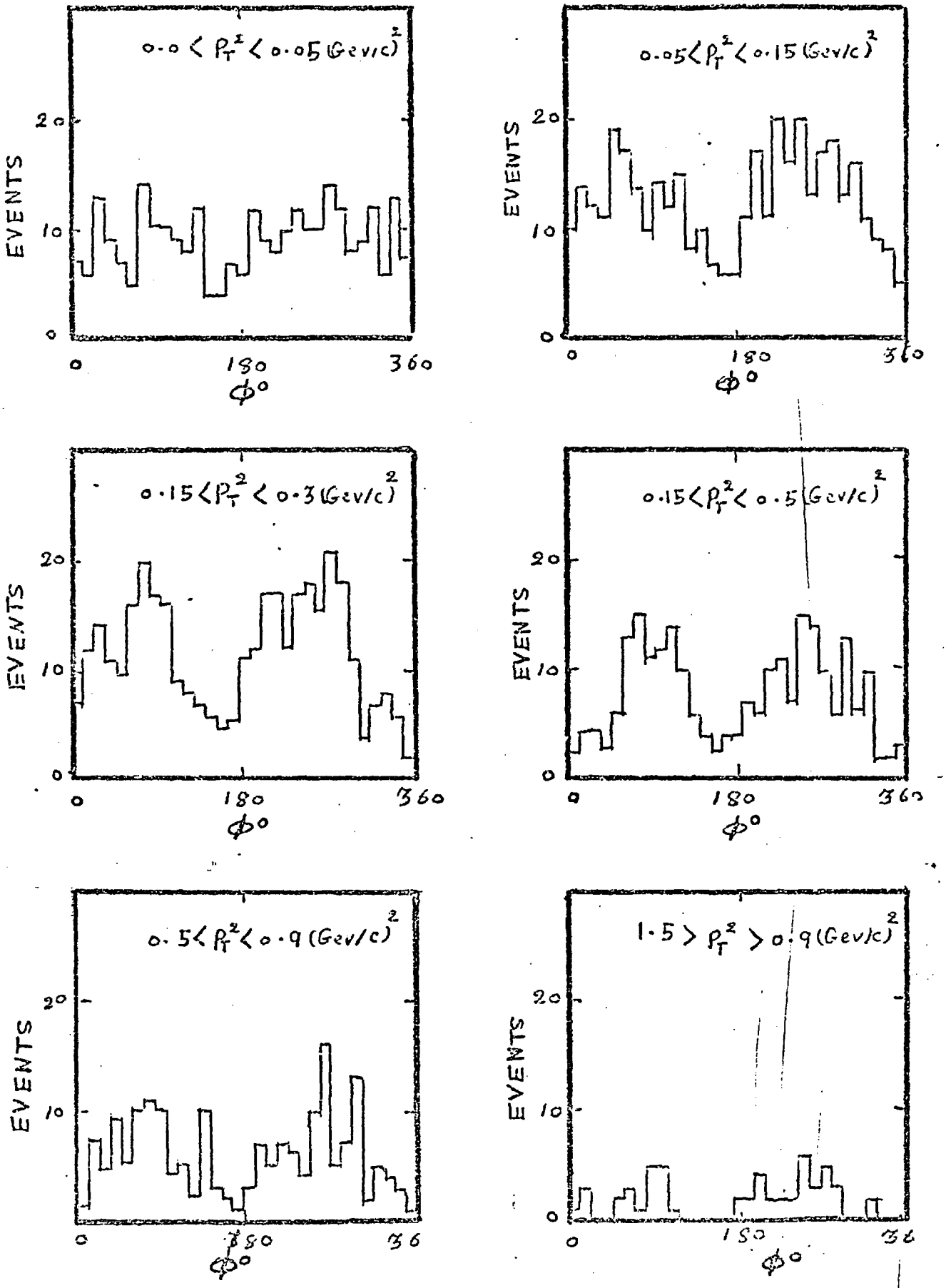

FIG (5-9-c-2)

FIG(5-10-a)

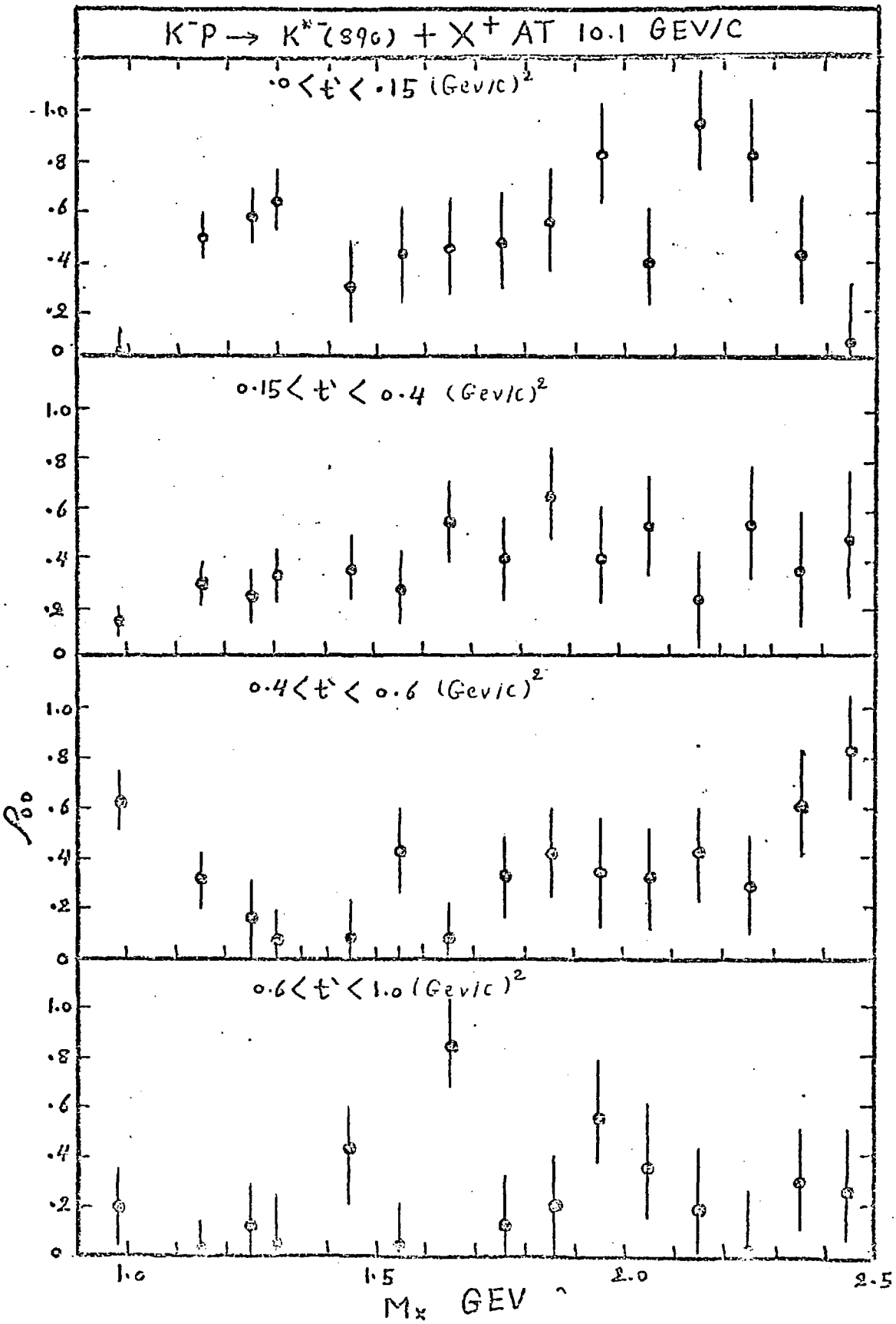
K⁻P → K*⁻(890) + X⁺ AT 10.1 GEV/C
0 < t' < .15 (Gev/c)²
0.15 < t' < 0.4 (Gev/c)²
0.4 < t' < 0.6 (Gev/c)²
0.6 < t' < 1.0 (Gev/c)²
ρ₀₀
1.0
.8
.6
.4
.2
0
1.0
1.5
2.0
2.5
Mx GEV

FIG(5-10-b)

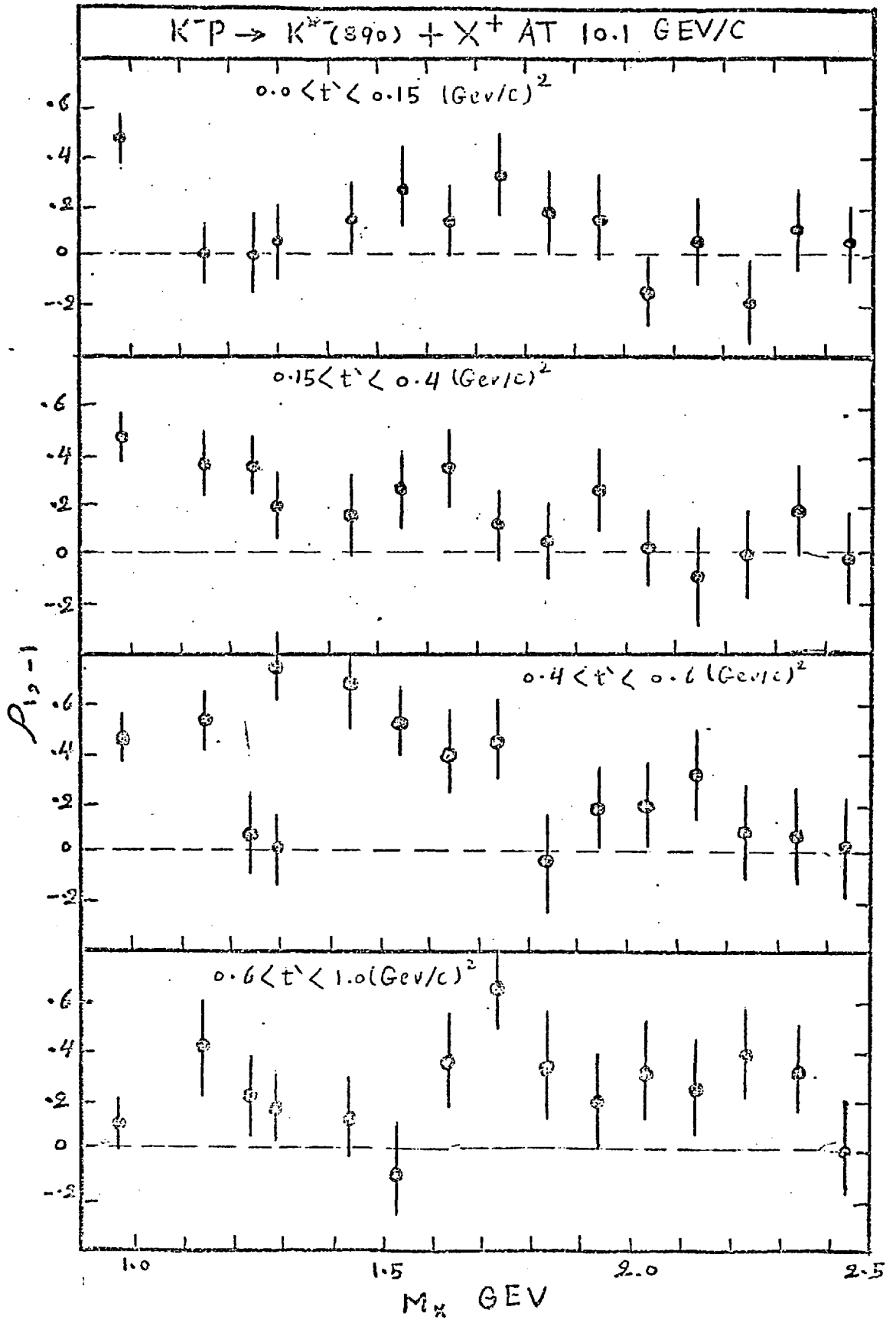
K⁻P → K*⁻(890) + X⁺ AT 10.1 GEV/C
0.0 < t' < 0.15 (Gev/c)²
0.15 < t' < 0.4 (Gev/c)²
0.4 < t' < 0.6 (Gev/c)²
0.6 < t' < 1.0 (Gev/c)²
ρ1,-1
.6
.4
.2
0
-.2
1.0
1.5
2.0
2.5
M_X GEV

FIG(5-10-c)

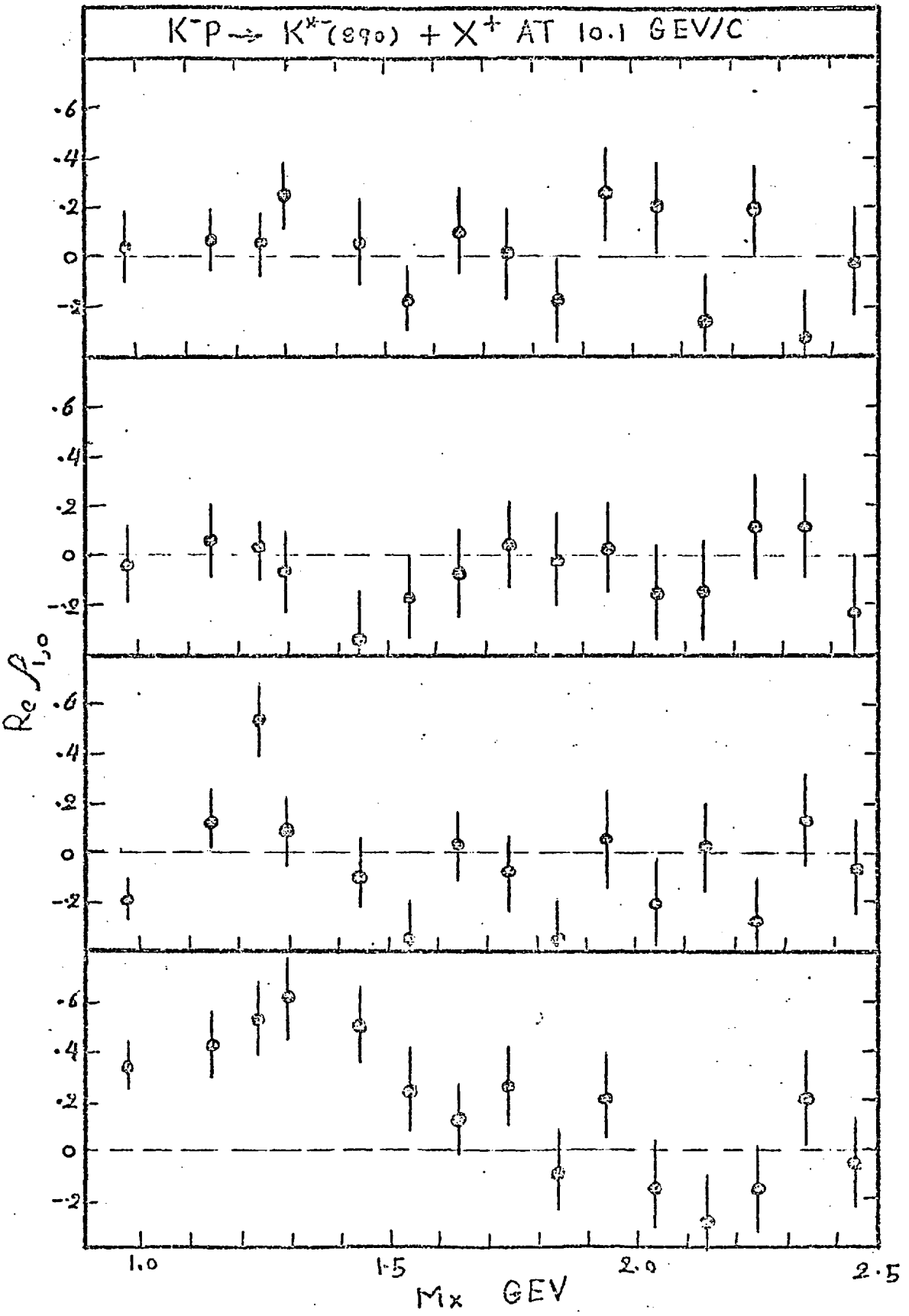

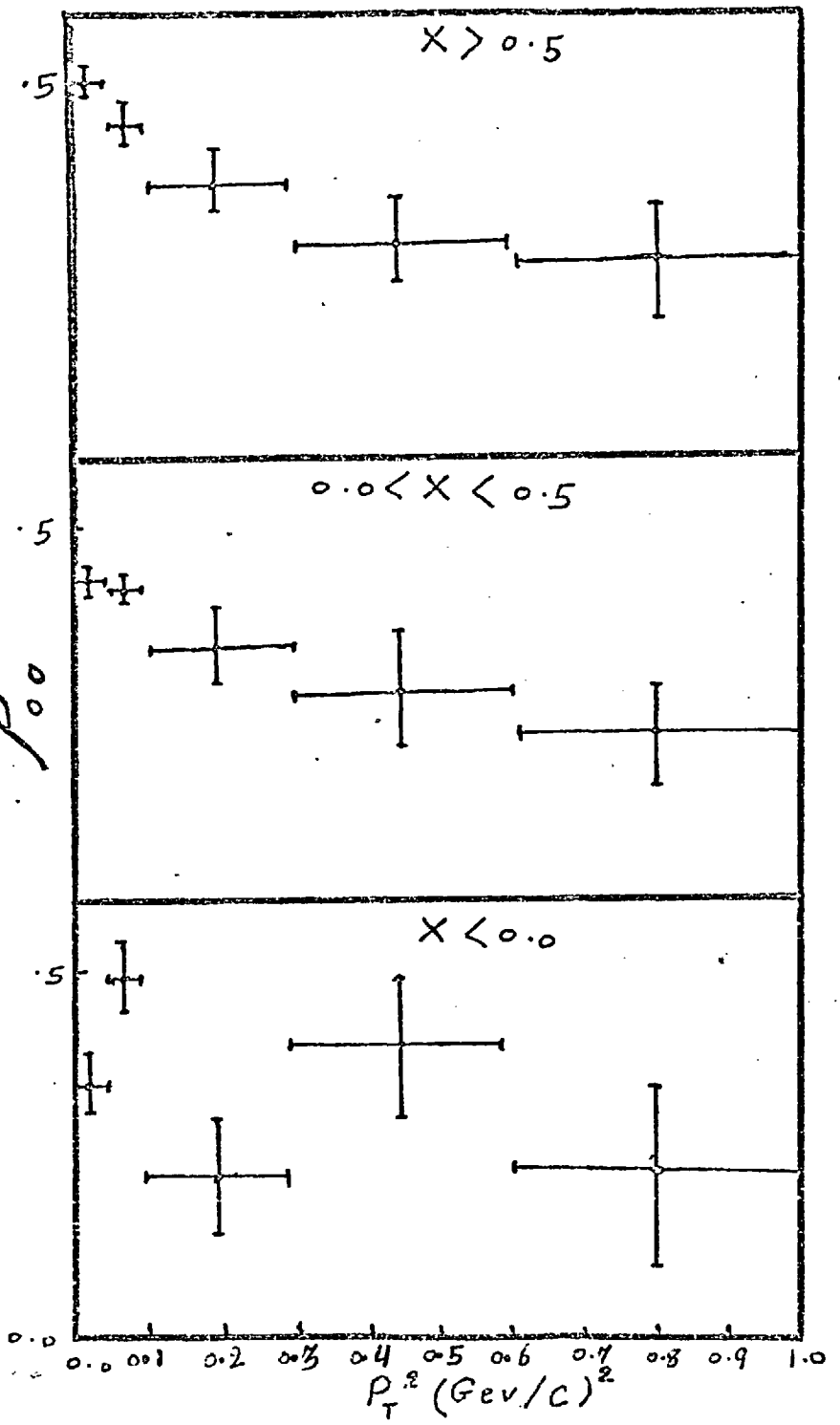
X > 0.5
0.0 < X < 0.5
X < 0.0
ρ_{00}
.5
.5
.5
0.0
0.0 0.1 0.2 0.3 0.4 0.5 0.6 0.7 0.8 0.9 1.0
P_T^2 (Gev/c)^2

FIG(5-11-a).

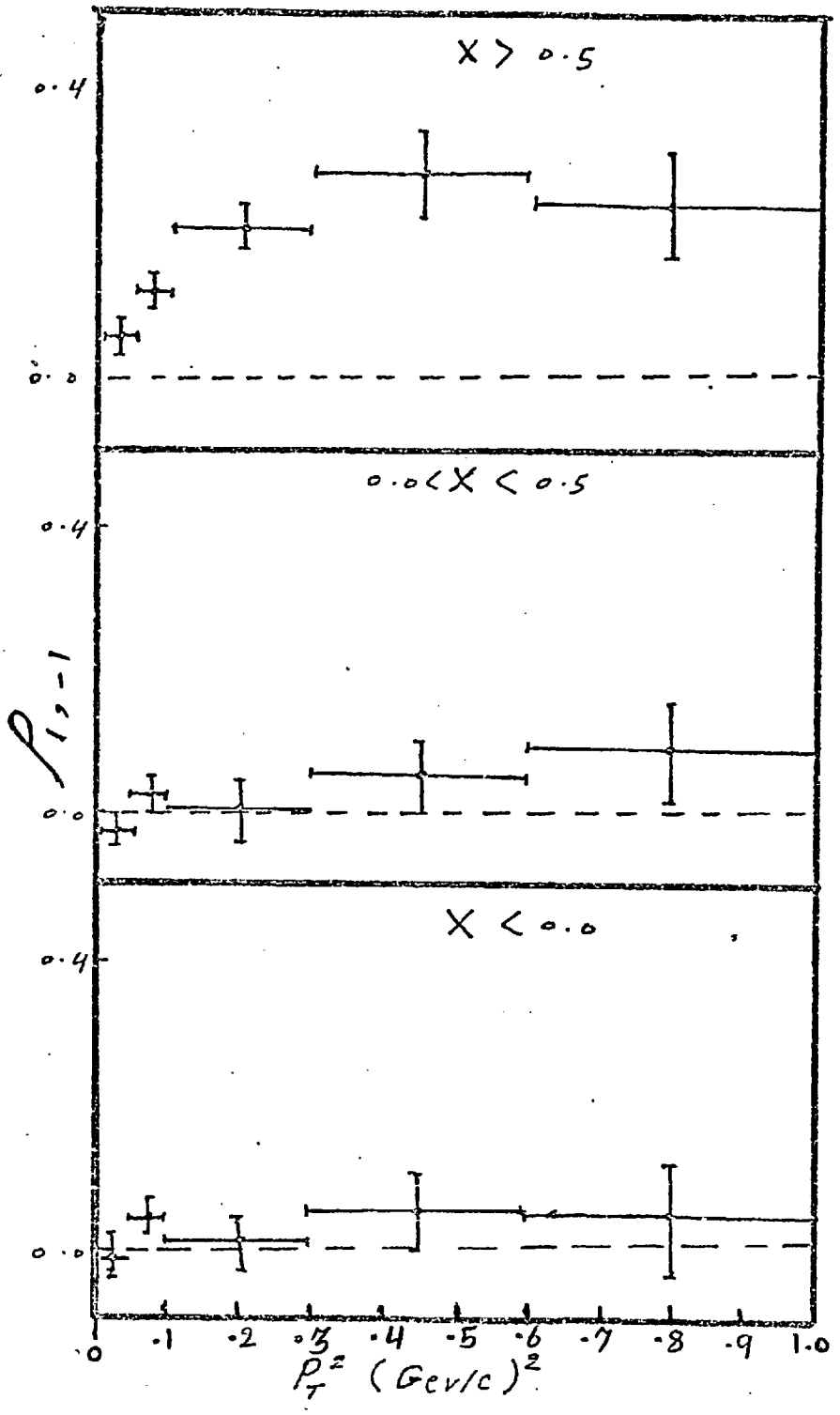

FIG(5-11-b)

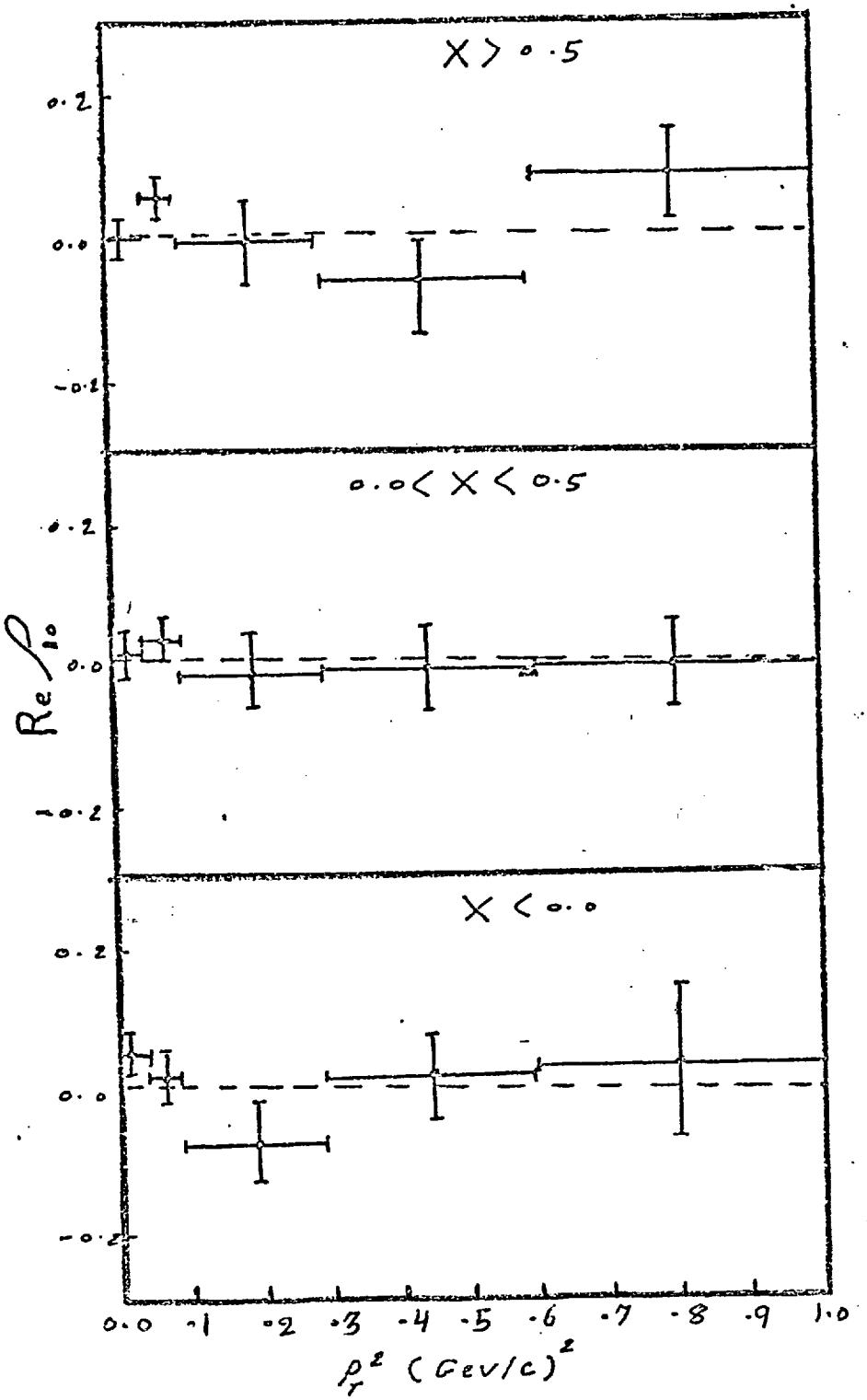

FIG(5-11-C)

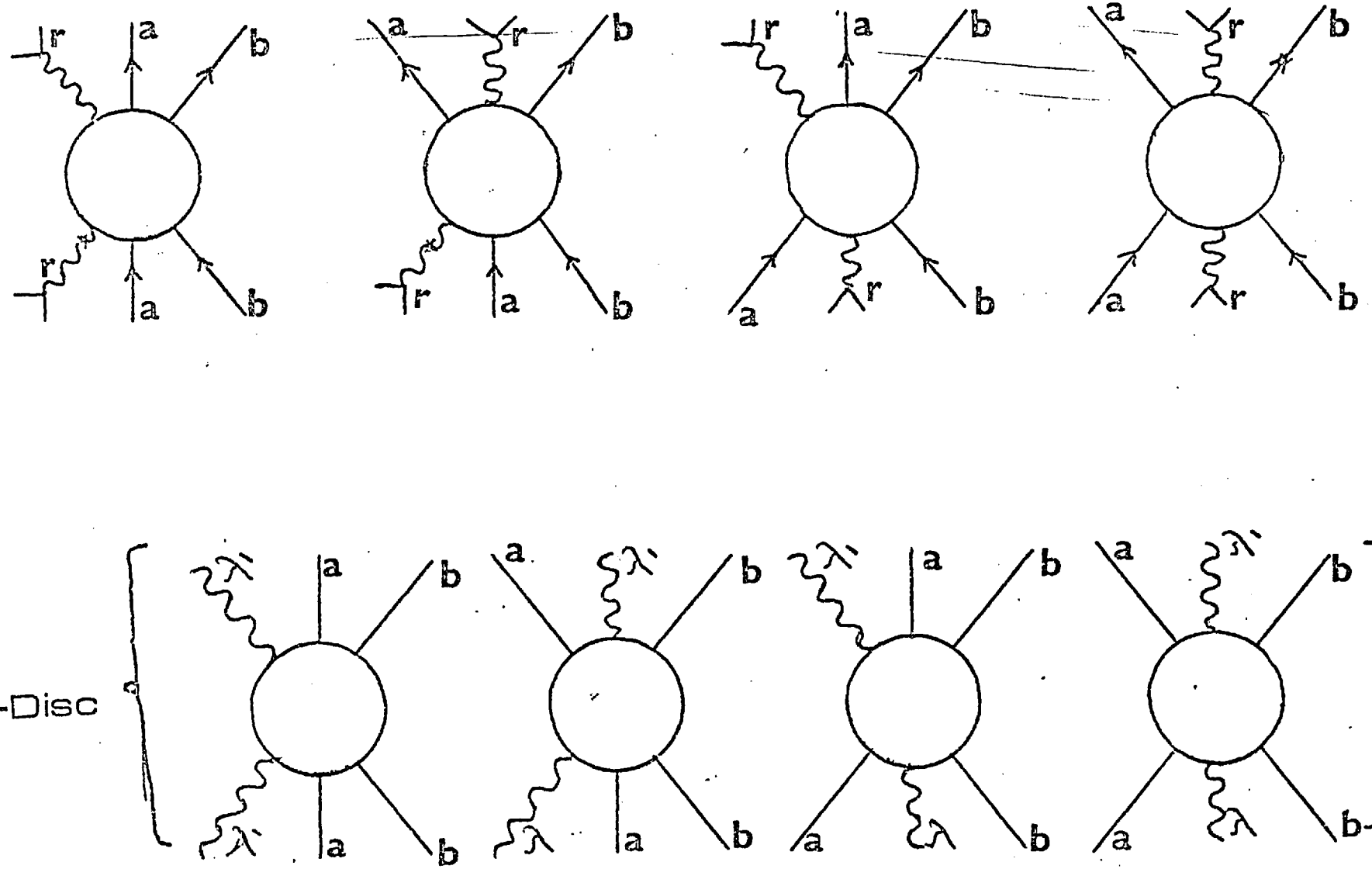
r
a
b
r
a
b
a
r
b
r
a
b
r
a
b
a
r
b
a
r
b
a
r
b
$\rho_{\lambda\lambda'} = \frac{1}{n}$ Disc
λ'
a
b
λ'
a
b
a
λ'
b
λ'
a
b
a
λ'
b
λ'
a
b
a
λ'
b
λ
a
b
a
λ
b
a
λ'
b
λ
a
b

FIG(5-12)

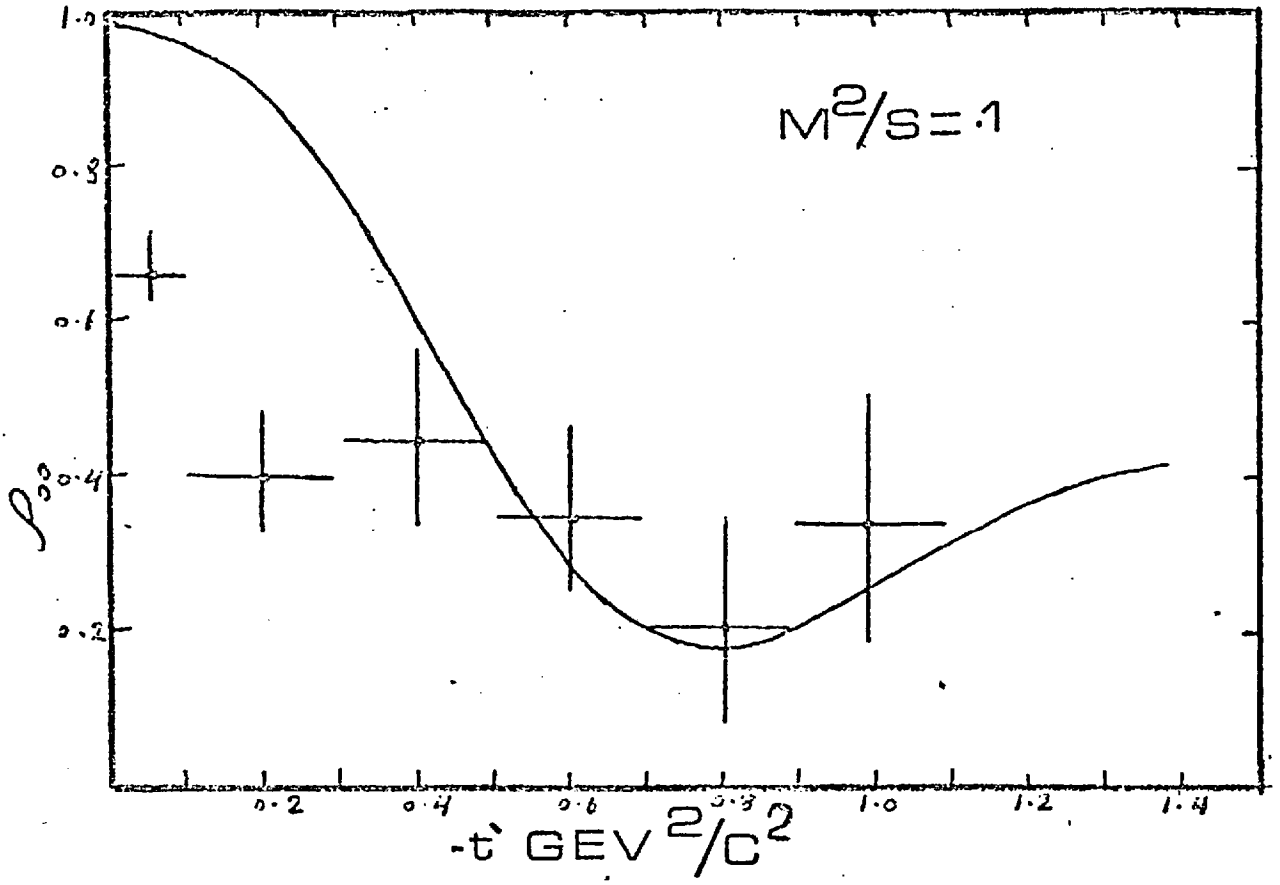
M²/s=.1
ρ₀₀⁰
1.0
0.8
0.6
0.4
0.2
0.2
0.4
0.6
0.8
1.0
1.2
1.4
-t` GEV²/c²

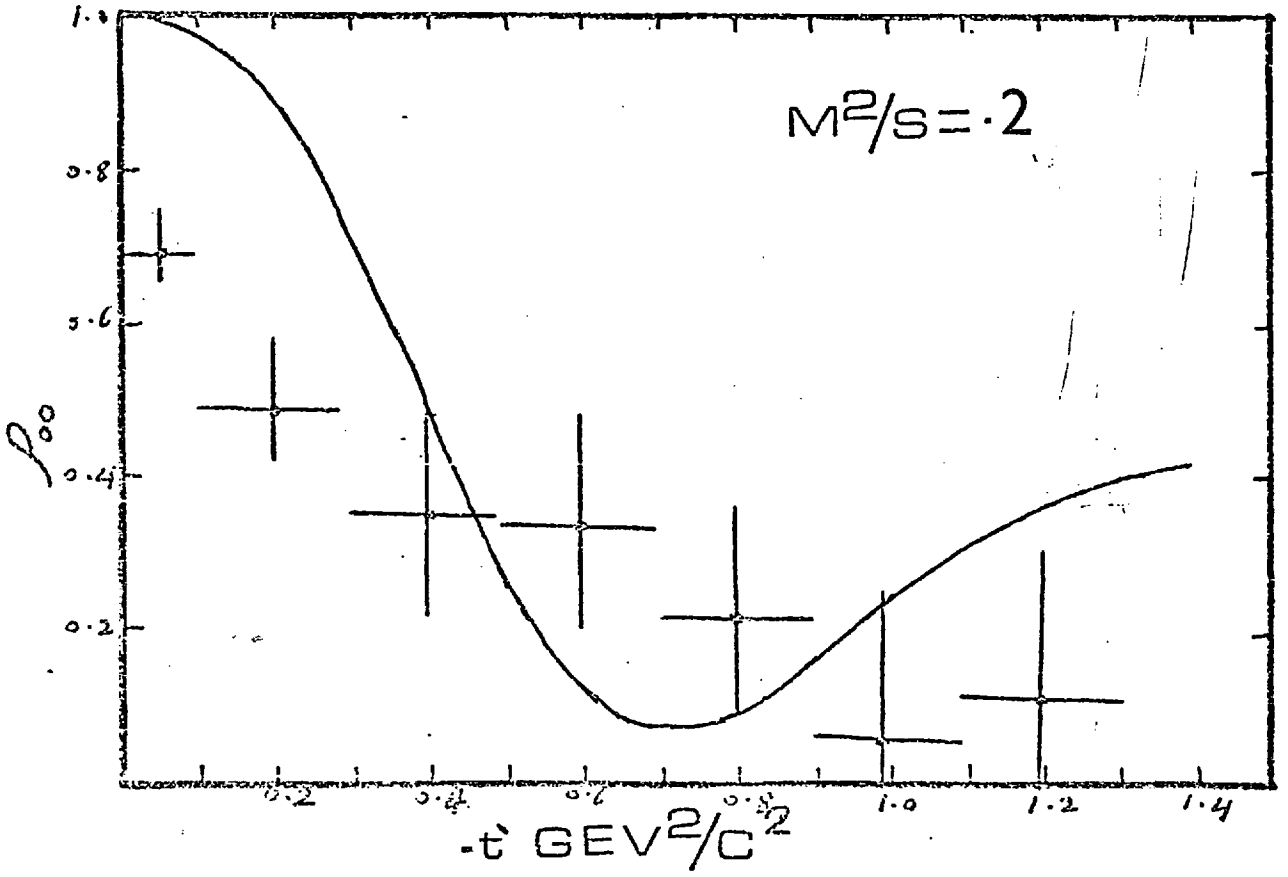
M²/s=.2
ρ₀₀
1.0
0.8
0.6
0.4
0.2
0.2
0.4
0.6
0.8
1.0
1.2
1.4
-t` GEV²/c²

FIG(5-13)

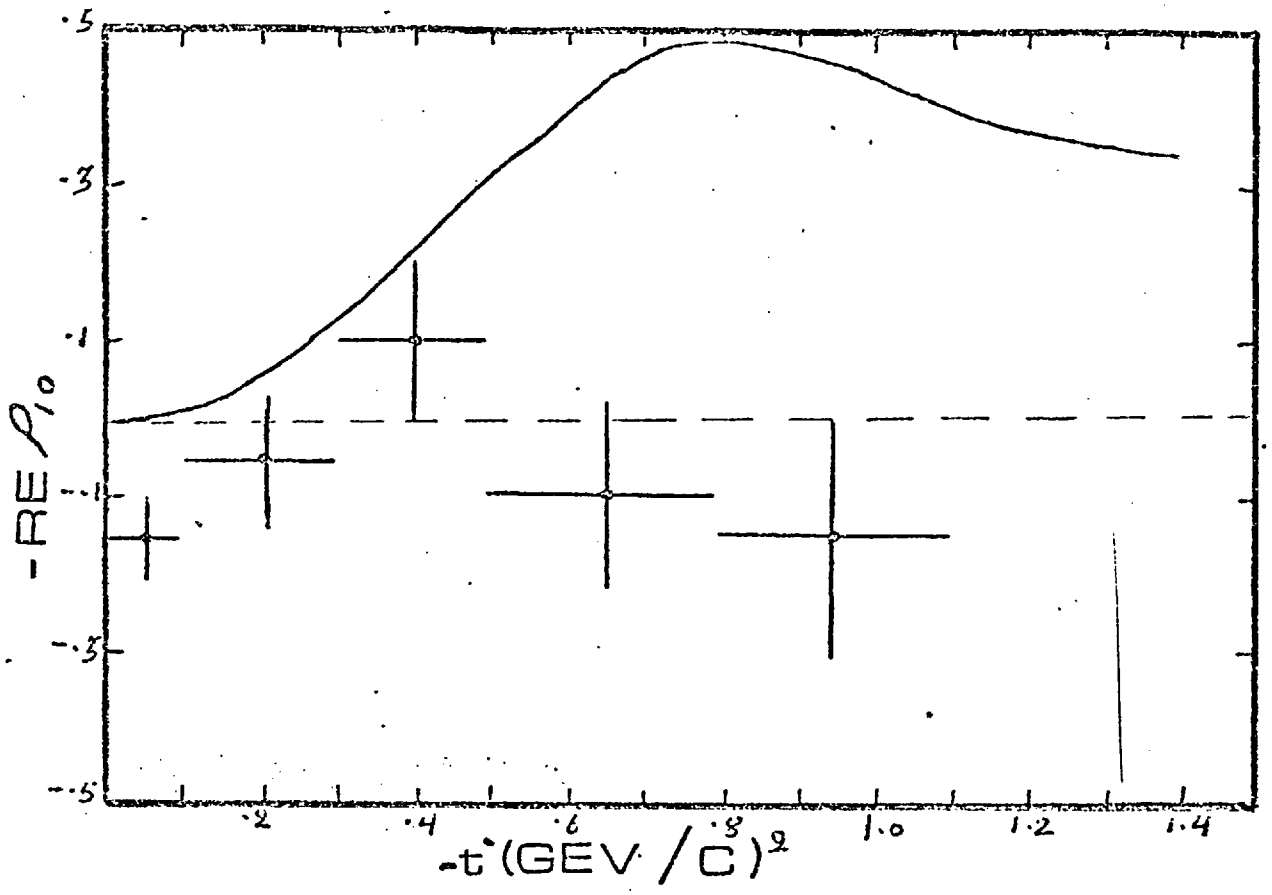
.5
.3
.1
-.1
-.3
-.5
-RE ρ10
.2
.4
.6
.8
1.0
1.2
1.4
-t (GEV/C)²

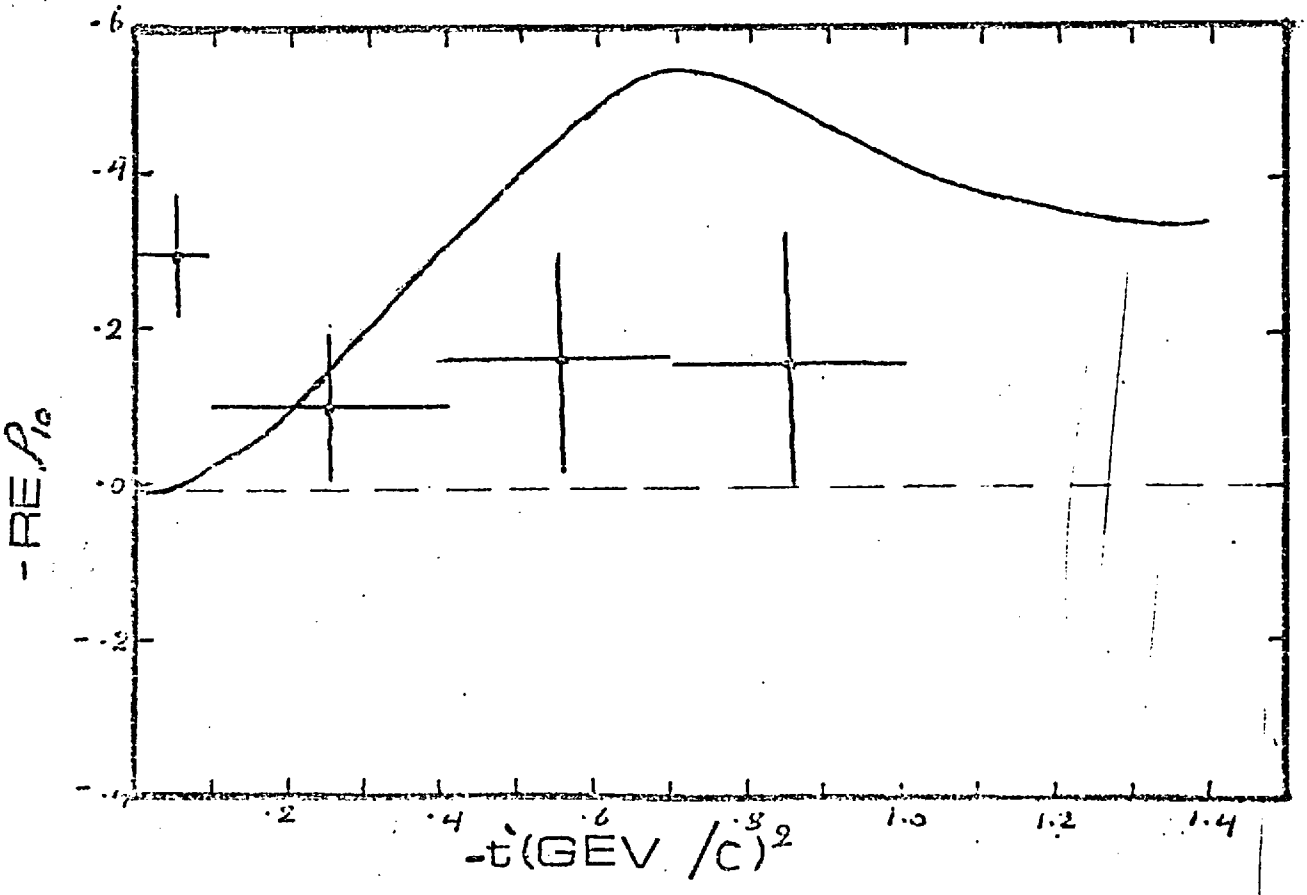
.6
.4
.2
.0
-.2
-.4
-RE ρ10
.2
.4
.6
.8
1.0
1.2
1.4
-t (GEV/C)²

FIG(5-14)

CHAPTER SIX

$K^-P \rightarrow \Delta^{++}(1236) + ANYTHING$

Production Features

The Δ^{++} resonance is produced most of the time, at our energies, in the backward hemisphere of the K^-p centre of mass system. This can be seen from the x-distributions of this resonance which are shown in fig. (6-1) for both 10 and 16 GeV/c data. It can also be observed in these distributions that although this resonance is produced in the backward direction, there is no strong peak in the region of $x = -1$.

The transverse momentum distribution of this resonance is similar in shape to that of the $K^{*-}(890)$. It differs from those of other particles discussed in Chapter Four in the sense that it does not deviate from the exponential form for small values of p_T^2, as can be seen from fig. (6-2). The average value of p_T^2 is about 0.4 $(GeV/c)^2$ which is higher than those observed for other particles but it does fall on the empirical line relating $\langle p_T \rangle$ to the mass of the particle.

The missing mass distribution of fig. (6-4) starts from threshold and increases smoothly, showing no strong features up to the kinematical limit. Such features are not to be expected anyway because of the exotic nature of the quantum numbers involved in the missing mass. This will be a great deal of help when one studies the behaviour in the Triple Regge limit because one can go to lower values of missing mass in defining the triple Regge limit, a procedure which could not be used in the $K^{*-}(890)$ case.

The Triple Regge Formula

The generalised optical theorem has been used intensively to formulate the mathematical form of the inclusive cross-section. After

the success of Regge theory in expressing the behaviour of the two body amplitude it was a logical step to use the same approach in the inclusive Mueller's optical theorem framework[1].

The basic assumption involved in the inclusive triple Regge analysis is that for small values of the squared four momentum transfer t, each narrow missing mass range M_x may be considered as a one particle state with the same trajectory $\alpha(t)$ being exchanged as in fig. (6-5-a)[2]. Now in the region of high values of missing mass the top vertex in fig. (6-5-a) can be approximated by the total cross section of the $a - \alpha(t)$ scattering with centre of mass energy M_x. This cross-section can then be represented by the imaginary part of the forward $a - \alpha(t)$ scattering amplitude which again may be expected to have a Regge behaviour as shown in fig. (6-5-c).

In general and for values of M_x above the resonance region the latter amplitude can be represented in terms of a trajectory $\bar{\alpha}(o)$ which will be the pomeron at large M_x, but an effective pomeron-reggion trajectory at lower values of M_x[3].

Such considerations lead to a dependence of the inclusive single particle cross-section on M and t given by

$$\frac{d^2\sigma}{dtdM} = \frac{1}{p_{Lab}^2} B(t) \left(\frac{s}{M_x^2}\right)^{2\alpha(t)} M_x^{2\bar{\alpha}(o) - 1} \qquad (6.1)$$

where p_{Lab} is the incident particle laboratory momentum and B(t) incorporate the various Regge residue functions involved[4].

For reasons outlined above, equation (6.1) is not expected to hold over the whole kinematical region but only in that part restricted by the following values of M_x and t [5].

1. $|t|$ must be small so that the Regge exchange argument can be expected to be valid.
2. The values of M_x ought to be chosen above the resonance region although

this condition has been relaxed by some authors using arguments based on semi-local duality, extracted from experimental observations, that Regge predictions of the asymptotic behaviour of two body total cross sections can be extrapolated to give the average cross section in the low energy resonance region.

3. Values of s/M_X^2 must be large in order to make sure that we are working in the inclusive asymptotic limit.

The same kind of relation in the above defined kinematical region has been derived by De Tar et al. using group theoretical arguments to expand the discontinuity in the 3-3 amplitude in Mueller's generalised optical theorem.

The kinematical limit defined above where this formula is expected to be valid is called the triple Regge limit and the formula itself is called the triple Regge formula because of the triple Reggion vertex involved in fig. (6-5-c).

Equation (6.1) is very useful in the sense that if it is valid and one has some prior idea of the exchange trajectories involved, one can predict the expected s dependence of the cross section from measurements of the M dependence at a single energy and vice versa.

The disadvantage involved in using this relation lies in the fact that the large M and small t restriction on the applicability of this formula means that one is necessarily working close to the kinematical boundary. Careful attention has to be paid to treatment of kinematical effects, particularly for a broad resonance like the Δ^{++}. Unfortunately such effects should be somewhat dependent on the form assumed for the Regge residue.

The applicability of the triple Regge formula has been tested in many single particle inclusive experiments. In table (6-1) [6] we quote some of these tests and the general conclusion drawn from them. In addition this table contains some of the Regge trajectories which were

found to give suitable parametrization of the data. In most cases, although the formulae did, indeed, provide a good parametrization of the inclusive cross-sections, the trajectories obtained using such parametrization are somewhat different from those obtained from two body and quasi two body reactions. This might be due mainly to the fact that in most inclusive studies one usually deals with effective trajectories which are mixtures of pomeron and degenerate reggion trajectories rather than with almost pure trajectories as in the case with two body and quasi two body reactions.

The Δ^{++} Resonance in the Triple Regge Limit

The Δ^{++} resonance inclusively produced from K^-p interactions possesses some properties which make it more useful than the $K^{*-}(890)$ resonance, discussed in Chapter Four, in testing the triple Regge formula. The first and possibly most important of all is that in the region of small values of the squared four momentum transfer from the proton to the Δ^{++}, which was chosen to be less than 0.6 $(GeV/c)^2$, the problem of background under the Δ^{++} is not serious, as can be seen in fig. (6-3). This greatly facilitates reliable analysis in this region.

The second important advantage associated with this reaction is that one reduces the problem of having to deal with effective trajectories. This can be expected if one believes that the CHQW scaling criterion discussed in Chapter Three is correct, because in this reaction we have a b $\bar{c}$ is indeed exotic and from the triple Regge formula one would expect the value of $\bar{\alpha}(o)$ to be equal to the intercept of the pomeron in order to take care of the energy independence in the triple Regge limit. Furthermore, this value should not contain any dependence on the squared four momentum transfer t and the values of the density matrix elements obtained should be compatible with those expected from exchanging the trajectory $\alpha(t)$.

The third advantage is related to the previous one and arises because the missing mass on the whole has exotic quantum numbers, thus circumventing the restriction that M_X should be large. This helps a great deal in taking a wider range in M_X within the available kinematical region, which helps to improve the quality of the fits and reduces effects due to the dependence on B(t).

Test of the Triple Regge Formula

The applicability of equation (6.1) has been tested in this reaction in the following manner:-

Equation (6.1) indicates that the Regge trajectory $\alpha(t)$ can be obtained from the s dependence at fixed M_X values. If the triple Regge formula is a valid parametrization of the data this trajectory $\alpha(t)$ should be the same as that obtained from the M_X dependence at fixed s. However, the M_X variation also depends on the intercept $\alpha(o)$ which can be obtained from the s dependence at fixed (s/M_X^2) as can be seen if we rearrange equation (6.1) to take the form:-

$$\frac{d^2\sigma}{dtdM} = \frac{1}{p_{Lab}^2} \; B(t) \left(\frac{s}{M^2}\right)^{2\alpha(t) - \bar{\alpha}(o) - \frac{1}{2}} s^{\bar{\alpha}(o) + \frac{1}{2}} \qquad (6.2)$$

Once $\bar{\alpha}(o)$ has been obtained in this way equation (6.1) can give $\alpha(t)$ from the M dependence at fixed s and this can be compared with $\alpha(t)$ from equation (6.1) using the s dependence at fixed M.

As mentioned before, the lower limit on M created no difficulty because we were able to use relatively low values of M where there are enough events to carry out the fitting. The upper limit was always affected by the position of the kinematical boundary. The missing mass distributions for the two energies in five ranges of the momentum transfer t from the proton to the Δ^{++} are shown in fig. (6-6) and fig. (6-7) in

bins of 0.1 GeV in the missing mass. We used a χ^2 minimization procedure to fit the data to the triple Regge formula (6.1). For each bin the theoretical curves given by the formula were integrated over a Breit Wigner shape with the Δ^{++} mass and width as given in the Particle Data Group tables[7]. This procedure was performed over the t range, up to the kinematical limit specified by the position of the boundary for the particular $p\pi^+$ effective mass. However, it was found that direct substitution with the Δ^{++} central mass value [7] does not produce results which are much different from the ones obtained using the above long procedure which is also dependent on the form assumed for B(t) which was left as a free parameter in our case. Fortunately, as it turned out, such effects are only important at the lowest t range where reliable results could not be obtained anyway.

The values of the parameter $\bar{\alpha}(o)$ obtained from the s dependence at fixed values of s/M_X^2 for the five t ranges are shown in fig. (6-8). The results represent the average values obtained from determinations in each t bin for various values of M_X chosen such that the quantity (s/M_X^2) remains the same for both 10 and 16 GeV/c. It is very interesting that the values of $\bar{\alpha}(o)$ do not show any significant t dependence except that we get a rather anomalous value of $\bar{\alpha}(o)$ for the lowest t bin. This is because, as was stated earlier, of the effect of the way we dealt with the Regge residue B(t). No attempt was made to substitute any functional form of B(t). The other very interesting feature which can be observed is that the values of $\bar{\alpha}(o)$ obtained are compatible with unity. Such a value is to be expected if one has the pomeron trajectory at the kaon vertex and one expects duality to be true. What is not well understood is that the values of $\bar{\alpha}(o)$ are slightly higher than expected. Different checks were applied and the whole calculation was repeated twice without any significant difference in the results. We suspect that this might be due to some error in the calculations of the microbarn equivalent per event in the 16 GeV/c data, which was the first batch of measurement to go

onto the DST. It would be very desirable if the whole analysis can be repeated when more statistics at 16 GeV/c become available.

Using values of $\bar{\alpha}(o)$ derived above we determined the Regge trajectory $\alpha(t)$ from the M dependence at 16 GeV/c in the range of M between 1.0 and 2.5 GeV/c. A number of separate determinations of $\alpha(t)$ were made from the s dependence between 10 and 16 GeV/c for narrow fixed values of M. The overall average of the values of $\alpha(t)$ for each t range are plotted in fig. (6-9). The slope and intercept of the trajectory $\alpha(t)$ were derived from the fitted values of $\alpha(t)$ though passing a straight line through the points in fig. (6-9). In this case we neglected the $\alpha(t)$ value in the lowest t range because it is biased due to kinematical effects. The trajectory obtained was of the form

$$\alpha(t) = 0.45 + 0.75\ t \quad .$$

The slope and intercept of this trajectory are compatible with those of the ρ [8].

From the above discussion one may conclude that the triple Regge formula provides a good parametrization of our data. The slope and intercepts of the Regge trajectories obtained are in good agreement with those expected from such a Regge picture. The value of $\bar{\alpha}(o)$, which is close to unity, can be considered as a demonstration of the duality principle where the pomeron is considered to be dual to the exotic a b $\bar{c}$ combination.

The Effect of the Regge Residue

It is clear that the values of both $\alpha(t)$ and $\bar{\alpha}(o)$ obtained from our parametrization of the data using the triple Regge formula were higher in the lowest t bin than in other t ranges. Furthermore, these values

are not in agreement with values expected if one assumes that our trajectories are compatible with well known Regge trajectories. This result is not very surprising, because of the way we treated the Regge residue function B(t) in our parametrization, where no explicit functional form was substituted for it. In this case one would naturally expect some anomalies in the small t region where kinematic corrections can be strongly dependent on the functional form of B(t). In this small t region our knowledge of the exchange mechanism and consequently the form of the Regge residue is very limited. For very small values of t one is very near to the pion pole exchange where the Regge residue function may have to contain in its structure a pion propagator of the form $\frac{1}{t - m^2}$. Such a propagator can give steep t dependence in the small t region. For higher values of t one might expect contributions from other exchanges such as the ρ and the A_2 as we move away from the pion pole. Such contributions can give a more gentle type of t dependence in the very small t region and the t dependence becomes weaker as t increases for both pion and other exchanges[9]. For this reason we have considered the values of $\bar{\alpha}(o)$ and $\alpha(t)$ above the lowest t bin as more reliable than the values in the lowest t bin because their values are not very dependent on the kinematic corrections due to the shape of B(t).

Decay Angular Distributions and Density Matrix Elements

In order to check the degree of reasonableness of the values of the slope and intercept of the Regge trajectory obtained from fitting the triple Regge formula, we studied the exchange mechanism of Δ^{++} production in terms of its decay angular distributions and the density matrix elements associated with them. In this case again we rely upon the results of Ader, Meyer and Salin in the same way we did in the K^{*-} case and assume that all relations derived for a quasi-two body angular distribution can be used for inclusive resonance production processes.

We studied the angular distributions in the Jackson frame which can be defined in the same way as in the K^{*-} case by interchanging the target proton and the projectile kaon directions in fig. (5-6)

For this case the decay angular distributions for a spin 3/2 baryon resonance is given by[10]

$$W(\cos\theta, \phi) = \frac{3}{4\pi}\left[\frac{1}{6}(1 + 4\rho_{33}) + \frac{1}{2}(1 - 4\rho_{33})\cos^2\theta - \frac{2}{\sqrt{3}}\rho_{3,-1}\right.$$
$$\left.\sin^2\theta\cos 2\phi - \frac{2}{\sqrt{3}}\,\mathrm{Re}\,\rho_{31}\sin^2\theta\cos\phi\right] . \qquad (6.3)$$

Fig. (6-10) and fig. (6-11) show the cos θ angular distributions for Δ^{++} produced at 10 and 16 GeV/c respectively. The t cuts used are the same as those used in the study of the triple Regge limit and all plots contain only events selected in the missing mass region of 1.0 to 2.5 GeV as used in the triple Regge fit.

The density matrix elements were calculated from the cos θ and φ angular distributions of fig. (6-10) and fig. (6-11). Using the method of moments applied to equation (6.3), the three density matrix elements are given by

$$\rho_{33} = \frac{1}{8}(7 - 15\,\overline{\cos^2\theta})$$
$$R\rho_{3,-1} = -\frac{5\sqrt{3}}{8}\,\overline{\sin^2\theta\cos 2\phi} \qquad (6.4)$$
$$\mathrm{Re}\,\rho_{3,1} = -\frac{5\sqrt{3}}{8}\,\overline{\sin 2\theta\cos\phi}$$

Because no detailed model analysis about the behaviour of decay angular distributions and density matrix elements exists, one does not really know what to expect. However, it is probable that the behaviour will not be much different from that in the quasi two body case, where

some predictions do exist.

Because our results concerning the trajectory $\alpha(t)$ show that it is very compatible with the ρ trajectory, we chose to compare our results for the density matrix elements with predictions made for the quasi two body case by the ρ exchange model of Stodolsky and Sakurai[11] where the vertex $p\text{-}\rho\text{-}\Delta^{++}$ is treated, in analogy to the vertex $N\gamma\Delta^{++}$, in terms of electromagnetic multipole transitions because the quantum numbers of the ρ are the same as those of the photon. They found that using such assumptions one gets the values of the three density matrix elements as

$$\rho_{33} = \frac{3}{8} , \qquad \text{Re } \rho_{3,-1} = \frac{\sqrt{3}}{8} , \qquad R\rho_{31} = 0.0 \quad .$$

These density matrix elements for our 10 and 16 GeV/c data are shown in fig. (6-12) and fig. (6-13) respectively. The values of ρ_{33}, Re $\rho_{3,-1}$ and Re $\rho_{3,1}$ and their t dependence are not in good agreement with the unmodified ρ exchange model. It is possible that better agreement would be obtained if one took into account absorption effects which could yield the t dependence observed.

Pomeron Factorization

Factorization of Regge trajectories can be useful in the sense that it provides many relations between scattering cross-sections of different particles. Many authors are inclined to believe that the pomeron is a factorisable pole[2, 6].

To check this property in the triple Regge limit we compared our data at 16 GeV/c with unpublished data from $\pi^- p$ interactions at the same energy[12].

On the triple Regge diagram of fig. (6-4-c) one would have an a b $\bar{c}$ combination exotic in both cases where a is K^- or π^-. Thus one would expect $\bar{\alpha}(o)$ to be that of the pomeron which, according to duality, is

expected to dominate. The only difference one would expect between the two cases is that due to different couplings between the pomeron and the projectile particle in each case. This is only true if the pomeron is a factorizable pole. In this instance one can write a relation between the partial cross-sections in the two cases given by

$$\frac{d^2\sigma/dtdM(p \overset{K^-}{\rightarrow} \Delta^{++})}{d^2\sigma/dtdM(p \overset{\pi^-}{\rightarrow} \Delta^{++})} = \frac{\gamma_{\pi^-P}}{\gamma_{K^-P}}$$

where γ_{K^-P} is the pomeron coupling to K^- and γ_{π^-P} is the pomeron coupling to the π^-.

The ratio of the two couplings can be obtained from the ratio of K^-p/π^-p total cross-sections where one again has to assume that the pomeron is a factorizable pole. In such a case we can write

$$\frac{d^2\sigma/dMdt(p \overset{K^-}{\rightarrow} \Delta^{++})}{d^2\sigma/dMdt(p \overset{\pi^-}{\rightarrow} \Delta^{++})} = \frac{\sigma_T(K^-p)}{\sigma_T(\pi^-p)} \quad .$$

Fig. (6-14) shows the partial cross-sections for production in t and M in both cases plotted on the same diagram at beam momentum of 16 GeV/c. The cross-section for K^-p case is multiplied by $\sigma_T(\pi^-p)$ $\sigma_T(K^-p)$. The two distributions seem to be in very good agreement with each other for all ranges in t after such normalisation. This supports the assumption that the pomeron is, indeed, a factorizable pole.

Summary and Conclusions

The main aim of this chapter was to perform a possible test on the triple Regge formula using the inclusively produced Δ^{++} resonance. The formula seems to provide a good parametrization of the data and the values of the parameters obtained for the slope and intercepts of the Regge

trajectories are in good agreement with those expected if the formula is applicable. The results deduced from studies of the decay angular distributions and the density matrix elements are not in disagreement with assumptions about the ρ exchange production mechanism which was the result obtained from the triple Regge fit.

The value of $\bar{\alpha}(o)$ is of a special importance because of its relation to the scaling behaviour of Δ^{++}. If one take the CHQW condition of a b $\bar{c}$ exoticity as sufficient in this case, one would expect $\bar{\alpha}(o)$ to be that of the pomeron, which is, indeed, compatible with what we obtain from our fits. This supports not only the triple Regge parametrization but also the exoticity condition for scaling predicted by CHQW.

It is interesting to note that agreement of the data with the triple Regge parametrization is good even in this relatively low energy region in spite of the fact that the triple Regge formula is an approximation to the asymptotic limit.

REFERENCES (6)

1. Chan Hong-Mo, C.S. Hsue, C. Quigg and Jiunn-Ming Wang, Phys. Rev. Letters 26, 672 (1971).
2. Hong-Mo Chan, Rutherford Laboratory Preprint RPP/T/21.
3. P. Chliapnikov, O. Czyzewski, J. Finkelstein and M. Jacob, Phys. Letters 35B, 581 (1971).
4. R.C. Arnold, NAL Preprint ANL/HEP 7139 (1971).
5. De Tar et al, Phys. Rev. D2, 425 (1971).
6. D.P. Roy, Rutherford Laboratory Preprint RPP/T/41 (1973).
7. N. Barash et al, Particle Data Group, Reviews of Modern Physics, Volume 45, No. 2 (1973).
8. Gerald E. Hite, Reviews of Modern Physics, Part I, 669 (1969).
9. E. Ferrari and F. Selleri, Nuovo Cimento 21, 1028 (1961).
10. N. Schmitz, Proceedings of the 1965 CERN Easter School, CERN Yellow Report, CERN 65-24 (1965).
11. L. Stodolsky and J.J. Sakurai, Phys. Rev. Letters 11, 90 (1963).
12. K.W.J. Barnham, Private Communication.

TABLE CAPTION (6)

(6-1) A compilation of results on using triple Regge parametrization of inclusive distributions from ref.(6).

TABLE (6-1)[6]

i	Reaction	$\alpha_i(t)$	Authors
p	$\pi^- p \to pX$ $pp \to pX$	O.K.	Chan, Miettinen, Roberts, Paige and Wang
ρ	$pK^- \to \bar{K}^0 X$ $pK^+ \to K^0 X$	O.K.	Chliapnikov et al. Rutherford-Saclay E.P.
K^*	$K^- p \to \Lambda^0 X$	O.K.	Rutherford-Saclay E.P.
π	$p\gamma \to \pi^- X$ $\pi^+ p \to \Delta^{++} X$	O.K.	Stanford-Berkeley-Tuft ABBCCHW Collaboration
Δ	$p\pi^- \to pX$	O.K.	Randa, Bishari and Yeshian
N	$pK^- \to \Lambda^0 X$	O.K.	Rutherford-Saclay-E.P.
Δ	$pp \to \pi^- X$ $\gamma p \to \pi^- X$	Too low	Risk, Ranft and Ranft Chen et al. Stanford-Berkeley-Tuft
N	$pp \to \pi^+ X$	Too low	=

FIGURE CAPTIONS (6)

(6-1) X distribution for inclusive Δ^{++} production from K^-p at

(a) 10 GeV/c

(b) 16 GeV/c.

(6-2) p_T^2 distribution for inclusive Δ^{++} production from K^-p at

(a) 10 GeV/c

(b) 16 GeV/c.

(6-3) $p\pi^+$ effective mass distribution for

(a) all Δ^{++}'s produced from K^-p at 10 GeV/c

(b) all Δ^{++}'s produced from K^-p at 16 GeV/c

(c) Δ^{++}'s produced with $t < 0.6$ $(GeV/c)^2$ from K^-p at 10 GeV/c

(d) Δ^{++}'s produced with $t < 0.6$ $(GeV/c)^2$ from K^-p at 16 GeV/c.

(6-4) Missing mass distributions for the reaction $K^-p \to \Delta^{++}$ + anything at

(a) 10 GeV/c

(b) 16 GeV/c.

(6-5) Schematic representation of the amplitude $ab\bar{c}$-$ab\bar{c}$ in the triple Regge limit.

(6-6) Triple Regge fits for the inclusive cross section $d^2\sigma(K^-p \to \Delta^{++} + X^{--})/dtdM_X$ at 10 GeV/c.

(6-7) Triple Regge fits for inclusive cross section $d^2\sigma(K^-p \to \Delta^{++} + X^{--})/dtdM_X$ at 16 GeV/c.

(6-8) Values of $\bar{\alpha}(o)$ obtained from fitting the triple Regge formula to our data for the reaction $K^-p \to \Delta^{++} + X^{--}$ at 10 and 16 GeV/c plotted against t.

(6-9) Values of $\alpha(t)$ obtained from fitting the triple Regge formula to our data for the reaction $K^-p \to \Delta^{++} + X^{--}$ at 10 and 16 GeV/c plotted against t. The dashed line represents the fitted Regge trajectory through four points.

(6-10) Cos θ and ϕ decay angular distribution for inclusive Δ^{++} produced from K^-p at 10 GeV/c plotted versus t, the missing mass range is between 1.5 and 2.5 GeV.

(6-11) Cos θ and ϕ decay angular distribution for inclusive Δ^{++} produced from K^-p at 16 GeV/c plotted versus t, the missing mass range is between 1.5 and 2.5 GeV.

(6-12) The Δ^{++} density matrix elements ρ_{33}, Re ρ_{31} and Re $\rho_{3,-1}$ calculated from the distribution in fig.(6-10).

(6-13) The Δ^{++} density matrix elements ρ_{33}, Re ρ_{31}, and Re $\rho_{3,-1}$ calculated from the distribution in fig. (6-11).

(6-14) Comparison of $\frac{d^2\sigma}{dMdt^2}$ ($\pi^-p \to \Delta^{++} + X^{--}$) with $\frac{\sigma_T(\pi^-p)}{\sigma_{TK^-}}$ $\frac{d^2\sigma}{dMdt}$ ($K^-p \to \Delta^{++} + X^{--}$) at 16 GeV/c.

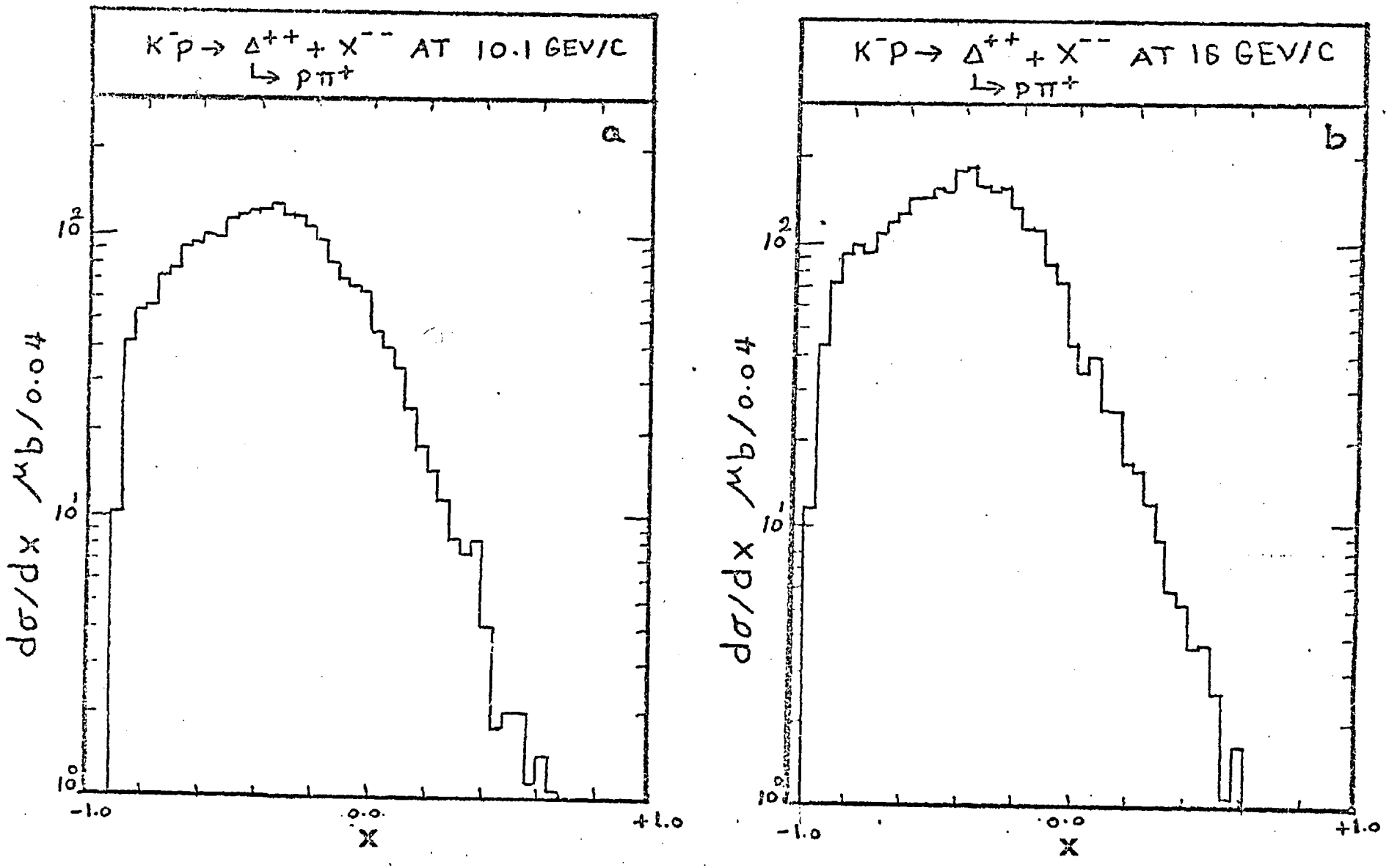
K⁻p → Δ⁺⁺ + X⁻⁻ AT 10.1 GEV/C
↳ pπ⁺
a
dσ/dx mb/0.04
10²
10¹
10⁰
-1.0
0.0
+1.0
X
K⁻p → Δ⁺⁺ + X⁻⁻ AT 16 GEV/C
↳ pπ⁺
b
dσ/dx mb/0.04
10²
10¹
10⁰
-1.0
0.0
+1.0
X

FIG(6-1)

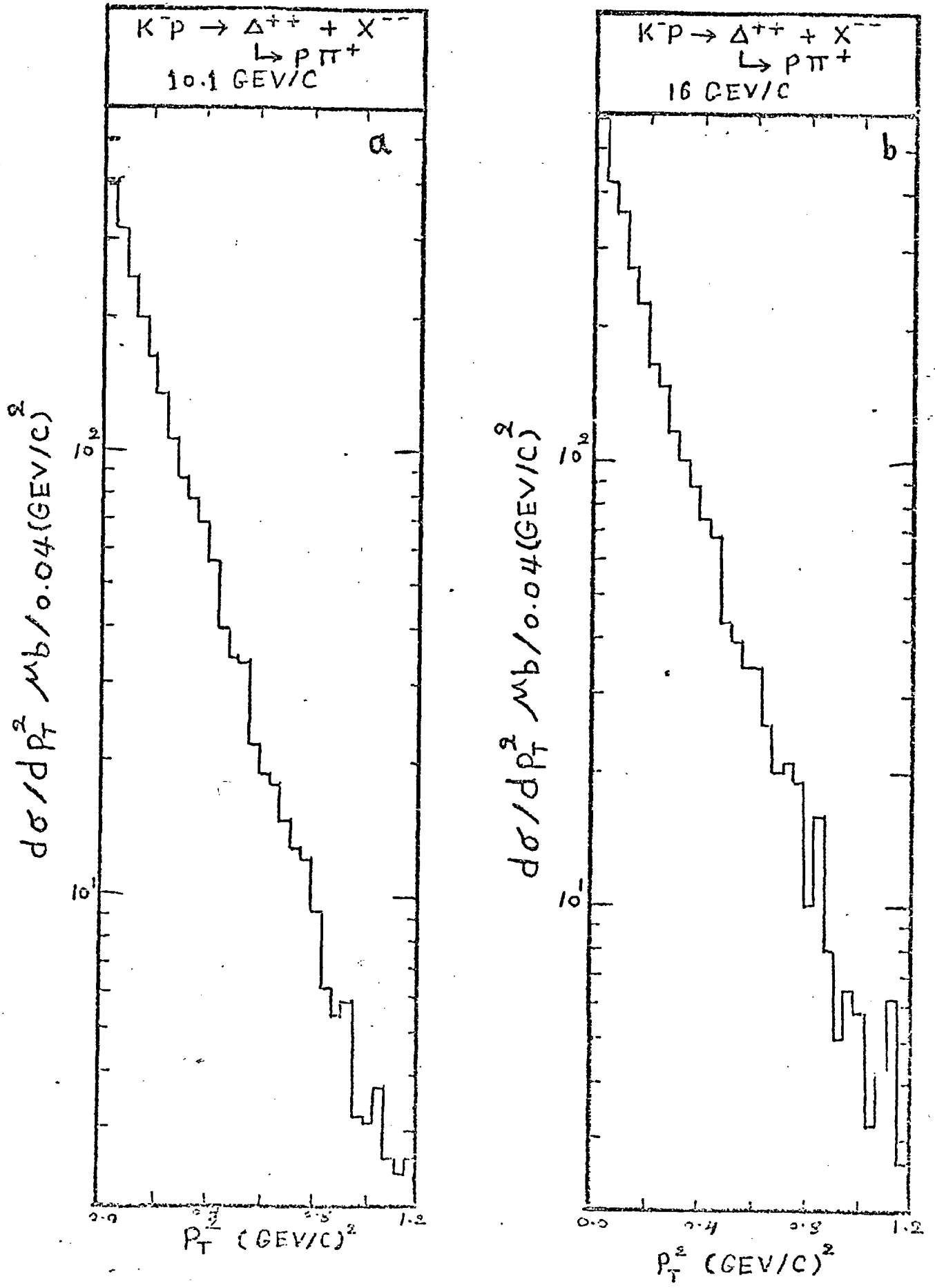
K⁻P → Δ⁺⁺ + X⁻⁻
↳ P π⁺
10.1 GEV/C
a
K⁻P → Δ⁺⁺ + X⁻⁻
↳ P π⁺
16 GEV/C
b
dσ/dP_T² mb/0.04(GEV/C)²
10²
10¹
0.0
0.4
0.8
1.2
P_T² (GEV/C)²

FIG(6-2)

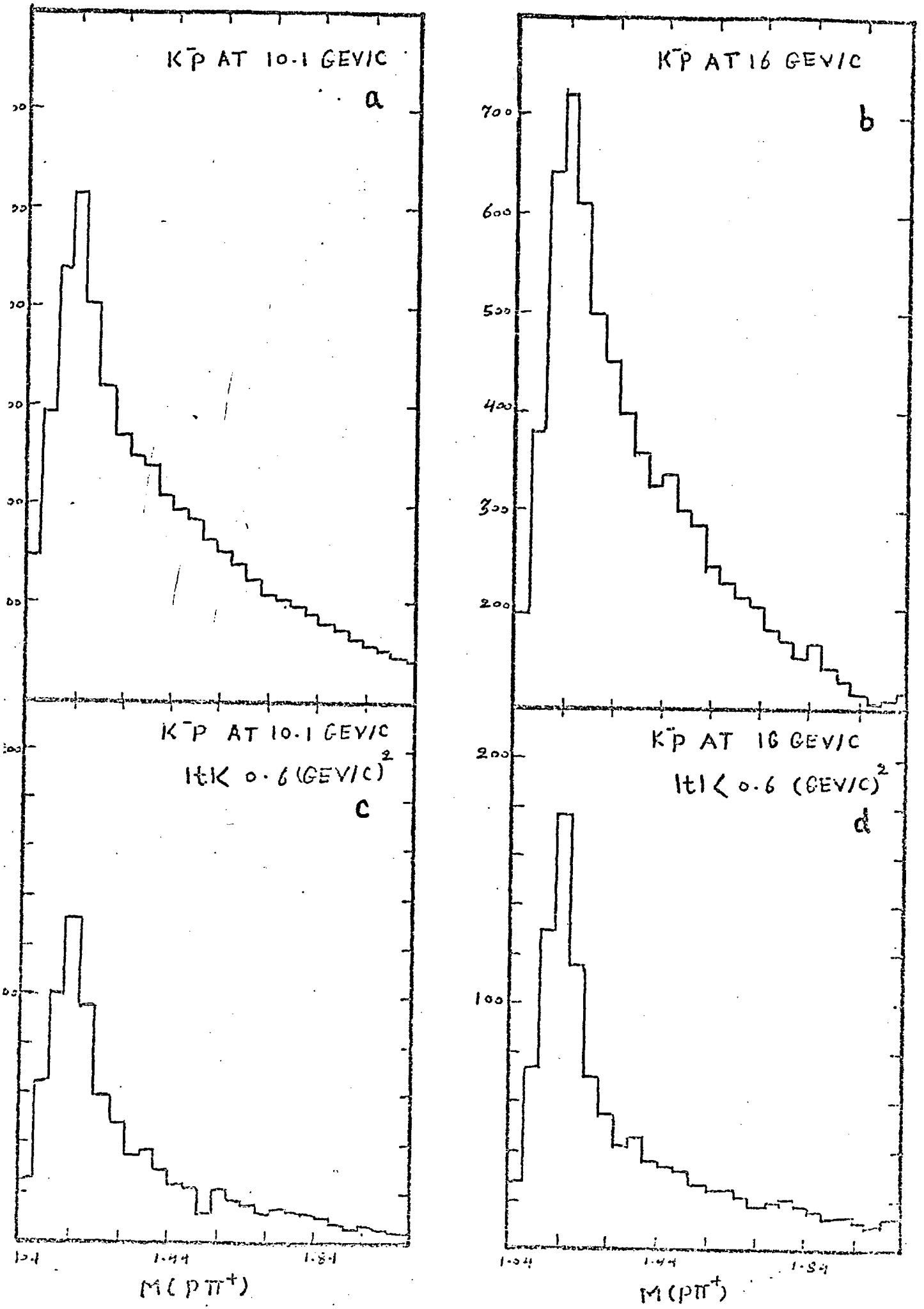
K⁻P AT 10.1 GEV/C
a
K⁻P AT 16 GEV/C
b
K⁻P AT 10.1 GEV/C
|t|< 0.6 (GEV/C)²
c
K⁻P AT 16 GEV/C
|t|< 0.6 (GEV/C)²
d
M(pπ⁺)
M(pπ⁺)

FIG(6-3)

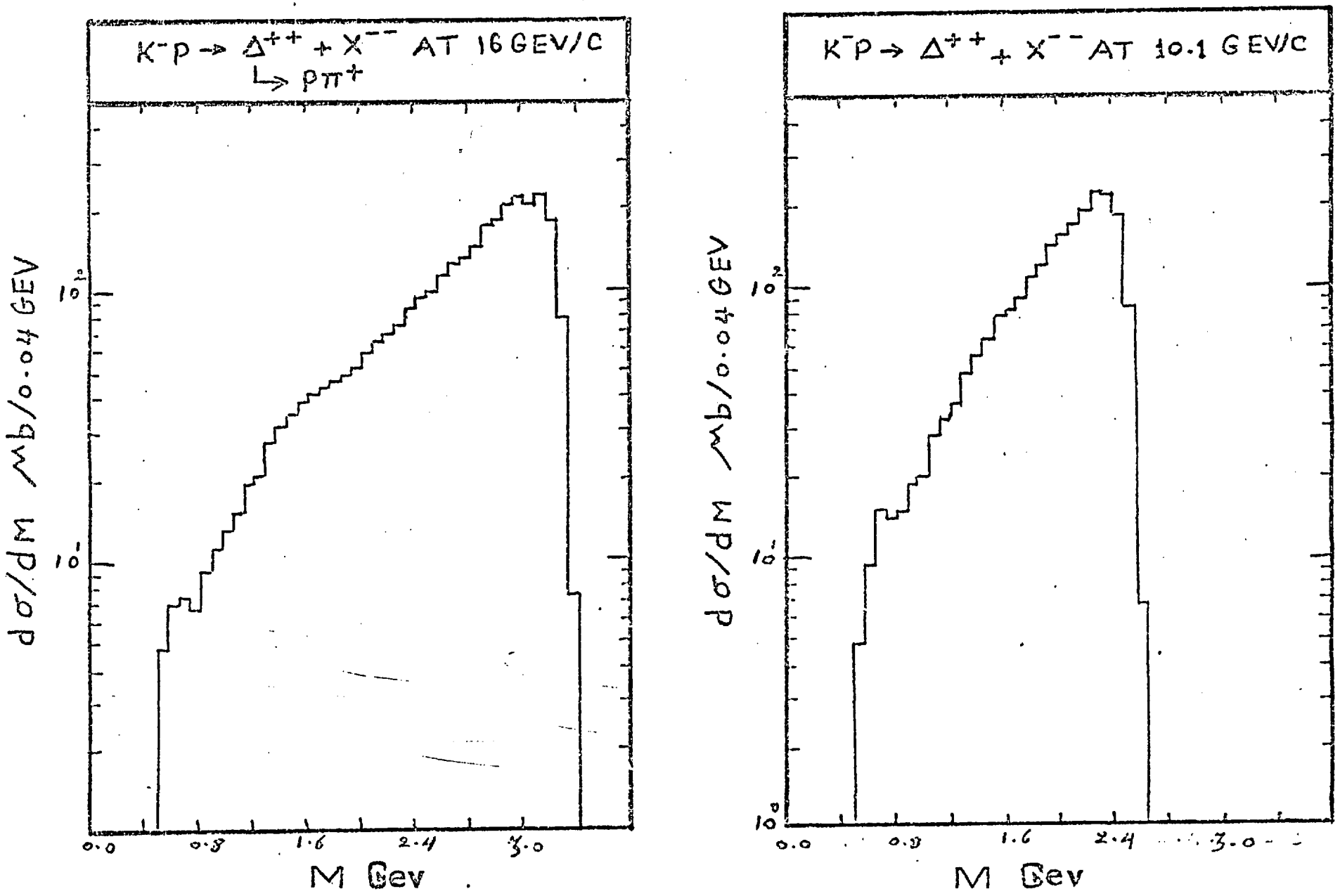
K⁻p → Δ⁺⁺ + X⁻⁻ AT 16 GEV/C
↳ pπ⁺
dσ/dM mb/0.04 GEV
M Gev
0.0
0.8
1.6
2.4
3.0
K⁻p → Δ⁺⁺ + X⁻⁻ AT 10.1 GEV/C
dσ/dM mb/0.04 GEV
M Gev
0.0
0.8
1.6
2.4
3.0

FIG(6-4)

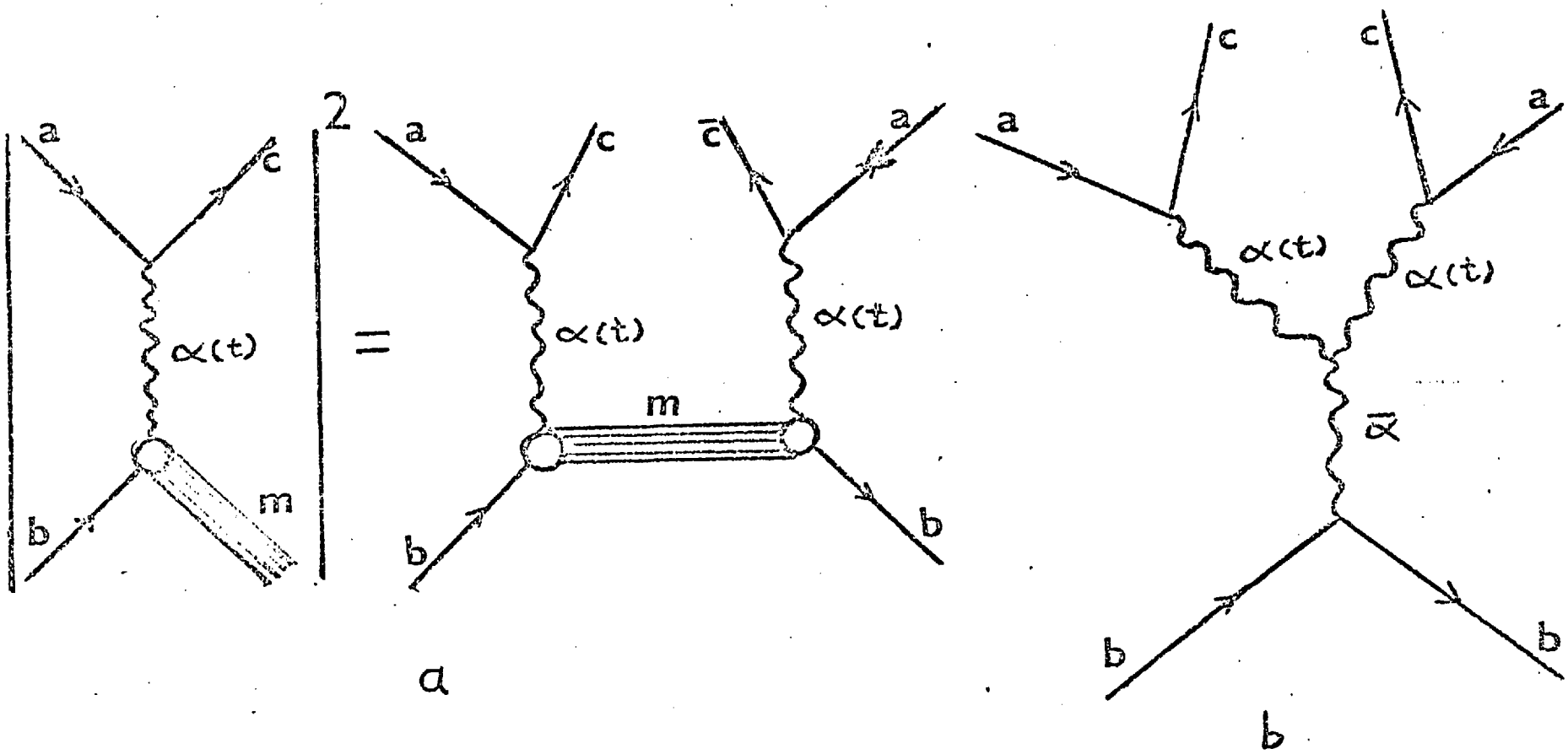

FIG(6-5)

FIG(6-6)

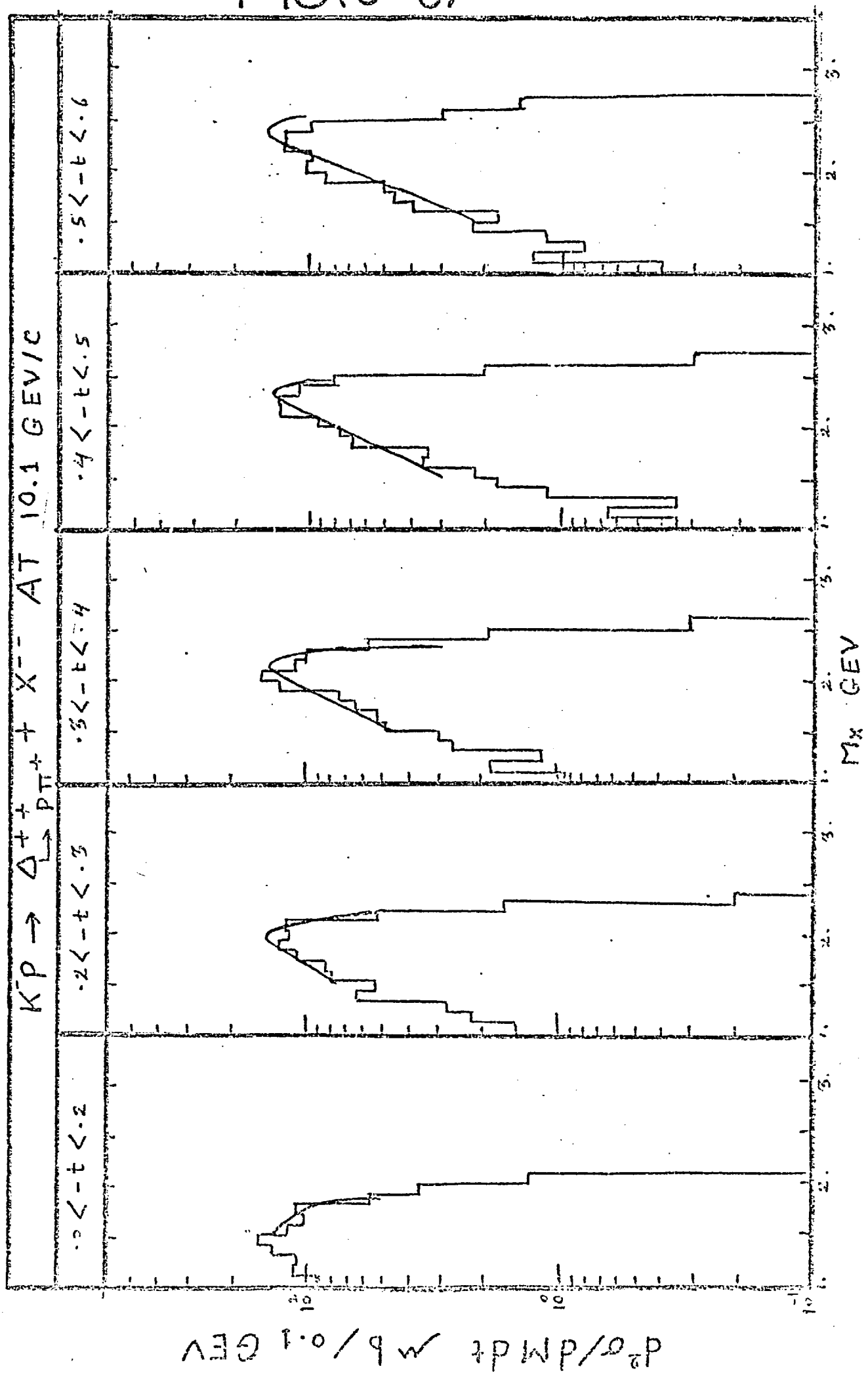

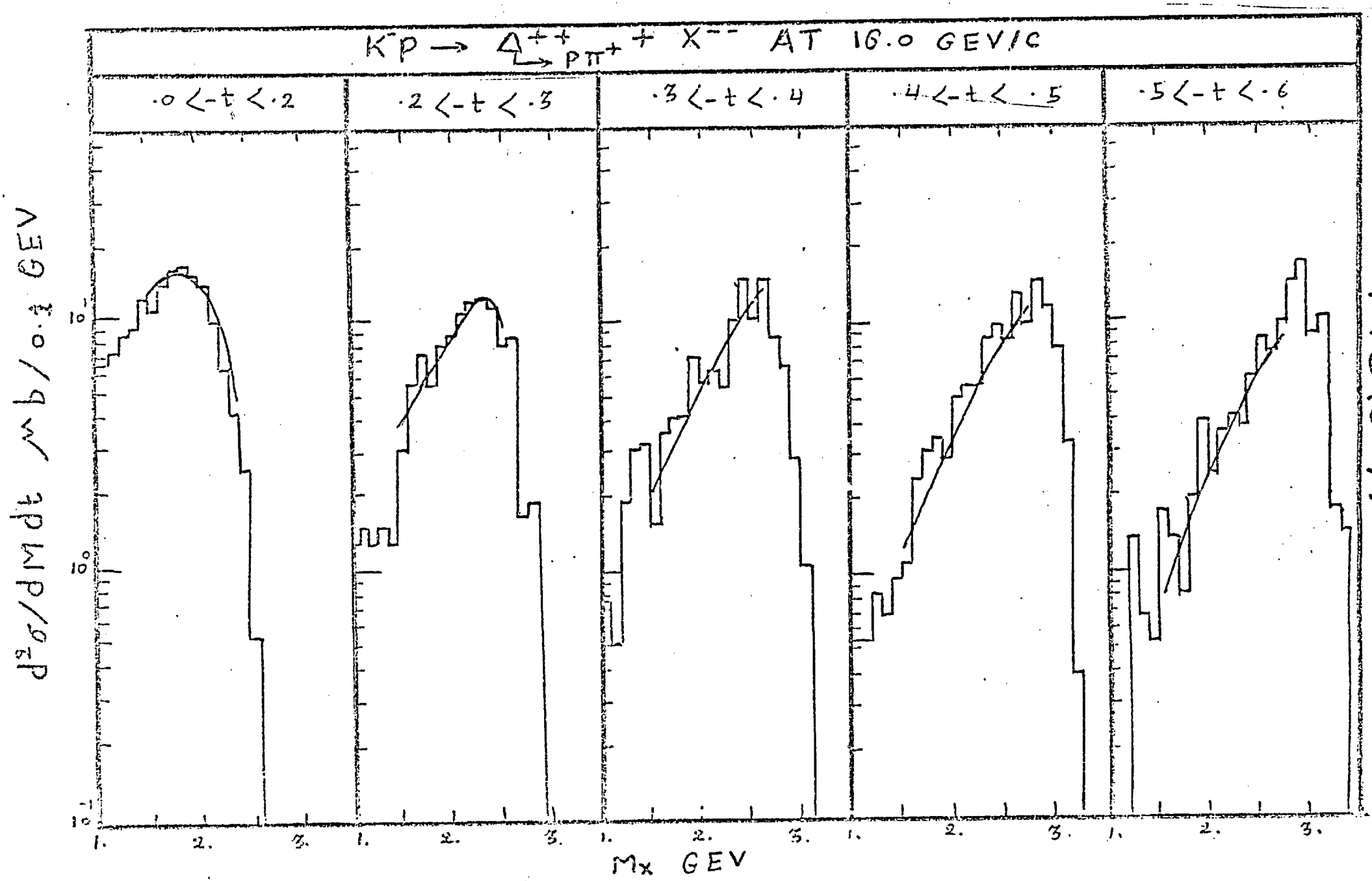
$K^-p \rightarrow \Delta^{++}_{\rightarrow p\pi^+} + X^{--}$ AT 16.0 GEV/C
$.0 < -t < .2$
$.2 < -t < .3$
$.3 < -t < .4$
$.4 < -t < .5$
$.5 < -t < .6$
$d^2\sigma/dMdt$ mb/0.1 GEV
M_X GEV

FIG(6-7)

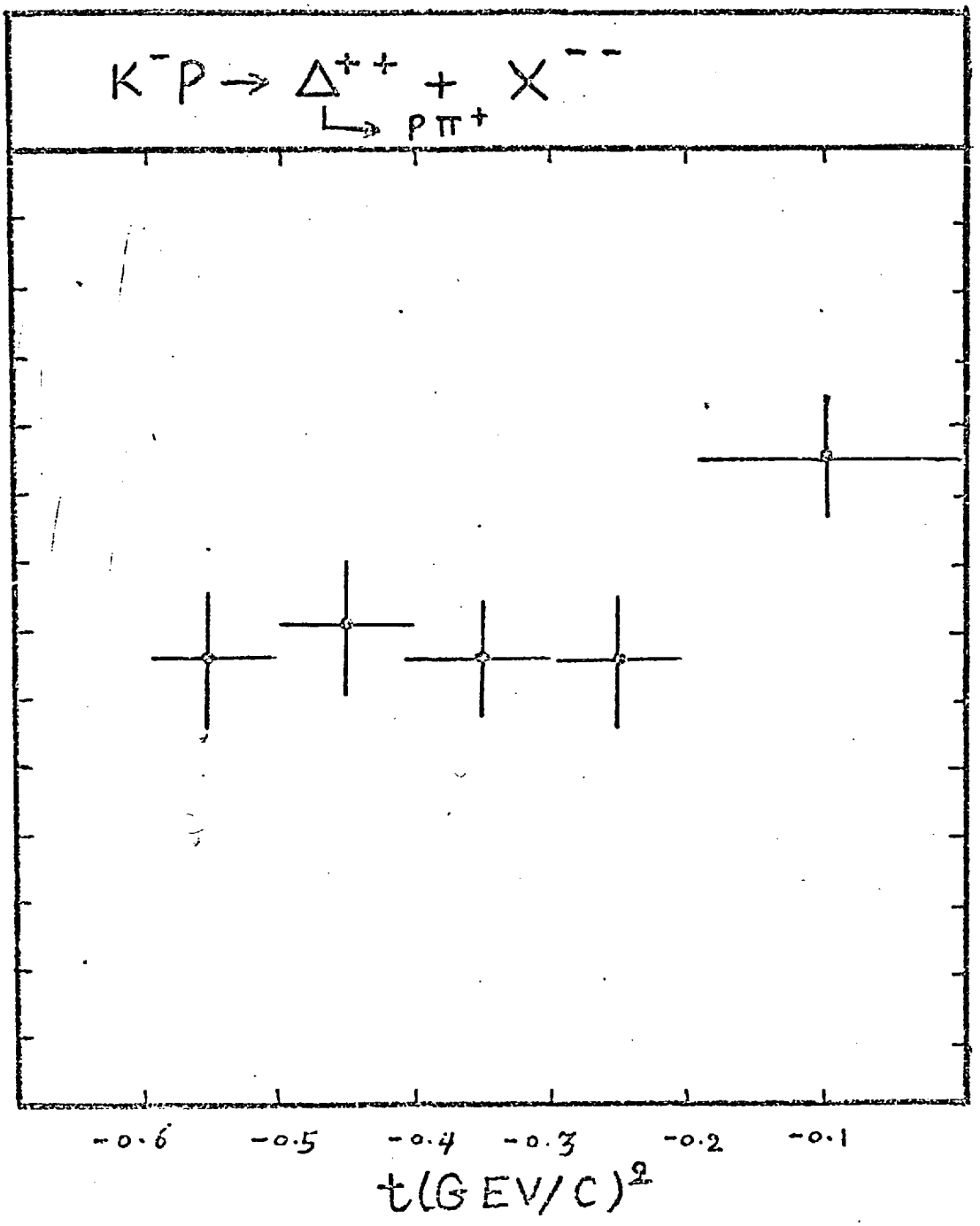
$K^- p \to \Delta^{++} + X^{--}$
$\Delta^{++} \to p\pi^+$
$\bar{\alpha}(0)$
2.0
1.0
-0.6
-0.5
-0.4
-0.3
-0.2
-0.1
$t(GEV/C)^2$

FIG(6-8)

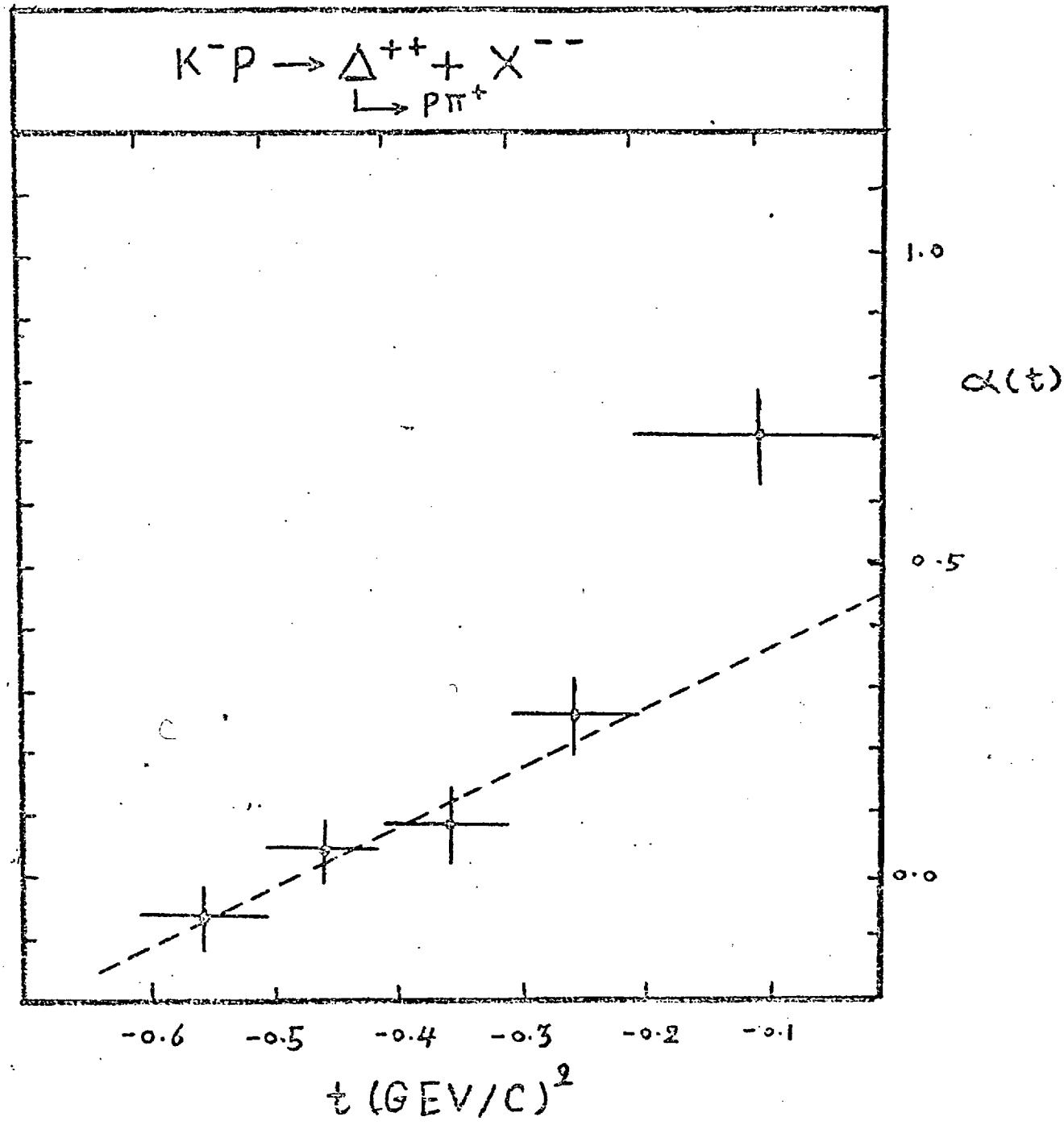

$\alpha(t) = 0.45 + 0.7\,t$

FIG(6-9)

$K^- p \rightarrow \Delta^{++} + X^{--}$ AT 10.1 GEV/C

$1.5 < M(X) < 2.5$ Gev

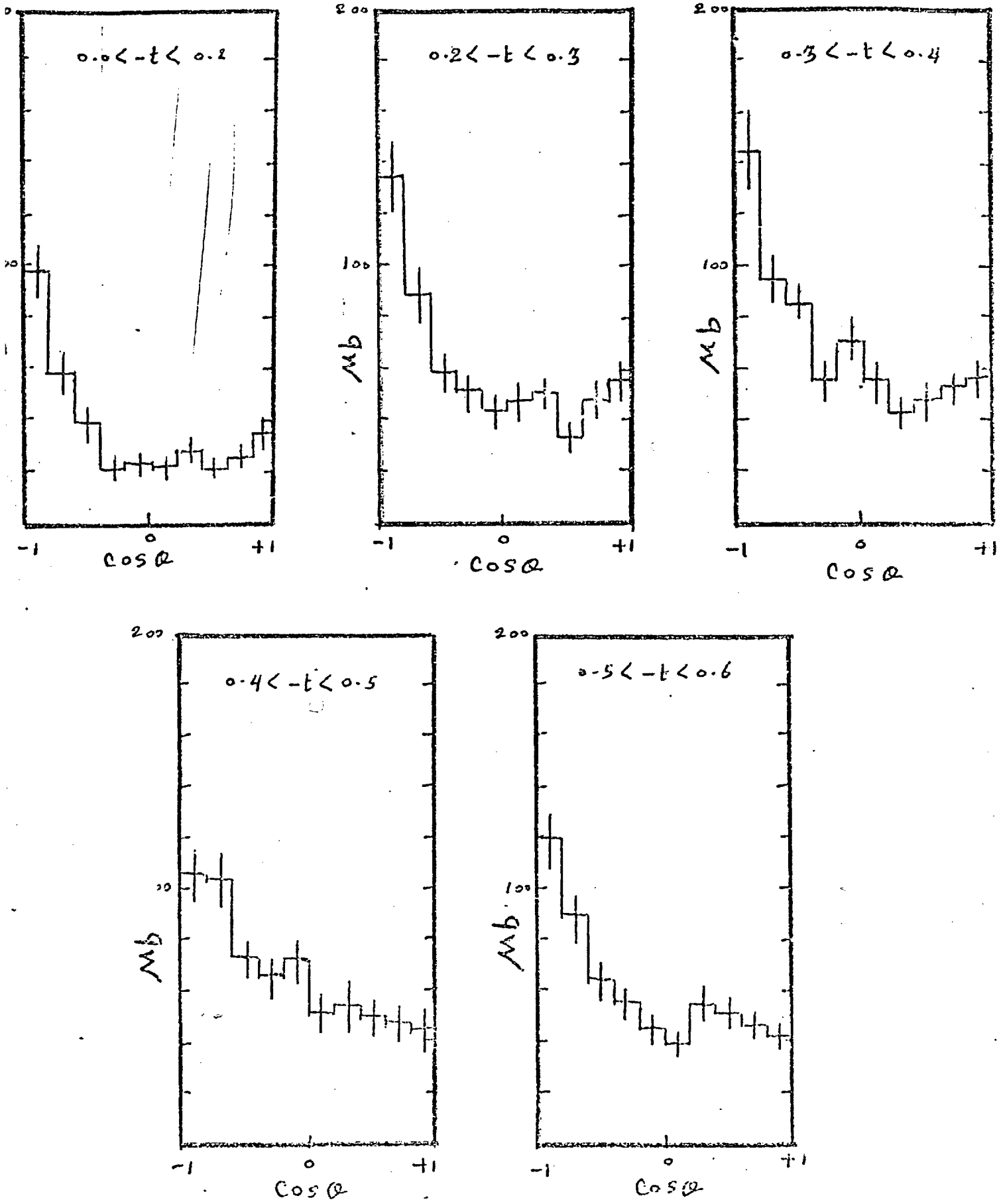

FIG(6-10-a)

$K^- p \rightarrow \Delta^{++} + X^{--}$ AT 10 GEV/c

$1.5 < M_X < 2.5$ Gev

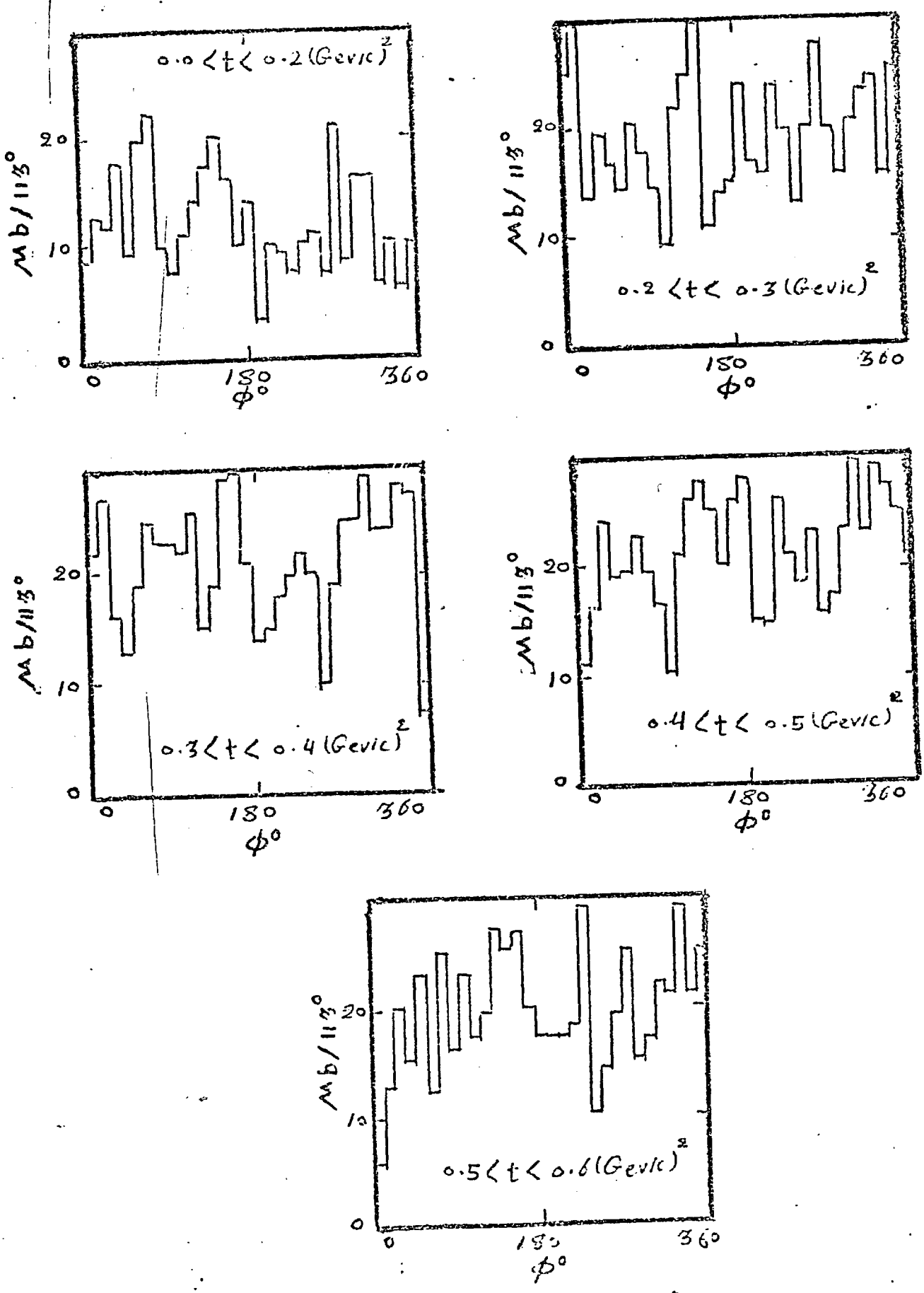

FIG (6-10-b)

$K^- p \to \Delta^{++} + X^{--}$ AT 16 GEV/C

$1.5 < M(X) < 2.5$ Gev

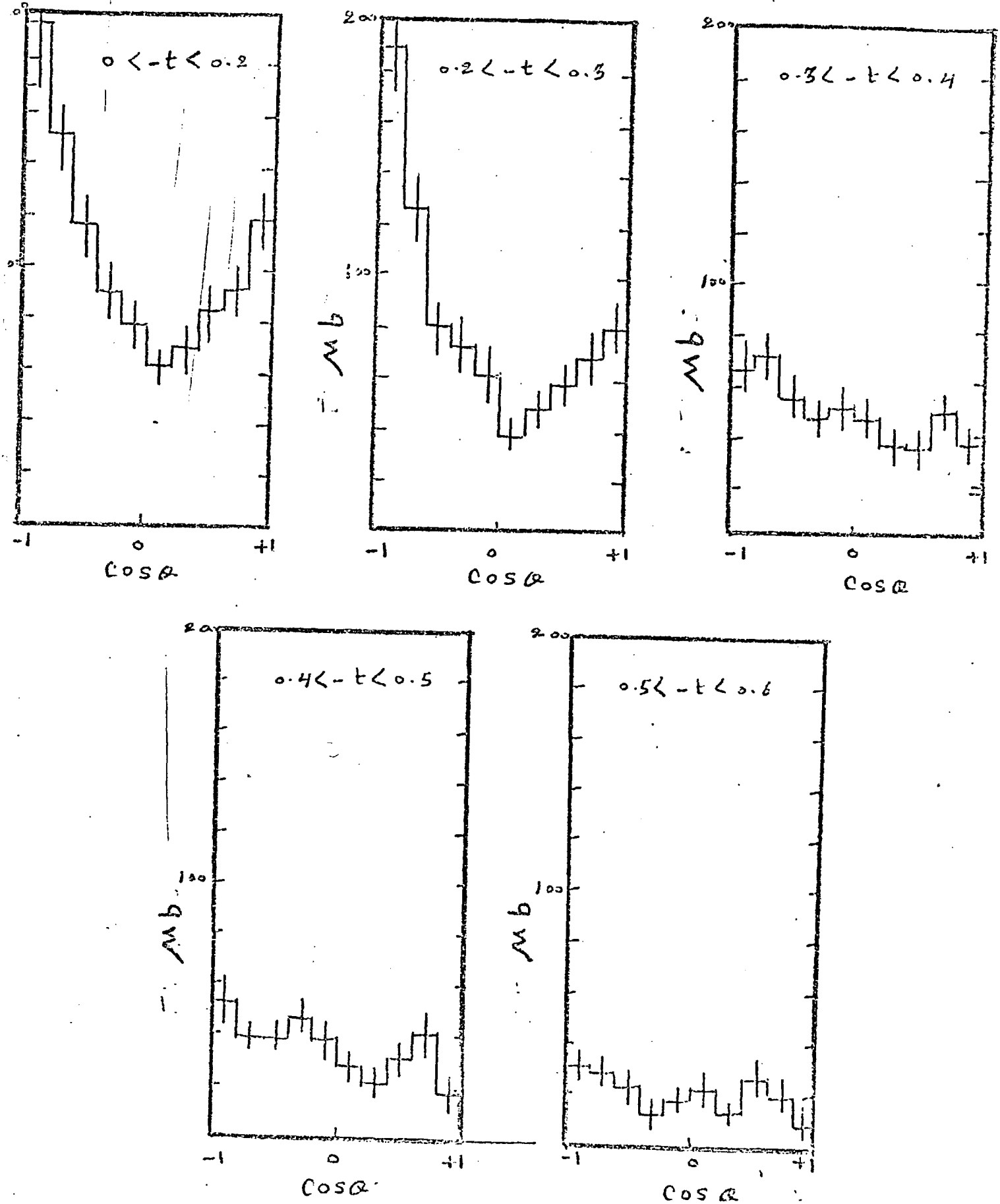

FIG(6-11-a)

$K^- p \rightarrow \Delta^{++} + X^{--}$ AT 16 GEV/C
$1.5 < M_X < 2.5$ Gev

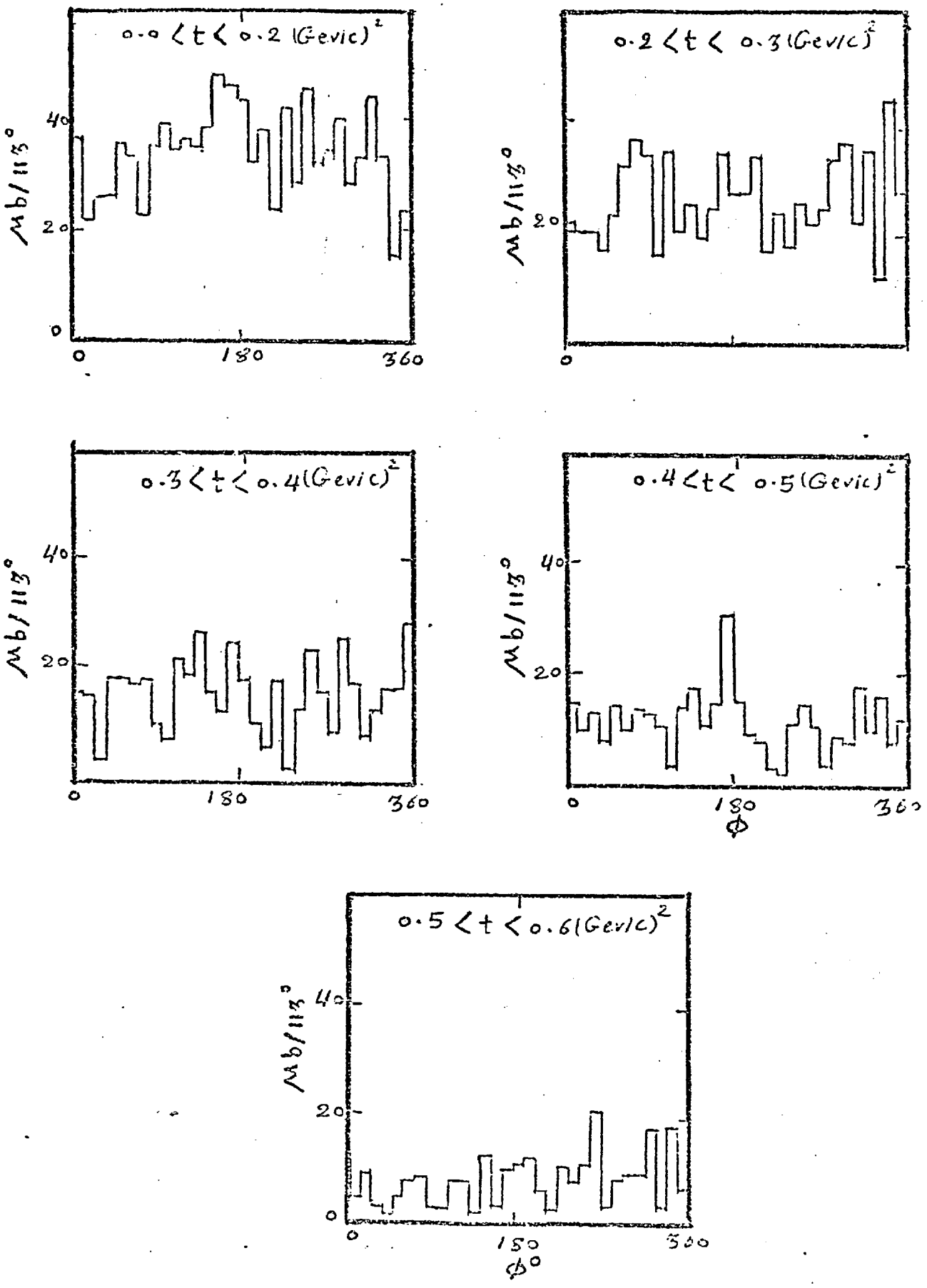

FIG (6-11-b)

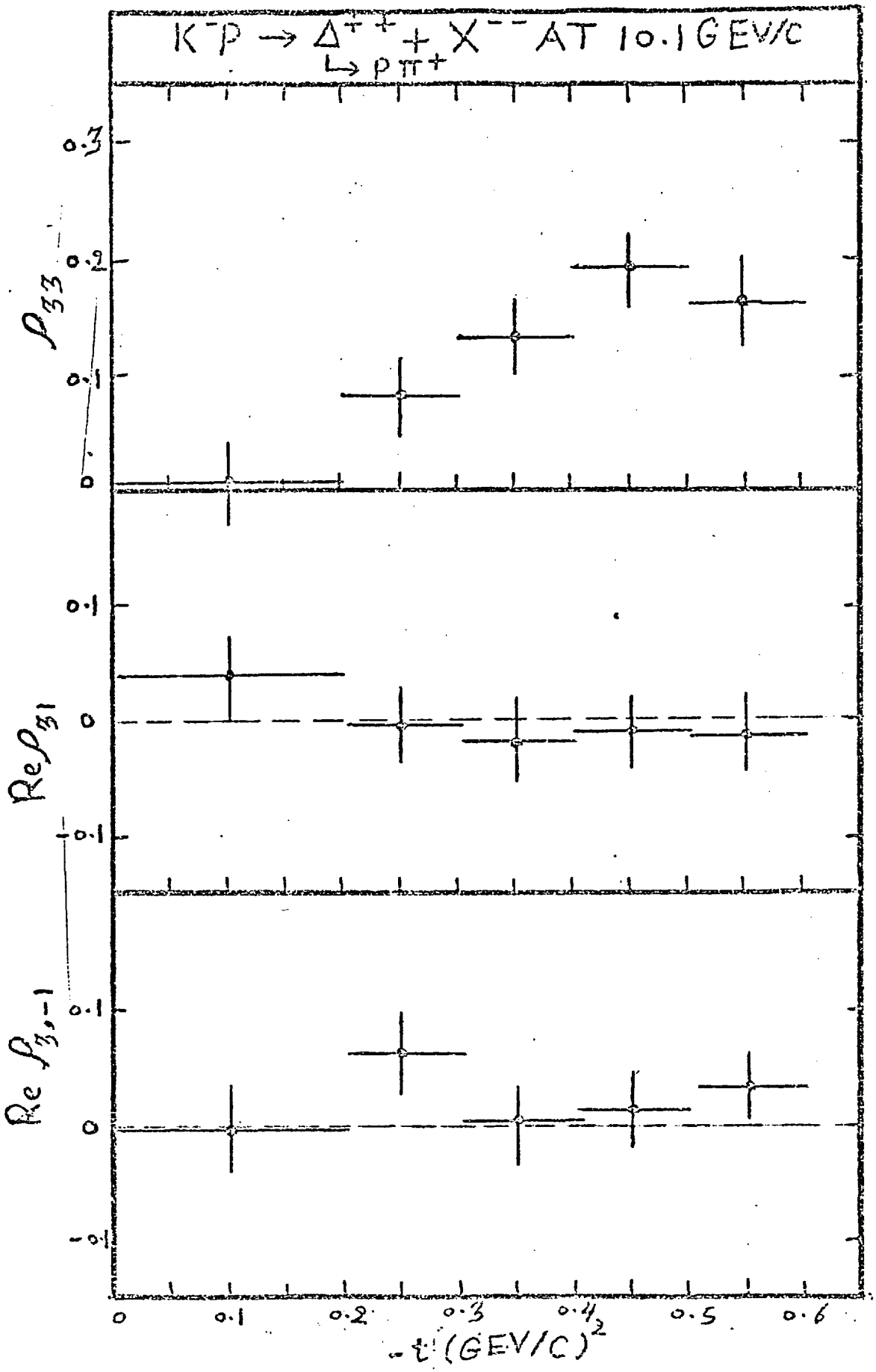
$K^- p \to \Delta^{++} + X^{--}$ AT 10.1 GEV/C
$\hookrightarrow p\pi^+$
ρ_{33}
$\mathrm{Re}\,\rho_{31}$
$\mathrm{Re}\,\rho_{3,-1}$
0.3
0.2
0.1
0
-0.1
0.1
0
-0.1
0.1
0
-0.1
0
0.1
0.2
0.3
0.4
0.5
0.6
$-t'\,(GEV/C)^2$

FIG(6-12)

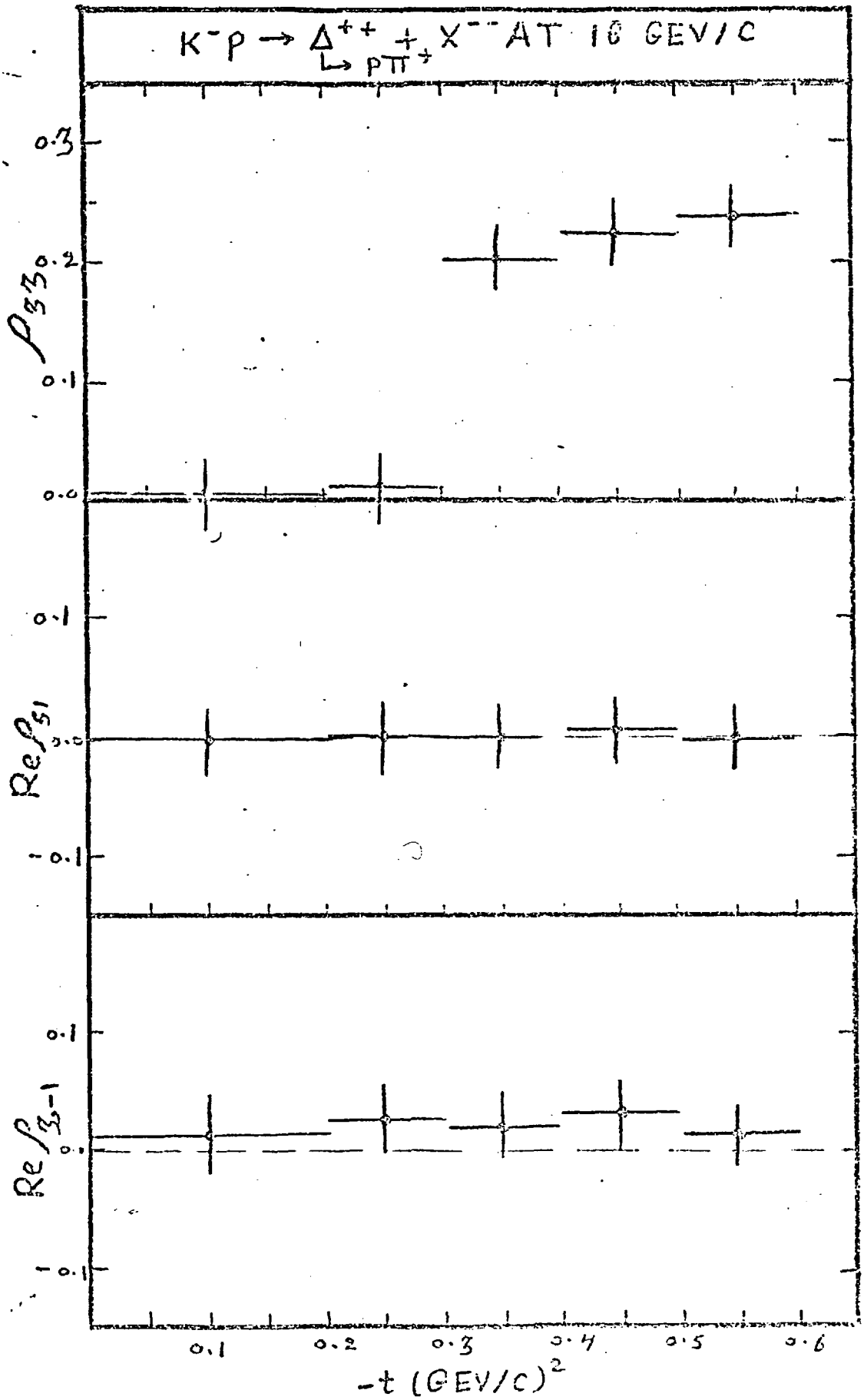
$K^- p \to \Delta^{++} + X^-$ AT 16 GEV/C
$\Delta^{++} \to p\pi^+$
ρ_{33}
$Re\rho_{31}$
$Re\rho_{3-1}$
0.3
0.2
0.1
0.0
0.1
0.0
0.1
0.1
0.0
0.1
0.1
0.2
0.3
0.4
0.5
0.6
$-t$ (GEV/c)^2

FIG(6-13)

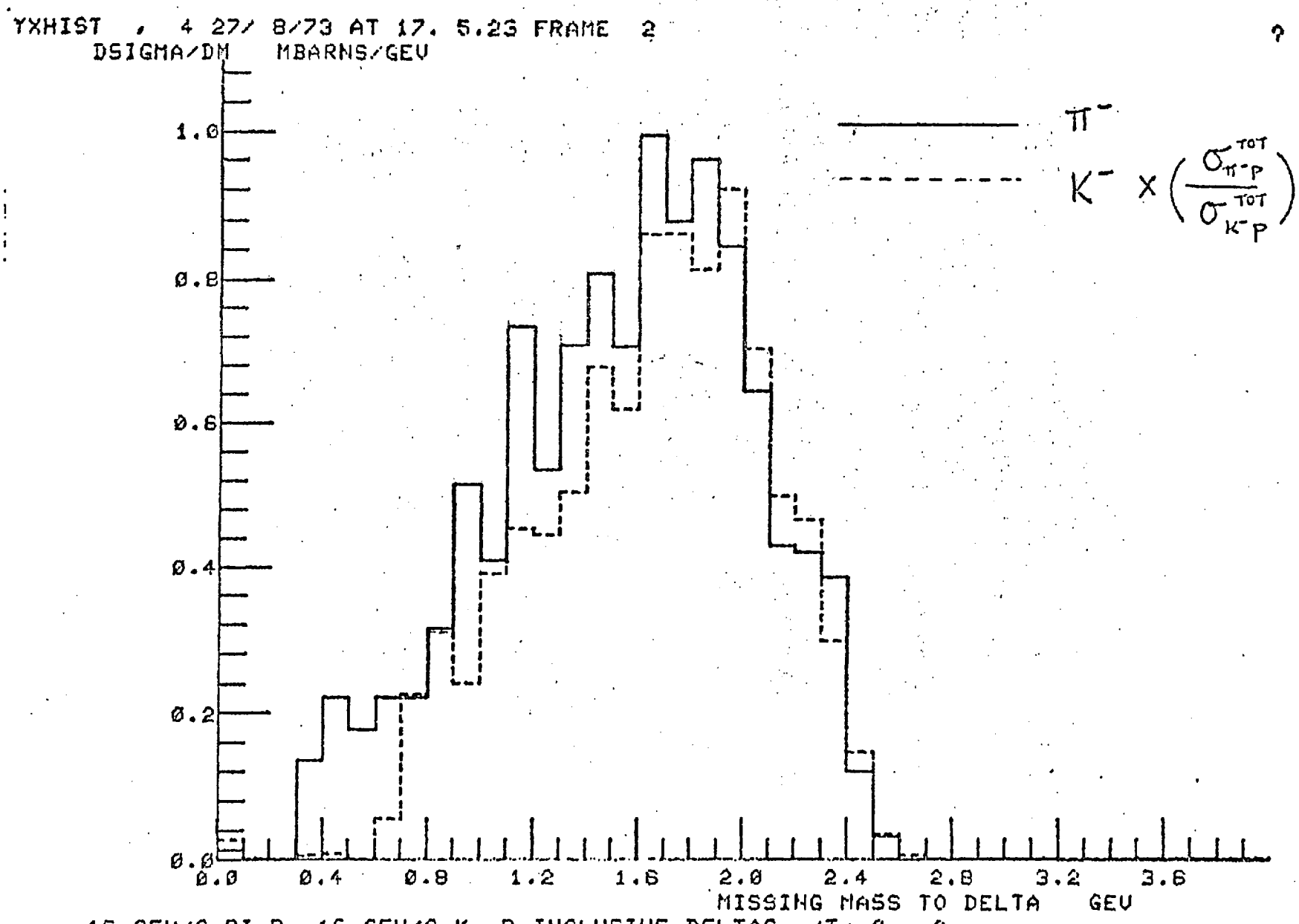

16 GEV/C PI-P, 16 GEV/C K- P INCLUSIVE DELTAS, /T/ 0.-.2

FIG(6-14-a)

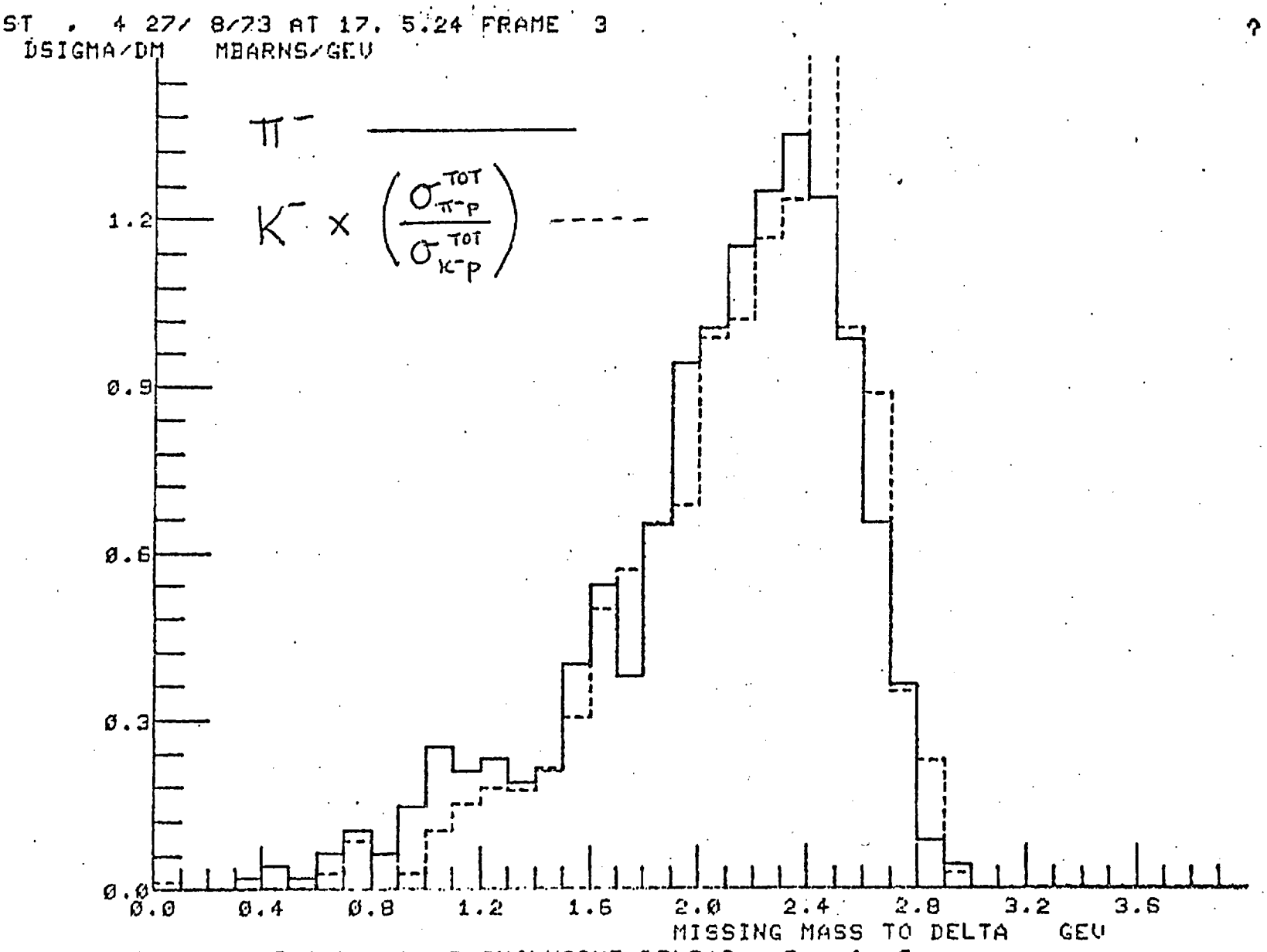

16 GEV/C PI-P, 16 GEV/C K- P INCLUSIVE DELTAS, /T/ .2-.3

FIG(6-14-b)

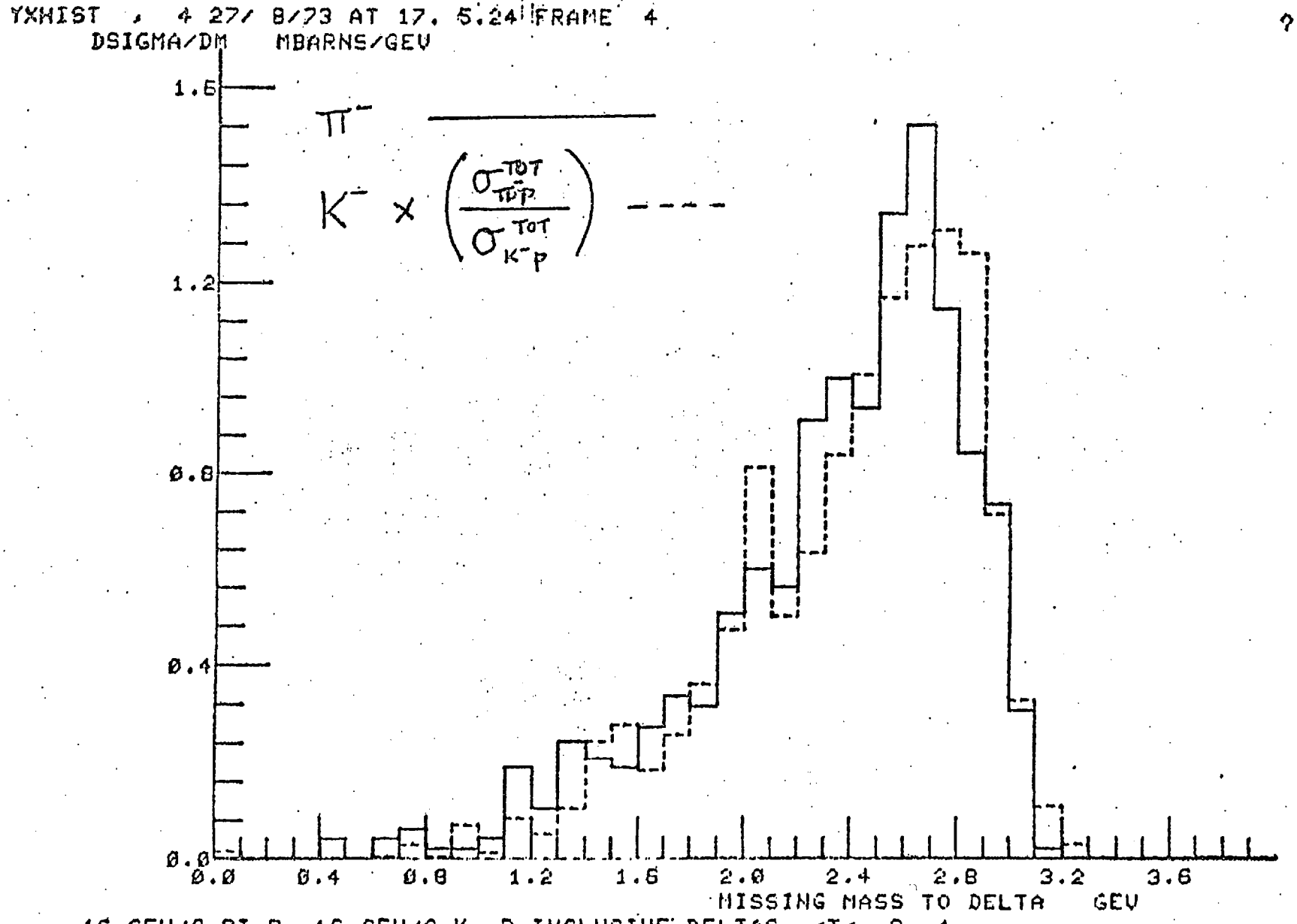

16 GEV/C PI-P, 16 GEV/C K- P INCLUSIVE DELTAS, /T/ .3-.4

FIG(6-14-c)

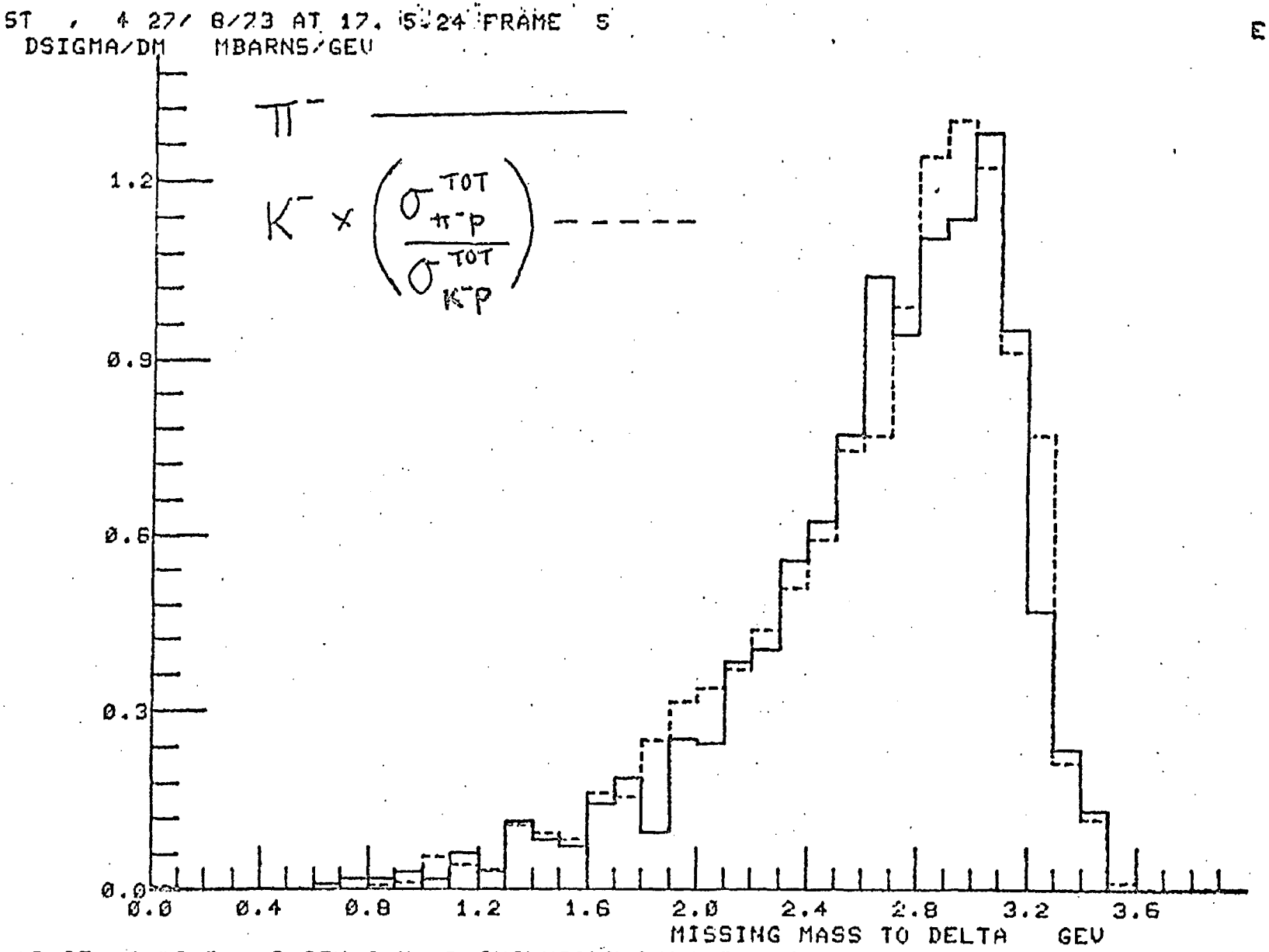

16 GEV/C PI-P, 16 GEV/C K- P INCLUSIVE DELTAS, /T/ .4-.8

FIG(6-14-d)

CHAPTER SEVEN

TWO PARTICLE CORRELATIONS

Introduction

The idea of studying correlations that might exist between particles produced in multibody final states in high energy collisions is not a very new one. This type of study forms a substantial part of the work done with such final states. The study of correlations appeared in its earliest form in analyses of effective mass distributions and in the hunt for new resonances in exclusive channels . This type of analysis can in principle be used in the inclusive framework. However, as evidenced in the previous two chapters, such analysis is not likely to teach us much about correlations in inclusive reactions. This is because when we sum over all exclusive channels which involve the particles between which correlations are intended to be studied, the background that exists under the resonance tends to dilute many effects that can be seen in exclusive channels. This makes inclusive effective mass distributions an unlikely place to look for resonances.

In the inclusive approach one follows a different line in studying correlations. In this case, one studies possible effects constraining the production of a particle or a group of particles by the production of another particle or group of particles. Such effects are called correlations in the inclusive terminology. One type of correlation is that imposed purely by kinematics, coming from energy-momentum conservation. Such effects do, indeed, exist and are likely to show up, in some form or another, in any study of correlations. Now the question arises, how do we separate these kinematical correlations from possible dynamical effects in which we are interested? Unfortunately, the answer to this question is not trivial. Methods employed in

exclusive types of analysis are not in general suitable for detecting such effects in inclusive correlations. For example, it is difficult to compare Monte Carlo generated events constrained by kinematics only with real events as in exclusive analysis.[1] This is because as well as being a lengthy process, one does not know everything about the real multiplicities of the contributing events which can contain an unknown number of neutrals. In such a case one is forced to use some assumptions about the number of these neutrals. These assumptions are usually model dependent. This means that one is imposing dynamics in the process of looking at kinematics. This would certainly lead to some wrong conclusions.

This leaves one with two choices in the method to employ in the study of correlations. The first one is to study some of the features of correlations which are not largely affected by the kinematics involved or features which are described by models which take into account correlations due to kinematics. The second method is to try to study some special cases where kinematical correlations can be accounted for experimentally.

Although the study of correlations on the basis of the two choices open to us is not expected to lead to full understanding of multibody correlations in high energy collisions, it might still be capable of providing us with some information about these interactions.

For the reasons outlined above and for other reasons associated with the fact that when studying correlations one is looking for a variety of known and unknown effects, the methods of studying correlations vary with the aim of the study. For this reason different methods have been used and at this stage one cannot decide which is the best method to obtain more information about correlations. Thus we shall discuss the advantages and disadvantages of some of these methods during the process of discussing their applications to our data.

Two Body Correlation Function

The Mueller-Regge approach to the study of inclusive reactions is one of the most fruitful ways of analysing data from inclusive experiments. Correlations between particles in inclusive reactions can be studied in the Mueller-Regge framework when they are expressed in terms of correlation functions[2]. The two particle correlation function, defined in equation (1.27), is dependent on seven independent variables. However, it is convenient to reduce those to three only by integrating over the transverse momenta of the two particles. In doing so equation (1.27) is reduced to the following when the rapidity variables are used[3].

$$C(s, y_1, y_2) = \frac{d^2\sigma}{dy_1\, dy_2} - \frac{1}{\sigma_T} \frac{d\sigma}{dy_1} \cdot \frac{d\sigma}{dy_2} \qquad (7.1)$$

Because rapidities are not Lorentz invariant quantities and because it is much simpler to plot correlation functions as one dimensional quantities, it is useful to study equation (7.1) in terms of rapidity separation instead of rapidities of the two particles. The quantity $\Delta y = y_1 - y_2$ is a Lorentz invariant quantity. Most theoretical predictions about correlation functions are usually made in terms of Δy rather than y_1 and y_2.

To study the behaviour of this correlation function as a function of Δy we calculated values of $C(s, y_1, y_2)$ for $\pi^+\pi^+$, $\pi^-\pi^-$ and $\pi^+\pi^-$ combinations from final states at 10 and 16 GeV/c. This was done by plotting the two particle distribution function $d\sigma/dy_1dy_2$ and summing over all cells of constant $y_1 - y_2 = \Delta y$. The product of the two single particle distributions in each case, which is a two dimensional diagram, was treated in the same way to find $(d\sigma/dy_1).(d\sigma/dy_2)$ for each range of Δy. After normalising by the total cross-section, values of $C(s, y_1, y_2)$ were calculated for each Δy bin for each set of particles. The correlation functions calculated by

this method for the three sets of particles are given in figs. (7-1), (7-2) and (7-3) for $\pi^+\pi^+$, $\pi^-\pi^-$ and $\pi^+\pi^-$ respectively.

The first feature one notices in all these figures is that c approaches zero when Δy becomes large. This approach is expected to depend on the leading Regge singularities which control the approach to scaling in the Regge expansion of the 4-4 amplitude[4]. If we assume that the intercept of such singularities is α_Q then one would expect

$$c(y_1, y_2) \simeq s_{12}^{\alpha_Q - 1}$$

where s_{12} is the invariant mass of the two particles. Now

$$s_{12} = m_1^2 + m_2^2 + 2(K_1K_2)^{\frac{1}{2}} \text{ Cos h } (y_1 - y_2) - 2\,\bar{p}_{T_1}.\bar{p}_{T_2}$$

$$= m_1^2 + m_2^2 - 2\,\bar{p}_{T_1}.\bar{p}_{T_2} + (K_1K_2)^{\frac{1}{2}}\, e^{|y_1 - y_2|}$$

$$\therefore \; s_{12}^{\alpha_Q - 1} = (K_1K_2)^{(\alpha_Q - 1)|y_1 - y_2|} \; .$$

When the correlation functions in the region of $\Delta y > 2.0$ were fitted with a simple exponential of the form $c(y_1, y_2) = e^{-K\Delta y}$ the value of K in all cases was found to be about 0.5 ± 0.05. This may be taken as an indication that the leading singularity is not the pomeron. This is in agreement with results obtained in Chapter Three from the study of the scaling behaviour of the two particle distribution function of the same sets of particles. This is because the region of large Δy corresponds to the case where the two particles are produced in different fragmentation regions. None of these two particle distribution functions showed any scaling behaviour in these regions. Such behaviour was shown, in Chapter Three, not to be expected from the study of the different contributions to the cross-sections from dual diagrams of the 4-4 amplitude.

The main disadvantage of the correlation function is that one does not know how much the correlation is due to kinematics[5]. The way such correlations show themselves on a correlation function plot is complicated. This problem becomes more serious in the region of small Δy where the values of the correlation functions usually peak sharply. Morrison has pointed out that such behaviour is expected simply because the single particle distribution peaks at values of small y.

One can resolve this problem partially through the study of correlations between different pairs of particles having approximately the same type of kinematical correlations. Such correlations are expected to give the same kind of reflections on the behaviour of the correlation function. For all our three cases one would expect these reflections to be the same. Hence, if no dynamical correlations exist one would expect all the three sets of correlation functions to be similar. However, as is apparent from figs. (7-1) to (7-3) this is not the case. Near $\Delta y = 0$ the values of $c(y_1, y_2)$ are positive and much higher for $\pi^+\pi^-$ than for $\pi^-\pi^-$. The latter are again higher than those for $\pi^+\pi^+$ which are always negative. This is direct evidence for the existence of different dynamical effects producing the correlations of the three sets of particles. We note that in the $\pi^+\pi^-$ case the two particles form a non-exotic combination while in the $\pi^-\pi^-$ and $\pi^+\pi^+$ cases the combinations are exotic. From this we may conclude that the amount of positive correlation between two particles is larger if the two particles form a non-exotic combination than if they form an exotic one.

Correlation Functions and Energy

The three sets of correlation functions studied so far do not show any significant differences between 10 and 16 GeV/c. Not many predictions exist about the nature of the energy dependence of the shape of correlation functions. However, an important quantity which is useful for distinguishing between different models is the integral overall values of Δy of the

correlation function. This is defined as the second multiplicity moment mentioned in Chapter One.

Unfortunately, the predictions about this quantity made by both the multiperipheral and the diffractive pictures are supposed to hold only at asymptotic energies[6,7]. Neither of these two models predict strong variation with energy for the second multiplicity moment in our energy range. However, we think it useful to report the values of this quantity for the three different cases at our two energies. These values are given in table (7-1).

It is clear from figs. (7-1) to (7-3) and from table (7-1) that statistical models which predict pure Poisson distributions for the charged multiplicities are not capable of explaining our correlation data[8]. This is because these models also predict a value of zero for the second multiplicity moments. The multiperipheral model predicts a log s dependence while diffractive models predict $s^{\frac{1}{2}}$ dependence. These two cannot be distinguished in our energy range.

Correlations in Different Kinematical Regions

We have seen that the correlation function is strongly dependent on Δy. The positive contributions to the correlation always tend to be stronger in the region of Δy near zero than anywhere else. Furthermore, this positive contribution is stronger for unlike pions than for like pions in the small region. The situation is still not well understood. The region of small Δy has contributions coming from three different kinematical regions. These arise when both particles are produced in the target fragmentation region, the projectile fragmentation region or the central region.

To gain more insight into the different positive and negative contributions, we divided our 10 GeV/c data in rapidity space into four regions depending on the rapidity of one of the particles for each set of

particles. The plots of the correlation functions in each case are shown in figs. (7-4), (7-5) and (7-6).

When both particles are produced in the projectile fragmentation region, one notices that in the $\pi^-\pi^-$ and $\pi^+\pi^+$ cases the values of the correlation functions are not very different from zero and that in the $\pi^+\pi^-$ case the correlations are positive as before. This is in contrast with the behaviour which can be observed if one of the particles is produced in the target fragmentation region, when the correlations tend to have negative values for $\pi^-\pi^-$ and $\pi^+\pi^+$. The similarity between the correlations of $\pi^+\pi^+$ and $\pi^-\pi^-$ in these regions leads us to believe that these correlations are nothing but kinematical effects due to energy and momentum conservation and possibly leading particle effects. This is interesting in the sense that one can at least get some idea about the nature of the correlations due to such effects. One expects some other effects to account for the $\pi^+\pi^-$ case where positive correlations have been observed but where kinematical effects are expected to be of the same nature as in the previous cases.

When one of the two particles is produced in the central region the behaviour of the correlation function follows a different pattern. The main feature in this case is that there are large positive correlations in all cases in the region of small Δy. The same kind of behaviour was observed in the data on $K^+p \to \pi^-\pi^-$ + anything of Ko and Lander[9]. However, we believe that this effect is not very surprising because the correlations in our case are not much different between $\pi^-\pi^-$, $\pi^+\pi^+$ on the one hand and the $\pi^-\pi^-$ cases in the K^+p case on the other hand. This effect is not difficult to explain on any model which predicts that a large number of pions are produced with small values of rapidity in the centre of mass. In particular, the Hagedorn thermodynamical model and the multiperipheral model contain the necessary ingredients for such predictions. What is more interesting is the fact that these positive correlations are stronger

for the $\pi^-\pi^-$ case than for $\pi^+\pi^+$ and both cases contain much smaller correlations than in the $\pi^+\pi^-$ case. The interest here is not in whether there are positive correlations for small Δy values, but in where do they occur in terms of y_1 and y_2. A more striking effect would be if there are strong positive correlations in the case of two particles produced in one fragmentation region. However, the positive correlations observed in the central region can be attributed mainly to kinematics in the $\pi^-\pi^-$ and $\pi^+\pi^+$ case with some dynamical reflections. The difference between these two cases and the $\pi^+\pi^-$ case in this region suggests that different dynamics are involved in the latter case. These could possibly be due to resonance production. If one accepts this explanation then one may deduce that correlations due to resonances between the two particles are not only positive in sign but tend to be of large magnitude when compared with negative correlations due to phase space and leading particle effects. Hence, one would expect any realistic model which tries to explain correlation data to take into account resonance production.

Azimuthal Correlations

Another method for looking for possible correlations between particles in multibody final states is through the study of the distribution of the azimuthal angle defined as

$$\phi = \mathrm{Cos}^{-1} \frac{\bar{p}_{T_1} \cdot \bar{p}_{T_2}}{|\bar{p}_{T_1}||\bar{p}_{T_2}|}$$

where p_T is the transverse momentum vector of the particle[10].

If the two particle are uncorrelated then one would expect the ϕ distribution to be isotropic. However, kinematical effects, especially energy-momentum conservation, can introduce anisotropy. The reflections of these effects on the ϕ distributions are not simple to predict. This severely limits the amount of information we can extract from the study

of such distributions. Again, we shall use the technique used previously of comparing correlations between pairs of particles with the same masses but different charge combinations, rather than trying to study absolute correlations between these particles. However, this method the problems associated with different kinematical boundaries for the two particles produced are not very important. For this reason here we can study correlations between leading or non-leading particles in the same way.

Using this method we looked for possible correlations in the following reactions:-

$$K^- p \rightarrow \pi^+\pi^+ + x$$
$$\rightarrow \pi^-\pi^- + x$$
$$\rightarrow \pi^+\pi^- + x$$

The ϕ distributions for the three reactions are shown in fig. (7-7). Although all three distributions show some kind of anisotropy in that more events populate the region of ϕ greater than 90 degrees than in the region of ϕ less than 90 degrees, the anisotropy is much stronger in the $\pi^+\pi^-$ case than in the other two cases. This behaviour confirms the effect observed through the study of the correlation functions of these three pairs of particles which indicated some different dynamical effects between $\pi^+\pi^-$ correlations on the one hand and $\pi^-\pi^-$ and $\pi^+\pi^+$ on the other.

One simple explanation for this type of behaviour is that we expect resonance production to play an important role in the observed correlations. To get some clearer idea about such a possible case we divided our data into two samples. The first sample included only those combinations with effective mass in the ρ region, which was defined to be $0.62 < M(\pi\pi) < 0.88$ GeV. The other sample contains all combinations outside this mass region. The ϕ distributions for the two samples are shown in fig. (7-8). One can observe that such a simple mass cut can produce a dramatic difference in

the ϕ distributions between the two samples. This difference indicates the existence of strong correlations between the two pions in the ρ indeed. However, a problem with the ρ resonance is that it is wide and rather close to the $\pi\pi$ threshold. Hence, one is not quite sure whether the effect observed is due to small values of the effective mass or whether it is a distinguishable effect associated with the ρ. To resolve this ambiguity we show in fig. (7-8-c) the ϕ distribution for $\pi^+\pi^-$ combinations which have effective masses smaller than 0.62 GeV. In this case one observes that although there exists some anisotropy in the ϕ distribution for these combinations, it is not as strong as that observed for those combinations inside the ρ^0 mass region. For this reason we tend to believe that the anisotropy in the ϕ distribution is strongly related to resonance production. However, kinematical reflections tend to give some anisotropy and, coupled with reflections from resonance production between pions and other particles, may form a reasonable basis for explaining the observed slight anisotropy in the ϕ distributions.

Cross Over Correlations

The method introduced in Chapter Four in connection with our investigation of the seagull effect may be called a cross over method of studying correlations. This is because we study correlations between values of two kinematical variables belonging to two different particles. Those two quantities were the longitudinal momentum of one particle versus the transverse momentum of the other.

Another similar method of studying correlations between average values of transverse momentum of the two particles was used in ref. (11). We tried this method for comparison with ours. Fig. (7-9) shows the average transverse momentum of pions versus that of protons produced at 10 GeV/c.

It is clear that the values of transverse momentum of negative pions are systematically higher than those of positive pions. Such behaviour can

be explained through suppression of transverse momentum values due to resonance production and the associated seagull effect. The difference in p_T^2 values extends over the whole range of $p_T^2(p)$. For this reason we find it more useful to study this type of correlation in terms of $x(p)$ rather than $p_T^2(p)$ where more information can be obtained about the kinematical region where suppression occurs.

Summary and Conclusions

In this chapter correlations between non leading particles as well as those between a leading and a non leading particle were studied qualitatively. The results suggest possible strong correlations between particles due to resonance production effects. This is in contrast with results obtained in ref. (12), where correlation between two leading particles could be explained on kinematical bases without the need to have any extra reflections on correlations due to resonance production.

REFERENCES (7)

1. Program FOWL, CERN Program Library.
2. E.L. Berger, ANL Preprint, ANL/HEP 7134 (1971).
3. K.G. Wilson, Acta Physica Austriaca 17, 37 (1963).
4. R.C. Arnold, ANL Preprint, ANL/HEP 7139 (1971).
5. D.R.O. Morrison, CERN Preprint, CERN/D.Ph.II/PHYS 72-25 (1972).
6. G. Ranft and J. Ranft, Leibzig Preprint, KMU-HEP-705 (1972).
7. M. Le Bellac, Phys. Letters 37B, 413 (1971).
8. Z. Koba, Proceedings of the Third International Colloquium on Multiparticle Reactions, Zakopane, June (1972).
9. Davis, W. Ko, Phys. Rev. Letters 28, 935 (1972).
10. Berkeley, J.H. Friedman, C. Risk and D.B. Smith, Phys. Rev. Letters 28, 191 (1972).
11. Aachen-Berlin-Bonn-CERN-Cracow-Heidelberg-Warsaw Collaboration, submitted to Nucl. Physics.
12. Aachen-Berlin-CERN-London-Vienna Collaboration, Phys. Letters 40B, 510 (1972).

TABLE CAPTION (7)

(7-1) Values of the overall correlation for the reactions

$K^-p \to \pi^+\pi^+ +$ anything

$K^-p \to \pi^-\pi^- +$ anything

$K^-p \to \pi^+\pi^- +$ anything

at 10 and 16 GeV/c.

TABLE (7-1)

Reaction	C mb at 10.1 GeV/c	C mb at 16 GeV/c
$K^- p \rightarrow \pi^- \pi^- + X^{++}$	-2.75	-1.87
$K^- p \rightarrow \pi^+ \pi^+ + X^{--}$	-2.24	-2.17
$K^- p \rightarrow \pi^+ \pi^- + X^0$	+6.90	+1.54

FIGURE CAPTIONS (7)

(7-1) Plots of the correlation function versus $\Delta y = (y_1 - y_2)$ for the reaction $K^- p \to \pi^+\pi^+$ + anything at 10 and 16 GeV/c.

(7-2) Plots of the correlation function versus Δy for the reaction $K^- p \to \pi^-\pi^-$ + anything at 10 and 16 GeV/c.

(7-3) Plots of the correlation function versus Δy for the reaction $K^- p \to \pi^+\pi^-$ + anything at 10 and 16 GeV/c.

(7-4) Plots of the correlation function versus Δy for the reaction $K^- p \to \pi^+\pi^+$ at 10 GeV/c when one π^+ is produced with a centre of mass rapidity y_1 where

(a) $y_1 < -1.0$

(b) $-1.0 < y_1 < 0.0$

(c) $0.0 < y_1 < 1.0$

(d) $y_1 > 1.0$.

(7-5) Plots of the correlation function versus Δy for the reaction $K^- p \to \pi^-\pi^-$ + anything at 10 GeV/c when one π^- is produced with centre of mass rapidity y_1 where

(a) $y_1 < -1.0$

(b) $-1.0 < y_1 < 0.0$

(c) $0.0 < y_1 < 1.0$

(d) $y_1 > 1.0$.

(7-6) Plots of the correlation function versus Δy for the reaction $K^- p \to \pi^+\pi^-$ + anything at 10 GeV/c when the π^+ is produced with centre of mass rapidity y_1 where

(a) $y_1 < -1.0$

(b) $-1.0 < y_1 < 0.0$

(c) $0.0 < y_1 < 1.0$

(d) $y_1 > 1.0$.

(7-7) Plots of the distributions of the azimuthal angle ϕ between the transverse momenta of the two pions in the reactions

(a) $K^- p \to \pi^+\pi^+$ + anything

(b) $K^- p \to \pi^-\pi^-$ + anything

(c) $K^- p \to \pi^+\pi^-$ + anything

at 10 GeV/c.

(7-8) Azimuthal angular distributions for the reaction $K^- p \to \pi^+\pi^-$ + anything plotted as a function of the $\pi^+\pi^-$ effective mass.

(7-9) Plot of $\langle p_T^2(\pi)\rangle$ versus $\langle p_T^2(p)\rangle$ for the reactions $K^- p \to p\pi^{\mp}$ + anything. The solid and dotted lines represent $\langle p_T^2(\pi^+)\rangle$ and $\langle p_T^2(\pi^-)\rangle$ respectively.

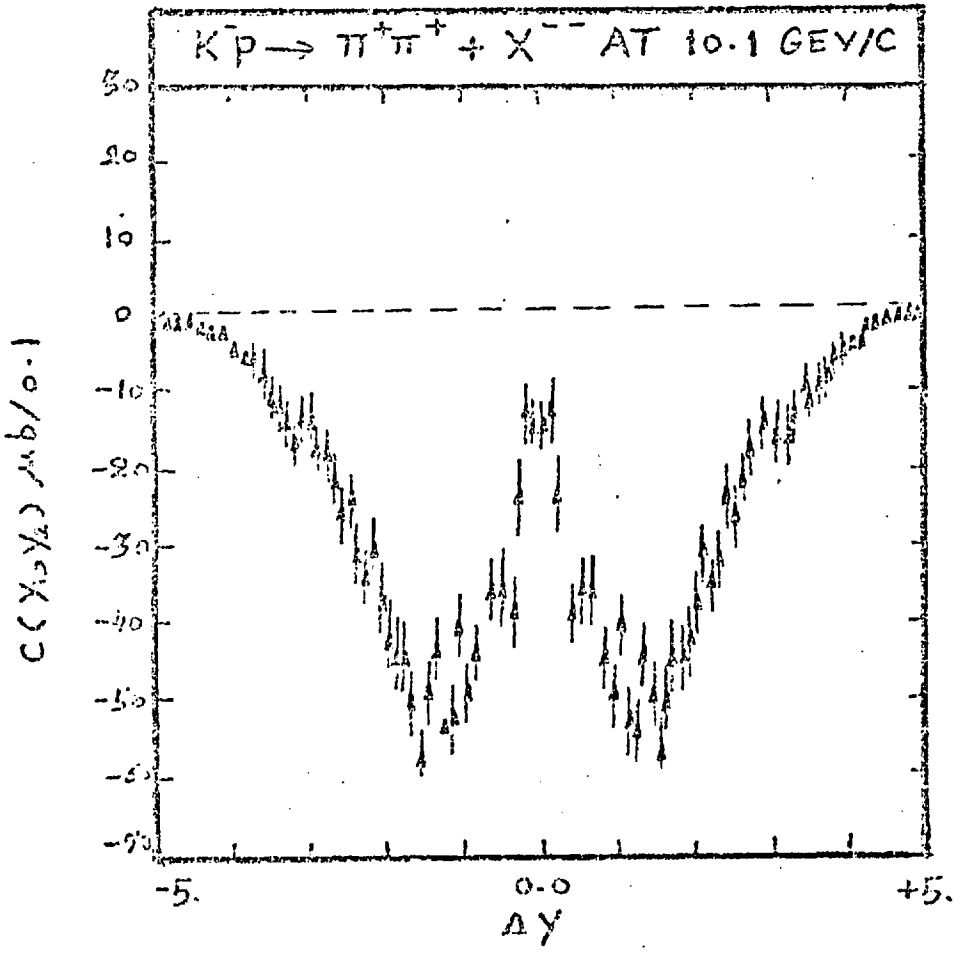
$K^-p \rightarrow \pi^+\pi^+ + X^{--}$ AT 10.1 GEV/C
$C(Y_1,Y_2)$ mb/0.1
30
20
10
0
-10
-20
-30
-40
-50
-5.
0.0
+5.
ΔY

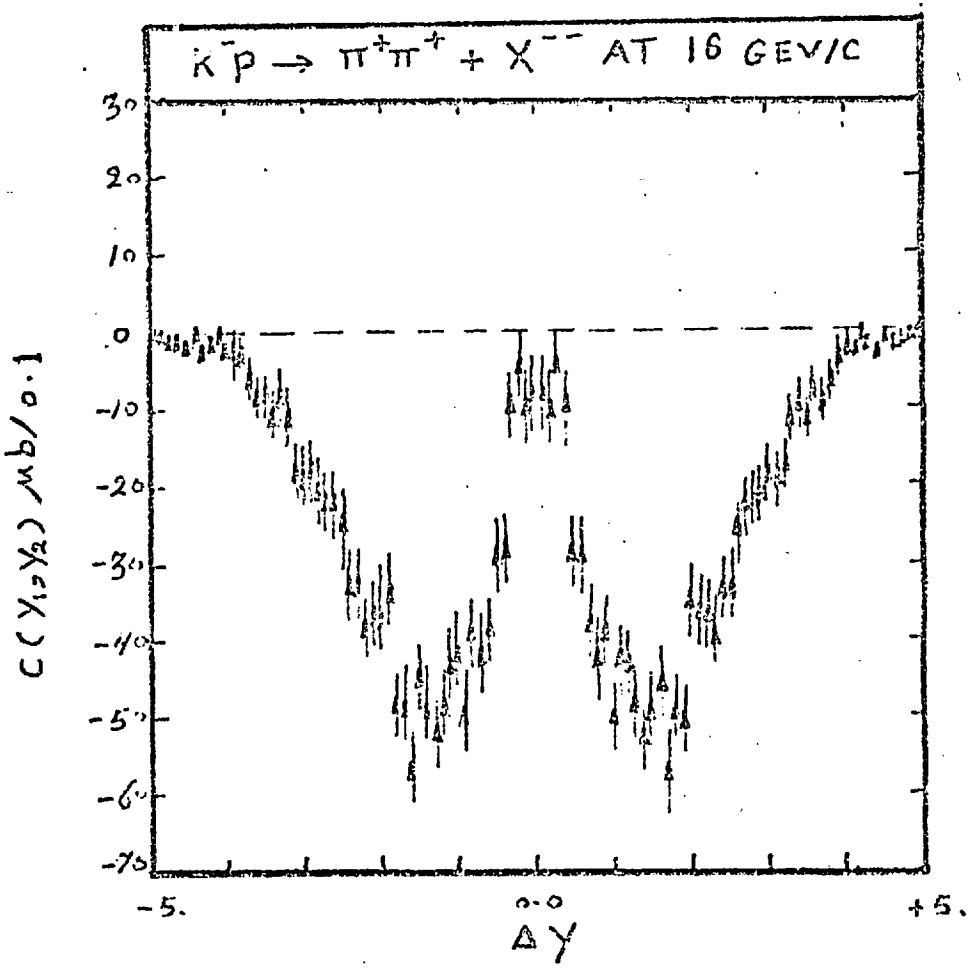
$K^-p \rightarrow \pi^+\pi^+ + X^{--}$ AT 16 GEV/C
$C(Y_1,Y_2)$ mb/0.1
30
20
10
0
-10
-20
-30
-40
-50
-60
-70
-5.
0.0
+5.
ΔY

FIG(7-1)

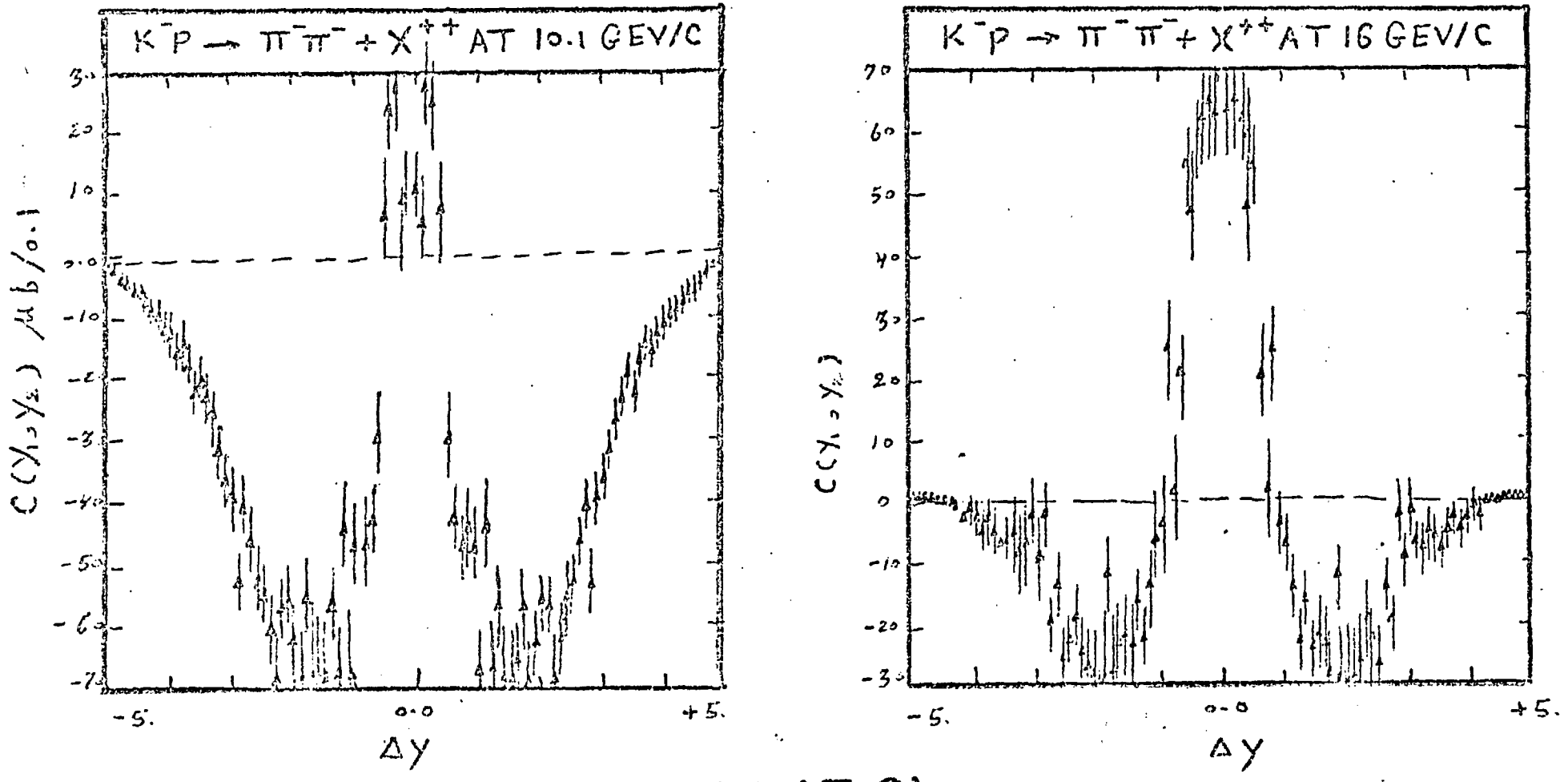
K⁻P → π⁻π⁻ + X⁺⁺ AT 10.1 GEV/C
C(Y1, Y2) /μb/0.1
3.0
2.0
1.0
0.0
-1.0
-2
-3
-4
-5
-6
-7
-5.
0.0
+5.
ΔY
K⁻P → π⁻π⁻ + X⁺⁺ AT 16 GEV/C
C(Y1, Y2)
70
60
50
40
30
20
10
0
-10
-20
-30
-5.
0.0
+5.
ΔY

FIG(7-2)

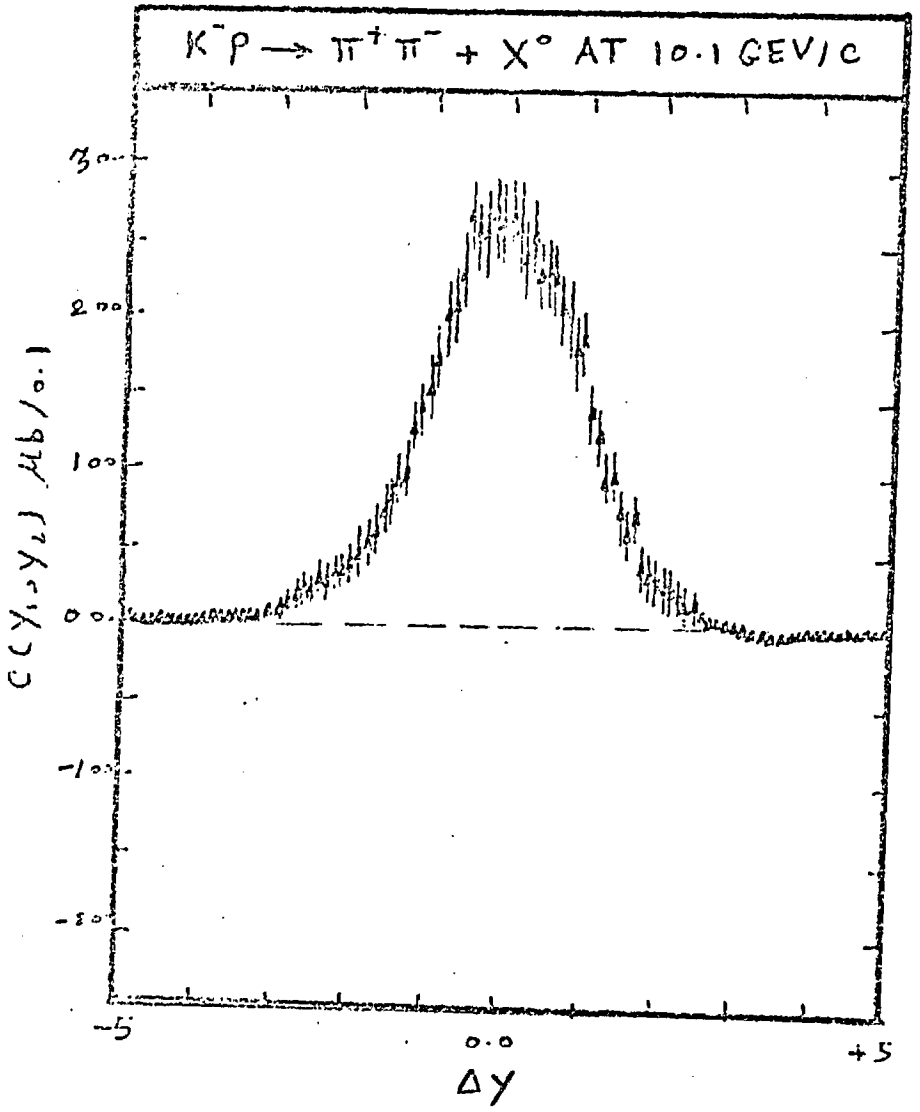
K⁻P → π⁺π⁻ + X° AT 10.1 GEV/c
C(Y1, Y2) μb/0.1
3.0
2.0
1.0
0.0
-1.0
-2.0
-5
0.0
+5
ΔY

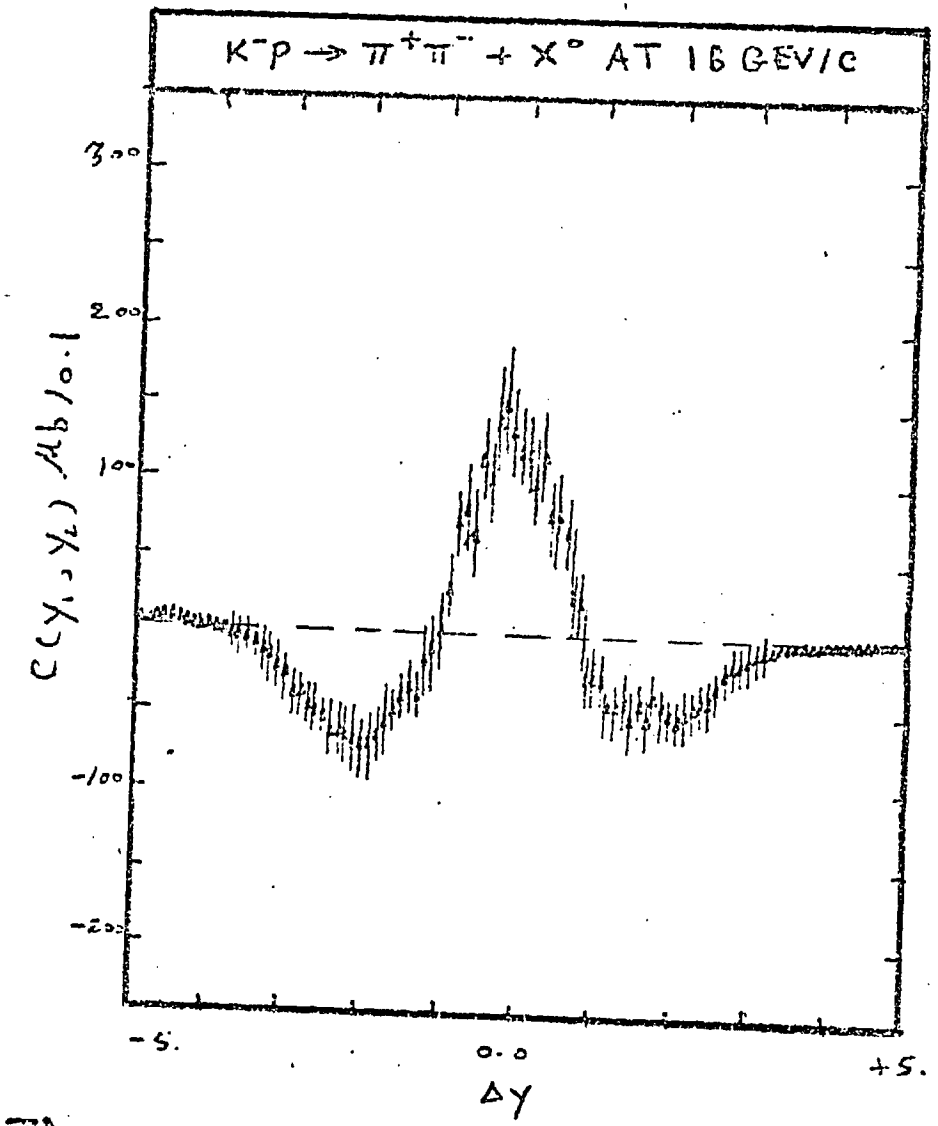
K⁻P → π⁺π⁻ + X° AT 16 GEV/c
C(Y1, Y2) μb/0.1
3.00
2.00
1.0
-1.00
-2.0
-5.
0.0
+5.
ΔY

FIG (7-3)

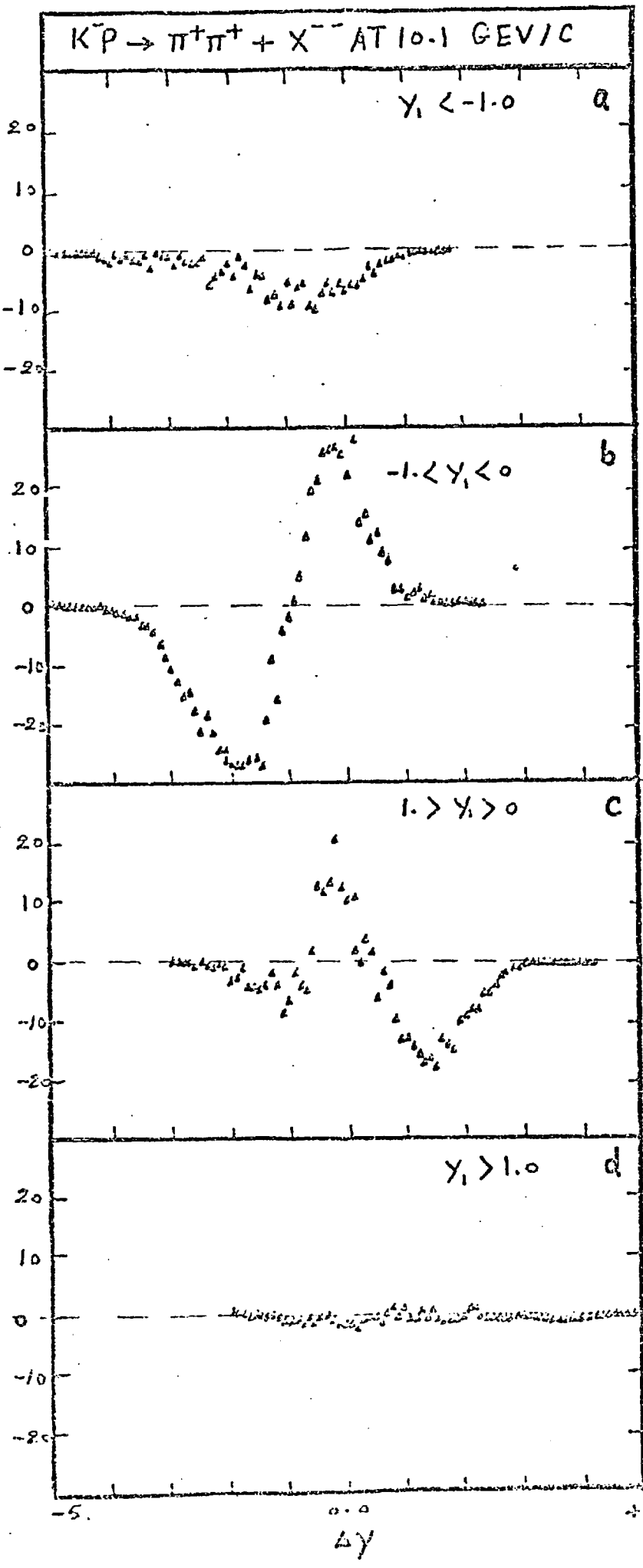
$K^-p \to \pi^+\pi^+ + X^{--}$ AT 10.1 GEV/C
$Y_1 < -1.0$
a
$-1. < Y_1 < 0$
b
$1. > Y_1 > 0$
c
$Y_1 > 1.0$
d
$C(Y_1, Y_2)$ mb/0.1
ΔY
-5.
0.0
+5.

FIG (7-4)

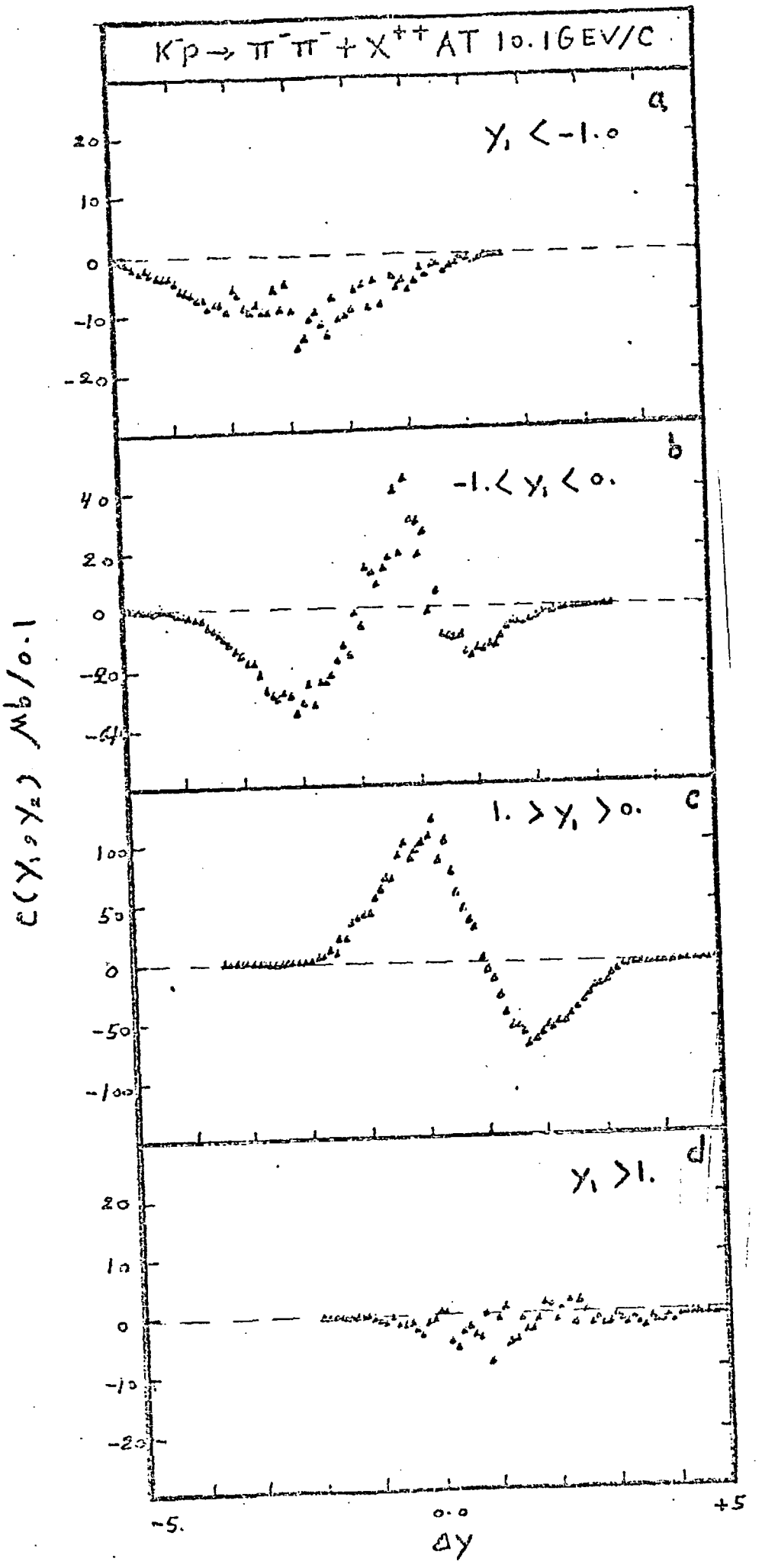

FIG(7-5)

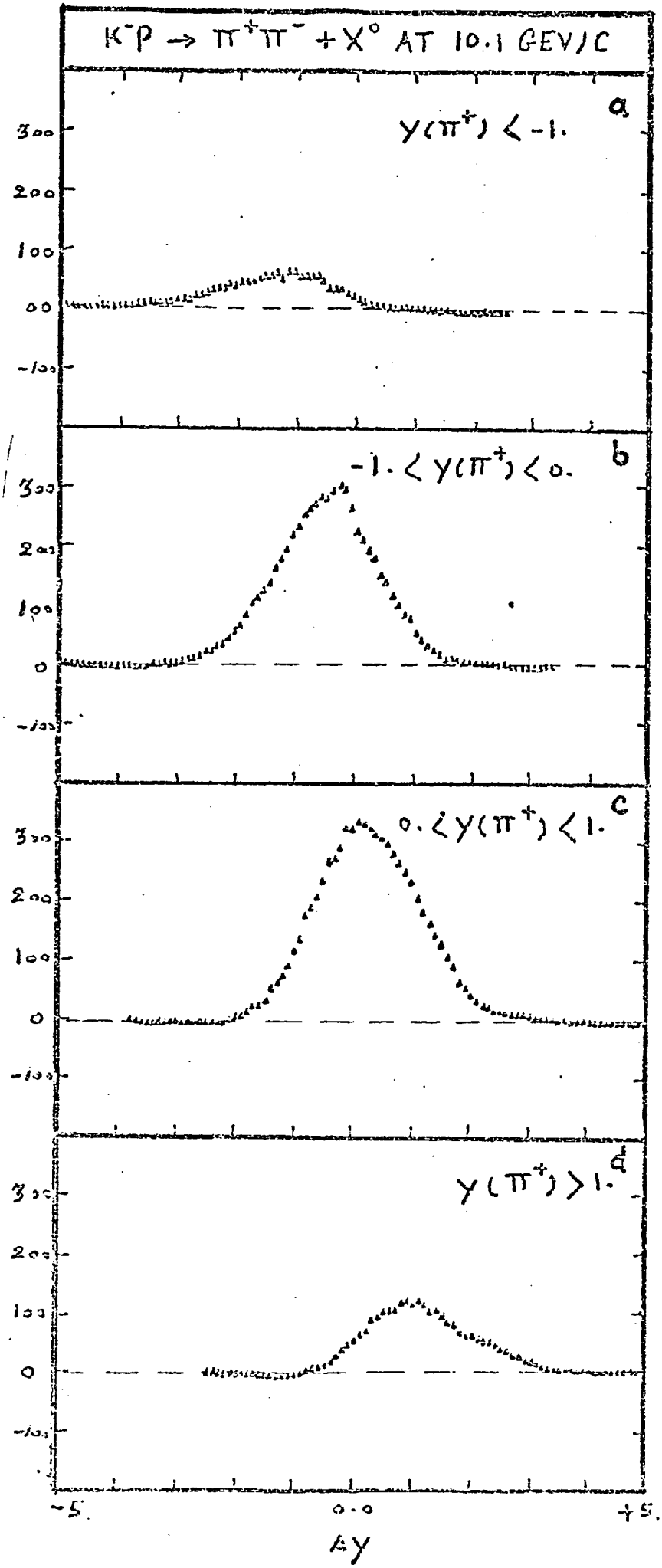
K⁻P → π⁺π⁻ + X° AT 10.1 GEV/C
a
y(π⁺) < -1.
b
-1. < y(π⁺) < 0.
c
0. < y(π⁺) < 1.
d
y(π⁺) > 1.
300
200
100
0
-100
C(Y1, Y2) μb/0.1
-5.
0.0
+5.
Δy

FIG (7-6)

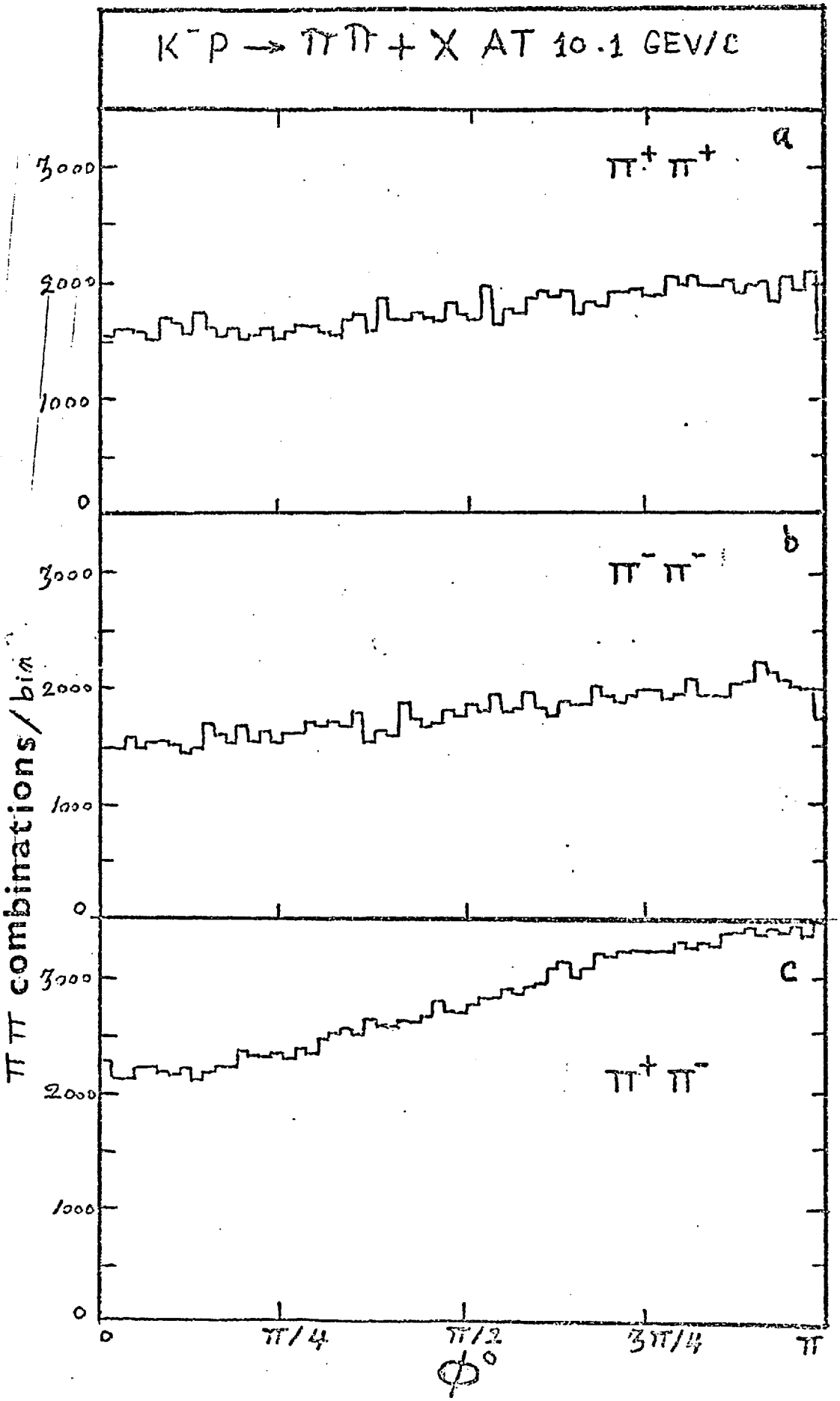
K⁻p → ππ + X AT 10.1 GEV/c
a
π⁺π⁺
b
π⁻π⁻
c
π⁺π⁻
3000
2000
1000
0
ππ combinations/bin
0
π/4
π/2
3π/4
π
φ°

FIG(7-7)

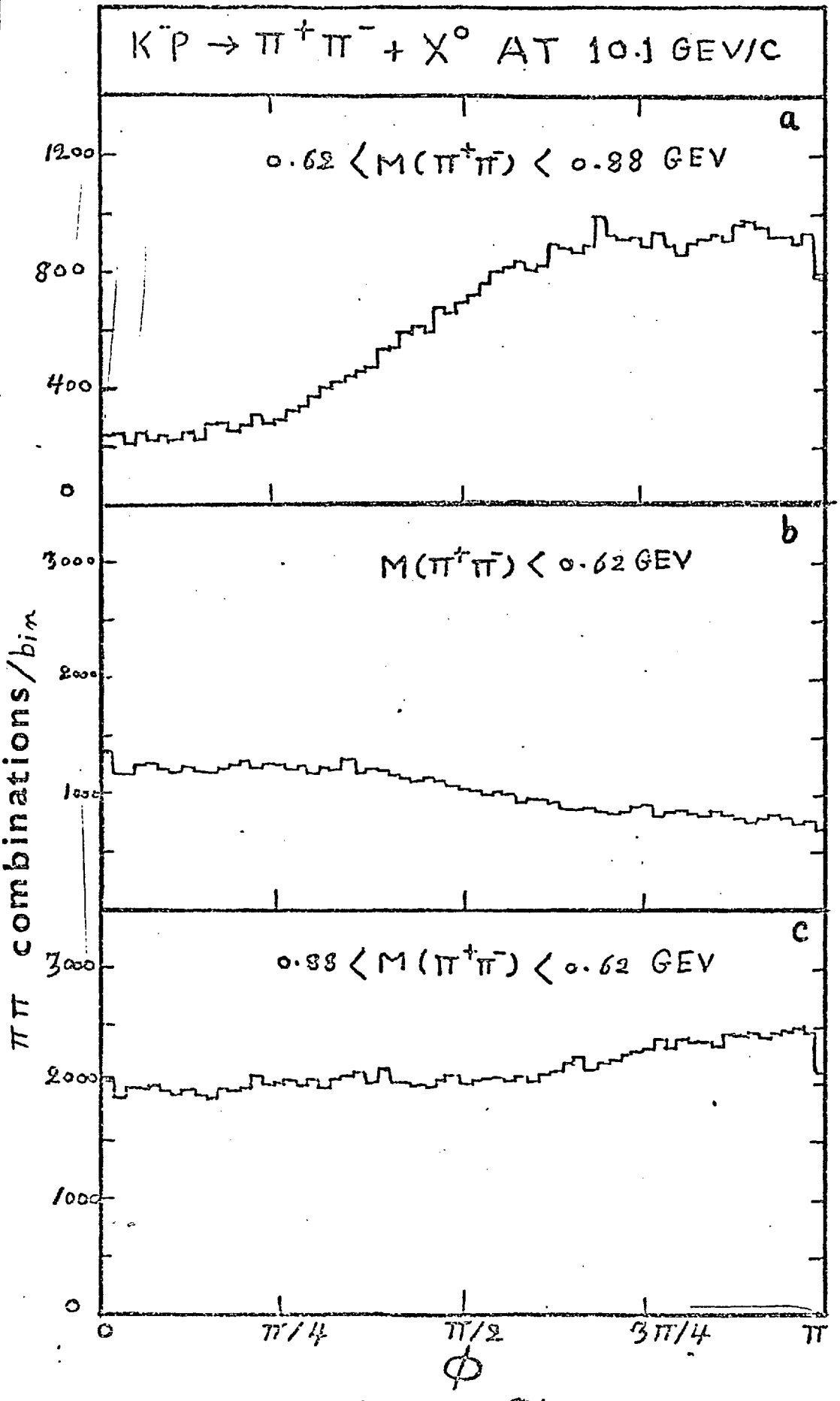
K⁻P → π⁺π⁻ + X° AT 10.1 GEV/C
a
0.62 < M(π⁺π⁻) < 0.88 GEV
1200
800
400
0
b
M(π⁺π⁻) < 0.62 GEV
3000
2000
1000
c
0.88 < M(π⁺π⁻) < 0.62 GEV
3000
2000
1000
0
ππ combinations/bin
0
π/4
π/2
3π/4
π
φ

FIG(7-8)

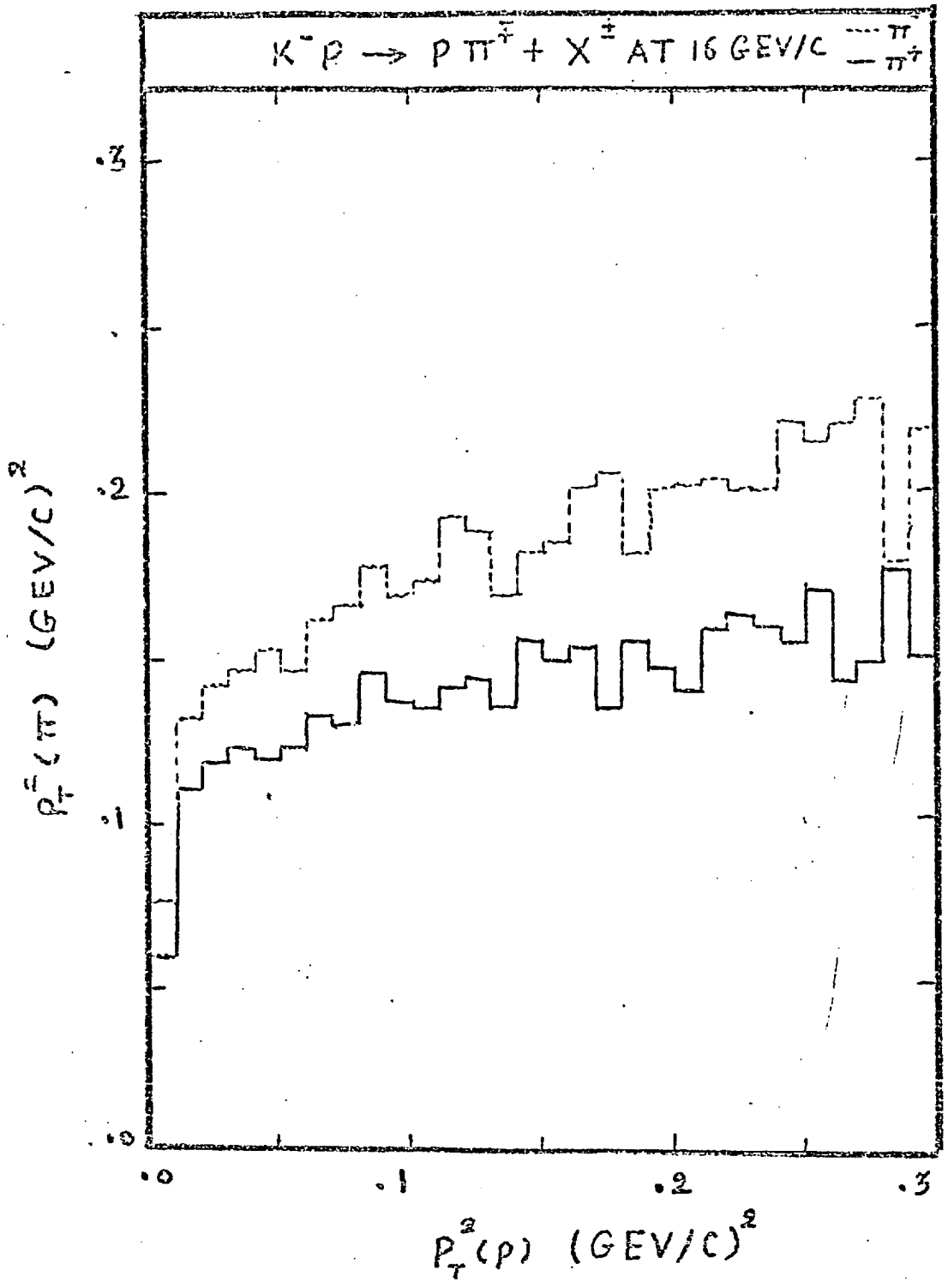
$K^- p \to p \pi^{\mp} + X^{\pm}$ AT 16 GEV/C π^- π^+
.3
.2
.1
.0
.0
.1
.2
.3
$P_T^2(\pi)$ (GEV/C)^2
$P_T^2(p)$ (GEV/C)^2

FIG(7-9)

CHAPTER EIGHT

$\bar{K}^0$ AND Λ^0 INCLUSIVE AND SEMI-INCLUSIVE PRODUCTION

Introduction

So far in our study we have treated inclusive reactions, in which a $\bar{K}^0$ or a Λ^0 are produced and detected, in the same way as we treated other reactions involving, for example, pions. Although such treatment is correct from an inclusive point of view, one may feel that it does not teach us many things we would like to know about the characteristic features of strange particle production. It is our aim in this chapter to investigate some of these features in more detail.

Semi-Inclusive Reactions

In an earlier stage, arguments were brought in support of the meaningfulness of the idea of studying inclusive reactions. Those arguments were mainly based on relations between inclusive and exclusive cross-sections and also on relations between these cross sections and n - n amplitudes through the Mueller generalised optical theorem. However, using those arguments only, one cannot achieve full understanding of particle interactions equivalent to that which follows from full analysis of all exclusive channels unless one is in an ideal situation where one can study all inclusive channels. In such an ideal situation full understanding may come from either inclusive or exclusive analysis and the separation between the two approaches from the experimental point of view becomes rather artificial. Unfortunately, we are not in that ideal situation and for this reason both types of reactions are being studied.

In bubble chamber experiments one feels that it is a pity to average over so many pieces of available information to study a lower order inclusive reaction. In order to try to make more use of the information available about each track in bubble chamber events, Koba, Nielsen and

Olesen (KNO)[1] introduced the so called "Semi-inclusive reactions".

The simplest two forms of this type of reaction are

$$a + b \rightarrow c^{\mp} + (n - 1) \text{ charged} + \text{Anything} \qquad (8.1.a)$$

$$a + b \rightarrow c^{o} + (n) \text{ charged} + \text{Anything} \quad . \qquad (8.1.b)$$

The advantage in studying this type of reaction is that one is using information about the charged multiplicity of each event, and looking for the dependence of cross sections on multiplicity. However, in this case one is dealing with cross sections which do not form complete sets of information from which exclusive or inclusive cross sections can be derived. Furthermore, exclusive cross sections can be related to a phenomenological picture related to 2-n body inelastic amplitudes and inclusive cross sections can be related to the discontinuities in n-n body elastic amplitudes through the Mueller generalised optical theorem while no such relations can be constructed for semi-inclusive cross sections.

Through lack of a theoretical picture to express semi-inclusive cross sections, predictions about these cross sections have been made starting with ordinary inclusive reactions. For such reasons one does not expect semi-inclusive data to have a theoretical importance equal to that enjoyed by exclusive or inclusive data. However, such data may be useful from an experimental point of view in yielding a qualitative feeling about distributions of particles observed at different multiplicities. This type of knowledge may help to a certain extent in understanding some phenomenological pictures of particle interactions at high energies.

For these reasons we decided to show data about semi-inclusive Λ^{o} and $\bar{K}^{o}$ production and we shall try to discuss our results in terms

of what we know about the inclusive cross section of these two particles.

The KNO Scaling Formula

Koba, Nielsen and Oleson[1], who argued that if an inclusive distribution of a particle produced at high energy shows some kind of energy independence then one may expect the individual semi-inclusive distributions of that particle to follow a simple formula at each multiplicity. They suggest this scaling formula to have the general form:-

$$\frac{Ed\sigma_n}{d^3\bar{p}_c}(a + b \rightarrow c + n \text{ charged} + \text{anything neutral}) = \sigma_n(s)\, h\,(x, p_T, \frac{n}{\langle n\rangle})(1 + 0\,\frac{1}{\langle n\rangle}) \qquad (8.2)$$

where 0 is a term of the order of zero. In this relation $\langle n\rangle$ and n are the average and real multiplicity and σ_n is the topological cross section for the reaction at a given asymptotic energy s.

Because the lns (s) dependence produces very slow variation of cross section with energy one would expect the main s dependence to be due to the variation of $\langle n\rangle$ with energy. In this case one might be able to check the correctness of relation (8.2) using the two sets of semi-inclusive cross sections derived from events involving $\bar{K}^0$ and Λ^0 production. This can be done through the use of our prior knowledge about the way the inclusive cross sections of these two reactions behave as a function of energy. In these two reactions we have on the one hand the inclusive cross section of $\bar{K}^0$ which shows no significant energy dependence in our energy range while on the other hand we have the Λ^0 inclusive cross section which is falling rapidly with increasing energy. If relation (8.2) is valid, then one would expect the same kind of energy dependence

in the corresponding semi-inclusive cross sections. This can be done because <n> does not vary too much between our two energies and, hence, for a given prong number n/<n> is nearly constant.

The Reaction $K^- p \to \bar{K}^0$ + n charged + neutrals

In fig. (8-1) we present semi-inclusive cross sections in x normalised by σ_n for this reaction for different multiplicities at 10 and 16 GeV/c. It can be seen from this figure that the shape of the distribution for a given multiplicity at one energy tends to be similar to that at the other energy. Such behaviour is very much in agreement with what one expects from relation (8.2) coupled with the fact that the $\bar{K}^0$ inclusive distribution discussed in Chapter Three does not show any strong energy dependence between the two energies.

From our previous studies concerning correlations between particles we have shown that such correlations do indeed exist. KNO have pointed out that in their absence, relation (8.2) reduces to a simple form given by:-

$$\frac{E d^3\sigma_n}{d^3 p_c} = \sigma_n f(x, p_T, s)$$

where $f(x, P_T, s)$ is the inclusive cross section of particle c.

It is true that the assumption of no correlations contradicts our previous conclusions concerning their existence. However, it is useful to check whether equation (8.2) is sensitive to such correlations.

From fig. (8-1) again one notices that although distributions with equal n values have the same shape at both energies they do change their shape to a large extent as we move from one multiplicity to another. Furthermore, all distributions at different multiplicities tend to have shapes which are rather different from the inclusive $\bar{K}^0$ distributions

of fig. (3-4). This is not only a simple check on the correctness of relation (8.2) and its sensitivity to correlations, but can be taken as a confirmation of our previous results concerning the existence of these correlations. From this we may conclude that our semi-inclusive $\bar{K}^0$ distributions are not in disagreement with relation (8.2) proposed by KNO.

The Reaction $K^- p \to \Lambda^0$ + n charged + neutrals

In contrast with the previous reaction where we had an energy dependent inclusive cross-section in our energy range, as mentioned in Chapter Three the inclusive cross-section for Λ^0 falls off quite significantly as the energy increases. In such a case one would expect the same kind of energy dependence of the individual semi-inclusive cross-sections at different multiplicities: i.e. scaling of semi-inclusive cross sections is not expected to occur if relation (8.2) is a good measure of the energy dependence of these cross sections.

In fig. (8-2) we show the topological semi-inclusive cross-sections for this reaction. From this figure it is apparent that distributions at different energies but for the same multiplicity tend to have different shapes. Scaling does not occur. The different shapes of the normalised semi-inclusive cross-sections tend to reflect the energy dependence of two different exchange mechanisms involved in the forward and backward directions. This is other evidence that what is called naive scaling is not satisfied in this energy range which is in contrast with previous results on Λ^0 inclusive production[2] between 4.2 and 10.1 GeV/c.

$\bar{K}^0$ and Λ^0 in the Triple Regge Limit

Comparison of inclusive cross sections of $\bar{K}^0$ and Λ^0 produced in $K^- p$ interaction at 14.2 GeV/c with predictions of the triple Regge formula was carried out by Paler et al.[3].

The results of their comparison showed that the triple Regge formula (6-1) provides good parametrization of the data. However, in their case, they fitted only for the parameter $\alpha(t)$. Values of $\bar{\alpha}(o)$ were considered to be known. For their $\bar{K}^o$ and backward Λ^o, $\bar{\alpha}(o)$ was assumed to be a meson trajectory intercept and $\bar{\alpha}(o)$ was set to equal to 0.5. For forward Λ^o, $\bar{\alpha}(o)$ was assumed to be equal to 0.0.

Study of triple Regge behaviour for these two particles in this energy range is not as simple as the corresponding one for the Δ^{++} case. This is mainly because in these two cases we have non-exotic quantum numbers in the missing mass. This leads to restrictions about the extent to which one can employ the triple Regge formula. This is because for a wide range of M values one has well known resonances while the assumptions made to obtain the triple Regge formula involve asymptotic Regge behaviour of $\alpha(t)$ b scattering. Such an assumption is valid only in the high mass region.

Thus triple Regge fits in this energy range for such reactions if successful are not only good support for the triple Regge parametrization but may be considered as evidence for the applicability of semi-local duality arguments[4] if such fits are carried out using events in the small M_x region.

Another problem associated with the triple Regge parametrization of these two reactions is that one cannot expect the trajectory derived in each case to correspond to a pure exchange mechanism. What one actually gets is an effective trajectory resulting from contributions from more than one Regge trajectory. Thus one is not in a situation to make definite conclusions about which trajectory is being exchanged in each case.

Triple Regge Parametrization of the $\bar{K}^o$ Cross Sections

The x distributions for $\bar{K}^o$ produced at our two energies shown in fig. (3-4) show that only a few $\bar{K}^o$'s are produced in the backward direction.

For this reason we cannot fit the triple Regge formula in the region of small momentum transfer from the incident proton. Parametrization can be performed on those $\bar{K}^o$'s produced in the K^- fragmentation region only.

The same kind of technique which was used in the Δ^{++} regge fits has been used here. The missing mass distributions for different t ranges between 0.0 and -0.6 $(GeV/c)^2$ are shown in fig. (8-3) and these were fitted with the triple Regge formula. Again the values of $\bar{\alpha}(o)$ were obtained from the s dependence at fixed values of M_x^2/s for each t range and in this case again no significant dependence of $\bar{\alpha}(o)$ on t was found.

Using these values of $\bar{\alpha}(o)$ the Regge trajectory $\alpha(t)$ was calculated from the M_x dependence for values of M between 1.5 and 2.5 GeV/c. The dependence of $\bar{\alpha}(o)$ and $\alpha(t)$ on t are shown in fig. (8-4) and fig. (8-5) respectively. An eye-ball fit to a straight line through the values of $\alpha(t)$ versus t yields a Regge trajectory given by

$$\alpha(t) = 0.15 + 0.87\ t.$$

The values of $\bar{\alpha}(o)$ are in agreement with a value of 1. within the errors. This is expected if one assumes that $\bar{\alpha}(o)$ is the intercept of the pomeron trajectory which may indeed be the case if one is to expect the observed early scaling in the $\bar{K}^o$ single particle distribution. This is not in agreement with the value of 0.5 for $\bar{\alpha}(o)$ assumed in the triple Regge fit of ref. (3).

Triple Regge Parametrization of Λ^o Cross Sections

Unlike the x distribution for $\bar{K}^o$, the corresponding one for Λ^o shows cross sections in the forward and backward directions which are of the same order of magnitude. The cross section in the backward direction is somewhat higher than in the forward direction. In this case one can study the behaviour in two triple Regge limits corresponding to fragmentation regions

of the proton and the kaon.

In both cases we have used the same technique employed previously. The missing mass distributions for different regions in the momentum transfer variables are shown in fig. (8-6) where for backward moving Λ^0's the momentum transfer was taken to be that from the protons and in fig. (8-7) where the momentum transfer was taken to be from the kaon for forward moving Λ^0.

For backward moving Λ^0's results of fits for the parameters $\bar{\alpha}(o)$ and $\alpha(t)$ for values of M between 1.5 - 2.5 GeV are shown in fig. (8-8) for each t range. From this figure it is apparent that $\bar{\alpha}(o)$ has no significant dependence on t. Furthermore, the average value of $\bar{\alpha}(o)$ is in agreement with the value of 0.5 which is what one would expect if $\bar{\alpha}(o)$ is an intercept of a meson trajectory. The values of $\alpha(t)$ for different ranges in t give a trajectory which seems to be in agreement with what one would expect if one has $K^*(890)$ exchange.

For forward moving Λ^0's one could not select on events with Λ^0 produced with very small squared four momentum transfers from the beam. This is because of the small number of events in the small t ranges. Thus we had to use values of t up to 1.1 $(GeV/c)^2$. The results of triple Regge fits in this case are shown in fig. (8-9). The values of $\bar{\alpha}(o)$ show no significant dependence on t. Furthermore, these values are in agreement with what one would expect from s^{-1} dependence of $p\bar{p}$ total cross-sections.

Polarization of Λ^0 at 10 GeV/c

We have studied the average polarization of inclusively produced Λ^0 in our 10 GeV/c data. This was done using the polarization formula for Λ^0 decay given by:

$$p = \frac{1'}{\alpha} \langle \text{Cos } \theta \rangle$$

where p is the polarization and θ is the angle between the direction of

pion coming from the Λ^o decay and the original direction of the Λ^o when this angle is calculated in the Λ^o rest frame. α is the Λ^o decay parameter which is known to be 0.62[5].

Such calculation could not be done for Λ's produced at 16 GeV/c because the data summary tape available did not contain measurements of the decay trakcs and for this reason our calculation was confined to the 10 GeV/c data.

The polarization of Λ^o as a function of the kinematical variables x, p_T^2, t and M is shown in fig. (8-10). In this figure one notices that the average polarization tends to have values which are slightly positive for negative values of X. This polarization changes sign going to negative values when x becomes positive. As a function of p_T^2 the polarization is zero for small values of p_T^2 becoming more negative toward higher values of p_T^2. This may be related to x dependence of the polarization through the seagull effect because selection on events where the Λ^o has small values of p_T^2 increases the proportion of events produced in the small x region where the average polarization is zero. An overall small negative polarization for large p_T^2 values comes from adding the positive polarization at negative x to the larger negative polarization at positive x.

The polarization changes sign as a function of t. It is negative for very small values of t and becomes positive for t in the range of 0.2 GeV^2/c^2. For higher values of t the polarization is negative. Zero values for the polarization are obtained for small values of the missing mass. However, for values of M greater than 2.5 GeV the polarization becomes negative.

All the above effects are expected to be related. What is most interesting is the fact that the polarization shows a change of sign as we go from negative to positive values of x. It was shown in a previous article that fits performed using the triple Regge formalism gave different trajectories which are assumed to be exchanged in the triple Regge limits for the positive and negative x regions. The difference between the two sets of trajectories exchanged may have something to do with the observed polarization in the two regions. As far as we know, there are no theoretical

predictions about such polarization effects. However, Berger in his review of inclusive phenomenology emphasizes that because the theoretical situation is not clear, it is important to obtain data showing the approximate magnitude and sign of the polarization in different kinematical regions.

Summary and Conclusions

In this chapter we dealt with some aspects of $\bar{K}^0$ and Λ^0 production in our experiments. Semi-inclusive cross sections for the production of these two particles were presented and compared with KNO predictions. Triple Regge analysis of these two reactions shows that the triple Regge formula produces good parametrization of the data. For $\bar{K}^0$ production the value of $\bar{\alpha}(o)$ seems to be in disagreement with the assumption made in ref.(3). For the Λ^0 case, although our statistics at 16 GeV/c are not very good the trajectories obtained were in good agreement with baryon exchange for Λ^0 produced in the forward direction and K^* exchange for Λ^0 produced in the backward direction. Polarization measurement reflect to some extent these two different exchange mechanisms.

REFERENCES (8)

1. Z. Koba, H.B. Nielsen and P. Olesen, Phys. Letters 38B, 25 (1972).
2. Aachen-Berlin-CERN-London-Vienna and Amsterdam-Nijmegen Collaborations, Nucl. Phys. B39, 287 (1972).
3. K. Paler et al., Rutherford Laboratory Preprint, to be published in Phys. Letters.
4. P. Hoyer, R.G. Roberts and D.P. Roy, Rutherford Laboratory Preprint RPP/T/35 (1973).
5. W. Koch, Proceedings of the 1964 CERN Easter School, CERN Yellow Report, CERN 64-13.

FIGURE CAPTIONS (8)

(8-1) Plots of the normalized semi-inclusive distributions in x for the reaction $K^-p \to \bar{K}^0$ + n charged + anything. Solid histograms represent values of h(x) from the 10 GeV/c data, dotted histograms represent the corresponding values of h(x) from the 16 GeV/c data.

(8-2) Plots of the normalized semi-inclusive distributions in x for the reaction $K^-p \to \Lambda^0$ + n charged + anything. Solid histograms represent values of h(x) from the 10 GeV/c data, dotted histograms represent the corresponding values of h(x) from the 16 GeV/c data.

(8-3) Missing mass distributions for different t ranges for the reaction $K^-p \to \bar{K}^0$ + anything

(a) at 10 GeV/c

(b) at 16 GeV/c.

The solid curves represent results of fitting those distributions with the triple Regge formula.

(8-4) Values of $\bar{\alpha}(o)$ obtained from fitting the missing mass distributions of fig.(8-3) with the triple Regge formula plotted versus t.

(8-5) Values of $\alpha(t)$ obtained from fitting the distributions of fig.(8-3) with the triple Regge formula plotted versus t. The solid line represents an eye ball fitted trajectory.

(8-6) Missing mass distributions for different $t_{p\Lambda^0}$ ranges for the reaction $K^-p \to \Lambda^0_{Backward}$ + anything at

(a) 10 GeV/c

(b) 16 GeV/c.

Solid curves represent results of fits using the triple Regge formula.

(8-7) Missing mass distributions for different $t_{K\Lambda^0}$ ranges for the reactions $K^-p \to \Lambda^0_{Forward}$ + anything at

(a) 10 GeV/c

(b) 16 GeV/c.

Solid curves represent results of fits using the triple Regge formula.

(8-8)
(a) Values of $\bar{\alpha}(o)$ obtained from triple Regge fits of the distributions in fig.(8-6) plotted as a function of t.

(b) Values of $\alpha(t)$ obtained from triple Regge fits of the distributions in fig.(8-6) plotted as a function of t. The solid line represents the K^* Regge trajectory.

(8-9)
(a) Values of $\bar{\alpha}(o)$ obtained from triple Regge fits of the distributions in fig.(8-7) plotted as a function of t.

(b) Values of $\alpha(t)$ obtained from triple Regge fits of the distributions in fig.(8-7) plotted as a function of t.

(8-10) Polarization of Λ^o's from the reaction $K^- p \to \Lambda^o$ + anything plotted as a function of x, p_T^2, $t_{p\Lambda^o}$ and missing mass.

FIG(8-1)

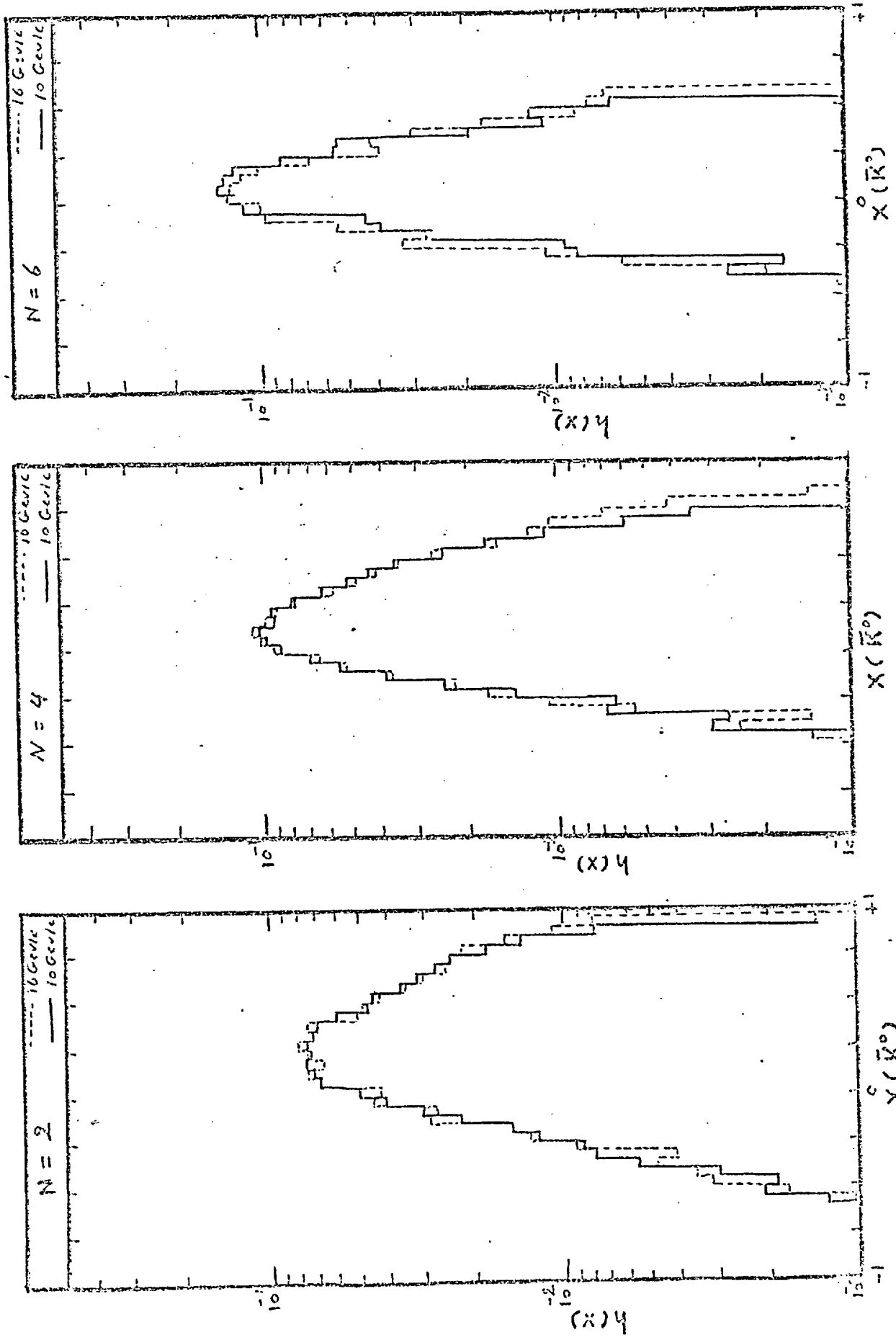

FIG(8-2)

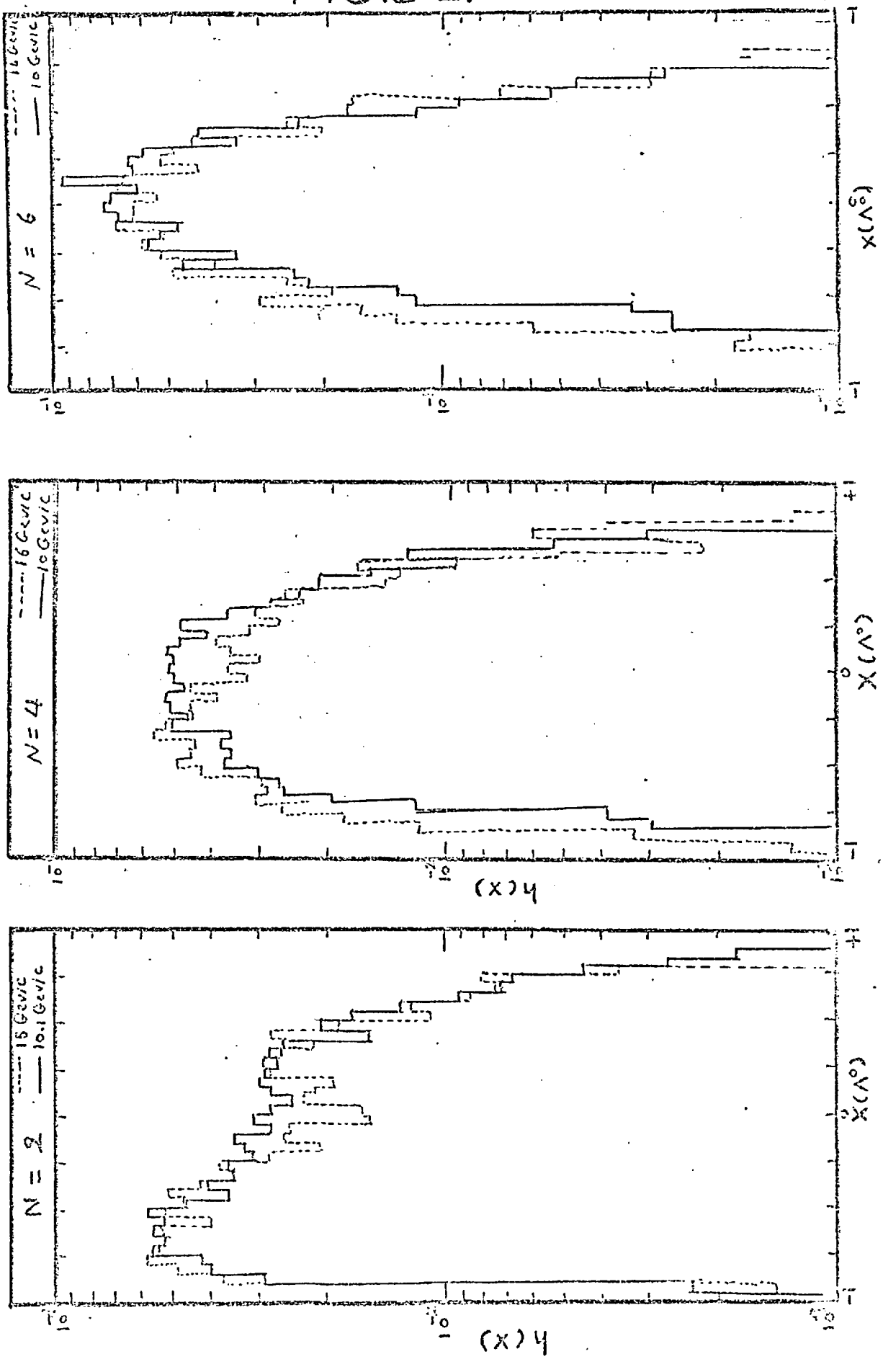
N = 6
16 Gev/c
10 Gev/c
X (°)
h(x)
N = 4
16 Gev/c
10 Gev/c
X (°)
h(x)
N = 2
16 Gev/c
10.1 Gev/c
X (°)
h(x)

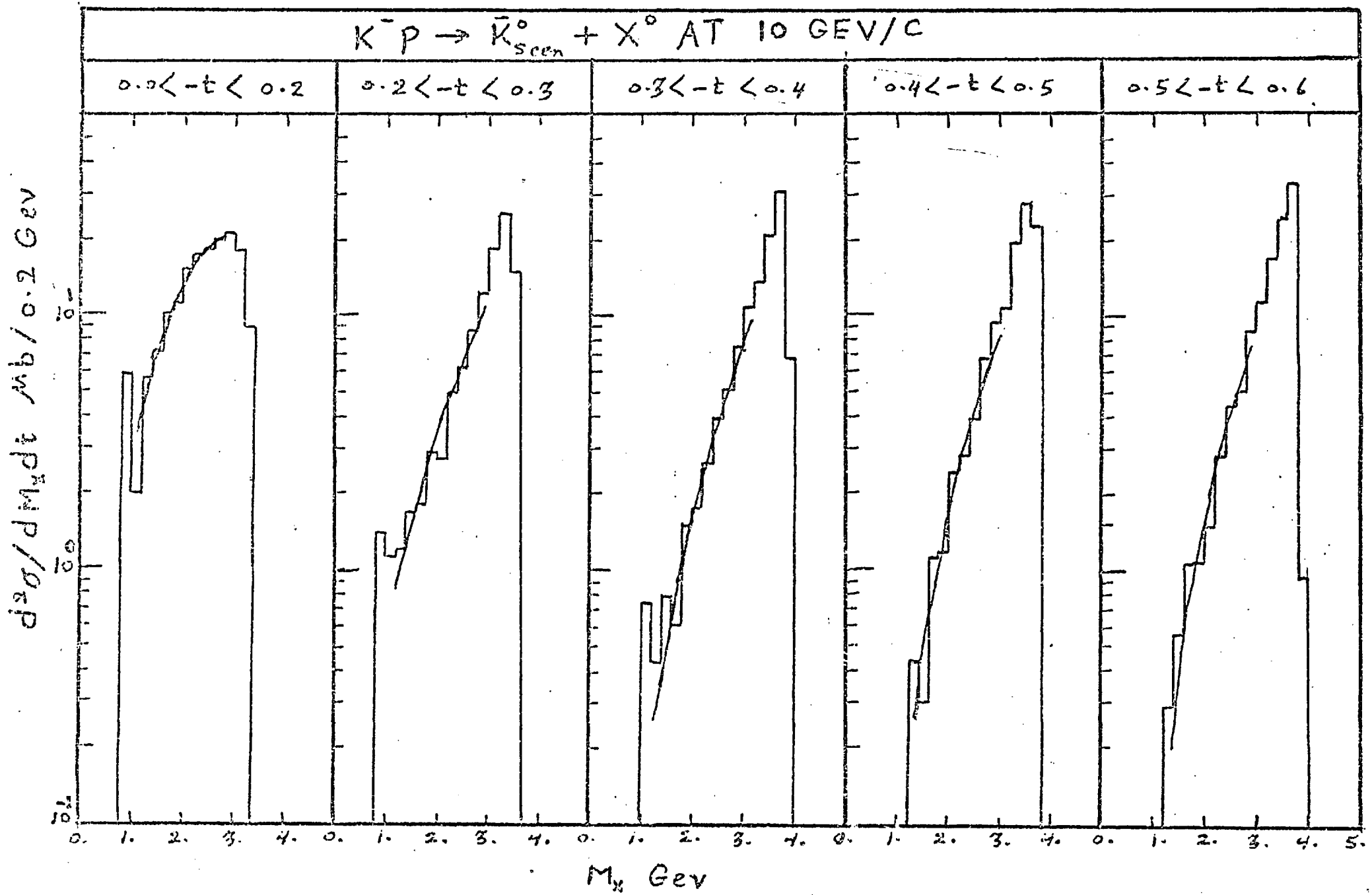
$K^- p \rightarrow \bar{K}^0_{scen} + X^0$ AT 10 GEV/C
0.0 < -t < 0.2
0.2 < -t < 0.3
0.3 < -t < 0.4
0.4 < -t < 0.5
0.5 < -t < 0.6
$d^2\sigma/dM_x dt$ mb/0.2 Gev
M_x Gev

FIG(B-3-a)

FIG(8-3-b)

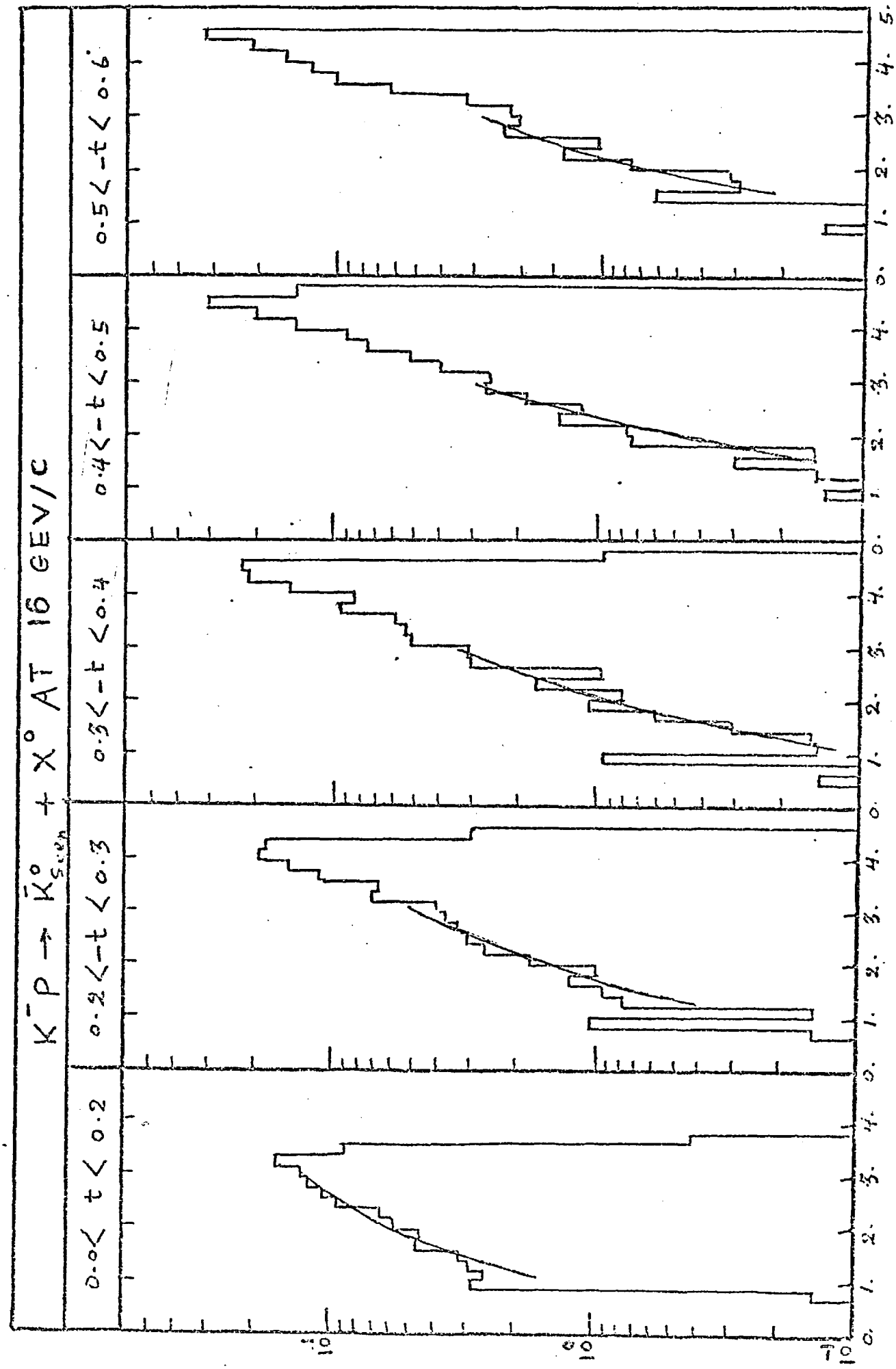
K⁻P → K°s.e.p + X° AT 16 GEV/C
0.0< t <0.2
0.2<-t <0.3
0.3<-t <0.4
0.4<-t <0.5
0.5<-t <0.6
dσ/dM_x dt mb/0.2 GeV

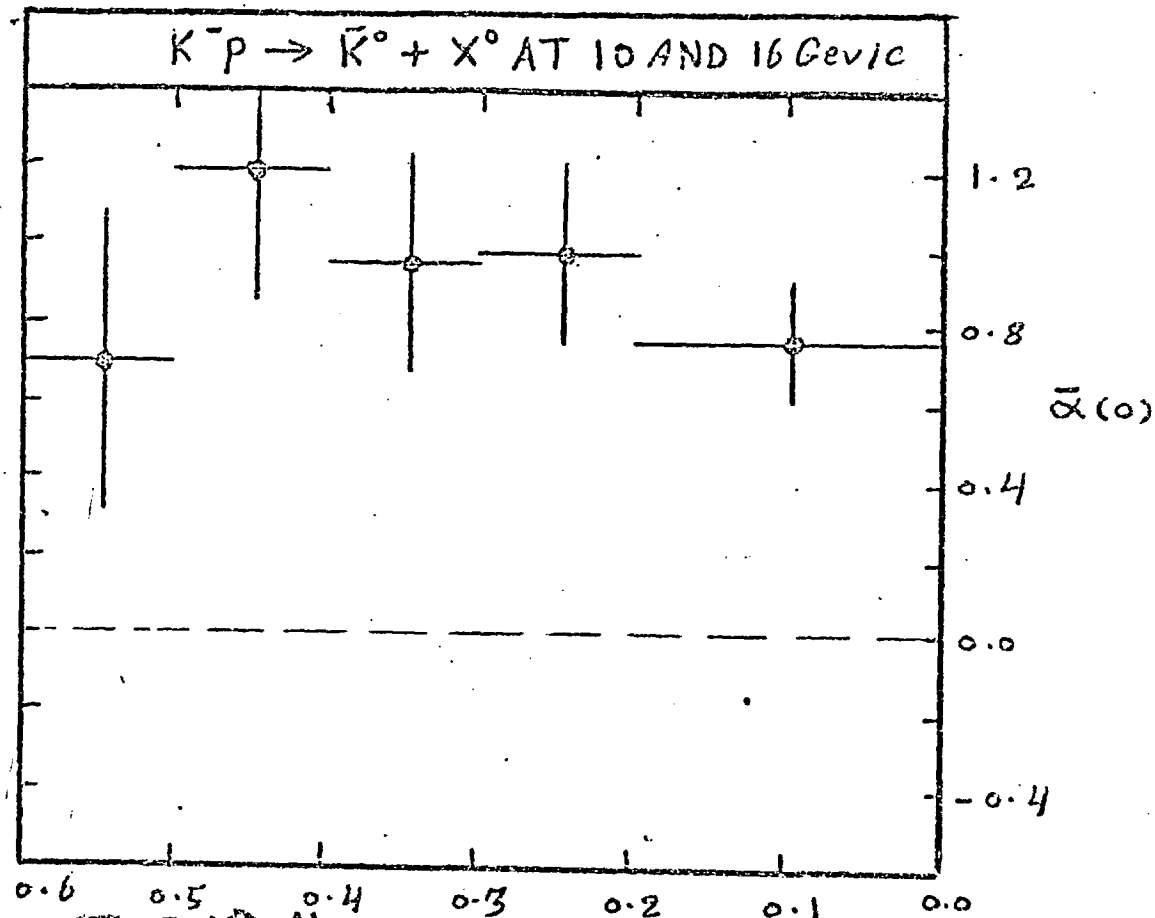
K⁻P → K̄° + X° AT 10 AND 16 Gev/c
1·2
0·8
0·4
0·0
-0·4
ᾱ(0)
0·6
0·5
0·4
0·3
0·2
0·1
0·0
-t Gev

FIG(8-4)

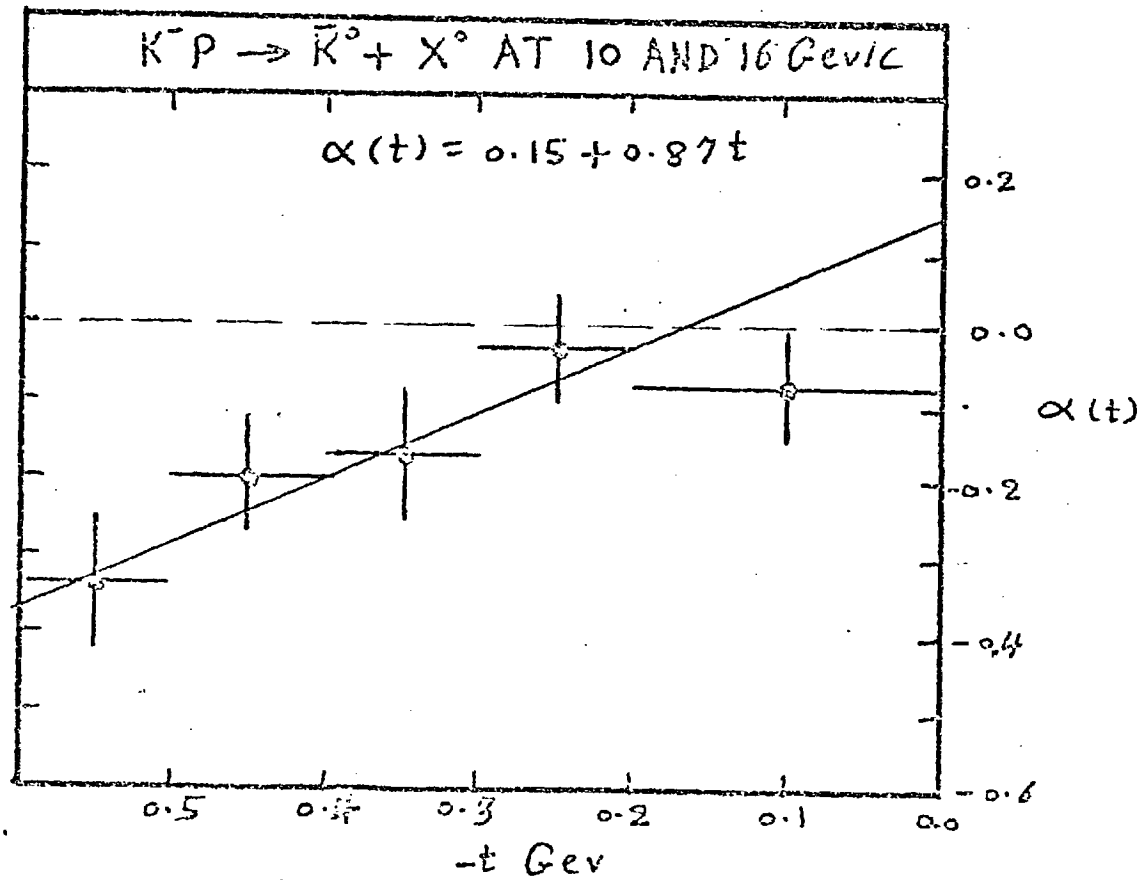
K⁻P → K̄° + X° AT 10 AND 16 Gev/c
α(t) = 0·15 + 0·87 t
0·2
0·0
-0·2
-0·4
-0·6
α(t)
0·5
0·4
0·3
0·2
0·1
0·0
-t Gev

FIG(8-5)

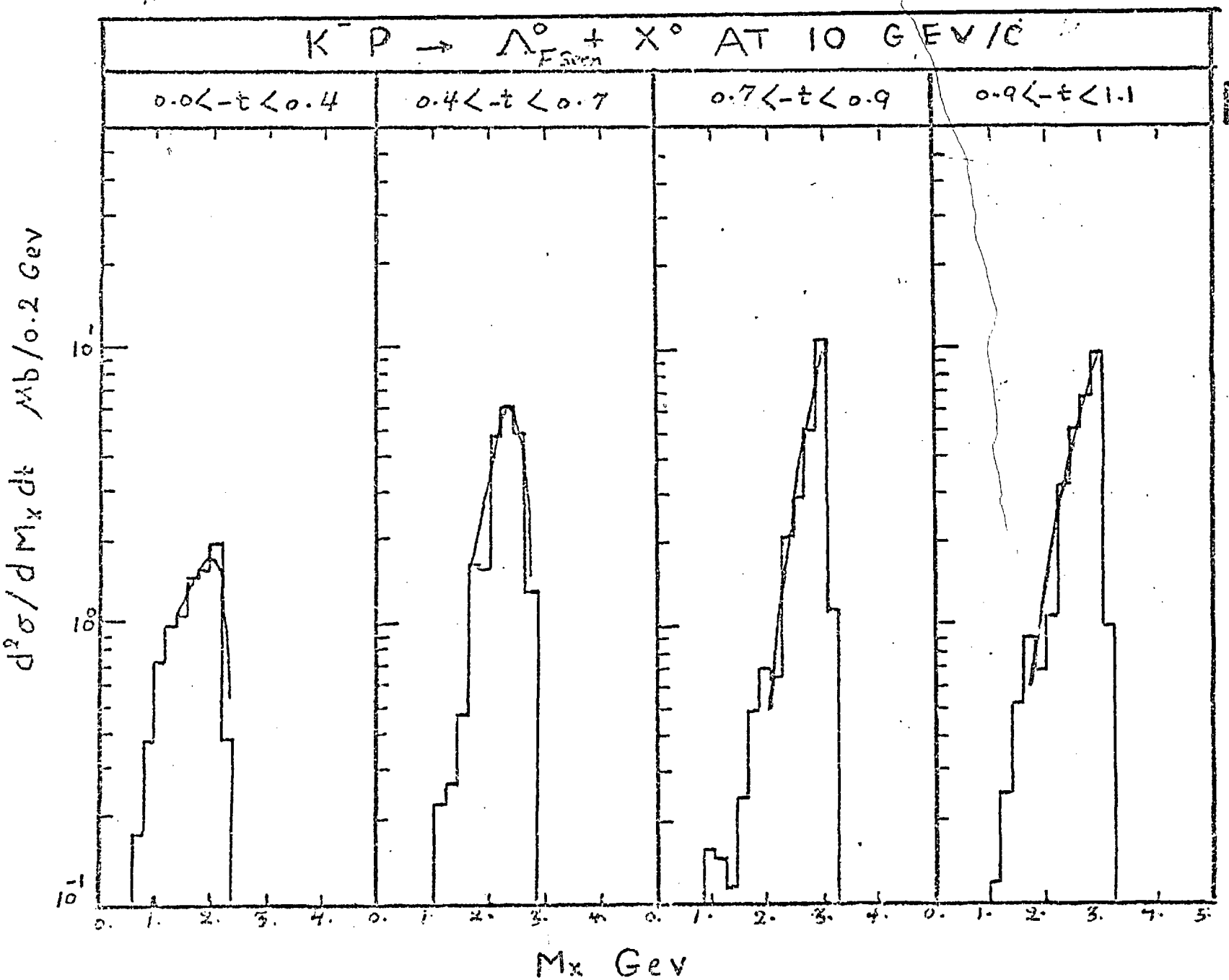
K⁻P → Λ°F seen + X° AT 10 GEV/C
0.0<-t<0.4
0.4<-t<0.7
0.7<-t<0.9
0.9<-t<1.1
d²σ/dMx dt Mb/0.2 Gev
1
10
0. 1. 2. 3. 4. 5.
Mx Gev

FIG18-6-a

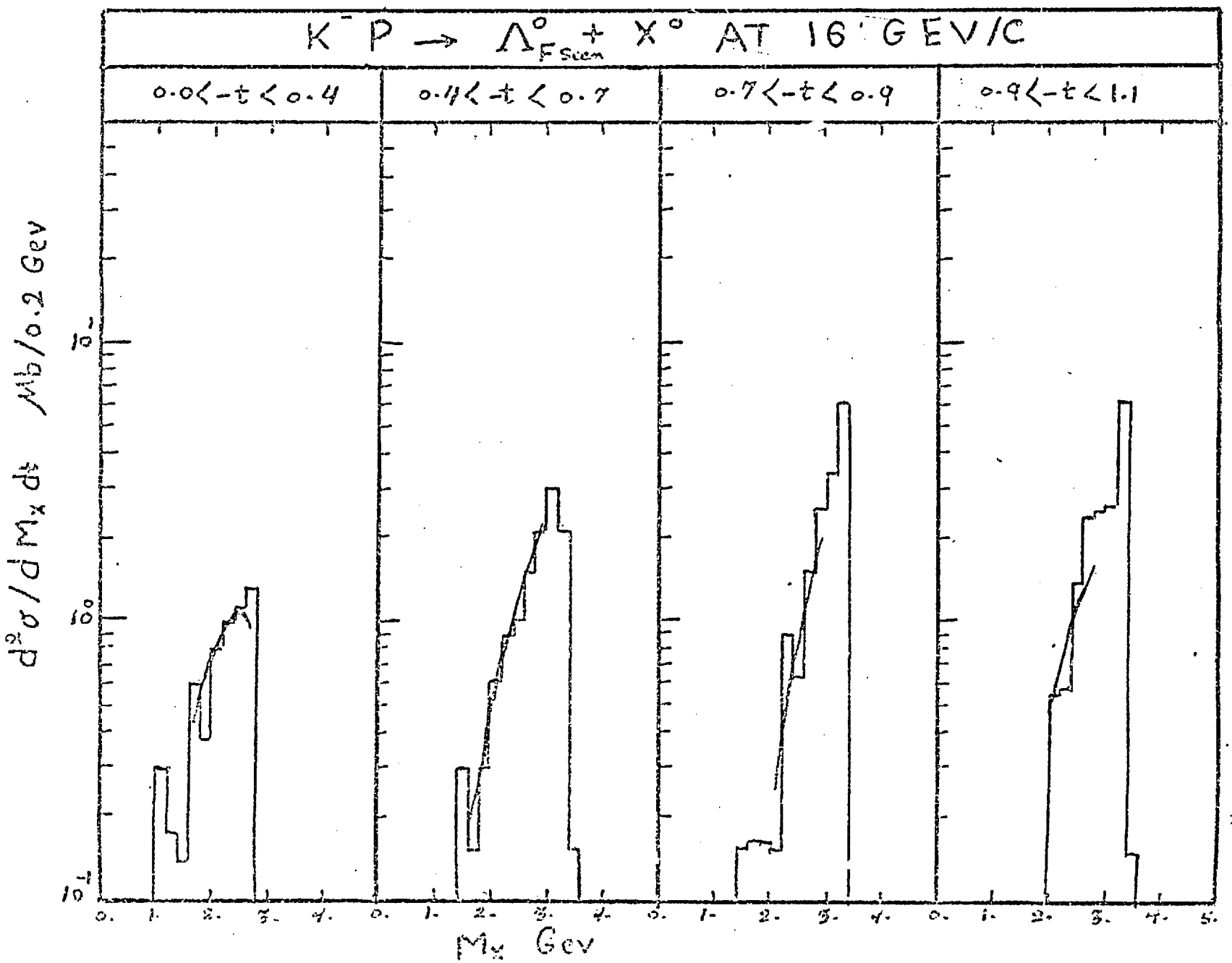
K⁻P → Λ°F Scan + X° AT 16 GEV/C
0.0 < -t < 0.4
0.4 < -t < 0.7
0.7 < -t < 0.9
0.9 < -t < 1.1
d²σ/dM_x dt Mb/0.2 Gev
10⁻¹
10⁰
10⁻
0. 1. 2. 3. 4. 5.
M_x Gev

FIG 8-6

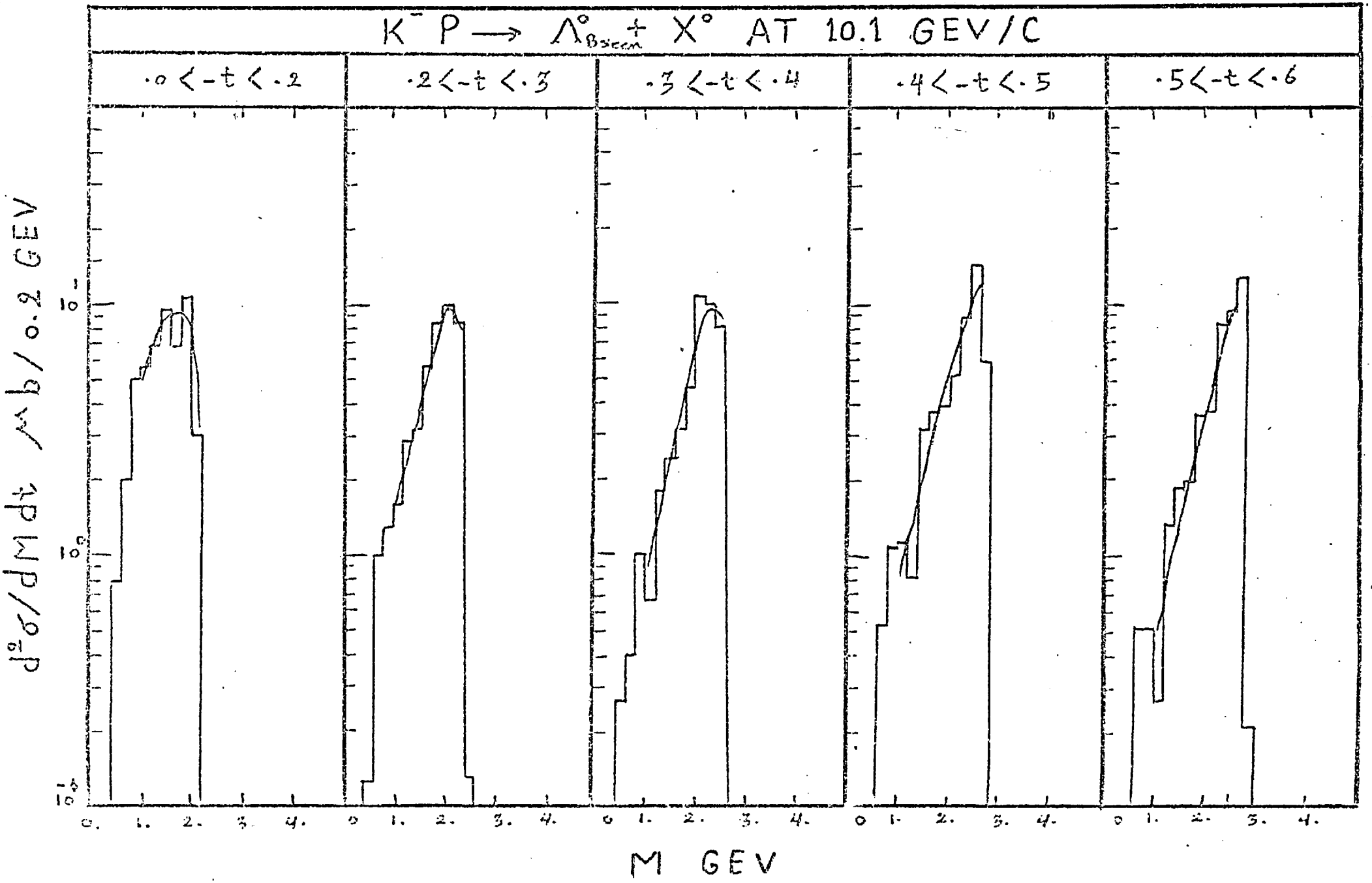
K⁻P → Λ°Beam + X° AT 10.1 GEV/C
·0 < -t < ·2
·2 < -t < ·3
·3 < -t < ·4
·4 < -t < ·5
·5 < -t < ·6
d²σ/dMdt μb/0.2 GEV
M GEV
0. 1. 2. 3. 4.

FIG 10-1

FIG(8-7-b)

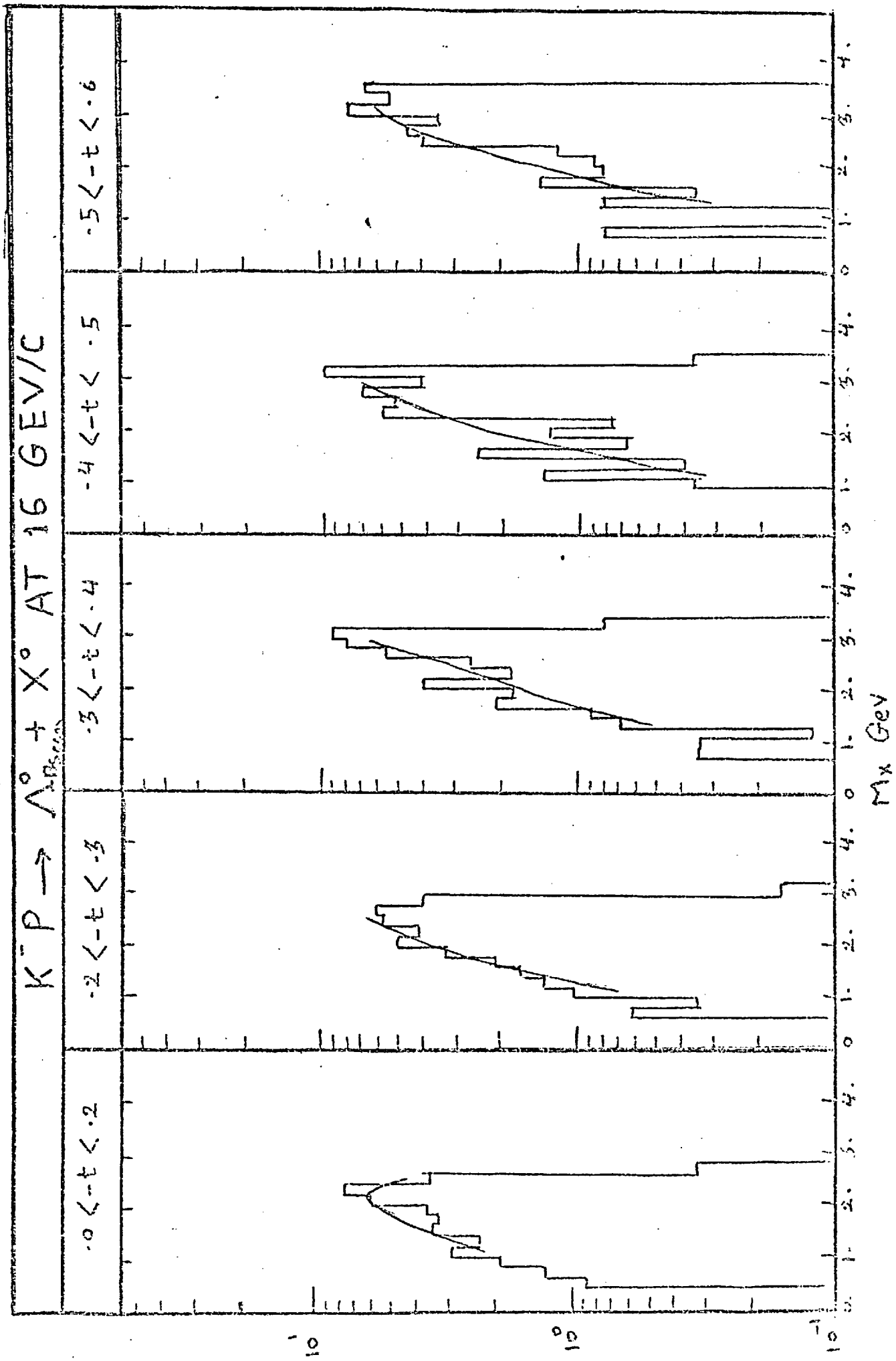
K⁻P → Λ°Beam + X° AT 16 GEV/C
-.5 < -t < .6
-.4 < -t < .5
-.3 < -t < .4
-.2 < -t < -.3
-.0 < -t < .2
Mx GeV
d²σ/dMdt mb/0.2 GEV

FIG(8-8)

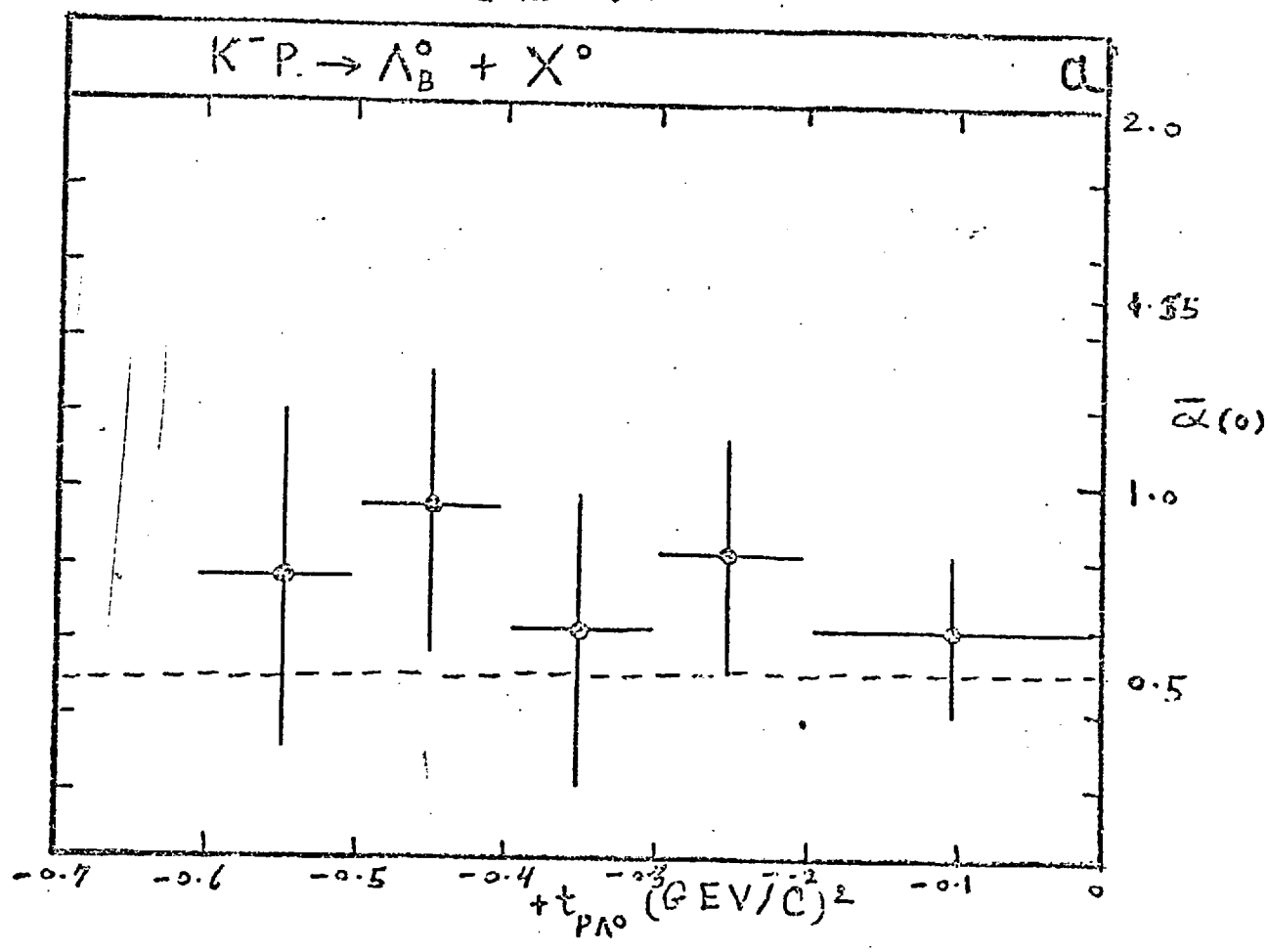
K⁻P → Λ°B + X°
a
2.0
1.55
1.0
0.5
ᾱ(0)
-0.7
-0.6
-0.5
-0.4
-0.3
-0.2
-0.1
0
+t PΛ° (GEV/C)²

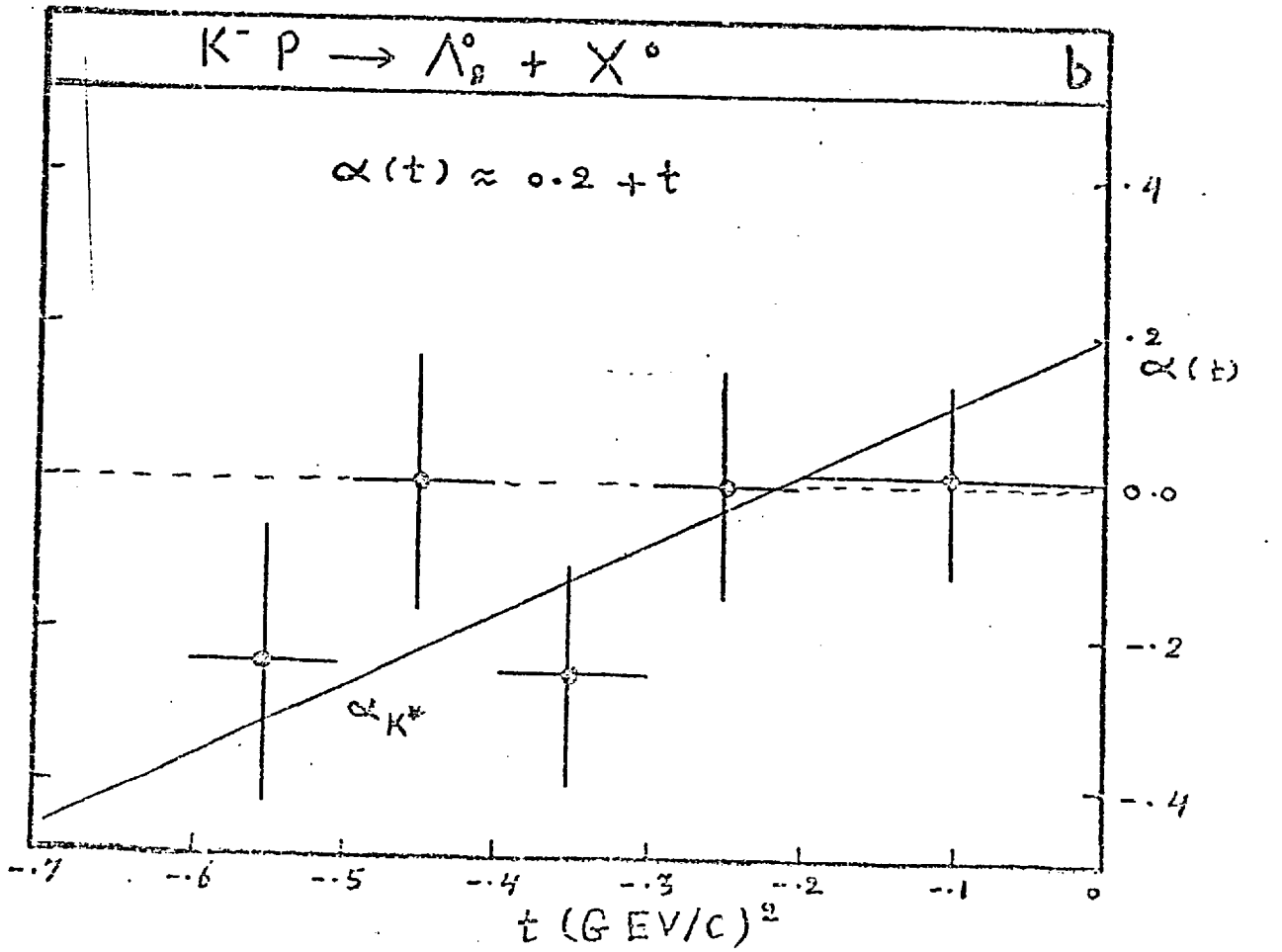
K⁻ P → Λ°B + X°
b
α(t) ≈ 0.2 + t
.4
.2
0.0
-.2
-.4
α(t)
α K*
-.7
-.6
-.5
-.4
-.3
-.2
-.1
0
t (GEV/C)²

FIG(8-9)

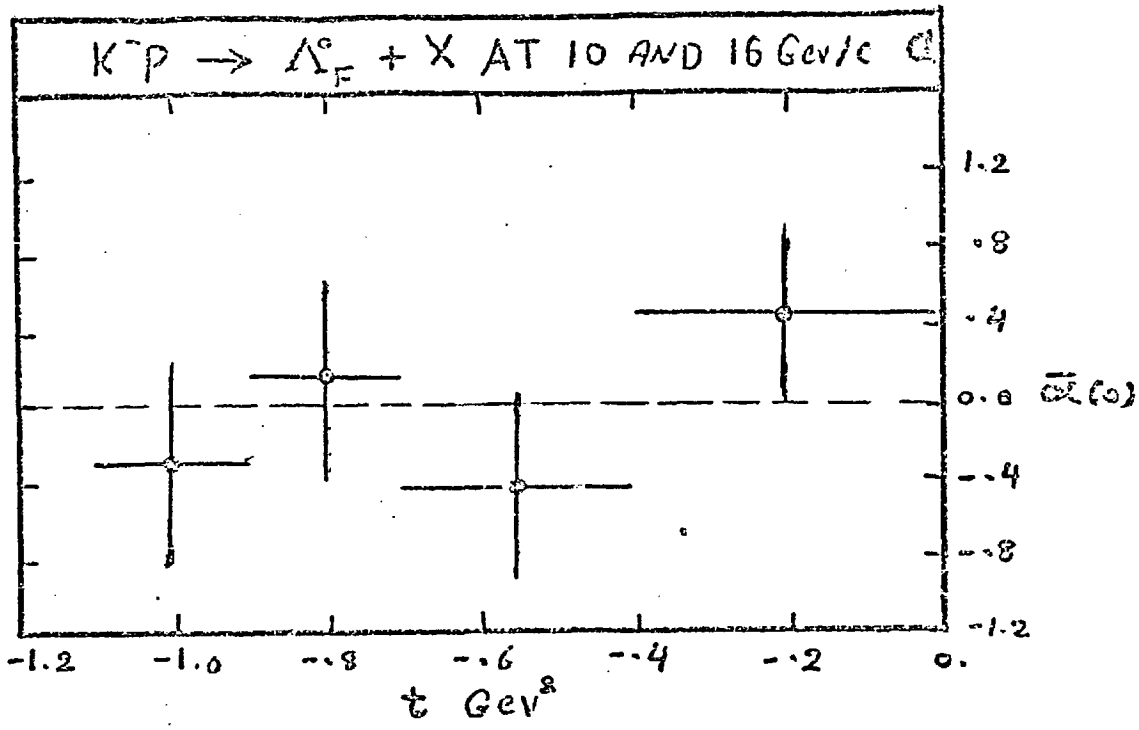
K⁻P → Λ°F + X AT 10 AND 16 Gev/c a
1.2
.8
.4
0.0
-.4
-.8
-1.2
α̅(0)
-1.2
-1.0
-.8
-.6
-.4
-.2
0.
t Gev²

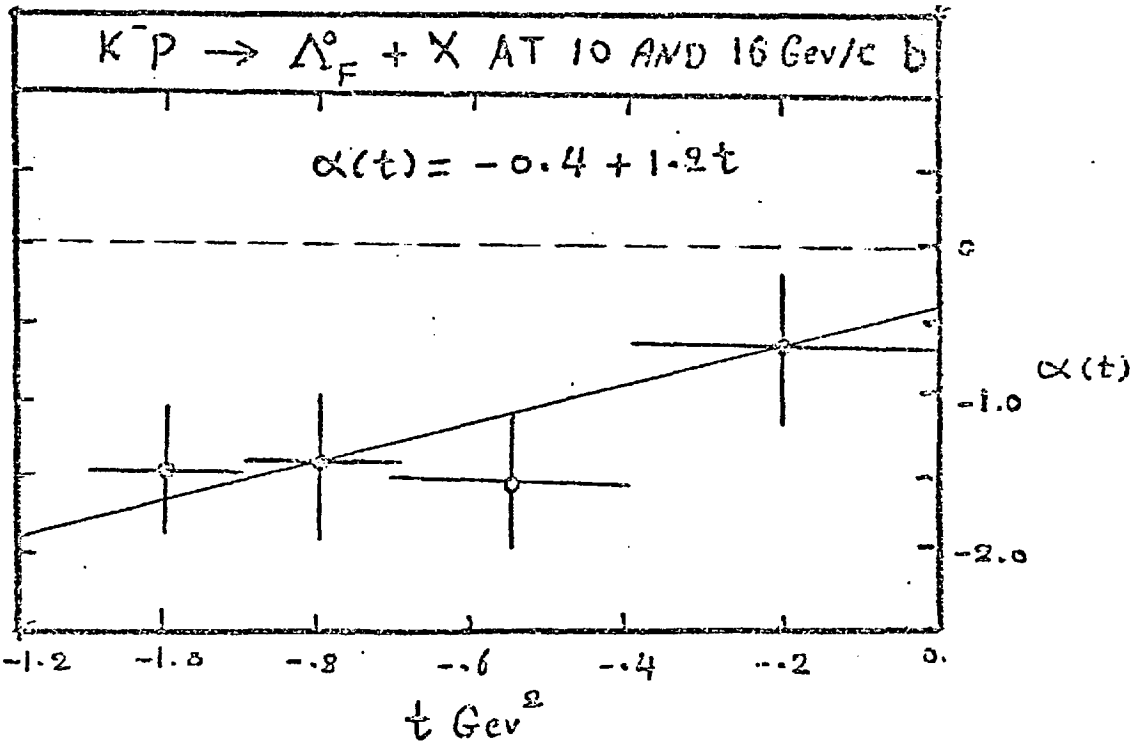
K⁻P → Λ°F + X AT 10 AND 16 Gev/c b
α(t) = −0.4 + 1.2t
0
-1.0
-2.0
α(t)
-1.2
-1.0
-.8
-.6
-.4
-.2
0.
t Gev²

FIG(8-10)

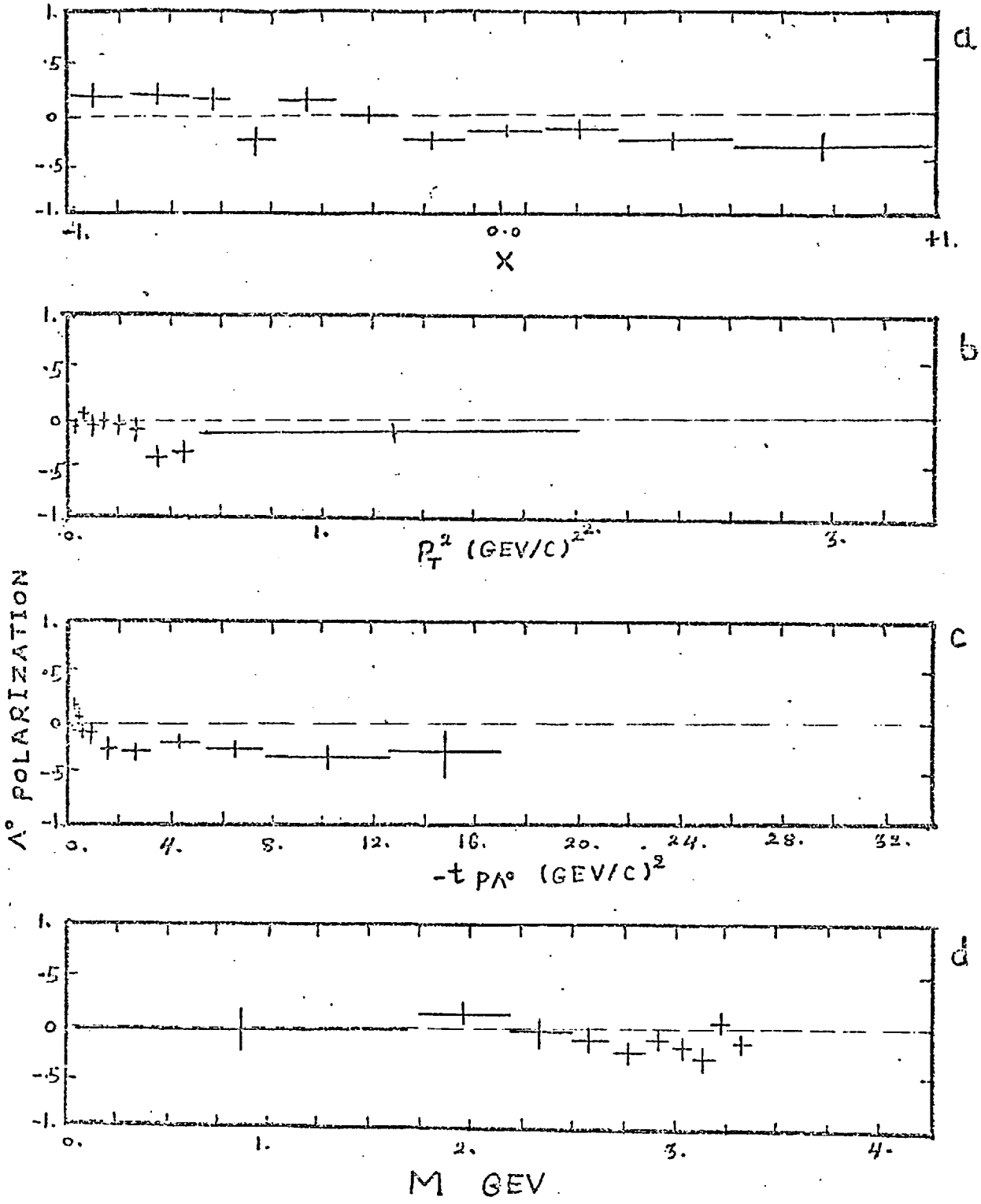

ACKNOWLEDGEMENTS

I thank Professor C.C. Butler and Professor I. Butterworth for giving me the opportunity to start and continue this work in the high energy physics group.

Thanks are due to Professor S.J. Goldsack for suggesting the idea of this work and also for supervising it during the first year.

I would like to express my deep gratitude to my supervisor, Dr. T.C. Bacon, for his valuable help and understanding during the last two years and also for reading and correcting the original manuscript.

My thanks are due to Dr. P.J. Dornan for his valuable criticism and advice. Thanks are also due to Dr. K.W.J. Barnham from whom I have benefitted from our discussions and also for giving me the data on $\pi^- p \to \Delta^{++} + X$ at 16 GeV/c.

Thanks to all the scanning, measuring and technical staff of all laboratories in the ABCLV Collaboration for their effort, without which this work would not have been possible.

My deep gratitude is to my parents for their patience and encouragement during the period of mutual suffering. Thanks are also due to all my brothers and sisters and to my friend Mr. Mahir Taka.

To Miss Mary Rusbridge are special thanks, not only for typing the first draft of this thesis, but also for being a very patient and understanding friend during the difficult period of this work.

My thanks to Miss M.S. Housden for typing the final draft.

This work has been supported by a grant from the Caloste Gulbunkian Foundation through the University of Mosul.